

**AZO-BENZOTHAZOLE CHROMOPHORE BASED
LIQUID CRYSTALLINE MONOMERS AND THEIR
POLYMERIZATION FOR NEW SIDE CHAIN
LIQUID CRYSTALLINE POLYMERS**

MD. RABIUL KARIM

**THESIS SUBMITTED IN FULFILLMENT OF THE
REQUIREMENTS FOR THE DEGREE OF
DOCTOR OF PHILOSOPHY**

**DEPARTMENT OF CHEMISTRY
FACULTY OF SCIENCE
UNIVERSITY OF MALAYA
KUALA LUMPUR**

2014

UNIVERSITI MALAYA
ORIGINAL LITERARY WORK DECLARATION

Name of Candidate: **MD. RABIUL KARIM** (Passport No: **AA8688495**)

Registration/Matric No: **SHC110055**

Name of Degree: **DOCTOR OF PHILOSOPHY**

Title of Project Paper/Research Report/Dissertation/Thesis ("this Work"):

**AZO-BENZOTHAZOLE CHROMOPHORE BASED LIQUID CRYSTALLINE
MONOMERS AND THEIR POLYMERIZATION FOR NEW SIDE
CHAIN LIQUID CRYSTALLINE POLYMERS**

Field of Study: **POLYMER CHEMISTRY**

I do solemnly and sincerely declare that:

- (1) I am the sole author/writer of this Work;
- (2) This Work is original;
- (3) Any use of any work in which copyright exists was done by way of fair dealing and for permitted purposes and any excerpt or extract from, or reference to or reproduction of any copyright work has been disclosed expressly and sufficiently and the title of the Work and its authorship have been acknowledged in this Work;
- (4) I do not have any actual knowledge nor do I ought reasonably to know that the making of this work constitutes an infringement of any copyright work;
- (5) I hereby assign all and every rights in the copyright to this Work to the University of Malaya ("UM"), who henceforth shall be owner of the copyright in this Work and that any reproduction or use in any form or by any means whatsoever is prohibited without the written consent of UM having been first had and obtained;
- (6) I am fully aware that if in the course of making this Work I have infringed any copyright whether intentionally or otherwise, I may be subject to legal action or any other action as may be determined by UM.

Candidate's Signature

Date

Subscribed and solemnly declared before,

Witness's Signature

Date

Name:

Designation:

ABSTRAK

Monomer cecair kristal yang boleh dijadikan polimer berasaskan kromorfor azo-benzothiazole, **M1-M10**, dengan pelbagai unit gantian (CH_3 , OCH_3 , OC_2H_5 , F, Cl dan sebagainya) pada kedudukan ke-enam pada rangka benzothiazole telah berjaya disintesis melalui gandingan azo diikuti dengan pengetheran dan kemudiannya tindakbalas pengesteran. Monomer-monomer baru ini menunjukkan kestabilan terma yang baik dengan suhu penguraian yang merujuk kepada 5% kehilangan berat dalam julat di antara $280\text{-}320^\circ\text{C}$. Kesemua monomer yang disintesis mempamerkan sifat-sifat cecair kristal berdasarkan pemerhatian daripada DSC dan POM. Monomer (**M1**, **M5** dan **M6**) mengandungi H, F and Cl pada kedudukan ke-enam pada rangka benzothiazole mempamerkan hanya fasa smektik wujud manakala monomer-monomer dengan CH_3 , OCH_3 dan OC_2H_5 (**M2**, **M3** and **M4**) mempamerkan fasa nematik dan smektik. Sebaliknya, monomer **M7** (tanpa sebarang unit gantian) mempamerkan fasa nematik dan smektik manakala monomer **M8-M10** (CH_3 , OCH_3 and OC_2H_5) mempamerkan fasa nematik sahaja. Pembentukan serta kestabilan mesofasa bagi monomer-monomer **M1-M10** kuat dipengaruhi oleh kedudukan kumpulan gantian di kedudukan ke-enam pada rangka benzothiazole dan kepanjangan sesuatu mesogen.

Polimer baru dengan rantaian sisi cecair kristal (SCLCPs), **P1-P10**, yang mengandungi mesogen azo-benzothiazole telah dihasilkan melalui pempolimeran konvensional rantai radikal bebas daripada monomer-monomer yang telah disintesis, **M1-M10**. Analisis thermogravimetric mengesahkan bahawa polimer-polimer **P1-P10** menunjukkan kestabilan terma yang baik dengan suhu penguraian yang merujuk kepada 5% kehilangan berat dalam julat di antara $310\text{-}340^\circ\text{C}$. Kesemua polimer mempamerkan sifat-sifat cecair kristal dan pembentukan mesofasa serta kepanjangan mesofasa bagi polimer-polimer sangat ketara dipengaruhi oleh unit gantian. Suhu peralihan kaca (T_g)

bagi polimer-polimer **P1-P10** didapati dalam julat suhu 134-81°C dan suhu ini beralih kepada suhu yang lebih rendah dengan kehadiran ekor yang pendek pada rantai sisi mesogenik. Kajian berkenaan penyerapan UV-vis menunjukkan penyerapan maksima (λ_{\max}) oleh polimer-polimer **P1-P10** adalah berada di penyerapan merah dengan kehadiran kumpulan penderma/penerima elektron di rantaian sisi polimer. Kajian terhadap photoluminescence menunjukkan bahawa polimer **P1-P6** memancarkan cahaya biru manakala polimer **P7-P10** memancarkan cahaya hijau. HOMO dan LUMO bagi polimer-polimer **P1-P10** adalah dalam julat -4.80 kepada -6.16 eV dan -2.14 kepada -3.53 eV masing-masing. Polimer yang mengandungi atom fluorin (**P5**) menunjukkan nilai HOMO pada -6.16 eV.

Sifat-sifat viscoelastik linear dan viscoelastik dinamik bagi polimer dengan rantaian sisi cecair kristal (SCLCPs) dikaji menggunakan reologi terhadap polimer **P1**, **P3** dan **P4**. Kesemua polimer menunjukkan viscoelastik linear pada amplitud tekanan kecil dan sederhana, manakala, ketidaklinearan diperhatikan pada amplitud tekanan yang tinggi. Smektik polimer, **P1** gagal mengikuti sifat-sifat terminal yang biasa ($G' \propto \omega^2$ and $G'' \propto \omega$) seperti yang ditunjukkan dalam sistem polimer yang homogenus; sebaliknya, ia mempamerkan sifat gel dalam wilayah terminal di mana ia merupakan ciri-ciri polimer smektik. Polimer **P3** dan **P4** juga menyimpang daripada sifat terminal yang biasa disebabkan oleh berat molekul yang rendah dan polidispersiti yang tinggi.

ABSTRACT

Azo-benzothiazole chromophore based new polymerizable liquid crystalline (LC) monomers, **M1-M10**, having different terminal substituents (CH₃, OCH₃, OC₂H₅, F, Cl etc.) at the sixth position on the benzothiazole moiety were successfully synthesized via azo coupling followed by etherification and esterification reactions. The newly synthesized monomers showed good to excellent thermal stability with decomposition temperatures corresponding to 5% weight loss in the range of 280-320°C. The LC properties of the synthesized monomers were confirmed via DSC and POM. Monomers (**M1**, **M5** and **M6**) bearing H, F and Cl at the sixth position on the benzothiazole moiety revealed only smectic phase whereas CH₃, OCH₃ and OC₂H₅ substituted monomers (**M2**, **M3** and **M4**) showed both nematic and smectic phases. On the other hand, monomer **M7** (without terminal substitution) exhibited both nematic and smectic phases while monomers **M8-M10** (CH₃, OCH₃ and OC₂H₅ substituted) showed only nematic phase. The mesophase formation as well as the mesophase stability of monomers **M1-M10** was greatly influenced by the terminal substituents and the length of the mesogen.

New side chain liquid crystalline polymers (SCLCPs), **P1-P10**, bearing azo-benzothiazole mesogen were prepared via conventional free radical polymerization from the synthesized LC monomers, **M1-M10**. Thermogravimetric analysis revealed that the SCLCPs, **P1-P10**, exhibited excellent thermal stability with decomposition temperatures corresponding to 5% weight loss in the range of 310-340°C. All the prepared polymers exhibited LC properties and the mesophase formation as well as mesophase length of the polymers were significantly influenced by the terminal substituents. The glass transition temperatures (T_g) of the polymers **P1-P10** as determined by DSC were in the range of 134-81°C and these values were shifted toward

lower temperature region with the incorporation of short terminal tails in mesogenic side chain.

The UV-vis absorption studies revealed that the absorption maxima (λ_{max}) of the **P1-P10** were red shifted with the incorporation of electron donating/pushing terminal substituents located in the side chain of polymers. The photoluminescence studies showed that the polymers **P1-P6** exhibited blue emission whereas the polymers **P7-P10** exhibited green emission. The highest occupied molecular orbital (HOMO) and the lowest unoccupied molecular orbital (LUMO) energy levels of the SCLCPs, **P1-P10**, were in the range of -4.80 to -6.16 eV and -2.14 to -3.53 eV respectively. Polymer having terminal fluorine atom (**P5**) exhibited the lowest HOMO value of -6.16 eV among all the studied polymers.

The extent of linear viscoelastic and the dynamic viscoelastic behaviours of the SCLCPs were investigated by rheology using selected polymers, **P1**, **P3** and **P4**. All the polymers showed linear viscoelastic region at small and medium strain amplitudes, while non-linearity is observed at high strain amplitude. Smectic polymer **P1** failed to follow the typical terminal behaviour ($G' \propto \omega^2$ and $G'' \propto \omega$) as shown by homogeneous polymeric system; instead, it exhibited gel-like behaviour in the terminal region which is characteristics of smectic polymers. SCLCPs **P3** and **P4** also deviated from the typical terminal behaviour due to the low molecular weight and high polydispersity of the polymers.

ACKNOWLEDGMENTS

First of all, I would like to express my greatest gratitude and sincere thanks to my supervisors; Professor Dr. Rosiyah Yahya, Dr. Md. Rezaul Karim Sheikh and Dr. H.N.M Ekramul Mahmud for their most valuable advice, encouragement and constant support at all the stages throughout this study.

I would also like to acknowledge and thank the entire staff of the Chemistry Department for all their assistance and support. I am very grateful to Noodini M. Salleh for her valuable suggestion and great help during my work. I would like to appreciate the help, support, and valuable hints given by my friends Ahmad Danial, Azhar Kamil, Wisam Naji, Farhana, Murni and the rest of the polymer group members.

I would like to acknowledge the financial support from University of Malaya during my candidature.

I owe my loving wife, Zannatun Ferdous, for her continuous care, inspiration, support and understanding throughout this entire journey.

Finally, I would like to express my utmost gratefulness and thanks to my beloved parents for their love, prayers, blessing and support.

TABLE OF CONTENTS

ABSTRAK.....	ii
ABSTRACT	iv
ACKNOWLEDGMENTS	vi
TABLE OF CONTENTS.....	vii
LIST OF FIGURES.....	xi
LIST OF TABLES	xvi
LIST OF ABBREVIATIONS AND SYMBOLS.....	xvii
LIST OF APPENDICES	xix
CHAPTER 1 : INTRODUCTION	1
1.1. Introduction	1
1.2. Research Objectives.....	5
CHAPTER 2 : LITERATURE REVIEW	6
2.1. Fundamentals of Liquid Crystals	6
2.2. Azo-chromophore containing materials	10
2.3. Azo-benzothiazole moiety based compounds	15
2.4. Liquid crystalline compounds bearing heterocyclic moiety	17
2.5. Photophysical and electrochemical properties of benzothiazole derivatives ...	28
2.6. Benzothiazole moiety based polymers	33
2.7. Side chain liquid crystalline polymers.....	36
CHAPTER 3 : EXPERIMENTAL.....	48
3.1. Materials and reagents	48
3.2. Instrumental Techniques Employed	49
3.2.1. Fourier Transform Infrared (FT-IR) spectroscopy	49
3.2.2. Nuclear Magnetic Resonance (NMR) spectroscopy	49
3.2.3. Thermogravimetric Analysis (TGA).....	50
3.2.4. Differential Scanning Calorimetry (DSC)	50
3.2.5. Polarized Optical Microscopy (POM)	50

3.2.6.	Small Angle X-ray Scattering (SAXS)	51
3.2.7.	Gel-permeation chromatography (GPC)	51
3.2.8.	UV-visible (UV-vis) and Photoluminescence (PL) Spectroscopy	52
3.2.9.	Cyclic voltammetric measurements	52
3.2.10.	Rheological measurements	52
3.3.	Synthesis and characterization of LC monomers, M1-M6.....	53
3.3.1.	Synthesis of monomer M1	53
3.3.2.	Synthesis of monomer M2	58
3.3.3.	Synthesis of monomer M3	60
3.3.4.	Synthesis of monomer M4	62
3.3.5.	Synthesis of monomer M5	64
3.3.6.	Synthesis of monomer M6	66
3.4.	Synthesis and characterization of monomers M7-M10	68
3.4.1.	Synthesis of azo-benzothiazole dyes, 1w-1z	68
3.4.2.	Synthesis of 4-(6-hydroxyhexyloxy)benzoic acid (HHBA).....	68
3.4.3.	Synthesis of 4-(6-methacryloxyhexyloxy)benzoic acid (MHBA)	69
3.4.4.	Synthesis of monomer M7	71
3.4.5.	Synthesis of monomer M8	73
3.4.6.	Synthesis of monomer M9	74
3.4.7.	Synthesis of monomer M10	75
3.5.	Synthesis and characterization of SCLCPs	76
3.5.1.	Synthesis of polymers P1-P6	76
3.5.1.	Synthesis of polymers P7-P10	78
CHAPTER 4 : RESULTS AND DISCUSSION		79
4.1.	Synthesis and characterization of LC monomers	79
4.1.1.	Synthesis of LC monomers M1-M6.....	79
4.1.2.	Synthesis of LC monomers M7-M10.....	81
4.1.3.	Characterization of LC monomers	83

4.2.	Synthesis and characterization of SCLCPs	88
4.2.1.	Synthesis of SCLCPs	88
4.2.2.	Characterization of polymers P1-P6	89
4.2.3.	Characterization of polymers P7-P10	91
4.3.	Thermal properties of LC monomers and their SCLCPs	91
4.3.1.	Thermal properties of LC monomers M1-M10	92
4.3.2.	Thermal properties of SCLCPs P1-P10	96
4.4.	Mesomorphic behaviour of monomers	100
4.4.1.	Mesomorphic behaviour of monomers M1-M6	100
4.4.2.	The effect of terminal substituents on mesophase behaviours of M1-M6 109	
4.4.3.	Mesomorphic behaviours of LC monomers M7-M10	112
4.4.4.	The effect of terminal substituent and mesogen length on mesomorphic behaviour of M7-M10	114
4.5.	Mesomorphic behaviour of SCLCPs	116
4.5.1.	Mesomorphic behaviour of polymers P1-P6	116
4.5.2.	Mesomorphic behaviour of polymers P7-P10	121
4.6.	Optical properties of SCLCPs	122
4.6.1.	Optical properties of polymers P1-P6	122
4.6.2.	Optical properties of polymers P7-P10	126
4.7.	Electrochemical properties of SCLCPs, P1-P10	128
4.8.	Rheology of SCLCPs P1, P3 and P4	132
4.8.1.	The strain sweep behaviour of polymer P1	133
4.8.2.	The linear viscoelastic response of smectic polymer P1	135
4.8.3.	The strain amplitude sweep behaviour of polymer P3	139
4.8.4.	The linear dynamic viscoelasticity of polymer P3	140
4.8.5.	The linear dynamic viscoelasticity of polymer P4	142
CHAPTER 5 : CONCLUSIONS.....		146
5.1.	Conclusions	146

5.2. Suggestions for further research.....	148
REFERENCES	150
APPENDICES	170

LIST OF FIGURES

Figure 1.1: The schematic representation of (a) crystalline solid, (b) liquid crystal and (c) isotropic liquid [2]	1
Figure 1.2: Structure of the first liquid crystalline compound, cholesteryl benzoate	2
Figure 1.3: Structure and phase transition of 4-pentyl-4'-cyanobiphenyl (5CB).....	2
Figure 2.1: General structural template of calamitic liquid crystals [60]	6
Figure 2.2: Schematic representation of molecular order in (a) nematic and (b) isotropic phases [67]	8
Figure 2.3: Schematic representation of molecular order in Smectic A and Smectic C phases [70]	9
Figure 2.4: Schematic representation of (a) MCLCPs and (b) SCLCPs [65].....	10
Figure 2.5: <i>Trans-cis</i> (E-Z) photoisomerization of azobenzene.....	11
Figure 2.6: Azo mesogen containing LC compounds	12
Figure 2.7: Azobenzene containing nonsymmetrical LC compounds	12
Figure 2.8: Photoresponsive LC compounds containing azobenzene chromophore	13
Figure 2.9: Structures of nonsymmetric dimers D4, D5, D6 and D12	13
Figure 2.10: Structure of benzothiazole azocalix[4]arene, BTC4 [52].....	16
Figure 2.11: Chemical structures of azo-benzothiazole derivatives 2, 4, 5 and 6.....	17
Figure 2.12: Structures of 4-methylthiazole derivatives, 1a-1e	18
Figure 2.13: Structures of series 7, 8, 9 and 10 compounds	19
Figure 2.14: General structure of azobenzene derivatives containing pyridine moiety .	19
Figure 2.15: Structures of 2,5-disubstituted thiophene compounds.....	20
Figure 2.16: Structure of conductive liquid crystalline compounds 6	21
Figure 2.17: Structure of 2-pyrazoline derivatives, 2, 3, 4, 5, 6 and 7.....	21
Figure 2.18: Structure of thiazole moiety based LC compounds (series A and series B)	22
Figure 2.19: Azomethine linked benzothiazole moiety based LC compounds [119-121]	23
Figure 2.20: Structure of benzothiazole mesogen based LC compounds, nEBTHDZ ...	24
Figure 2.21 : Azo-benzothiazole moiety based LC compounds [118]	25
Figure 2.22: Structure of azomethines BTA1 and BTA2 with benzothiazole core	25
Figure 2.23: Chemical structure of compounds 3a, 3b, 3c, 3d and 3e.....	26
Figure 2.24: Structure of calamitic liquid crystalline compounds, nBPEP	26
Figure 2.25: Structure of compounds, series E and series F.....	27

Figure 2.26: Benzothiazole moiety based donor-acceptor type LC materials a and b...	28
Figure 2.27: Azomethines BTA1 and BTA2 with benzothiazole core	29
Figure 2.28: Molecular structure of BBPA, BBNA, and BPNA.....	30
Figure 2.29: Chemical structure of PIB, F-N-Me, F-N,N-Me and O-FEt-PIB	31
Figure 2.30: Structure of benzothiazole derivatives PP-BT-1 and PP-BT-2 for optical imaging of β A in AD.....	32
Figure 2.31: Chemical structure of azo-chromophore containing polymers pDRSAM, pDRASM, pDR1M and pBTAMC.....	35
Figure 2.32: Molecular structure of polymer pBAMA	35
Figure 2.33: Chemical structure of P-2AT, P-2ABT and P-EtO-2ABT.....	36
Figure 2.34: Chemical structure of SCLCPs, pXMAN	37
Figure 2.35: Structure of polymers Pn-F and Pn-C.....	38
Figure 2.36: Chemical structures of SCLCPs, C _n MeO	39
Figure 2.37: Structure of side chain liquid crystalline polymers P _x	39
Figure 2.38: Structure of SCLCPs having azobenzene chromophore with donor-acceptor groups.....	40
Figure 2.39: Structure of SCLCPs PAMeAPr, PMADe and PMAM	41
Figure 2.40: Structure of SCLCP which was adopted from [180]	42
Figure 2.41: Polymer structure adopted from [182].....	43
Figure 2.42: Structure of norbornene based SCLCPs	44
Figure 2.43: Structure of SCLCP, PI-14-5CN and MCLCP, PSHQ9.....	45
Figure 2.44: Structure of SCLCP, PI-nCN	46
Figure 2.45: Structure of SCLCP, PBSiCB5	47
Figure 3.1: ¹ H NMR spectrum of monomer M1	57
Figure 3.2: ¹ H NMR spectrum of monomer M2	59
Figure 3.3: ¹ H NMR spectrum of monomer M3	61
Figure 3.4: ¹ H NMR spectrum of monomer M4	63
Figure 3.5: ¹ H NMR spectrum of monomer M5	65
Figure 3.6: ¹ H NMR spectrum of monomer M6	67
Figure 3.7: ¹ H NMR spectrum of monomer M7	72
Figure 3.8: ¹ H NMR spectrum of monomer M8	73
Figure 3.9: ¹ H NMR spectrum of monomer M9	74
Figure 3.10: ¹ H NMR spectrum of monomer M10	76
Figure 3.11: FT-IR spectrum of polymer P1	77
Figure 3.12: ¹ H NMR spectrum of polymer P1.....	78

Figure 4.1: Representative FT-IR spectrum of monomer M1	83
Figure 4.2: Representative ¹ H NMR spectrum of monomer M1	86
Figure 4.3: Representative ¹³ C spectrum of monomer M1	86
Figure 4.4: FT-IR spectra of monomer M1 and polymer P1	90
Figure 4.5: ¹ H NMR spectra of (a) monomer M1 and (b) polymer P1	90
Figure 4.6: TG curves of LC monomers M1-M6	92
Figure 4.7: DTG curves of LC monomers M1-M6	93
Figure 4.8: TG curves of LC monomers M7-M10	95
Figure 4.9: DTG traces of LC monomers M7-M10	95
Figure 4.10: TG traces of polymers P1-P6	96
Figure 4.11: DTG curves of polymers P1-P6	97
Figure 4.12: TG curves of polymers P7-P10	99
Figure 4.13: DTG traces of polymers P7-P10	99
Figure 4.14: DSC thermograms of M1 on heating and cooling at 5°C/min	101
Figure 4.15: POM images of M1 (a) smectic phase emerged as bâtonnet at 90.3°C upon cooling from isotropic liquid; (b) fan-shaped smectic A phase at 89.5°C (magnification: 50×)	101
Figure 4.16: DSC thermograms of M2 on heating and cooling at 5°C/min	102
Figure 4.17: POM images of M2: (a) nematic phase at 112.0°C; (b) smectic A phase at 101.5°C (magnification: 50×)	102
Figure 4.18: DSC thermograms of M3 on heating and cooling at 5°C/min	103
Figure 4.19: POM images of M3: (a) nematic phase at 105.8°C; (b) smectic C phase at 76.5°C (magnification: 50×)	103
Figure 4.20: DSC thermograms of M4 on heating and cooling at 5°C/min	104
Figure 4.21: POM images of M4: (a) nematic phase at 109.8°C; (b) smectic A phase at 75.5°C (magnification: 50×)	104
Figure 4.22: DSC thermograms of M5 on heating and cooling at 10°C/min	105
Figure 4.23: POM images of M5: (a) smectic phase emerged as bâtonnet at 125.8°C upon cooling from isotropic liquid; (b) fan-shaped smectic A phase at 124.5°C (magnification: 50×)	105
Figure 4.24: DSC thermogram of M6 on heating and cooling at 10°C/min	106
Figure 4.25: POM images of M6 (a) smectic phase emerged as bâtonnet at 134.5°C upon cooling from isotropic liquid; (b) fan-shaped smectic A phase at 133.5°C (magnification: 50×)	106
Figure 4.26: SAXS patterns of M1- M4 at 80°C, 95°C, 67°C and 65°C respectively .	107

Figure 4.27: Molecular structures and molecular lengths of M1-M4. The molecular lengths of the studied compounds were calculated from the most extended conformation with optimized energy level by simple molecular modelling (ChemBio3D Ultra 11.0).	108
Figure 4.28: DSC traces of monomers M7-M10 on first heating scan at 10°C/min....	112
Figure 4.29: POM images of compounds M7- M10: (a) & (b) M7 displays schlieren texture of nematic phase at 196.8°C and smectic C phase at 140.5°C; (c) M8 shows nematic phase at 225.5°C; (d) M9 exhibits nematic phase at 229.4°C (e) M10 reveals nematic (threaded) phase at 226.5°C (magnification: 50×)	113
Figure 4.30: DSC curves of P1-P4 on (a) second heating scan rate at 20°C and (b) first cooling scan at 10°C/min	117
Figure 4.31: DSC traces of P5 and P6 on heating at 20°C/min and cooling at 10°C/min	119
Figure 4.32: POM images of P1- P6: (a) P1 exhibits smectic phase at 164.8°C; (b) P2 shows nematic phase at 179.8°C; (c) P3 displays nematic phase at 180.2°C; (d) P4 reveals nematic phase at 169.9°C; (e) P5 exhibits smectic phase at 209.5°C and (f) P6 shows smectic phase at 233.8°C (magnification: 50×)	120
Figure 4.33: DSC traces of polymers P7-P10 under heating scan at 20°C/min	121
Figure 4.34: POM images of polymers P7- P10: (a) P7 shows nematic phase at 200.5°C; (b) P8 exhibits nematic phase at 210.8°C; (c) P9 displays nematic phase at 220.4°C; (d) P10 reveals nematic phase at 215.6°C (magnification: 50×)	122
Figure 4.35: UV-vis spectra of P1-P6 in dilute CHCl ₃ solutions (1×10 ⁻⁶ M).....	123
Figure 4.36: PL spectra of P1-P6 in dilute CHCl ₃ solutions (1×10 ⁻⁶ M).....	125
Figure 4.37: UV-vis absorption spectra of P7-P10 in dilute CHCl ₃ solutions (1×10 ⁻⁶ M)	126
Figure 4.38: PL spectra of P7-P10 in dilute CHCl ₃ solutions (1×10 ⁻⁶ M).....	127
Figure 4.39: PL spectrum of standard compound pyrene in dilute CHCl ₃ solutions (1×10 ⁻⁶ M).....	128
Figure 4.40: Cyclic voltammograms of P4 in CHCl ₃ with 0.1M tetrabutylammonium perchlorate (Bu ₄ NClO ₄) as supporting electrolyte. Inset figure shows CV of ferrocene, run under identical condition as P4	130
Figure 4.41: Cyclic voltammogram of P7 in CHCl ₃ with 0.1M tetrabutylammonium perchlorate (Bu ₄ NClO ₄) as supporting electrolyte. Inset figure shows CV of ferrocene run under identical condition as P7	131

Figure 4.42: Storage (G') modulus and loss modulus (G'') vs strain amplitude sweep at a constant frequency 10 rad/s for polymer P1 at 182°C	133
Figure 4.43: Steady shear viscosity (η) as a function of shear rate ($\dot{\gamma}$) for polymer P1 at indicated temperatures (°C)	134
Figure 4.44 : (a) Storage modulus (G') and (b) loss modulus (G'') as a function of frequency for polymer P1 at indicated temperatures (°C)	136
Figure 4.45: Complex viscosity ($ \eta^* $) as a function of frequency (ω) for P1 at indicated temperatures (°C).....	137
Figure 4.46: Storage modulus (G'), loss modulus (G'') and complex viscosity ($ \eta^* $) as a function of frequency (ω) for polymer P1 (a) at 182°C and (b) at 122°C.....	138
Figure 4.47: Storage (G') modulus and loss modulus (G'') vs strain amplitude sweep at a constant frequency 10 rad/s for polymer P3 at 190°C	139
Figure 4.48: (a) Storage modulus (G') and (b) loss modulus (G'') as a function of frequency for polymer P3 at indicated temperatures (°C)	141
Figure 4.49: Complex viscosity ($ \eta^* $) as a function of frequency (ω) for P3 at indicated temperatures (°C).....	142
Figure 4.50: (a) Storage modulus (G') and (b) loss modulus (G'') as a function of frequency for polymer P4 at indicated temperatures (°C)	143
Figure 4.51: Storage modulus (G'), loss modulus (G'') and complex viscosity ($ \eta^* $) as a function of frequency (ω) for polymer P4 at 115°C.....	144
Figure 4.52: Complex viscosity ($ \eta^* $) as a function of frequency (ω) for P4 at indicated temperatures (°C).....	145

LIST OF TABLES

Table 4.1: FT-IR absorption frequencies of monomers M1-M10.....	84
Table 4.2: ¹ H NMR chemical shifts of different type of protons present in monomers M1-M10	85
Table 4.3: ¹³ C NMR chemical shifts of different type of carbons present in monomers M1-M10	87
Table 4.4: Yields and GPC results of polymers P1-P10	88
Table 4.5: Thermal analysis data of LC monomers M1-M10	94
Table 4.6: Thermal analysis results of polymers P1-P10	98
Table 4.7: Scattering vector q (nm ⁻¹), layer spacing, d (nm), calculated molecular length, l (nm) and data collecting temperature (°C) of monomers M1-M4	109
Table 4.8: Mesophase lengths, phase transition temperatures and enthalpy changes for monomers M1- M6 upon heating and cooling scans.	110
Table 4.9: Mesophase lengths, phase transition temperatures and enthalpy changes for M7-M10 upon first heating scan.	115
Table 4.10: Phase transition temperatures and corresponding enthalpy changes of P1-P6 upon second heating and first cooling scans	118
Table 4.11: UV-vis and photoluminescence results of polymers P1-P10	124
Table 4.12: Cyclic voltammetric results of polymers P1 - P10.....	129

LIST OF ABBREVIATIONS AND SYMBOLS

ATR	Attenuated Total Reflectance
BPO	Benzoyl peroxide
CHCl ₃	Chloroform
CDCl ₃	Deuterated chloroform
DCC	<i>N, N'</i> -dicyclohexylcarbodiimide
DCM	Dichloromethane
DMAP	Dimethylaminopyridine
DMF	<i>N,N</i> -dimethylformamide
DMSO	Dimethyl sulfoxide
DMSO-d ₆	Deuterated dimethyl sulfoxide
DSC	Differential Scanning Calorimetry
FT-IR	Fourier Transform Infrared Spectroscopy
GPC	Gel Permeation Chromatography
LC	Liquid crystalline
MCLCP	Main chain liquid crystalline polymer
M_n	Number average molecular weight
M_w	Weight average molecular weight
NMR	Nuclear Magnetic Resonance Spectroscopy
PDI	Polydispersity index
POM	Polarized Optical Microscopy
SAXS	Small Angle X-ray Scattering
SCLCP	Side chain liquid crystalline polymer
T_d	Decomposition temperature

T_g	Glass transition temperature
TGA	Thermogravimetric analysis
THF	Tetrahydrofuran
G'	Storage modulus
G''	Loss modulus
ω	Frequency
η	Shear viscosity
$ \eta^* $	Complex viscosity
$\dot{\gamma}$	Shear rate

LIST OF APPENDICES

APPENDIX A : FT-IR spectra of monomers and polymers	170
APPENDIX B : ^1H NMR spectra of monomers and polymers	174
APPENDIX C : Cyclic voltammograms of polymers	179
APPENDIX D : Publications.....	181

CHAPTER 1 : INTRODUCTION

1.1. Introduction

Liquid crystals are compounds which show intermediate characteristic between crystalline solid and isotropic liquid. Liquid crystalline (LC) phases possess many properties correspond to liquid, e.g., they can still flow like liquid and can coalesce to droplets. On the other hand, they are similar to crystal as they exhibit anisotropy in their optical, mechanical, electrical, and magnetic properties. Materials that exhibit such unusual phases are often called mesogens (i.e., they are mesogenic) and the various phases in which they could exist are termed mesophases [1]. The schematic representation of crystalline solid, liquid crystal and isotropic liquid are depicted in Figure 1.1.

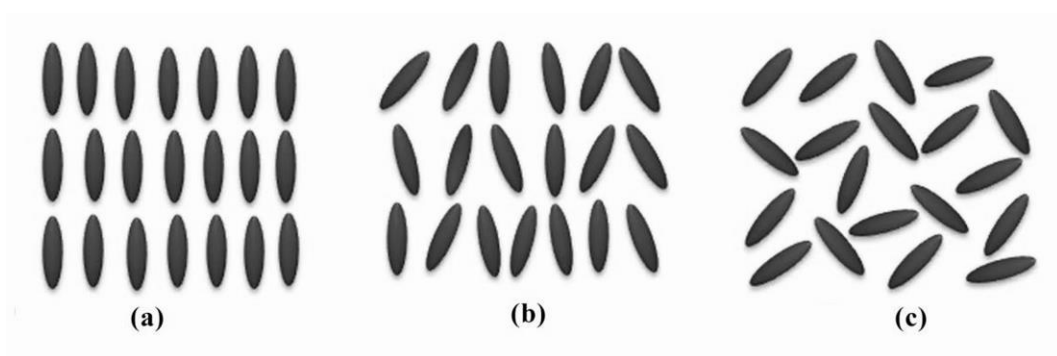


Figure 1.1: The schematic representation of (a) crystalline solid, (b) liquid crystal and (c) isotropic liquid [2]

The history of liquid crystals began in 1888 when an Austrian botanist, Friedrich Reinitzer observed ‘double melting’ behaviour of cholesteryl benzoate (Figure 1.2). Cholesteryl benzoate melted into a cloudy liquid at 145.5°C; as the temperature rose to 178.5°C, it suddenly became clear. He also observed some unusual colour behaviour upon cooling; a pale blue colour appeared as the clear liquid turned cloudy and followed by a bright blue-violet colour as the cloudy liquid crystallized [3]. A German physicist,

Otto Lehmann later made detailed observations using polarising optical microscope and named this state of matter as ‘liquid crystal’ [2]. Following this wonderful discoveries, scientists in the relevant fields turned their attention towards a growing number of compounds, which exhibited LC properties.

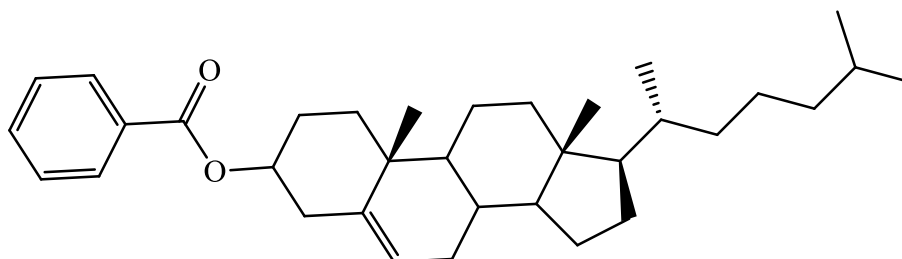


Figure 1.2: Structure of the first liquid crystalline compound, cholesteryl benzoate

In order to establish a relationship between molecular structure and the exhibition of LC properties, systematic modifications of the structures of mesogens were begun in 1973 when Gray et al. [4] reported the most technologically and commercially important class of LC compounds, 4-alkyl-4'-cyanobiphenyl (CB). The structure and phase transition of 4-pentyl-4'-cyanobiphenyl (5CB), an example of CB is illustrated in Figure 1.3.

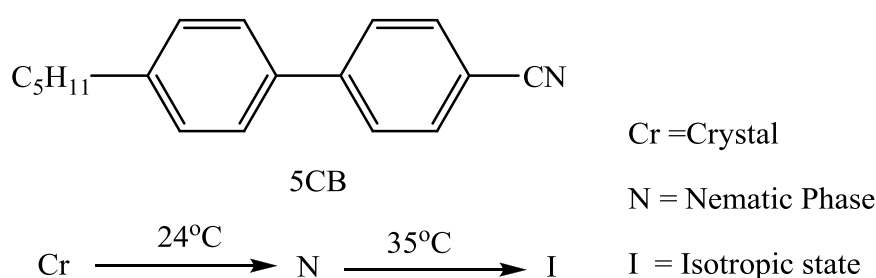


Figure 1.3: Structure and phase transition of 4-pentyl-4'-cyanobiphenyl (5CB)

These LC materials have still dominated electro-optical flat panel display devices, such as watches, clocks, stereos, calculators, personal organizers, laptop computers, portable notebooks computers, vehicle clocks, speedometers, navigation and positional aids, mobile phones, flat desktop monitors, wave plates, polarizers, notch filters, and so forth.

More recently, liquid crystals have been utilized in many new applications, such as medical displays, spectrometers, chemical and biological sensors, actuators, and so on [5, 6]. Over the last three decades, the quest of new LC materials has enormously increased due to their slim shape, low weight, low-voltage operation and low power consumption [7]. LC displays provide an interface between humans and machines and are expected to play an even bigger role in the future as the need of displaying information grows [8].

Side chain liquid crystalline polymers (SCLCPs) are a class of macromolecular compounds, which exhibit combined properties of low molar mass liquid crystals with mechanical properties of polymers. Over the last three decades, the work of Finkelmann et al. [9, 10] aroused substantial attention in the systematic synthesis and study of SCLCPs. A SCLCP comprises three structural components: a polymer backbone, a semi-rigid anisometric or mesogenic group and a flexible spacer. The flexible spacer in SCLCPs plays a vital role in determining the properties of polymers by decoupling the mesogenic side groups from the polymer backbone and renders the mesogenic unit into an order [11]. Consequently, SCLCPs exhibit electro-optic characteristics of low molar mass liquid crystalline materials combined with polymeric properties, such as glassy behaviour [12]. Due to the unique duality of properties, SCLCPs exhibit some improved properties such as high stability against humidity and/or various chemical substances, heat resistance, low flammability, low density, low product costs and the ability of spontaneous self-organization into liquid crystalline mesophases. These polymers find numerous applications as high-tensile strength fibres, self-strengthened materials, optoelectronic materials, reversible data storage devices, elastomeric products, thermal or barometric sensors, chromatographic separations, solid polymer electrolytes, separation membranes and display materials [13, 14].

Azo chromophore containing materials, either low molar mass or polymeric in nature, have attracted tremendous attention due to their unique optical, thermal and mechanical properties. The photoinduced *trans-cis* isomerization makes them potential in variety of applications, e.g., optical data storage devices [15-17], nonlinear optics [18-22], photo switching materials [23-30], liquid crystal display [31-34] and so on. The introduction of heterocyclic moiety, such as, benzothiazole unit into azo backbone, enhances some optoelectronic properties [35-38]. Theoretical and experimental studies have revealed that azo-benzothiazole chromophores possess large molecular hyperpolarizability [39, 40], indicating they are a good choice for the non-linear optical (NLO) materials. Moreover, benzothiazole incorporated molecules exhibit interesting photophysical properties, which make them possible candidate in organic light-emitting diodes [41-43], photovoltaic cell [44], memory devices [45-47], potential sensitizers for photodynamic therapy [48], fluorescent tracer for diseases diagnosis [49-51], chromogenic chemosensor for metal ions detection [52-54] and so forth. In addition, the introduction of benzothiazole unit in the mesogens of calamitic molecules has substantial influence on mesophase formation, the phase transition temperatures, dielectric constants and other properties of the mesogens [55]. As a result, a lot of attention has been paid on benzothiazole incorporated molecules to study their liquid crystalline behaviours as well as photophysical properties [56].

Scientific communities are devoted to prepare different devices with their prepared compounds. The most challenging task to fabricate a device is to achieve favourable alignment of molecules to enable efficient charge transport through the semiconducting medium [56]. However, LC materials can offer more ordered or closely packed structures, which are possible candidates to resolve the difficulties with providing highly ordered structure [57, 58]. In addition, SCLCPs may provide more ordered structure because flexible spacer decouples the mesogen from the polymer

backbone and renders the mesogenic unit into an order [11, 59]. Thus, azo-benzothiazole chromophore based SCLCPs may provide multifunctional materials with desirable properties. Until recently, very few reports have been published on azo-benzothiazole mesogen containing LC materials. Moreover, most of the published articles are focused mainly on varying terminal alkyl spacer length to establish structure-property relationship. In addition, azo-benzothiazole mesogen containing SCLCPs have not been studied and reported yet.

1.2. Research Objectives

As azo-heterocyclic moiety based materials exhibit improved optical, electrochemical and mechanical properties compared to their benzenoid analogues, azo-benzothiazole chromophore containing SCLCPs may exhibit excellent photophysical, electrochemical and mechanical properties. However, to fabricate multifunctional materials with desirable properties, azo-benzothiazole chromophore containing SCLCPs have not been studied and reported in the literature yet. Keeping these facts in mind, the objectives of this research are summarized as follows:

- To synthesize new polymerizable liquid crystalline monomers containing azo-benzothiazole chromophore
- To study the effect of terminal substituent and mesogen length on thermal and mesomorphic behaviours of monomers
- To synthesize new side chain liquid crystalline polymers from the prepared monomers by radical polymerization
- To study thermal, mesomorphic, optical, electrochemical and rheological properties of the synthesized SCLCPs

CHAPTER 2 : LITERATURE REVIEW

2.1. Fundamentals of Liquid Crystals

After discovery of the first LC compound (cholesteryl benzoate), the search for new LC materials has attracted tremendous attention over the last hundred and thirty years. Until recently, a great variety of new LC compounds have been synthesized and the molecular structure required to generate liquid crystal phase is well understood. In order to form a liquid crystal phase, a molecule is likely to be structurally anisotropic and often have to possess a permanent dipole as well as high polarizable anisotropy.

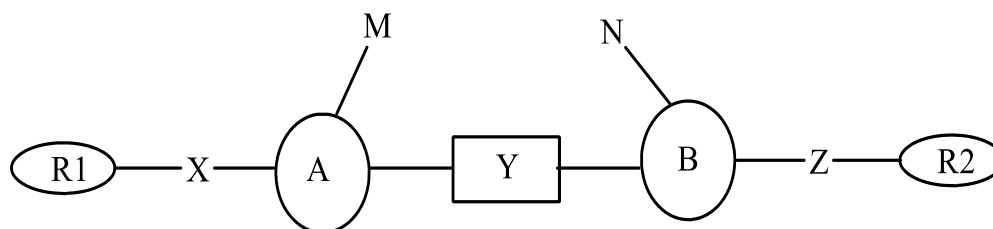


Figure 2.1: General structural template of calamitic liquid crystals [60]

Figure 2.1 shows a general structural template of rod-like rigid molecule, which is the most common feature of LC compounds and these molecules are also called calamitic liquid crystals. A and B are core units that are most frequently aromatic (e.g., 1,4-phenyl, 2,6-naphthyl, 2,5-pyrimidinyl, etc.) and can also be alicyclic (e.g., trans-1,4-cyclohexyl). Recently, heterocyclic compounds such as pyridine, thiophene, benzoxazole and benzothiazole have been used as a core unit [61-64]. To maintain linearity and polarizability anisotropy of the core, the rings can be directly linked or may be joined by a linking group Y, which can be stilbene (-CH=CH-), ester (-COO-), imine (-CH=N-), azo (-N=N-) and acetylene (-C≡C-) groups. The rigid cores themselves are usually not sufficient to generate liquid crystal phases. Flexible terminal groups (R1 and R2) are often introduced to the rigid cores directly or through linking groups X and Z in order to lower the melting point and stabilize the molecular

alignment in the liquid crystal phase. Alkyl (C_nH_{2n+1}) or alkoxy ($C_nH_{2n+1}O$) chains are the most frequently used terminal groups. Both flexibility and rigidity must be in balance in order to exhibit LC properties [65]. M and N are small lateral substituents (e.g., -F, -Cl, -CH₃, -CN, etc.) that are often used to modify the mesophase type and physical properties. Lateral substituents can disrupt the molecular packing, yet are often advantageous for the formation of liquid crystal phases [3].

Types of liquid crystals

A proper molecular design is necessary for a material to exhibit liquid crystalline properties. A large number of new LC compounds have been developed and these materials show quite different LC properties. LC materials are generally classified into two main categories, the thermotropic and the lyotropic liquid crystals. Thermotropic liquid crystals consist of only mesogenic molecules and the mesophase formation is temperature dependent. On the other hand, lyotropic liquid crystals contain mesogenic unit and solvent molecules as well. The mesophase transitions occur in lyotropic liquid crystals as a function of concentration and temperature. Some mesogens may exhibit both lyotropic and thermotropic phases; these materials are named amphotropic. As this thesis is mainly focused on thermotropic LC materials, discussion on lyotropic liquid crystals will not be addressed further.

Thermotropic LC materials can further be divided into two groups: (i) low molar mass liquid crystal and (ii) high molar mass liquid crystal (i.e., liquid crystalline polymers). Low molar mass thermotropic LC materials are generally further distinguished with respect to the molecular shape of the constituent molecules, being called calamitic for rod-like, discotic for disk-like, and sennidic for brick- or lath-like molecules. Depending on the types of mesophase, calamitic LC materials can be categorized into nematic and smectic phases [66].

Nematic phase

The nematic (N) phase is the simplest liquid crystal phase. This is the least ordered mesophase (closest to the isotropic liquid state) and it is usually very easy to identify by optical polarizing microscopy. In this phase the molecules have long-range orientational order and short-range positional order, where the centers of gravity of the mesogens are isotropically distributed. In the nematic phase all molecules are aligned approximately parallel to each other. In each point a unit vector \hat{n} can be defined, parallel to the average direction of the long axis of the molecules in the immediate neighborhood (Figure 2.2).

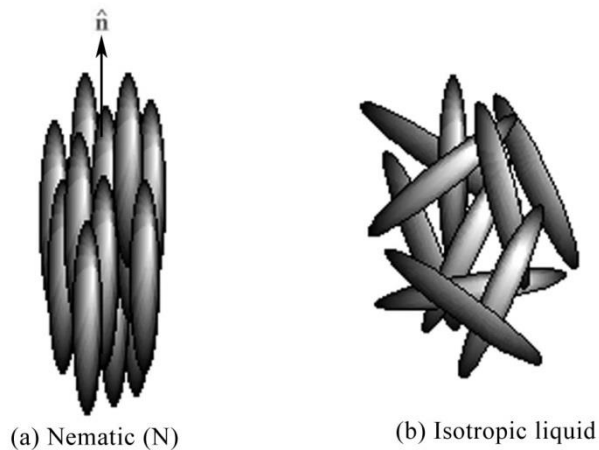


Figure 2.2: Schematic representation of molecular order in (a) nematic and (b) isotropic phases [67]

Smectic phase

The smectic phases usually appear at lower temperatures than the nematic phases and have some positional order along with orientational order. In the smectic phases, the centers of gravity of the molecules are arranged in layers in which they can flow and this mesophase shows more solid-like properties than nematic phase. This type of properties is due to the strong lateral forces and weak interlayer attractions between the molecules which allow the layers to slide over one another easily [1]. There are a

number of different categories of smectic phases amongst which the best known are the smectic A (SmA) and smectic C (SmC) phases. If the long axis of the molecules are parallel to the layer normal N (Figure 2.3a), the mesophase is called SmA, if the director \hat{n} is tilted in a certain θ angle with respect to the layer normal N (Figure 2.3b), the mesophase is called SmC. The tilt is caused by dipole-induced intermolecular interactions [68]. Both SmA and SmC phases have unstructured layers and they possess one-dimensional (1D) layer periodicity [69].

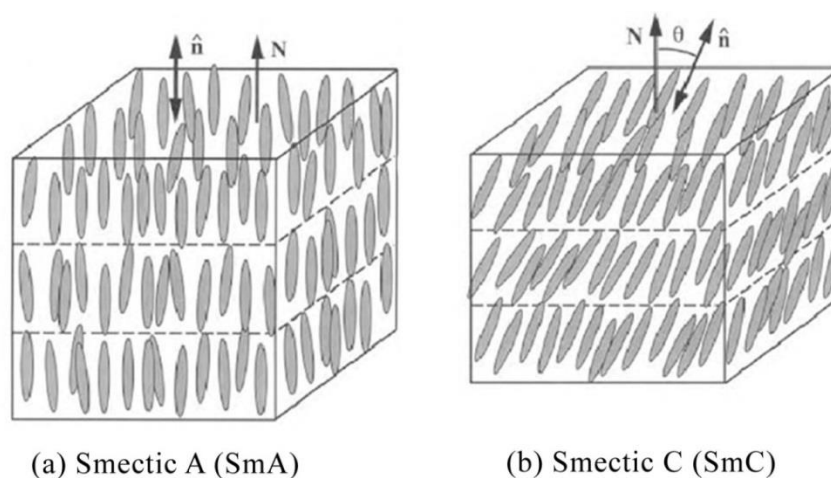


Figure 2.3: Schematic representation of molecular order in Smectic A and Smectic C phases [70]

Liquid crystalline polymers

Liquid crystalline polymers (LCPs) are a kind of macromolecular compounds, which combine the properties of polymers with those of liquid crystals. These systems show the anisotropic optical, electrical and mechanical characteristics of the liquid crystals and at the same time, demonstrate many useful and versatile properties of polymers. In order to observe liquid crystallinity, a polymer generally requires the presence of rigid mesogenic groups and sufficient conformational freedom to allow the mesogenic units to form stacks or organized domains. Based on the location of the rigid low molar mass mesogens relative to the polymer backbone, LCPs can be divided into

two categories: (i) main chain liquid crystalline polymers (MCLCPs) and (ii) side chain liquid crystalline polymers (SCLCPs). In MCLCPs (Figure 2.4a) mesogenic units are structural moieties with sufficient rigidity and are mostly in the shape of straight rods. On the other hand, in SCLCPs (Figure 2.4b) mesogenic units are connected to the main chain (backbone) of polymer by side on attachment and SCLCPs are the focus of this study.

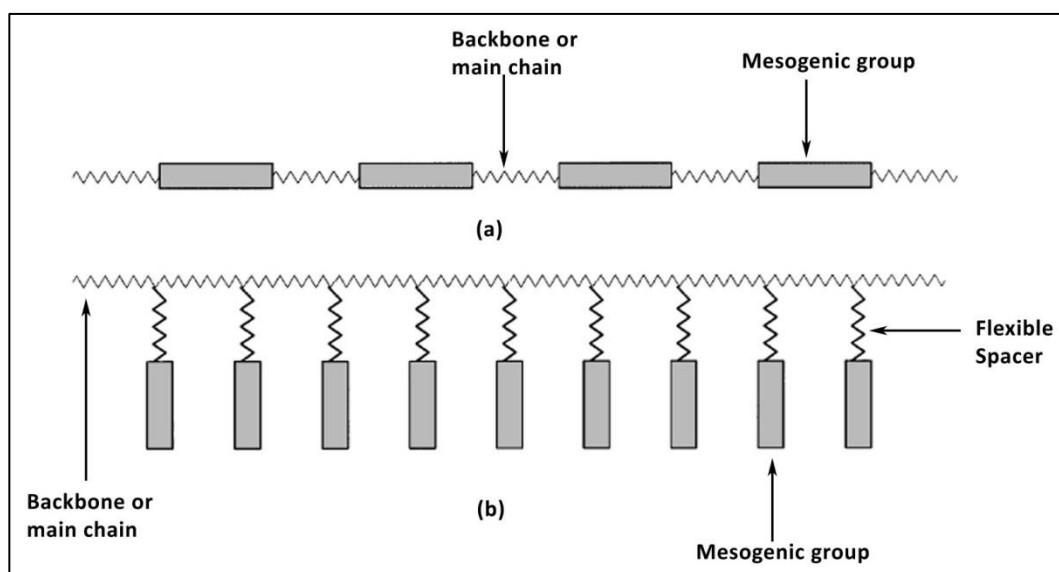


Figure 2.4: Schematic representation of (a) MCLCPs and (b) SCLCPs [65]

SCLCPs generally consist of three structural components: polymer backbone, mesogenic groups and flexible spacer. The flexible spacer plays a critical role in determining the properties of the polymer by decoupling the opposing tendency of the liquid crystal groups to self-assemble from that of the polymer backbones to adopt random coil conformations [12].

2.2. Azo-chromophore containing materials

Azobenzene is a broad class of azo aromatic compounds in which the azo linkage ($-N=N-$) bridges two phenyl rings. A large number of azo compounds can be prepared by substituting the aromatic rings with various substituents to change the

geometry and the electron donating/withdrawing character. Because of the rod-like rigid structure and anisotropic nature of molecular core, azo compounds can generate ideal liquid crystal mesogens with appropriate ring substitution [71]. Azo-chromophore containing materials either low molecular weight or polymeric in nature, are versatile and promising class of molecules due to their unique electrical, optical and mechanical properties. The most startling and intriguing property of all azobenzenes (and their derivatives) is the efficient and fully reversible photoisomerization which occurs upon absorption of a photon (Figure 2.5).

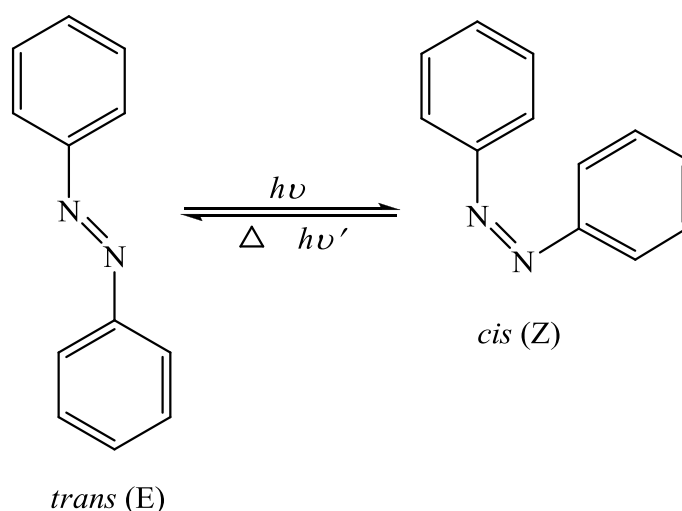
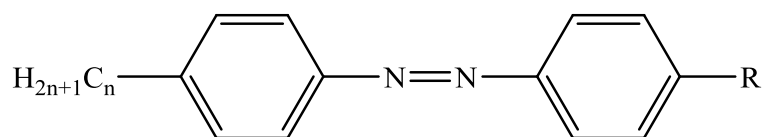


Figure 2.5: *Trans-cis* (E-Z) photoisomerization of azobenzene

The photochemical properties of azo compounds make them potential in variety of optical and optoelectronic applications such as, optical data storage [15-17], nonlinear optical devices [18-22], photo switching materials [23-30], LC display devices [31-34] and so forth.

Over the last several decades, much effort has been devoted to the synthesis and properties due to the robust and versatile moieties of azo compounds. The choice of linking groups in LC compounds is very crucial for overall molecular length as well as polarisable anisotropy which may improve the stability of the compounds and the

temperature range of the mesophase [60]. In addition, a suitable molecular design could allow achieving an anticipated mesophase as well as multifunctional material. Many mesogenic compounds containing azo central linkage have been studied as most of them exhibit LC properties above room temperature.



R = alkyloxy ($C_mH_{2m+1}-O-$) or acyloxy ($C_mH_{2m+1}-COO-$)

Figure 2.6: Azo mesogen containing LC compounds

The design of wide variety of LC compounds bearing azo chromophore in the central linkage is a feasible task for modern chemistry using new advanced techniques in the field of organic synthesis. In 1971 Steinstrasser and Pohl published their first substantial work on ‘an interesting new class of nematic LC compounds having azobenzene moiety’. They synthesized 43 azo compounds with varying terminal alkyl substituents in one end and alkyloxy/ acyloxy terminal on the other end (Figure 2.6). Among the 43 LC compounds, many of them exhibited enantiotropic nematic phase and melting points of some of them were near to room temperature. Kelker [72] and Murase [73] also synthesized series of analogous nematic LC compounds bearing azo mesogen.

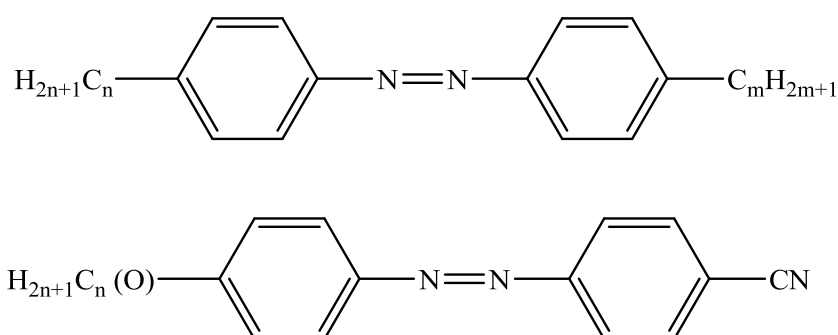
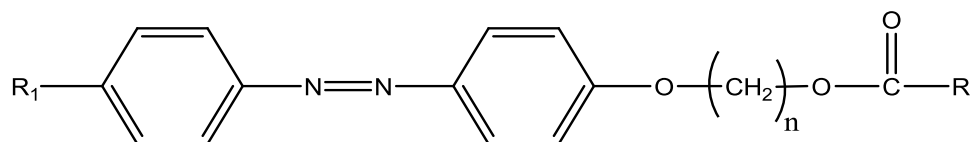


Figure 2.7: Azobenzene containing nonsymmetrical LC compounds

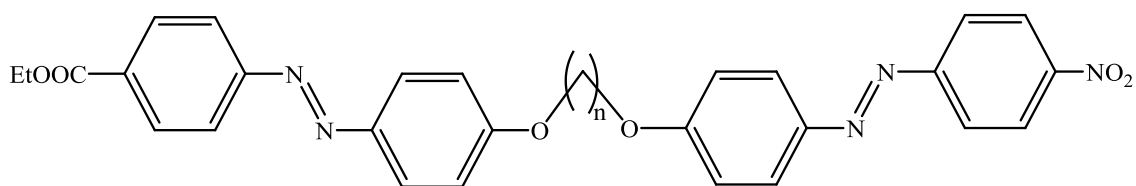
Hrozhyk et al. [74] synthesized two nonsymmetrical compounds, viz. 4,4'-di-n-alkyl azobenzenes and 4-n-alkyl(alkoxy)-4'-cyanoazobenzenes (Figure 2.7) and studied the LC properties of the prepared compounds.



R1 = NO₂ or OCH₃; R = Cholesteryl

Figure 2.8: Photoresponsive LC compounds containing azobenzene chromophore

In their finding, they revealed that the inclusion of two different alkyl groups into the azobenzene molecule drastically changed the mesogenic properties compared to the arrangement of alkyl-alkoxy substituents or combination of two symmetrical alkyl substituents. On the other hand, the inclusion of alkoxy or alkyl chains in the para-position of 4-cyanoazobenzene led to compounds with high melting points. Yang et al. [75] synthesized a series of photoresponsive azobenzene containing chromophores end-capped with cholesteryl group (Figure 2.8). They investigated the effect of terminal groups and spacer length on mesomorphic properties and photoreactivity of the photochromic compounds.



D4 : n = 4 D6 : n = 6

D5 : n = 5 D12 : n = 12

Figure 2.9: Structures of nonsymmetric dimers D4, D5, D6 and D12

Compounds with long methylene segments exhibited cholesteric LC mesophase while compound with electron withdrawing nitro group in the terminal position increased Z to E isomerization rates in darkness. Rahman et al. [76] synthesized a series of nonsymmetric dimers (D4, D5, D6 and D12) containing azobenzene mesogen (Figure 2.9) and investigated their LC properties with respect to the various length of alkyl chain. Compound D4 displayed only crystalline phase whereas compounds D5, D6 and D12 showed both nematic and smectic LC phases. Al-Hamdani [77] reported a homologous series of thioalkyl terminated mesogenic azobenzene compounds and found that the mesomorphic properties of the studied compounds are influenced by the length of thioalkyl chains.

In recent years, azo-chromophore containing liquid crystalline polymers (LCPs) have aroused substantial research interest because of their multifunctional properties. LCPs exhibit a unique duality of properties and show the electro-optic characteristics of low molar mass liquid crystals together with macromolecular properties such as glassy behaviour and mechanical integrity [78]. Moreover, azobenzene containing polymers are of great interest because azo chromophores can undergo reversible *trans-cis* photoisomerization which can be utilised to modification of phase behaviour and alignment [79-82]. *Trans*-azobenzene moieties possess rod like structure which exhibit liquid crystallinity, while the bent *cis*-azobenzene moieties do not show mesomorphic behaviour and act as impurities. As a result, the *trans-cis* photoisomerization of azobenzene may lower the nematic-isotropic phase transition temperature and can induce a nematic-isotropic phase transition at the given temperature [83]. Besides the unique photomechanical effect, azobenzene moiety based LC polymers have also been explored for various important applications such as, self-assembly [84-89], surface relief gratings [90-95] and energy transfer [96-99].

2.3. Azo-benzothiazole moiety based compounds

Azo aromatic dyes are the most diverse group of synthetic organic dyes which have been used as colorants in textile fibres, plastics, leather, paper and bio-medical studies. In recent years, heteroaromatic azo dyes, have gained great importance due to their better tinctorial strength, brightness, washing and sublimation fastness, and chromophoric strength in comparison with corresponding azo aromatic analogues. Moreover, the replacement of an aromatic diazo component with a heteroaromatic system is interesting from the toxicological point of view [100]. Heteroaromatic azo dyes, e.g., benzothiazole moiety based disperse dyes, have received substantial research attention and considered to be the first example of a successful commercial exploitation of heterocyclic amines with the use of 2-aminobenzothiazole nucleus as diazonium component in the production of red dyes [101]. The ever increasing interest of azo benzothiazole dyes as disperse and cationic dyes in the textile applications is due to their low-cost, brightness, and dyeing performance. In addition, azo benzothiazole moiety based dyes are of great importance as they show bathochromic absorptions compared to their corresponding benzenoid analogues and these dyes are considered to be environmental friendly [102]. Besides their usage as new functional dyes, the emerging applications of azo benzothiazole compounds have recently been reported in biological-medical studies, potential sensitizers for photodynamic therapy (PDT), optical data storage, non-linear optics and liquid crystal displays (LCDs) [19, 48, 103-105].

Very recently, azo-benzothiazole compounds have been investigated for detecting various toxic metal ions in the water and environment. Bingol et al. [52] synthesized benzothiazole azocalix[4]arene, **BTC4** (Figure 2.10) as chromogenic chemosensor and investigated its binding and sensing properties with heavy metal ions (Pb^{2+} , Hg^{2+} , Ni^{2+} ,

Cd^{2+} , Cu^{2+} , Zn^{2+} , Co^{2+} , Fe^{2+} , Mn^{2+} , Cr^{3+} , Ag^+) by UV–vis spectroscopy and voltammetric techniques.

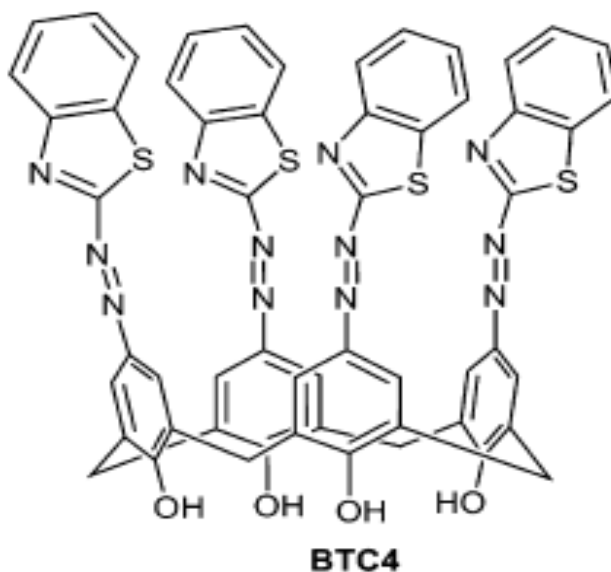


Figure 2.10: Structure of benzothiazole azocalix[4]arene, **BTC4** [52]

The colorimetric sensing ability of **BTC4** for heavy metal ions (Pb^{2+} , Hg^{2+} , Ni^{2+} , Cd^{2+} , Cu^{2+} , Zn^{2+} , Co^{2+} , Fe^{2+} , Mn^{2+} , Cr^{3+} , Ag^+) in DMF was monitored by naked eye (visual) and UV–vis absorption (optical) methods. The solution of **BTC4** showed dramatic changes in colour from light orange to reddish in the presence of Hg^{2+} while other metals did not result in appreciable change in colour. Finally, they concluded that the chromogenic chemosensor (**BTC4**) exhibited high selectivity towards Hg^{2+} ion over the other heavy metal ions investigated by spectroscopy and voltammetric technique. Misra and Shahid [53] synthesized some azo-benzothiazole chromophore based receptors, **2**, **4**, **5** and **6** (Figure 2.11) via azo coupling reaction. They investigated chromo and fluorogenic properties of their prepared compounds to recognise different metal ions of varying solvents by enhanced fluorescence. The detailed optical investigation revealed that the nitro substituted azo derivative, **2**, exhibited promising optical behaviour in the absence as well as in the presence of different transition metal ions in aqueous-acetonitrile solution.

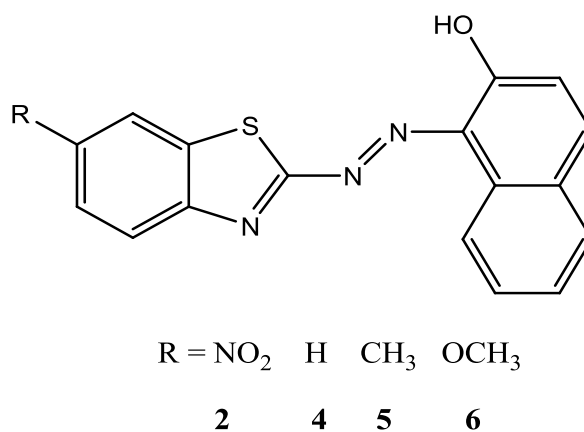


Figure 2.11: Chemical structures of azo-benzothiazole derivatives **2**, **4**, **5** and **6**

They concluded that the receptor **2**, upon interaction with Hg^{2+} ion, exhibited significant change in both absorption and fluorescence spectra making recognition of Hg^{2+} ion by naked-eye easy.

2.4. Liquid crystalline compounds bearing heterocyclic moiety

The mesomorphic behaviour of an organic compound is basically dependent on its molecular architecture in which a slight change in the molecular geometry brings about considerable change in its mesomorphic properties. The introduction of heterocyclic ring in the mesogens of calamitic molecules has substantial influence on mesophase formation, the phase transition temperatures, dielectric constants and other properties of the mesogens [55]. In addition, the incorporation of heterocyclic core in the thermotropic LC leads to the increase in molecular dipole and dielectric anisotropy thereby producing the molecular level polar organizations through generating electrostatic and molecular shape dependent interactions between the molecules [106, 107].

Over the past few decades, thermotropic LC compounds having heterocyclic core in the mesogen have received overwhelming research attention due to their unique properties [108]. A great variety of LC compounds with benzenoid structure have been

reported in the literature, but heterocyclic moieties containing LC compounds have been less explored [109]. However, a significant number of articles on LC materials containing heterocyclic moieties have been found in the literature in the recent years. Dorota et al. [61] synthesized a series of structurally related compounds having pyridine, oxidopyridinium, thienyl and furyl moieties in the mesogen and investigated the mesogenic properties of the prepared compounds. Their study revealed that the six-membered heterocyclic compounds with achiral as well as chiral ester chains generally melt higher than the corresponding phenyl analogues and the clearing temperatures were also lowered. On the other hand, for the series with five-membered heterocycles, both the clearing and melting temperatures were decreased. Comparison of the properties of chiral pyridyl and thienyl compounds with their phenyl analogues showed that the presence of a heteroatom significantly influenced the magnitude of spontaneous polarisation and the length of the helical pitch.

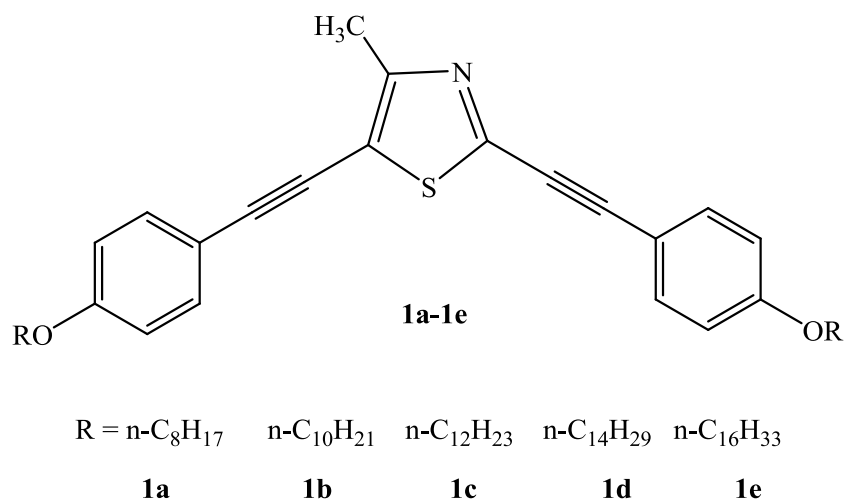


Figure 2.12: Structures of 4-methylthiazole derivatives, **1a-1e**

Lee and Yamamoto [110] synthesized 4-methylthiazole derivatives, **1a-1e** (Figure 2.12) having long alkoxy groups with bent-rod structure by palladium-catalyzed cross-coupling reaction. Their investigation revealed that all the prepared compounds exhibited nematic liquid crystal phase. Parra et al. [111] synthesized azomethine linked

LC compounds containing five-membered 1,3,4-thiadiazole (series **7**, **9**) and 1,3,4-oxadiazole (series **8**, **10**) rings in the mesogen (Figure 2.13).

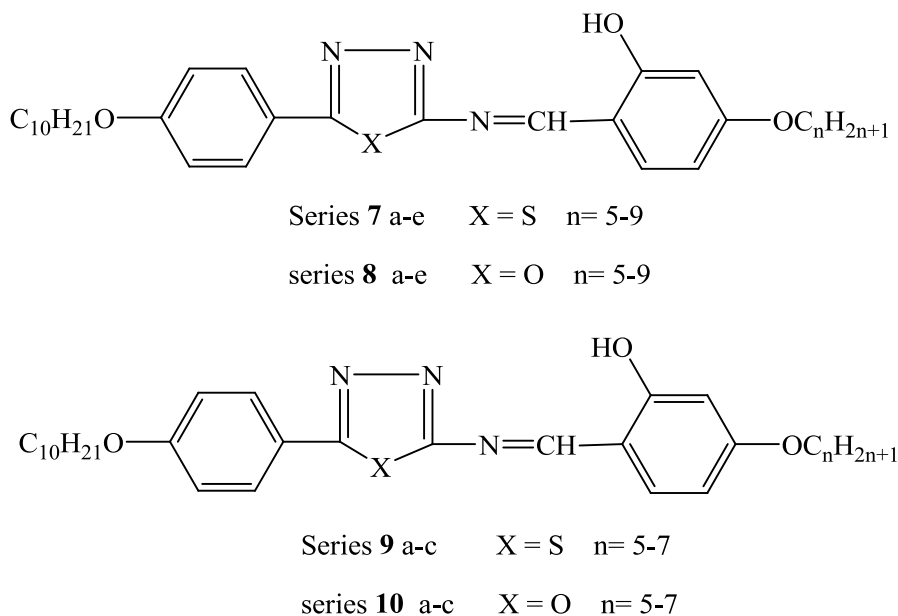


Figure 2.13: Structures of series **7**, **8**, **9** and **10** compounds

They studied the effect of the heterocyclic ring and the position of the lateral alkoxy group on the LC properties of the prepared compounds. They recognized that all the compounds of series **7** exhibited an enantiotropic smectic C phase while no LC properties were observed for the compounds of series **8–10**. Dave and Menon [112] synthesized twelve azobenzene derivatives containing pyridine moiety (Figure 2.14) and investigated the effect of variation of terminal group on the mesomorphic characteristics.

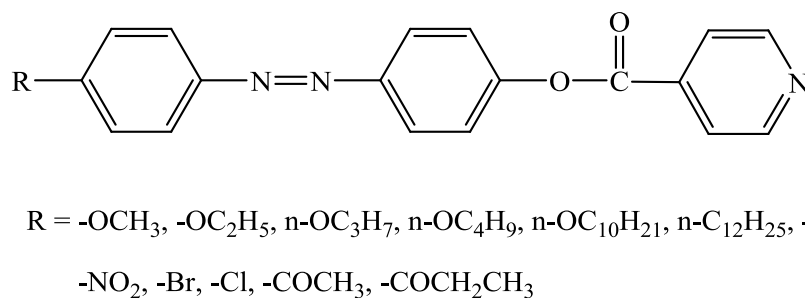


Figure 2.14: General structure of azobenzene derivatives containing pyridine moiety

The lower n-alkoxy derivatives i.e. from methoxy to n-butoxy members were found to show nematic phase while higher n-alkoxy derivatives viz. n-decyloxy and n-dodecyloxy, exhibited an additional smectic C phase along with nematic mesophase. Compounds with $-\text{CH}_3$, $-\text{NO}_2$, $-\text{Cl}$ and $-\text{Br}$ end groups were also noticed to exhibit only nematic phases whereas those with more polarisable terminal groups like $-\text{COCH}_3$ and $-\text{COCH}_2\text{CH}_3$, exhibited nematic as well as smectic A mesophases. Wu et al. [62] synthesized and characterized six series of 2,5-disubstituted thiophene containing LC materials (Figure 2.15).

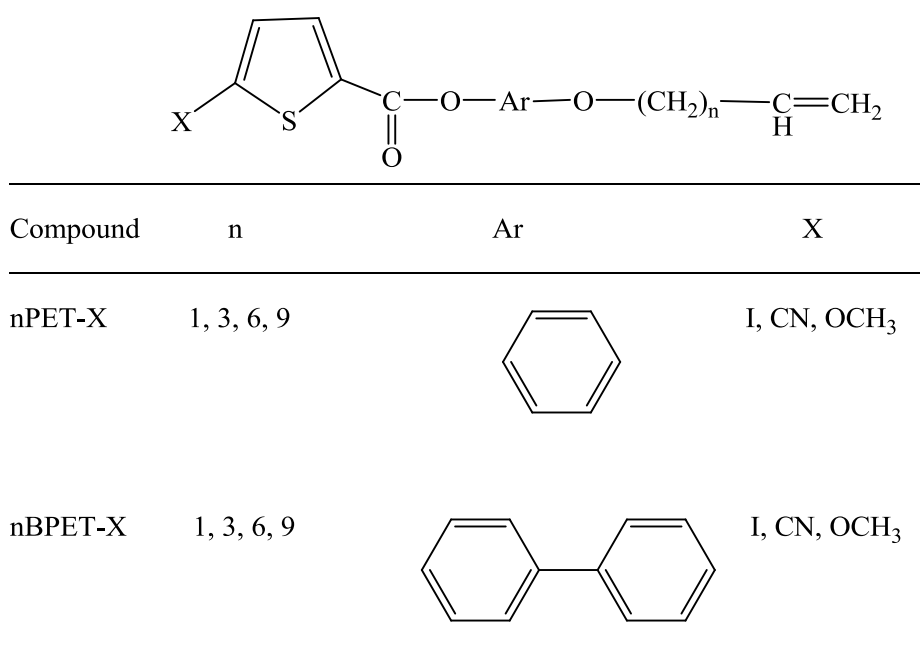


Figure 2.15: Structures of 2,5-disubstituted thiophene compounds

The LC properties of prepared compounds as a function of spacer units, number of aromatic core rings and different terminal moieties were investigated. Compounds having thiophene ring and one phenyl ring connected by an ester group, did not exhibit mesophase, while those containing biphenyl ring showed mesophases. The polarity of terminal groups and the flexible spacer length were found to have significant effect on the thermal behaviour of these compounds. In addition, the nematic transition range of cyano-containing compounds decreased with increasing length of the flexible spacer

and long alkanoyloxy chains facilitated to form smectic phase. Haramoto et al. [113] reported conductive thermotropic LC materials having a piperazine ring in the central core: 1-[4-(9-decenyloxy)phenyl]-4-alkylpiperazines **6** (Figure 2.16).

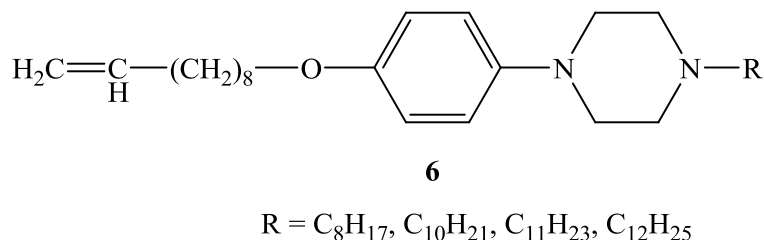


Figure 2.16: Structure of conductive liquid crystalline compounds **6**

The mesophase behaviour and electrical dark current of the synthesized compounds **6** were investigated. Results showed that compounds **6** exhibited natural smectic B (SmB) phase around room temperature and showed a dark current of $310\text{--}430 \mu\text{A cm}^{-1}$, which was the largest value seen in the thermotropic LC materials. Barbera et al. [114] synthesized and studied fluorescence, NLO and mesogenic properties of a series of 2-pyrazoline derivatives (Figure 2.17). The non-substituted or substituted with a 4-methoxy, 4-chloro or 4-carboxy group, the pyrazoline compounds exhibited fluorescent properties.

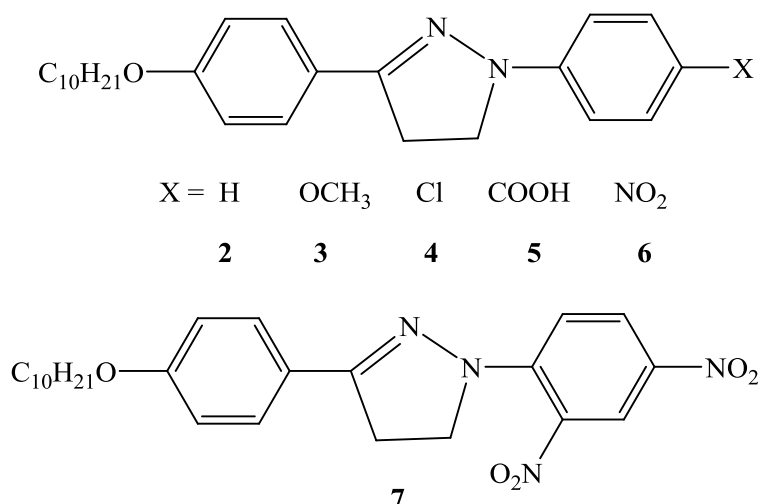
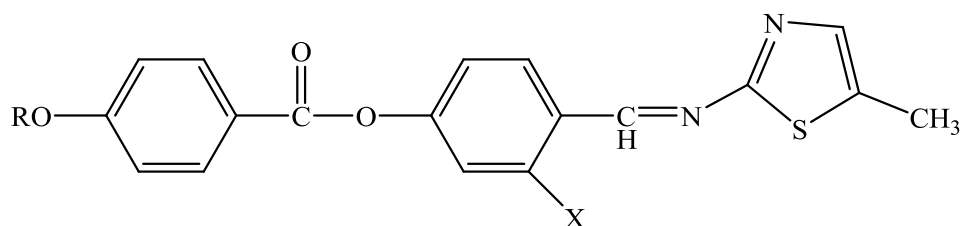


Figure 2.17: Structure of 2-pyrazoline derivatives, **2**, **3**, **4**, **5**, **6** and **7**

Pyrazoline with 4-nitro or 2,4-dinitro substituted derivatives showed interesting second-order NLO properties, while the 4-nitro substituted compound showed a higher first hyperpolarizability than the 2,4-dinitro derivative. The 4-nitro derivative also displayed LC behaviour, showing a monotropic smectic A phase while other derivatives were non-mesogenic. Campbell et al. [115] synthesized a large number of 2,5-disubstituted thiophene derivatives and studied their mesomorphic behaviour in order to systematically investigate the correlation between the molecular structure and mesomorphism of thiophene derivatives with different shapes, polarisability and polarity. In their finding, they reported that 2,5-disubstituted thiophene derivatives were the first LC materials that exhibited a nematic phase at room temperature. They concluded that their new thiophene compounds could be used to induce a high birefringence in nematic mixtures for LCDs.



X = H in series **A**, X = OH in series **B**

R = C_nH_{2n+1} n = 1- 8, 10, 12, 16

Figure 2.18: Structure of thiazole moiety based LC compounds (series **A** and series **B**)

Thaker et al. [116] synthesized and characterized two homologues series (series **A** and series **B**) of ester-azomethine linked LC compounds having thiazole moiety (Figure 2.18) and investigated the mesogenic properties of the prepared compounds. All the compounds of the 1,4-disubstituted series (series **A**) showed an enantiotropic nematic phase only whereas the compounds of the 1,3,4-trisubstituted series (series **B**) exhibited smectic and nematic phases.

In recent years, LC compounds containing fused heterocyclic ring systems, e.g., benzothiazole incorporated compounds have aroused a great research interest because of their interesting photophysical and fluorescent properties [117]. A benzothiazole ring which has been considered as an effective core in mesogens, containing the electron-rich sulphur atom, can contribute to a low ionisation potential and can also induce the smectic phase. Benzothiazole moiety containing LC compounds exhibit higher mesophase transition temperatures than other fused heterocyclic ring containing LC compounds because of the difference in degree of aromatization of the azole cycles that is degree of conjugation of heteroatom *p*-electrons with π -electrons of cycle [118].

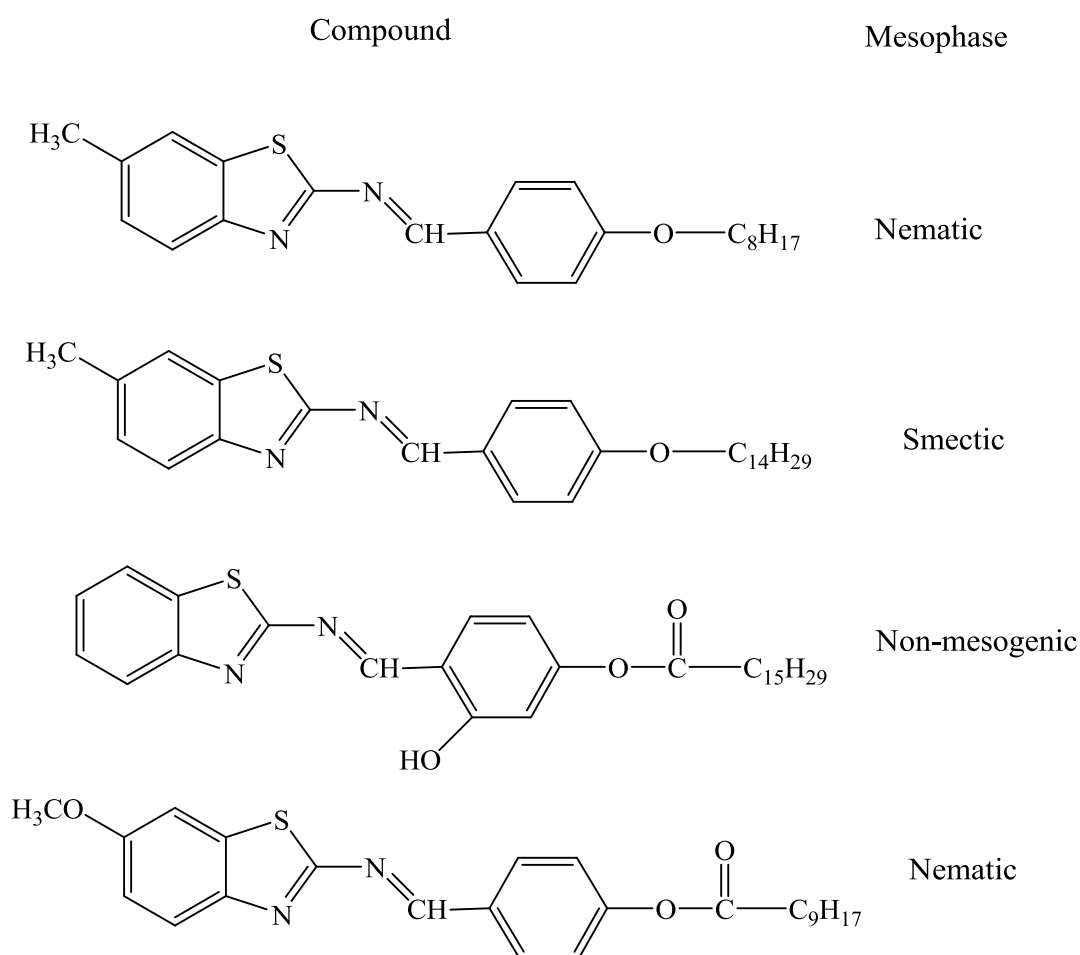


Figure 2.19: Azomethine linked benzothiazole moiety based LC compounds [119-121]

Until recently, a limited number of reports have been found in literature on benzothiazole moiety based LC compounds containing azomethine ($-C=N-$), azo

(-N=N-) and ester (-COO-) as central linkage. Ha et al. [119-121] reported azomethine linked LC compounds (Figure 2.19) bearing benzothiazole moiety and studied the effect of spacer lengths, terminal tails and lateral substituents on mesophase length and mesophase stability. The mesophase formation, phase stability as well as length of mesophase were found to be greatly influenced by the spacer lengths, terminal tails and lateral substituents. The higher spacer lengths were shown to facilitate the formation smectic phase while lateral substitution sometimes disrupts mesophase formation.

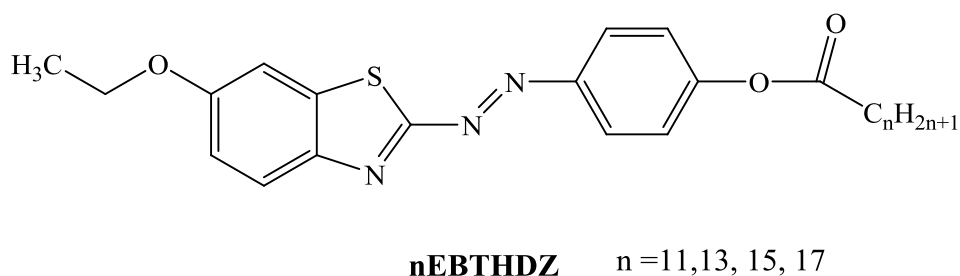


Figure 2.20: Structure of benzothiazole mesogen based LC compounds, **nEBTHDZ**

Yeap et al. [122] synthesized a series of azo-benzothiazole mesogen based LC compounds (**nEBTHDZ**) with electron donating ethoxy group at the sixth position on the benzothiazole moiety (Figure 2.20). It was found that all the compounds exhibited enantiotropic nematic phase and the melting and clearing temperatures were affected by the length of terminal alkoxy chain. A series of benzothiazole based LC compounds having azo central linkage with electron pushing methoxy group at the sixth position on benzothiazole ring (Figure 2.21) has also been prepared [118] and the lower members, i.e., up to ten carbons containing alkyl chain showed nematic phase. As for the series of LC compounds bearing azo-ester bridged benzothiazole moiety, it was found that nematic–isotropic transition temperatures exhibited a falling tendency with increase in terminal alkoxy tail.

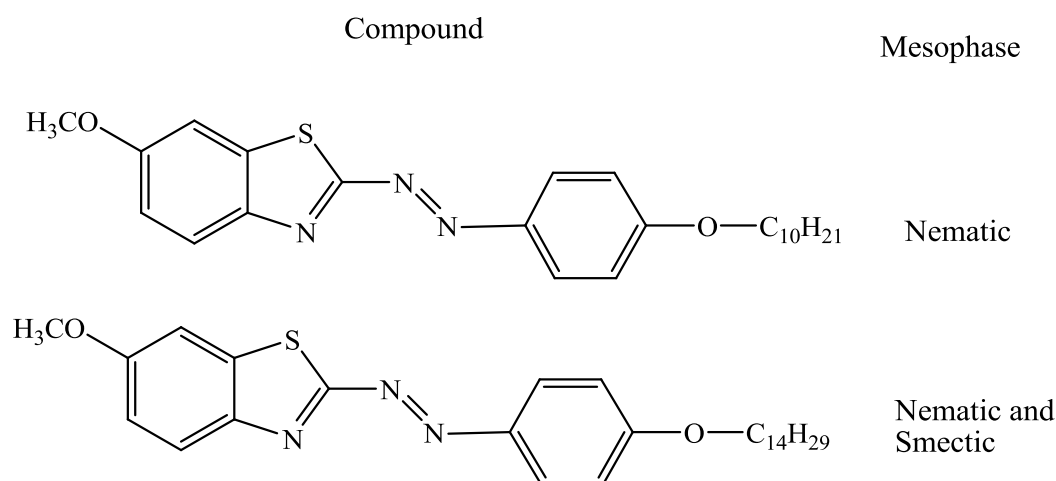


Figure 2.21 : Azo-benzothiazole moiety based LC compounds [118]

Iwan et al. [123] synthesized two unsymmetrical azomethines **BTA1** and **BTA2** (Figure 2.22) with benzothiazole core. **BTA2** was found to be thermally more stable than **BTA1**. Compound **BTA1** exhibited LC property while **BTA2** was non-mesogenic. The presence of fluorine atoms in **BTA1** was observed to trigger the increase in the isotropization temperature as well as the appearance of mesophase in comparison with **BTA2**.

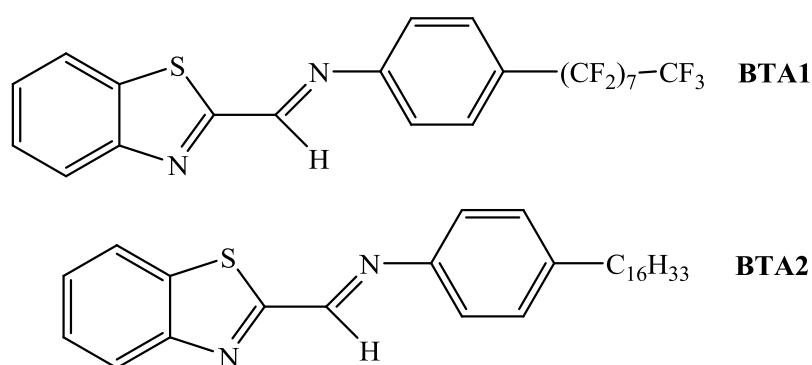


Figure 2.22: Structure of azomethines **BTA1** and **BTA2** with benzothiazole core

A series of catechol, 4,5-dibromocatechol, resorcinol, hydroquinone and 4,4'-dihydroxybiphenyl derivatives possessing two benzothiazole moieties at respective positions of 1,2, 1,3, 1,4 and/or 4,4' have also been synthesized and characterized [124]. The chemical structures of the synthesized compounds are shown in Figure 2.23. The

thermal transition temperatures and mesophase behaviours of the prepared compounds were investigated. Compounds with 1,2-substituted benzene (**3a**, **3b**) exhibited enantiotropic nematic and smectic A phases.

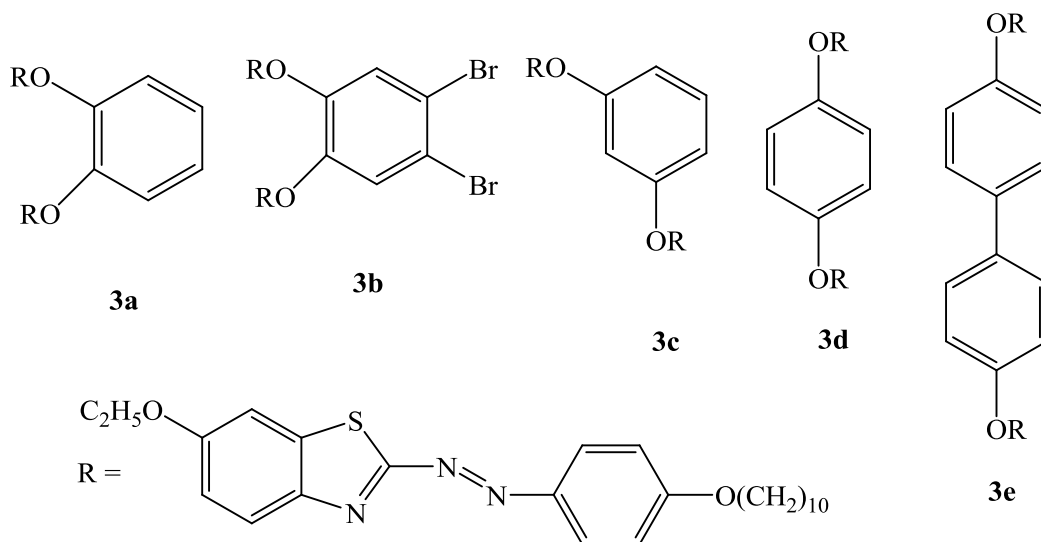


Figure 2.23: Chemical structure of compounds **3a**, **3b**, **3c**, **3d** and **3e**

On the other hand, derivatives **3c** and **3e** showed enantiotropic nematic phase while **3d** formed predominantly monotropic nematic phase. Compound **3e** was shown to exhibit higher nematic phase stability as compared to other members due to the increase in the breadth of the molecule. Ha et al. [125] synthesized and studied the phase transition behaviours of a series of calamitic liquid crystals comprising phenylbenzothiazole core, **nBPEP** (Figure 2.24) varying flexible spacer lengths.

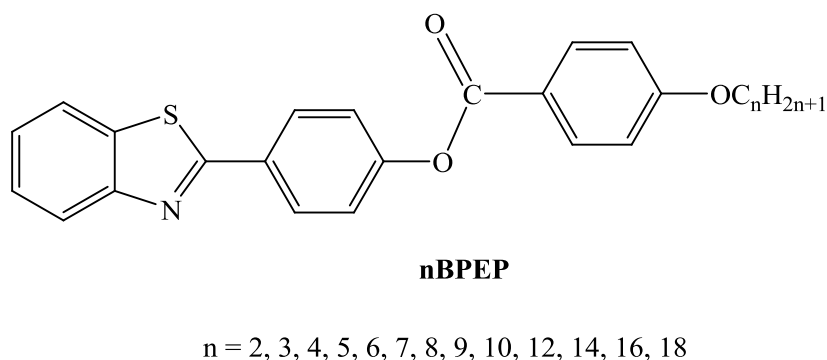


Figure 2.24: Structure of calamitic liquid crystalline compounds, **nBPEP**

It was observed that the mesophase started to form for the lowest member ($n = 2$), indicating phenylbenzothiazole might be considered as a good mesogenic core for mesophase formation. The emergence of monotropic SmA phase was also observed to start from n-nonyloxy derivative while enantiotropic SmA phase was detected from C₁₂ derivative onwards. Thaker et al. [64] synthesized and characterized two series (Series **E** and Series **F**) of 6-fluorobenzothiazole mesogen containing LC compounds (Figure 2.25) differing at the central linkage (an azo or ester group) and in the core unit (naphthalene or benzene). The series **E** derivatives with C₁ to C₇ chain length exhibited enantiotropic SmC and nematic mesophases. The C₈ homologue showed enantiotropic SmC, SmA and nematic mesophases, while the longer chain homologues (C₁₀ to C₁₄) showed enantiotropic SmC and SmA mesophases. The C₁₆ and C₁₈ homologues possessed only SmA mesophases. In series **F** all the compounds (C₁ to C₁₈) exhibited only the enantiotropic nematic mesophase.

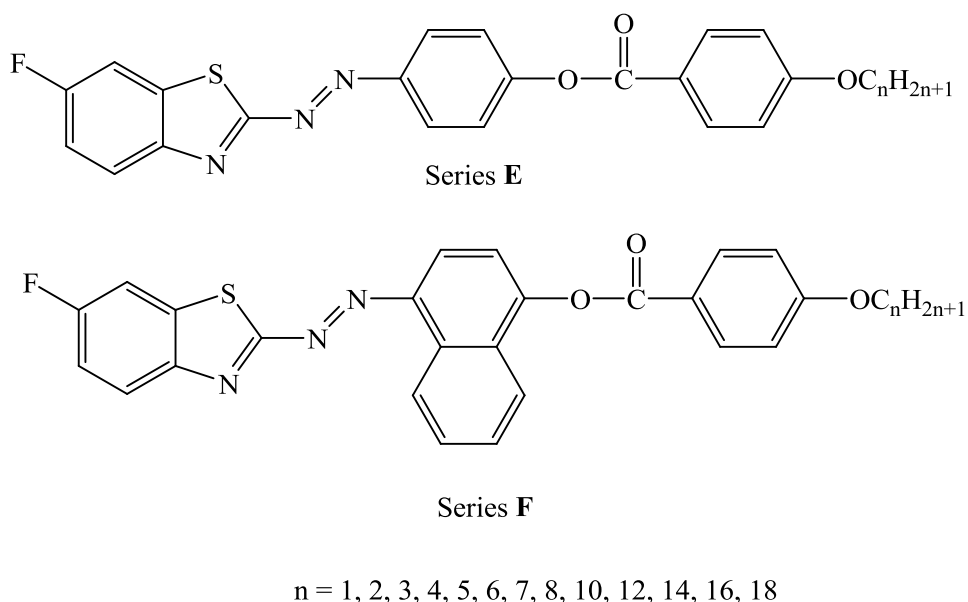


Figure 2.25: Structure of compounds, series **E** and series **F**

Meanwhile, compounds of series **E** exhibited higher mesophase thermal stability compared to those of series **F** due to the presence of a phenyl ring in place of a naphthyl

group. It was concluded that the naphthalene analogue of the benzothiazole ring favoured the formation of the nematic mesophase.

2.5. Photophysical and electrochemical properties of benzothiazole derivatives

Over the last two decades, organic and polymer light-emitting diodes (OLEDs and PLEDs) have attracted remarkable interest because of their potential applications in full-colour flat-panel displays and portable electronic devices [126-130]. It is very crucial to properly design molecule for improved OLEDs performance as well as to develop highly efficient materials with desirable properties [131-134]. Due to the strong electron withdrawing capabilities, relatively better chemical, thermal and photo-chemical stabilities and excellent fluorescence properties [135-139], heterocyclic molecules have received tremendous attention in recent years. Benzothiazole is a heteroaromatic compound with electron rich sulphur and nitrogen atoms in its molecular constituent and exhibits strong fluorescence in solutions as well as in solid state [140-142]. As a result, benzothiazole incorporated compounds have attracted overwhelming research interest in OLEDs application owing to their unique electro-optical properties [35-38]. Recently, a lot of attention has been paid on benzothiazole incorporated molecules to study their LC as well as photophysical properties together

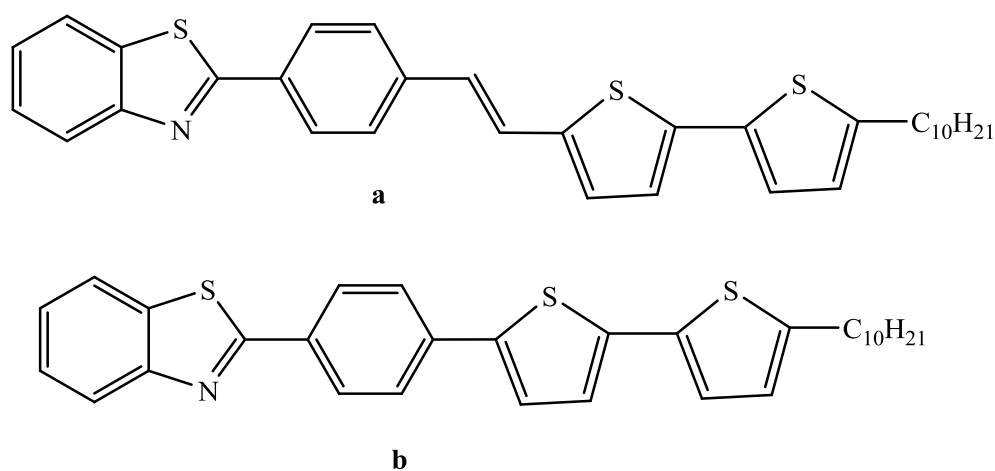


Figure 2.26: Benzothiazole moiety based donor-acceptor type LC materials **a** and **b**

Dutta et al. [56] synthesized donor-acceptor type two LC compounds (**a** and **b**) having benzothiazole moiety (Figure 2.26) and studied their optical, electrochemical and field-effect transistor properties. Both of the molecules exhibited SmA LC phase in the temperature range from 160°C to 240°C and the fabricated device showed p-channel behaviour with hole mobilities of 10^{-2} cm²/V s. Iwan et al. [44] prepared two unsymmetrical azomethines, **BTA1** and **BTA2** (Figure 2.27) having benzothiazole core and investigated their optical, electrochemical and photovoltaic performances. Both compounds exhibited blue photoluminescence with electrochemical band gap values as estimated by cyclic voltammetry were in the range of 2.31-2.81 eV and that band gap values were influenced by the introduction of fluorine atoms.

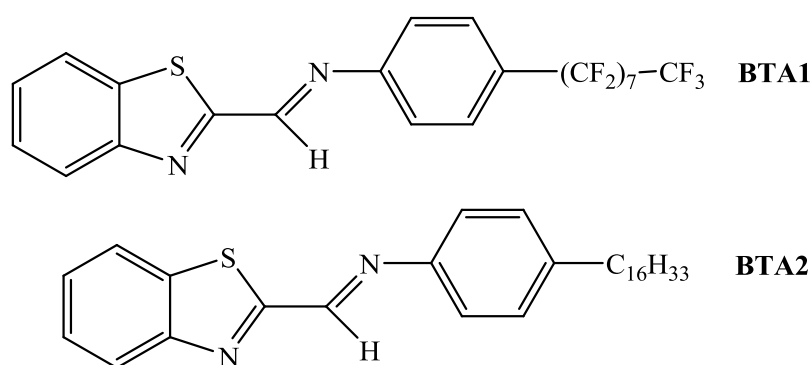


Figure 2.27: Azomethines **BTA1** and **BTA2** with benzothiazole core

BTA2 also showed very low photovoltaic performance while **BTA1** exhibited photovoltaic response and could have potential as an acceptor in bulk heterojunction (BHJ) devices. Wang et al. [42] synthesized benzothiazole-based derivatives with various π -electron donors as novel bipolar fluorescent compounds. These compounds exhibited high fluorescence quantum yield, desirable HOMO levels and high thermal stability. Optical study revealed that increasing conjugation length reduced the optical band gap up to 3.05 eV. The electrochemical and UV-vis spectroscopic results were used to estimate the actual HOMO and LUMO levels, which showed good match with the data obtained from density functional theory (DFT) calculations. It was concluded

that the newly synthesized compounds would be promising candidate in the application of OLEDs as a multifunctional material. Fu et al. [41, 43, 143] synthesized some benzothiazole derivatives (BBPA, BBNA, BPPA, BPPA-2CN, BPNA and BPNA-2CN) and investigated electroluminescent property (Figure 2.28). Compounds BBPA and BBNA exhibited excellent blue electroluminescent property and highly efficient blue-emitting electroluminescent devices were fabricated with BBPA or BBNA as the blue emitter. Considering the broad emission characteristics and electroluminescent performance, compounds BBPA and BBNA would be excellent candidates for blue light-emitting diodes in future OLED application compared to the other reported blue emitters [144, 145].

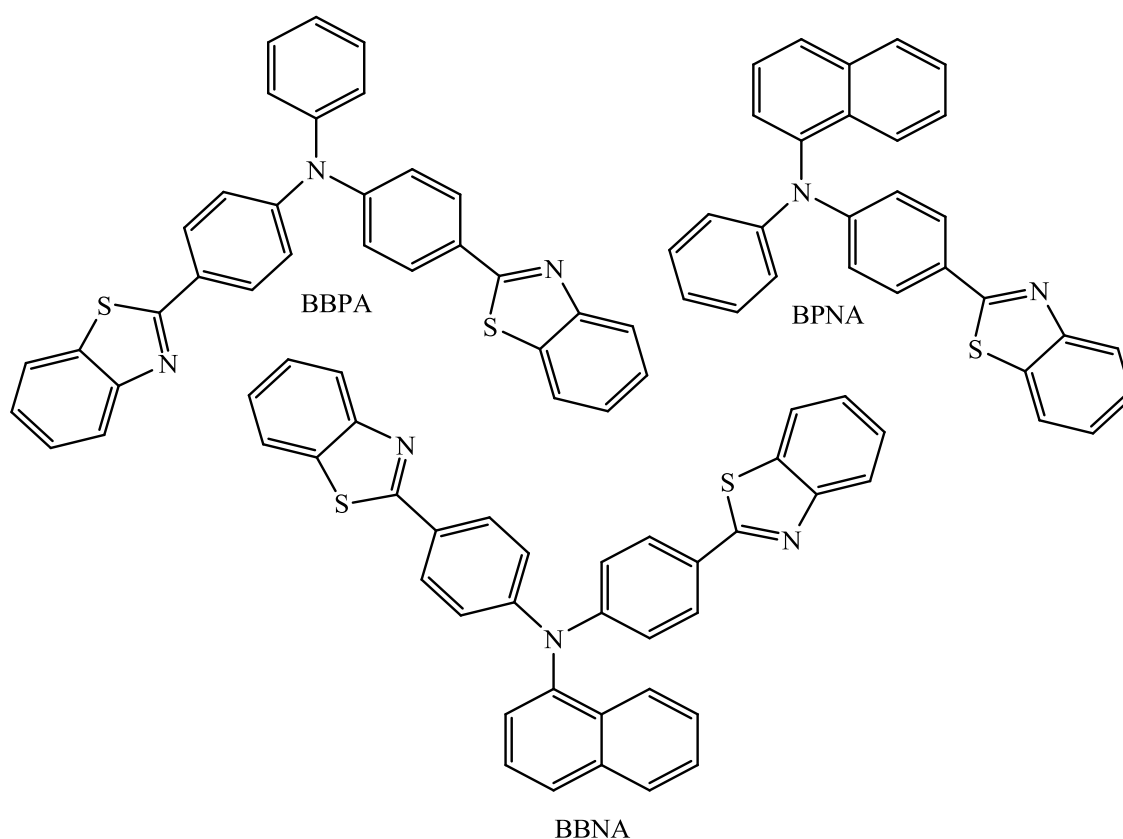


Figure 2.28: Molecular structure of BBPA, BBNA, and BPNA

On the other hand, compound BPNA showed bright yellowish-white emission and may be expected to serve as a new promising emission material for white organic electroluminescent devices. Raposo et al. [146] designed and synthesized two series of

novel thienyl pyrrole azo dyes bearing benzothiazole acceptor groups. The electrochemical as well as the linear and non-linear optical properties of well-defined asymmetric push-pull π -conjugated systems can be readily tuned by varying the linkage position of benzothiazole heterocycle (2 or 6) to the azo bridge. New dendrimers with benzothiazole as surface group and triazole as branching unit have also been synthesized and investigated for their photophysical, electrochemical and dye-sensitized solar cell (DSSC) performance [147]. It was shown that the presence of more number of benzothiazole and triazole units increased the molar absorption coefficient and altered the fluorescence as well as electrochemical behaviours in the dendrimers. Dye-sensitized solar cell (DSSC) studies revealed that dendrimers with more number of benzothiazole and triazole groups exhibited better current generating capacity than the dendrimers with lesser number of benzothiazole and triazole groups.

In recent years, benzothiazole derivatives have gained great importance in biomolecules detection due to their favourable spectral properties, particularly long wavelength absorption and fluorescence maxima positions, high values of molar extinction coefficient and fluorescence quantum yields [148]. Zheng et al. [49] synthesized three fluorine contained benzothiazole derivatives (F-N-Me, F-N,N-Me and O-FEt-PIB) (Figure 2.29) and studied their activity as potential tracers for β -amyloid plaques in Alzheimer's disease (AD).

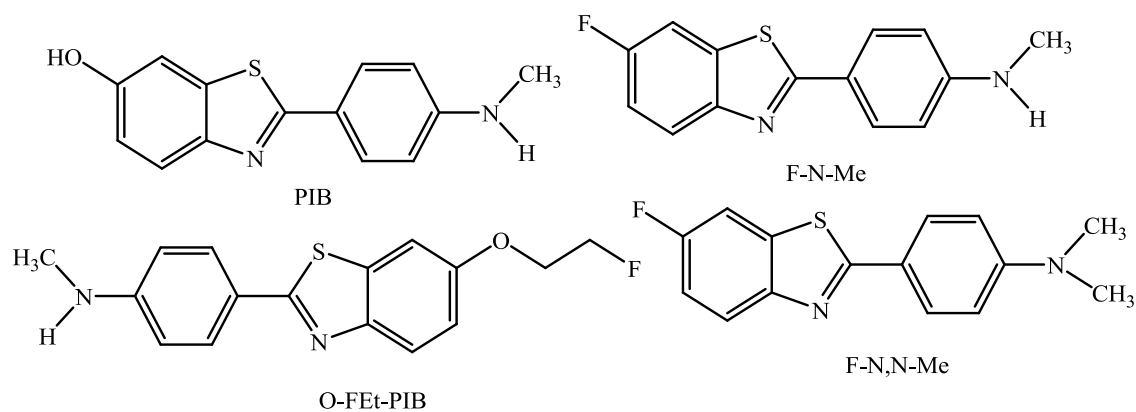


Figure 2.29: Chemical structure of PIB, F-N-Me, F-N,N-Me and O-FEt-PIB

considered to be potential as antimicrobial, anticancer and photosensitizing agents [150-153].

2.6. Benzothiazole moiety based polymers

Heteroaromatic compounds have attracted considerable research interest in recent years because of their better optoelectrical performance compared to benzenoid analogues. Both the theoretical and experimental [154-157] studies have revealed that heteroaromatic compounds, such as pyrrole, thiophene or benzothiazole can lead to enhance molecular hyperpolarizability [39, 40] compared to aryl derivatives due to the lower electron delocalization energy of the heteroaromatic system. Compounds having heterocyclic moiety have extensively been investigated because heteroaromatic compounds can offer a large molecular hyperpolarizability which is one of the desired criteria for NLO materials [158-161]. Recently, a remarkable attention has been paid on azo-benzothiazole chromophore containing compounds as NLO and optical data storage materials. Chen et al. [162] synthesized azo-benzothiazole chromophore based materials to study nonlinear optical applications. The replacement of benzene ring by a less aromatic heterocycle facilitated shift in UV-visible absorption band bathochromically and exhibited large molecular hyperpolarizability. Leng et al. [159] and Tambe et al. [163] synthesized nonlinear optical polyimides containing benzothiazole moiety and studied their electro-optical and thermal properties. The synthesized polymers exhibited substantial molecular hyperpolarizability. They also found that as the stability of the NLO chromophore increased, the glass transition temperature of the polyimides increased accordingly. He et al. [164] reported that soluble fluorinated polyimides containing azo-benzothiazole chromophore showed large hyperpolarizability and excellent temporal stability. Series of second-order NLO responsive polyurethanes containing nitro-substituted thiazole, benzothiazole and thiadiazole chromophores have also been synthesized [165]. These polymers exhibited glass transition temperatures in

the range of 140-165°C and most of the polymers showed high thermal stability. The second-order NLO response study revealed that all the poled films showed outstanding orientational stability up to 120°C without any measurable decay in the second harmonic generation signal. Among all the studied polyurethanes, nitro-substituted azobenzothiazole moiety showed the best dynamical thermal stability of the poling-induced dipole alignment up to ~150°C. As for polymethacrylates having pendant π -conjugated benzothiazole moiety synthesized via atom transfer radical polymerization (ATRP), the homo-polymer emitted blue fluorescence in DMF solution while the copolymer emitted orange fluorescence [166]. The intensity of the orange fluorescence decreased whereas the intensity of the blue fluorescence increased with the increase in molecular weight. Park et al. [167] reported NLO polymers having a chromophore with a π -conjugated imine bridge between phenyl and benzothiazole groups, for all-optical wavelength converters in optical fibre communication. Cao et al. [168] synthesized azobenzothiazole polyurethane-urea and investigated its thermo-optic property and simulation of 1×2 Y-branched and 2×2 Mach-Zehnder interferometer switch.

Cristina and Paul [46] synthesized amorphous high- T_g azo polymer having benzothiazole moiety in the side chain (pBTAMC) (Figure 2.31) and investigated its optical storage properties. In order to study the effect of chromophore structure on optical storage properties, they compared their results with other three push-pull azobenzene polymers (pDR1M, pDRASM and pDRSAM). Among four polymers, pBTAMC which contains the strongest pair of donor-acceptor substituents in the azo chromophoric side chain exhibited the highest stability of the induced order. The rate constant of thermal isomerization was found to increase with the increase in dipole moment of the azo moiety in the order of pDRSAM < pDRASM < pDR1M < pBTAMC.

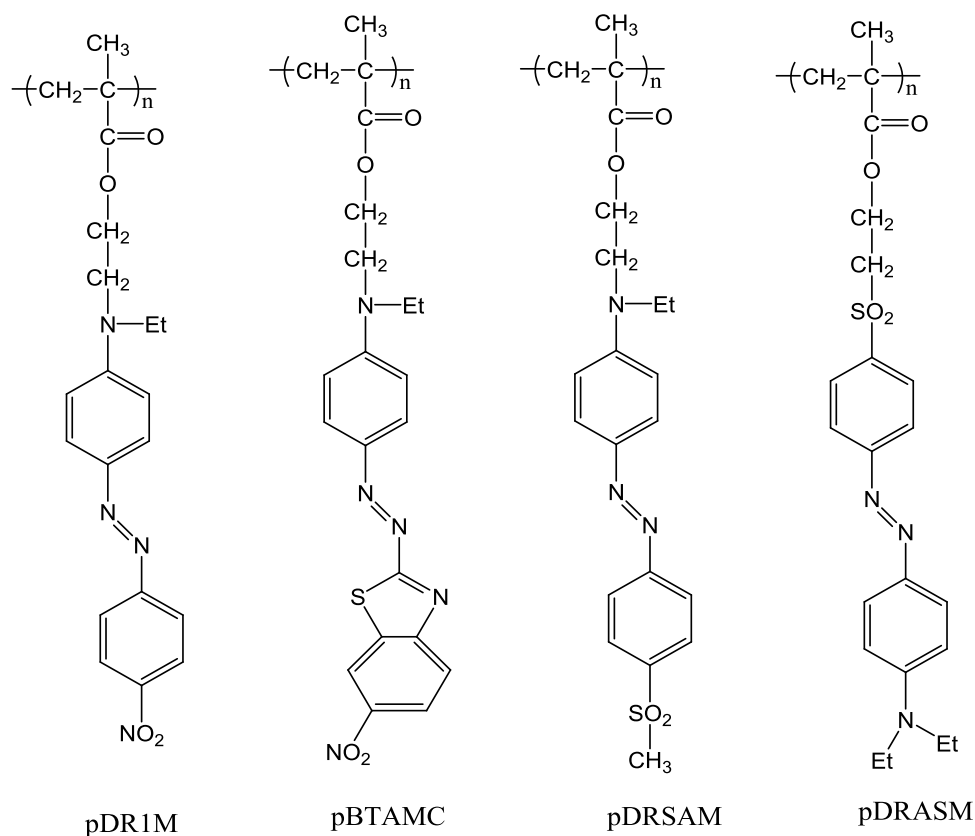


Figure 2.31: Chemical structure of azo-chromophore containing polymers pDRSAM, pDRASM, pDR1M and pBTAMC

Li et al. [45] prepared polymethacrylate containing pendant azo-benzothiazole, pBAMA (Figure 2.32) via free radical polymerization and investigated memory characteristic varying film thickness.

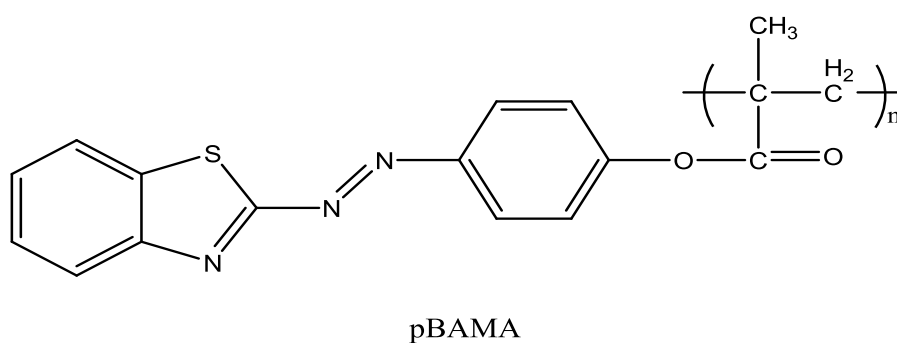


Figure 2.32: Molecular structure of polymer pBAMA

The synthesized polymer showed good solubility as well as thermal stability. The films of pBAMA showed the excellent FLASH memory behaviours or write once read many times (WORM) behaviours depending on the film thickness. Wang et al. [47] studied

dynamic random access memory (DRAM) characteristic with poly-methacrylate bearing pendant benzothiazole moiety. They concluded that their synthesized polymer exhibited excellent electrical properties and good film-forming capability and promising material for DRAM memory devices.

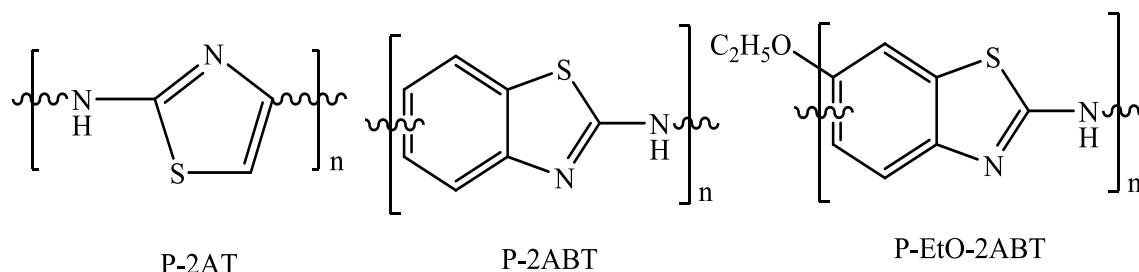


Figure 2.33: Chemical structure of P-2AT, P-2ABT and P-EtO-2ABT

Yıldırım and Kaya [169] synthesized 2-aminothiazole and 2-aminobenzothiazole based polymers (P-2AT, P-2ABT and P-EtO-2ABT) (Figure 2.33) via chemical oxidative polymerization method. Photoluminescence study revealed that polymers P-2AT and P-2ABT emitted bluish light under UV irradiation while P-EtO-2ABT emitted red colour with lower intensity. Electrochemical investigations of polymers showed lower band gaps than corresponding monomers, indicating their poly-conjugated structures.

2.7. Side chain liquid crystalline polymers

Side chain liquid crystalline polymers (SCLCPs) bearing azobenzene mesogen in the side chain have received substantial attention over the past decade because of their potential applications in optical information storage, optical switching, and nonlinear optics [170]. A great number of reports have been published on SCLCPs containing azobenzene moieties to explore their unique photochromic properties. Labarthe et al. synthesized and characterized a series of azobenzene containing SCLCPs, **pXMAN** (Figure 2.34) with varying methylene spacer lengths from 4 to 12 carbons. Polymers with short spacer lengths (**p4MAN-p8MAN**) induced a

hypsochromic shift during annealing process while longer spacers containing polymers (**p9MAN-p12MAN**) induced a large bathochromic shift. These effects may be due to the strong dipolar interaction and interdigitation of the side chain chromophores in an antiparallel orientation [171]. The irradiation of organized films with either circularly or linearly polarized light induced a bathochromic shift by breaking the antiparallel organization. This was a consequence of the angular reorientation of the azobenzene moieties as a result of *trans-cis* photoisomerization.

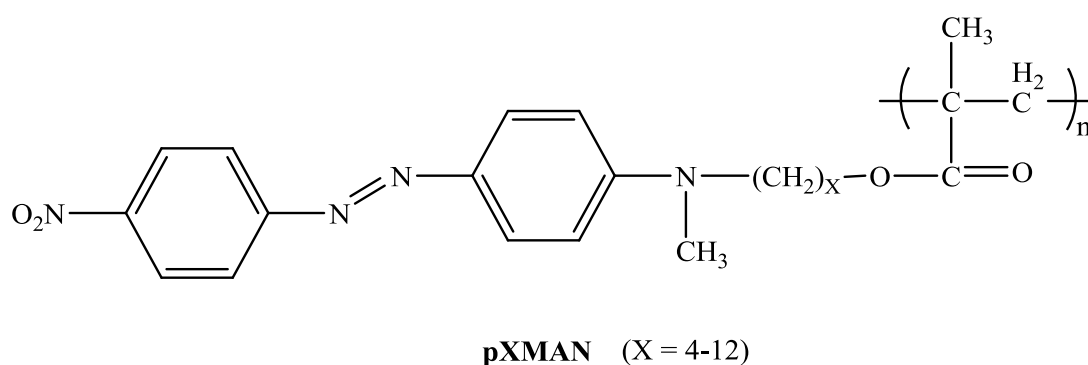
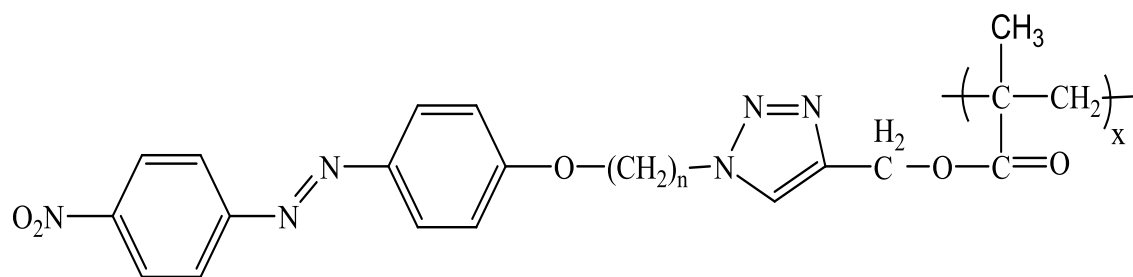


Figure 2.34: Chemical structure of SCLCPs, **pXMAN**

Freiberg et al. [172] reported a series of azobenzene containing SCLCPs and investigated the effect of spacer length on liquid crystallinity as well as photoinduced birefringence. The shortest spacer length containing polymer exhibited both nematic and smectic phases whereas all other polymers showed smectic phase. The systematic photoinduced birefringence measurements revealed that the maximum and remnant levels of birefringence decreased with the increasing of spacer length. Li et al. [173] synthesized high molecular weights (up to 303000) photoresponsive SCLCPs (Figure 2.35) containing azobenzene mesogens by click chemistry. They studied the phase transition behaviours and photosensitivity of synthesized polymers and compared the results with those of low molecular weight SCLCPs prepared by free radical polymerization.



Pn-F (n= 4, 6, 10) F refers to free radical polymerization

Pn-C (n= 4, 6, 10) C refers to click chemistry

Figure 2.35: Structure of polymers **Pn-F** and **Pn-C**

Both the high and low molecular weight azo polymers with a flexible spacer of $(\text{CH}_2)_{10}$ showed smectic C liquid crystal phase and the temperature range of the mesophase phase was influenced by in the molecular weights whereas the highly reversible photoisomerization of the polymer in solutions was independent of molecular weights. Photochromic SCLCPs containing azobenzene mesogen with short spacer lengths also facilitate the formation of nematic phase while smectic A_1 phase emerges with increasing spacer length [78]. Meanwhile, azobenzene chromophore containing SCLCPS with longer polymeric chain provides a higher volume variation with a slower process dynamics, indicating increased relaxation times. Polymers with higher molecular weight might be more suitable for applications requiring higher volume variation, since they could store more free volume [174]. Han and Ichimura [175] studied optical anisotropy of side chain liquid crystalline poly-methacrylates $C_n\text{MeO}$ (Figure 2.36) by irradiation with linearly polarized 365 nm light and by oblique irradiation with non-polarized 365 nm light. Irradiation of spin-coated polymers films with linearly polarized 365 nm light of around $10\text{-}20 \text{ mJ/cm}^2$ doses followed by annealing at temperatures nearly to the glass transition temperatures (T_g) of polymers led to a marked enhancement of azimuthal reorientation of the azobenzene giving birefringent films exhibiting excellent thermostability of the optical anisotropy.

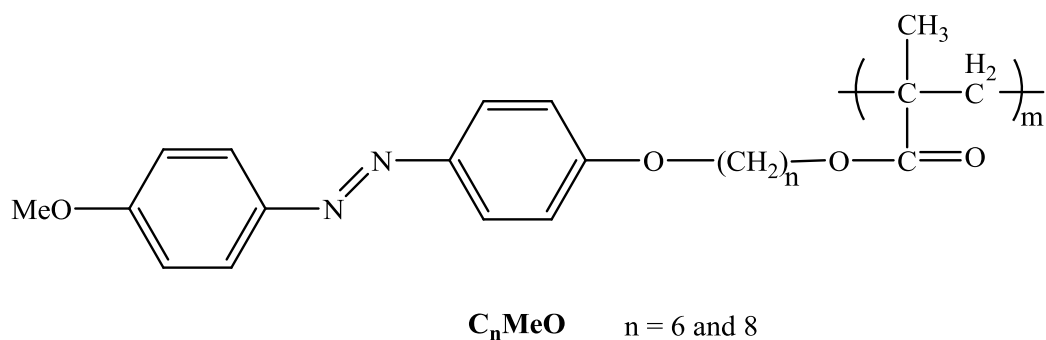


Figure 2.36: Chemical structures of SCLCPs, **C_nMeO**

On the other hand, exposure of spin-coated polymers films to obliquely non-polarized 365 nm light of about 15 mJ/cm² doses and subsequent annealing spatially manipulated reorientation of the azobenzene groups was realized, accompanied by the formation of H-aggregation. In both the cases, the photoinduced optical anisotropy was noticeably reduced or disappeared with the increasing of exposure doses (about 50 mJ /cm²).

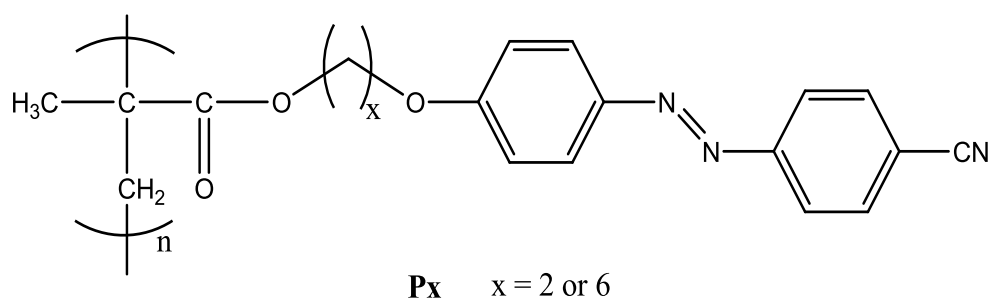


Figure 2.37: Structure of side chain liquid crystalline polymers **P_x**

The phase behaviour after photoinduced orientation of azobenzene chromophore containing SCLCPs, **P_x** (Figure 2.37) have been shown to exhibit banded texture (nematic state) upon heating the irradiated **P₂** film at 125°C which was just above its T_g (123°C). However, no banded texture was observed on heating the irradiated **P₆** film at 75°C (T_g : 72°C). During thermal treatment, the formation of the banded texture may be ascribed to the co-existence of in-plane and out-of-plane orientated mesogens in **P₂** film. The formation of the banded texture was influenced by the experimental conditions such as irradiated light intensity, film thickness and heating rate [176]. Very recently, Alicante et al. [177] synthesized, characterized and studied NLO properties of a series

of LC monomers and SCLCPs having azobenzene chromophores with piperazine as a strong donor group (Figure 2.38) and different acceptor groups (DCN, NO₂, CN).

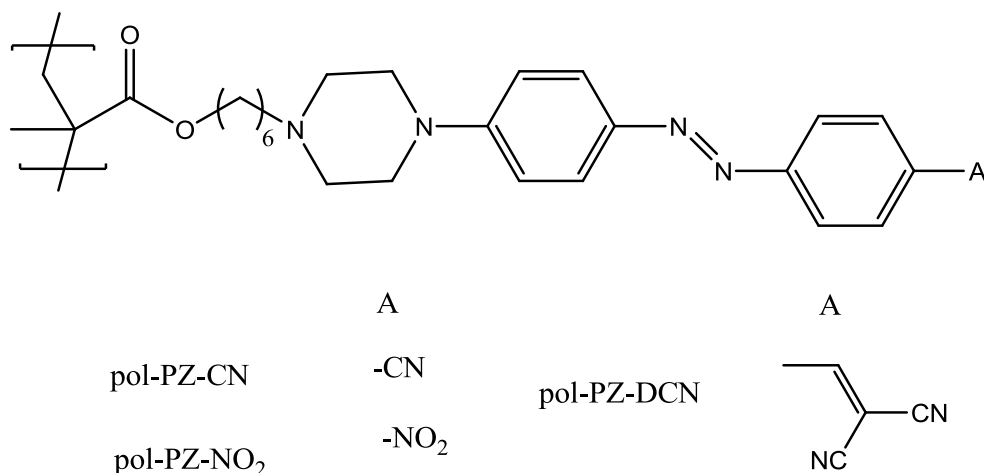


Figure 2.38: Structure of SCLCPs having azobenzene chromophore with donor-acceptor groups

Monomers having terminal cyano or nitro groups and the corresponding polymers, exhibited smectic A phases. The molecular nonlinearities study revealed that molecular hyperpolarizabilities ($\mu\beta$ values) showed the expected tendency by considering the strength of the electron withdrawing groups (DCN > NO₂ > CN). UV-vis absorption study revealed an out-of-plane orientation of azo chromophores as well as the presence of azo aggregates in the as-prepared films. The thermal annealing induced a significant amplification of the out-of-plane optical anisotropy while irradiation with 440 nm light induced some disruption of aggregates. The second order NLO properties of pol-PZ-CN films showed a noticeable degree of polar order remained for several months after the poling in films kept at room temperature.

SCLCPs are attractive for a variety of potential commercial applications (optical data storage, nonlinear optical materials and stress sensors) due to the combination of anisotropic phase structure, capacity to freeze liquid crystalline order into the glassy state, and the ability to manipulate the orientation of their optical axis using applied

fields. To realize these applications, it is imperative to understand the rheology of these materials and the effect of flow history on molecular alignment, which controls their optical and mechanical properties. Although considerable work has been done on main-chain and rigid-rod polymer liquid crystals, relatively little research has been devoted to the rheological behaviour of SCLCPs. Over the past two decades, several research groups have conducted experimental investigations on the rheological behaviour of SCLCPs. Colby et al. [178] investigated the linear viscoelasticity of three SCLCPs (**PAMeAPr**, **PMADe** and **PMAM**) with poly-acrylate and poly-methacrylate backbone (Figure 2.39) having *trans*-azobenzene pendent mesogen attached via six carbons flexible spacer to main polymer backbone.

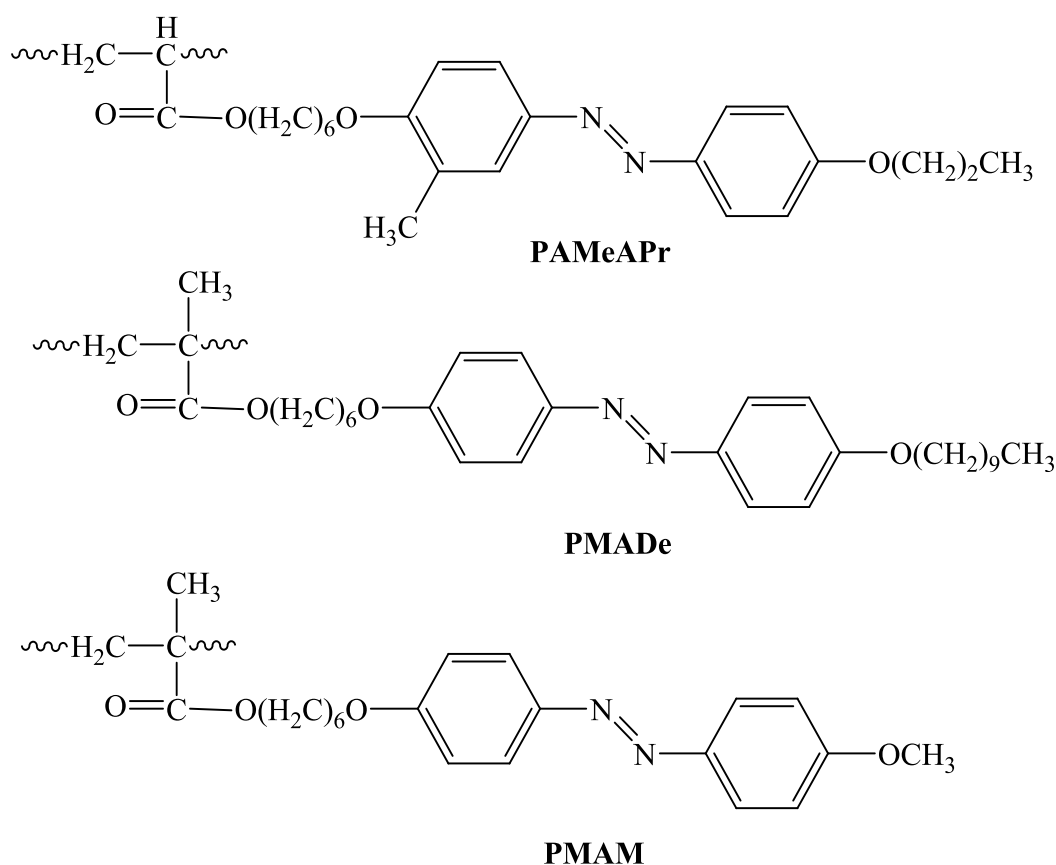


Figure 2.39: Structure of SCLCPs **PAMeAPr**, **PMADe** and **PMAM**

In contrast to main chain liquid crystalline polymers (MCLCPs), nematic SCLCPs showed linear viscoelastic response over a wide range of strain amplitudes that was

independent of thermal and shear histories. It was concluded that the viscoelastic response was very sensitive to smectic-nematic and smectic-isotropic transitions, but insensitive to the nematic-isotropic transition. Investigation on the oscillatory shear response of three thermotropic smectic LC materials: two were polymers (one MCLCP and one SCLCP) and the other was a low molecular weight liquid crystalline molecule [179] showed all three LC materials exhibited smectic phase showing classical linear response to oscillatory shear flow of a viscoelastic solid at sufficiently small strain amplitude and frequencies. Above certain strain amplitudes, these three materials showed a strong nonlinear response to strain.

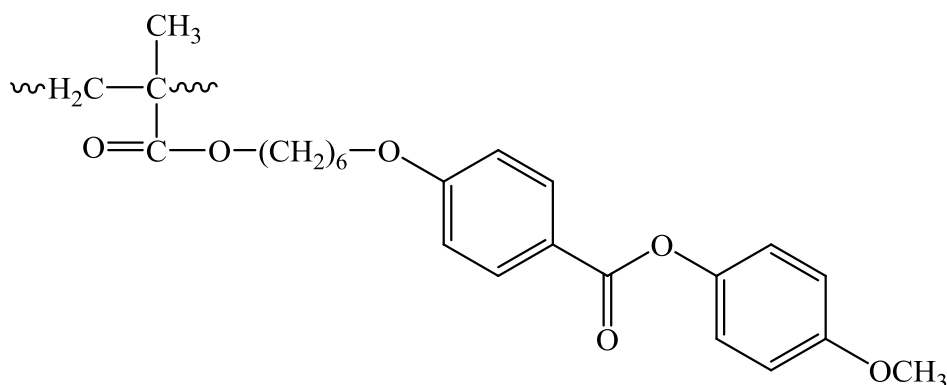


Figure 2.40: Structure of SCLCP which was adopted from [180]

Kannan et al. [180] investigated the dynamics of nematic SCLCP using transient stress and birefringence measurements. In their study, they used a SCLCP which was composed of a methacrylate backbone, a six-methylene spacer, and a phenyl benzoate mesogenic group with the chemical structure shown in Figure 2.40. At sufficiently low frequency, the studied SCLCP exhibited a noticeable drop in the dynamic moduli upon passing through the transition from the isotropic to the nematic state. They also found that prolonged large amplitude oscillatory shear dramatically reduced turbidity and dynamic moduli in the nematic phase and increased birefringence of the sample. They concluded that shearing also induced a preferred alignment in this SCLCP melt.

Rubin et al. [181] studied the effect of mesophase order and molecular weight on the dynamics of nematic and smectic SCLCPs. Four different SCLCPs with methacrylate backbone having hexamethylene spacer and phenyl benzoate mesogens were used. Nematic order produced a significant change in the dynamics of high molecular weight SCLCPs relative to the isotropic phase while there was virtually no difference in rheological behaviour between the nematic and isotropic phases of the low-molecular weight SCLCPs. Berghausen et al. [182] investigated the shear orientation of a nematic SCLCP with side-on fixed mesogenic units (Figure 2.41) by means of rheo-birefringence and rheo-small angle light scattering.

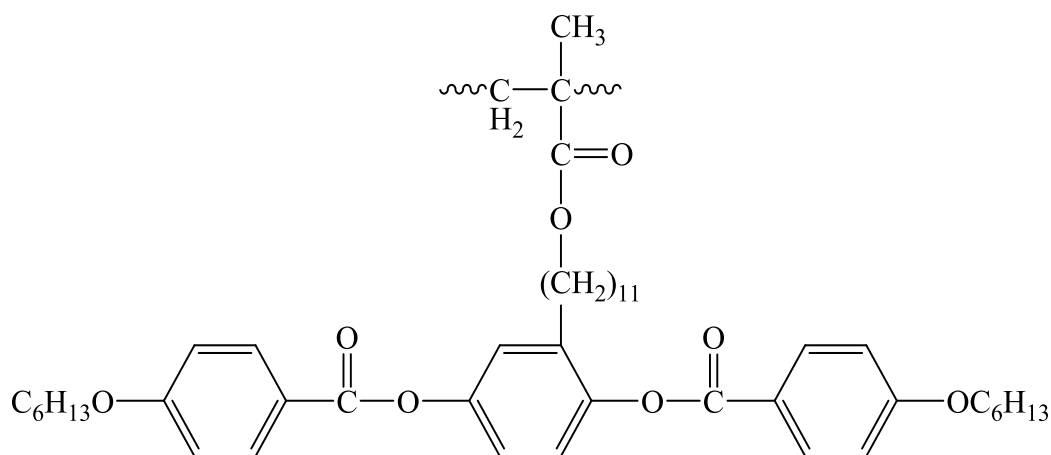


Figure 2.41: Polymer structure adopted from [182]

They observed that the rheological properties of the SCLCPs were influenced by the molecular weights. The shear modulus of a low molar mass sample in the nematic and isotropic phase superposed to exhibit a common master curve. The low-frequency modulus of a high molar mass sample, however, decreased at the phase transition, and time-temperature superposition was not possible. Rheo-birefringence measurements revealed a clear influence of molar mass on both the final value and the orientation state after cessation of shear. Rheo-small angle light scattering also showed a strong influence of molecular weight. Wewerka et al. [183] synthesized norbornene based

SCLCPs (homopolymer and copolymer) with different spacers (Figure 2.42) and investigated phase transitions and rheological behaviour.

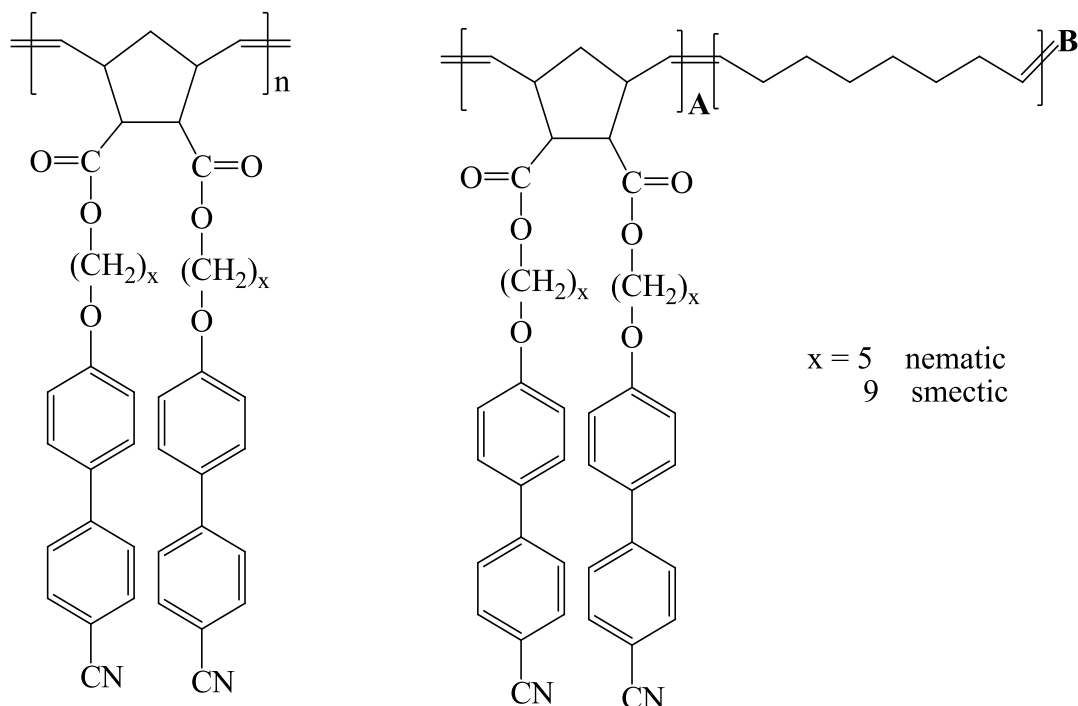
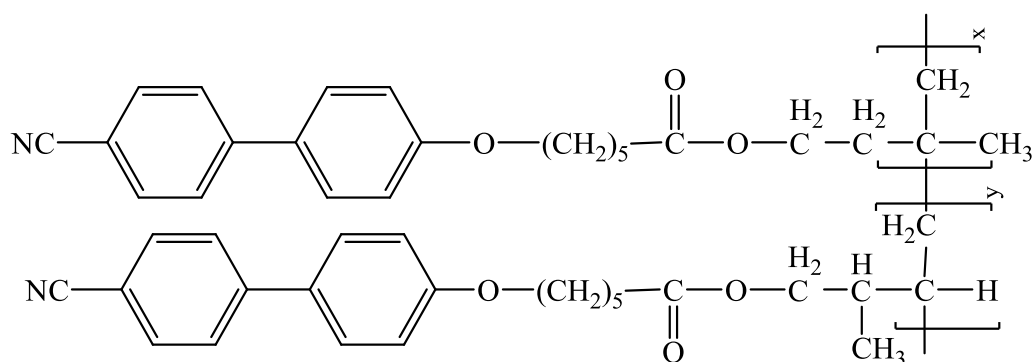
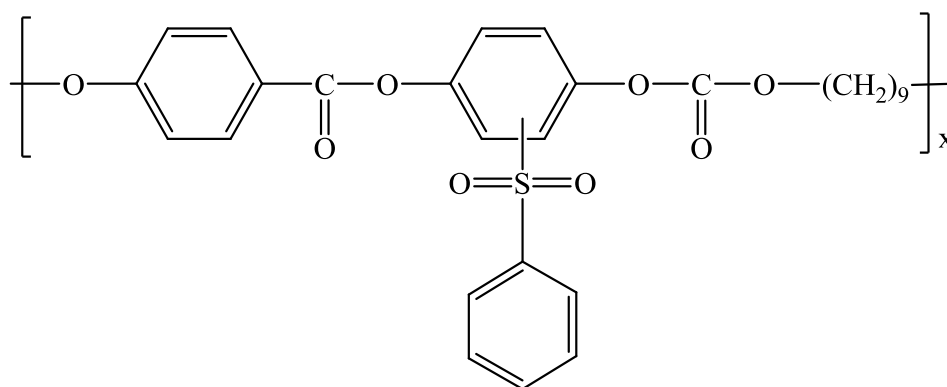


Figure 2.42: Structure of norbornene based SCLCPs

Like other LC materials, SCLCPs with the chemical structure having short methylene groups ($x = 5$) formed a nematic phase while SCLCPs having long methylene groups ($x = 9$) showed a smectic A mesophase. Although, nematic-isotropic transition temperature was affected by the degree of polymerization of the backbone, the mesophase dynamics was not. The smectic and nematic liquid crystalline polymers exhibited non-Newtonian low-frequency response and violated the empirical principle of time-temperature superposition with the effect being more pronounced in the former. Lee and Han [184] synthesized a nearly mono-dispersed (polydispersity = 1.05) nematic SCLCP and compared the rheological properties of SCLCP, **PI-14-5CN** with an MCLCP, **PSHQ9** (Figure 2.43). The linear dynamic viscoelasticity, steady shear flow, transient and intermittent shear flows and stress relaxation of **PI-14-5CN** and **PSHQ9** were investigated in their study.



PI-14-5CN



PSHQ9

Figure 2.43: Structure of SCLCP, **PI-14-5CN** and MCLCP, **PSHQ9**

They found that the steady-state shear viscosity (η) of the SCLCP exhibited a Newtonian behaviour at shear rates as low as 0.01 s^{-1} followed by a shear thinning behaviour at higher shear rates, similar to ordinary flexible polymers, while the η of the MCLCP exhibited a shear-thinning behaviour at low shear rates followed by a Newtonian region at intermediate shear rates and then another shear-thinning behaviour at higher shear rates. They also observed that upon cessation of steady shear flow, the dynamic storage and loss moduli (G' and G'') of the SCLCP increased very rapidly initially and then levelled off within ca. 40 min, whereas the G' and G'' of the MCLCP did not level off in the same period. Upon cessation of steady shear flow, both shear stress and first normal stress difference of the SCLCP relaxed much faster than those of the MCLCP. The effect of flexible spacer length on the rheology of SCLCP, **PI-nCN**

(Figure 2.44) has been investigated. It was observed that the flexible spacer length has a profound influence on the rheological responses of polymers [185]. At temperatures below isotropic point the complex viscosity ($|\eta^*|$) of **PI-5CN** exhibited a very weak frequency dependence but the frequency dependence of $|\eta^*|$ for **PI-nCN** became progressively stronger as the number of methylene spacer groups increased from 5 to 7 and to 11.

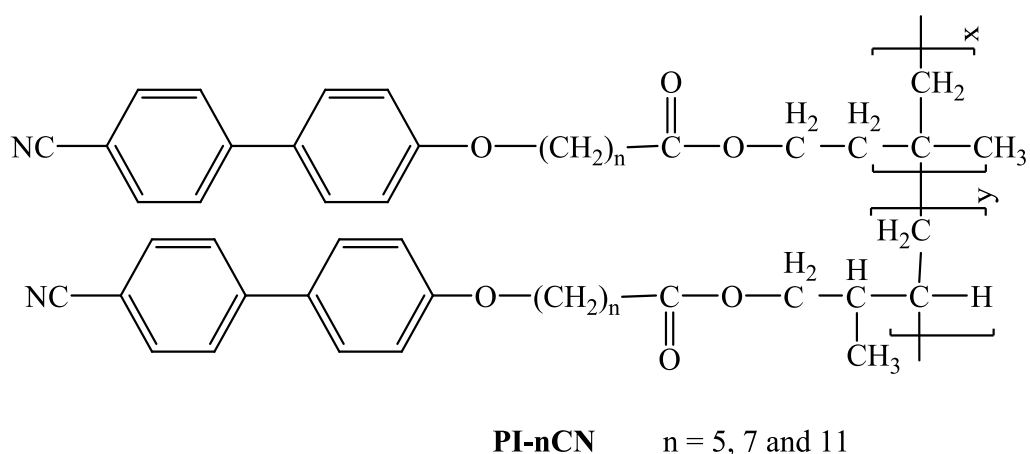


Figure 2.44: Structure of SCLCP, **PI-nCN**

The steady-state shear viscosity (η) and first normal stress difference (N_1) of **PI-nCN** decreased as the number of methylene spacer groups was increased from 5 to 11. Rendon et al. [186] reported combined rheological and in situ X-ray scattering investigations of large amplitude oscillatory shear (LAOS) induced alignment in smectic SCLCPs, **PBSiCB5** (Figure 2.45). Rheological measurements of the dynamic moduli confirmed that the application of LAOS induced a noticeable decrease in G' , which was in accord with general observations made for layer-like fluids. Larger strains directed to both higher degrees of layer alignment, and sharper reductions in modulus. X-ray and rheological data demonstrated that increasing strain promoted higher degrees of orientation, while increasing molecular weight impeded development of smectic alignment. Andreozzi et al. [187] investigated the shear rheological behaviour of a series of high molar mass SCLCPs having an azobenzene mesogenic group in the side

chains. The focus of their study was the entanglement effects and tested selected reptation models to ascertain the ability to reproduce the complex shear modulus of the copolymers.

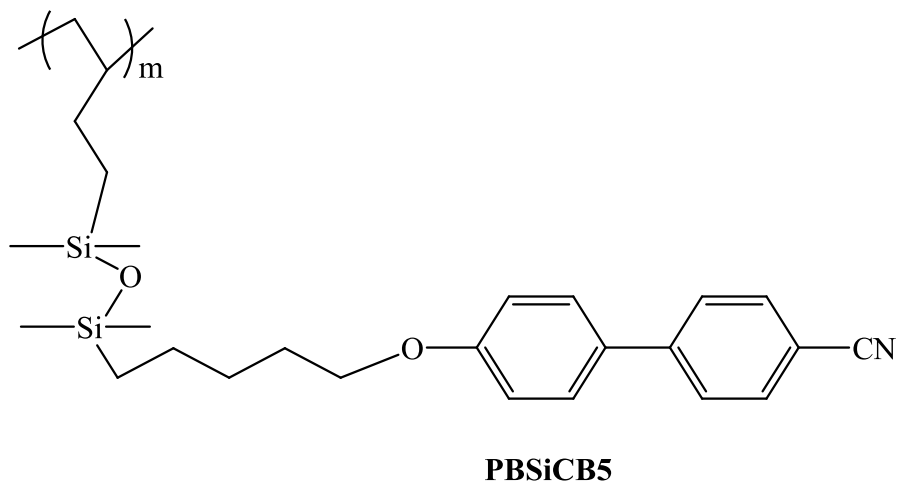


Figure 2.45: Structure of SCLCP, **PBSiCB5**

It was found that ordinary dynamic models worked nicely for the nematic copolymers and also observed reproducible rheological response of the materials. They were able to obtain microscopic information of the materials, such as Rouse time and entanglement molar mass as well as got insight on the macroscopic effects of tube dilatation induced by the nematic order on the master curves of the entangled polymers.

CHAPTER 3 : EXPERIMENTAL

3.1. Materials and reagents

All chemicals and solvent were of reagent grade unless otherwise stated. 2-Aminobenzothiazole (Aldrich, Germany, 97%), 2-amino-6-methylbenzothiazole (Aldrich, Japan, 98%), 2-amino-6-methoxybenzothiazole (Aldrich, Germany, 98%), 2-amino-6-ethoxybenzothiazole (Aldrich, Switzerland, technical grade), 2-amino-6-fluorobenzothiazole (Acros Organics, 99%), 2-amino-6-chlorobenzothiazole (Acros Organics, 99%), 1-chloro-6-hexanol (Acros Organics, 95%), 4-hydroxyethylbenzoate (Acros Organics, 99%) benzoyl peroxide (BPO) (Merck, Germany, 72-77%), concentrated sulfuric acid (Friendemann Schmidt Chemical, 95-97%), glacial acetic acid (J.T Baker, USA, 99.9%), sodium nitrite (System, 98.0%), sodium hydroxide (R & M Chemicals, UK 99.0%), phenol (Sigma-Aldrich, Germany, 99%), 1,6-dibromohexane (Aldrich, India, 96%), potassium carbonate (John Kollin Corporation, 99%), acetone (J.T Baker, USA, 99.8%), methacrylic acid (Sigma-Aldrich, 99%), potassium hydrogen carbonate (Hamburg Chemicals, 99.5%), potassium iodide (R & M Chemicals, UK 99.9%), hydroquinone (Merck, Germany, 99.5%), silica gel 60 (Merck, Germany), tetrabutylammonium perchlorate (Acros Organics, 99%), N,N-dimethylformamide, (Merck, Germany, 99.8%), dimethyl sulfoxide-D₆, (DMSO-D₆) (Merck, Germany, 99.8%), chloroform-D₁, (CDCl₃) (Merck, Germany, 99.8%), chloroform (Friendemann Schmidt Chemical, 99-99.5%), toluene (Merck, Germany, 99.8%), chlorobenzene (Merck, Germany, 99.8%), ethanol (Merck, Germany, 99.8%), dichloromethane (Merck, Germany, 99.8%), tetrahydrofuran (Merck, Germany, 99.8%). Initiator benzoyl peroxide (BPO) was recrystallized from ethanol and toluene was distilled before used. Other chemicals and solvents were used without further purification.

3.2. Instrumental Techniques Employed

The prepared monomers and their corresponding polymers were characterized and studied by the different instrumental techniques as described in the following parts.

3.2.1. Fourier Transform Infrared (FT-IR) spectroscopy

Infrared spectroscopy is an important tool to identify and study the presence of functional groups in a molecule. The purity or specific impurities in a compound can be recognized and verified by absorption bands. The FT-IR spectra were recorded with a Spotlight 400 Perkin Elmer spectrometer with 16 scanning numbers using attenuated total reflectance (ATR) method and a resolution of 4 cm^{-1} . The wavelength was recorded from region 450 to 4000 cm^{-1} at room temperature. All the investigated samples were placed over the ATR crystal and maximum pressure applied using the slip-clutch mechanism.

3.2.2. Nuclear Magnetic Resonance (NMR) spectroscopy

The chemical structure and purity of the prepared compounds were investigated by NMR spectroscopy. ^1H NMR and ^{13}C NMR measurements were performed with a JEOL JNM-LA 400 MHz spectrometer, JEOL ECA 400 MHz spectrometer and Bruker AVN 400 MHz. Samples were dissolved in appropriate deuterated solvent to obtain viscous solution in NMR tube and concentrations were maintained at 2.5% (w/v) and 15% (w/v) for the ^1H NMR and ^{13}C NMR analysis respectively. The chemical shifts were referenced against TMS as 0 ppm and the deuterated chloroform showed a typical peak at δ value of 7.26 ppm for ^1H NMR and 77.0 ppm for ^{13}C NMR. On the other hand, the deuterated DMSO showed peaks at 3.33 ppm and 2.5 ppm for ^1H NMR and 40.6 ppm for ^{13}C NMR.

3.2.3. Thermogravimetric Analysis (TGA)

Thermogravimetric analysis was employed primarily for determining thermal stability of synthesized monomers and their polymers. Thermogravimetric investigation was performed using a SDT Q600 thermogravimetric analyser (TGA Instrument). All the investigations were carried out under steady flow of nitrogen atmosphere 20 mL min⁻¹ at a heating rate of 20°C min⁻¹ from 50°C to 900°C with a digital resolution of 2550 points. The sample weight used was between 8 and 15 mg during measurements. Data were processed using the instrument built in Pyris v9.1.0.0203 software.

3.2.4. Differential Scanning Calorimetry (DSC)

Thermal transition temperatures and corresponding enthalpy changes of the prepared monomers and polymers were investigated by DSC. DSC thermograms in nitrogen atmosphere were recorded with a Parkin Elmer Pyris DSC6 instrument calibrated with indium. For the monomers about 4-6 mg and for polymers about 8-12 mg of samples were weighed in a standard sample aluminium pan. The same empty pan was utilized as a reference. During DSC measurements, the samples were heated up to their isotropization temperature and annealed for two minutes and then cooled down to room temperature. The samples were again heated up to their isotropization temperature to erase any previous thermal history. The second heating and first cooling data were evaluated to ensure equivalent thermal histories of the analysed samples.

3.2.5. Polarized Optical Microscopy (POM)

The liquid crystal phase transitions were investigated by a Mettler Toledo FP82HT hot stage and viewed with an Olympus BX51 microscope fitted with crossed polarizing filters. A small amount of the sample was placed on a glass slide and covered with a cover slip. Each sample was heated up to its isotropization temperature and then

cooled at $1^{\circ}\text{C min}^{-1}$. Most of the optical photomicrographs were taken upon cooling process to obtain better images.

3.2.6. Small Angle X-ray Scattering (SAXS)

Small angle X-ray scattering (SAXS) experiments were performed with Nano-Viewer equipped with a CCD camera (Rigaku Corp. Japan). The X-ray experiment was performed by using the Cu K_{α} radiation beam ($\lambda = 1.541 \text{ \AA}$) which was converged and monochromatized by a Confocal Max Flax (CMF) mirror. X-ray generator was a Rigaku Micro7 rotating anode generator (40 kV, 30 mA). The diameter of the X-ray beam controlled by a 3-slit optical system was set to $250 \mu\text{m}$. The samples were filled into capillary tubes and put into a temperature-controlled sample holder attached to Mettler FR-82 hot stage (Mettler Toledo Inc. Switzerland) and FP-80 Control Processor. The accuracy of the temperature control was $\pm 0.1^{\circ}\text{C}$.

3.2.7. Gel-permeation chromatography (GPC)

Molecular weight determinations were performed using a gel permeation chromatography (GPC) instrument (Waters 2414 refractive index detector coupled with a Waters 717 plus Auto sampler and Waters 600 Controller) with polystyrene standards as reference and tetrahydrofuran (THF) as the eluent at flow rate 1 ml per minute. A weight of 5 to 10 mg of the polymer sample was dissolved in 5 mL of tetrahydrofuran. The samples were filtered through a Waters GHP Acrodisc® that has a minispikes diameter of 13 mm and a pore size of $0.45 \mu\text{m}$ (to protect the chromatography instrument from un-dissolved particulates) into a sample vial of about 1 ml capacity. The total run time for each sample was set to 55 minutes and the injection volume was $100 \mu\text{l}$ for each vial. All of the data processing was done using the instrument's built in Empower v2.0 software.

3.2.8. UV-visible (UV-vis) and Photoluminescence (PL) Spectroscopy

UV-vis absorption spectra were recorded with a Cary 60 UV-vis spectrophotometer. The dilute polymer solutions (1×10^{-6} M) were prepared in chloroform and fresh chloroform was used as blank. The polymer solutions were placed into 4 sided clear quartz cuvette and the measurements were carried out from 200 nm to 700 nm with medium scan rate. The fluorescence emission spectra were obtained by a Cary Eclipse spectrophotometer and the measurements were conducted from 300 nm to 700 nm. The wavelengths, at which polymers exhibited maximum absorption in UV-vis spectra, were chosen for the excitation wavelength of fluorescence measurement.

3.2.9. Cyclic voltammetric measurements

Cyclic voltammetry (CV) measurements were performed using a potentiostat/galvanostat (AUTOLAB/PGSTAT 302N) which was run by General Purpose Electrochemical System software (GPES) installed in computer. All the experiments were done under nitrogen atmosphere at room temperature. The system consisted of a CV cell containing glassy carbon (GCE) as the working electrode, platinum wire as the counter electrode, and Ag/AgCl as the reference electrode. The electrochemical potential of Ag/AgCl electrode was calibrated with respect to the ferrocene/ferrocenium (Fc/Fc⁺) couple.

3.2.10. Rheological measurements

The rheological behaviour of the polymers was investigated using a Rheometer Physica MCR301 with 15 mm parallel plates. Prior to any test the zero-gap between the parallel plates was calibrated at 5°C above their clearing temperature. In every measurement, the sample was placed between preheated fixtures and 15 min were allowed to reach thermal equilibrium before the gap was set to 0.2 mm. For temperature

changes, the control system needed about 5 min to reach a target equilibrium temperature with an error of 1~2°C. For dynamic oscillatory shearing the linear viscoelastic region of 1% strain was first obtained by strain sweep tests and no pre-shear was applied.

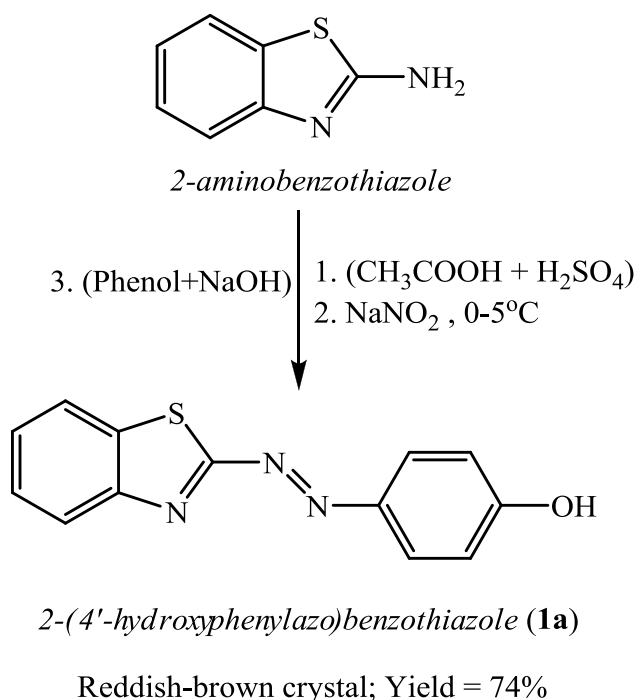
3.3. Synthesis and characterization of LC monomers, M1-M6

The synthetic method and structural characterization of intermediate and final compounds (LC monomers) are described in the following sections. The structural characterization of compounds was conducted by ¹H NMR, ¹³C NMR and FT-IR spectroscopic techniques. The synthesis of intermediate compounds **1a** and **2a** and monomer **M1** is described in detail as an example.

3.3.1. Synthesis of monomer M1

2-(4'-hydroxyphenylazo)benzothiazole (1a)

The synthesis of *2-(4'-hydroxyphenylazo)benzothiazole (1a)* is presented in Scheme 3.1. *2-Aminobenzothiazole* (1.5020 g, 10 mmol) was dissolved in glacial acetic acid (38 mL) containing concentrated sulphuric acid (22 mL) and cooled to 0-5°C in an ice bath. The ice-cold solution of sodium nitrite (14 mmol, 0.9700 g) in water (5.0 mL) was added dropwise to the reaction mixture with constant stirring to obtain the diazonium salt. After complete addition, the resultant mixture was left in an ice bath for 1 h and alkaline phenolic (10 mmol, 0.9400 g) solution (15% NaOH, 20 mL) was added dropwise to the ice cold diazonium salt solution to obtain a red coloured azo compound. The resultant reaction mixture was further stirred for 2 h and then filtered. The obtained red solid was washed with water, warm ethanol and finally crystallized from DMF-CHCl₃ (2:1) mixture to obtain reddish-brown crystal, *2-(4'-hydroxyphenylazo)benzothiazole (1a)*.

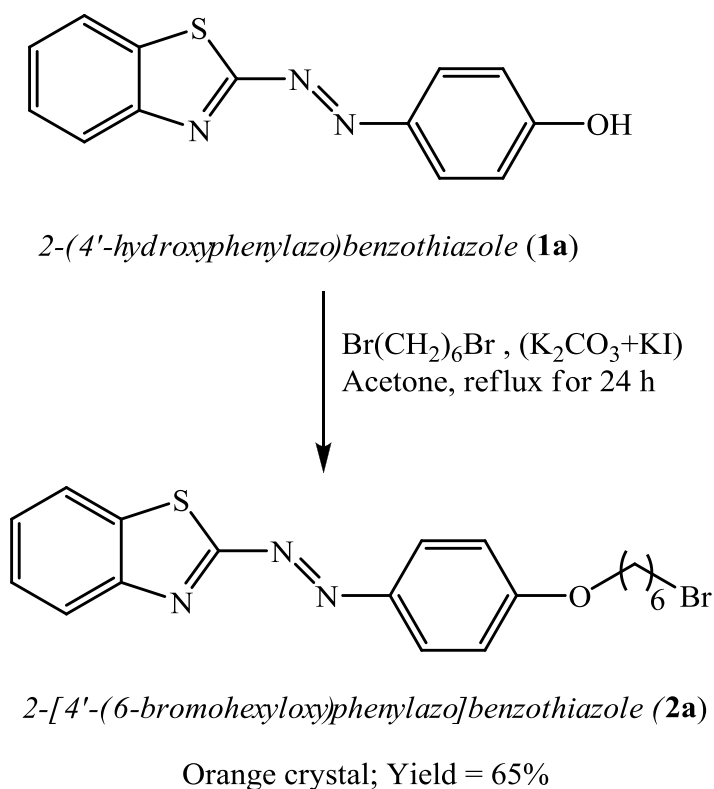


Scheme 3.1: Synthesis of *2-(4'-hydroxyphenylazo) benzothiazole (1a)*

Yield: 74%, mp: 286-288°C, ¹H NMR (400 MHz, DMSO-D₆) δ (ppm): 11.01 (s, 1H, -OH), 8.15-8.05 (d, 2H, benzo-H), 7.98-7.90 (d, 2H, Ar-H), 7.60-7.50 (t, 2H, benzo-H), 7.08-6.98 (d, 2H, Ar-H), ¹³C NMR (400 MHz, DMSO-D₆) δ (ppm): 176.2 (benzo-C-N=N-), 164.5 (Ar-C-OH), 152.8 (benzo-C-N), 145.1 (benzo-C-S), 134.0 (Ar-C-N=N-), 127.9, 127.5, 127.4, 124.6, 123.4, 117.7 (Ar-C), FT-IR (cm⁻¹): 3030 (C-H, aromatic), 2938, 2881, 2677, 2599, 2370, 1605 (C=N), 1578 (C-C, aromatic), 1458 (-N=N-), 1379 (C-N), 1296 (C-O), 1234, 1194, 1139, 1060 (benzothiazole), 898, 841, 758, 724, 645 (C-S-C).

2-[4'-(6-bromohexyloxy)phenylazo]benzothiazole (2a)

The synthesis of *2-[4'-(6-bromohexyloxy)phenylazo]benzothiazole (2a)* is depicted in Scheme 3.2. A mixture of *2-(4'-hydroxyphenylazo)benzothiazole* (2.3500 g, 9.2 mmol), potassium carbonate (1.9044 g, 13.8 mmol), potassium iodide (50 mg) and acetone (200 mL) was refluxed with stirring for 2 h at 80°C followed by addition of 1,6-dibromohexane (13.4100 g, 55 mmol) and was further refluxed for 22 h at 80°C.



Scheme 3.2: Synthesis of 2-[4'-(6-bromohexyloxy)phenylazo] benzothiazole (**2a**)

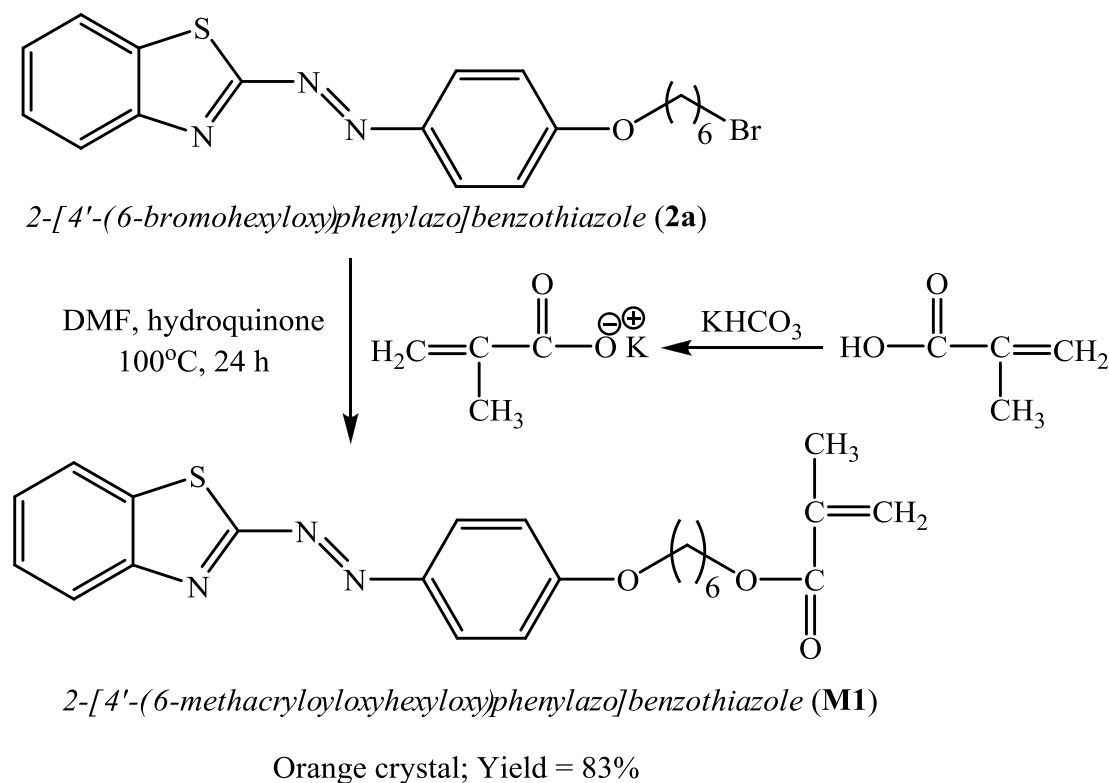
The reaction mixture was filtered under hot condition and the solvent was removed under reduced pressure. 100 mL petroleum ether (40-60°C) was added to the obtained concentrated mixture and kept overnight in refrigerator. The solid was filtered off and hot filtration was carried out using ethanol-chloroform (2:1) mixture and then recrystallized three times with ethanol-chloroform mixture. The orange crystal 2-[4'-(6-bromohexyloxy)phenylazo]benzothiazole (**2a**) was filtered off, washed with cold ethanol and dried at 40°C in vacuum oven.

Yield: 65%, mp: 146-148°C, ¹H NMR (400 MHz, CDCl₃) δ (ppm): 8.12-8.07 (d, 1H, benzo-H), 8.04-8.97 (d, 2H, Ar-H), 7.84-7.80 (d, 1H, benzo-H), 7.46-7.36 (m, 2H, benzo-H), 7.17-6.96 (d, 2H, Ar-H), 4.08-4.00 (t, 2H, -O-CH₂-), 3.42-3.36 (t, 2H, -CH₂-Br), 1.91-1.75 (4H, m, -CH₂-), 1.49-1.43 (4H, m, -CH₂-). ¹³C NMR (400 MHz, CDCl₃) δ (ppm): 176.3 (benzo-C=N=N-), 164.0 (Ar-C-O-), 152.8 (benzo-C-N), 146.2 (benzo-C-S), 134.4 (Ar-C-N=N-), 127.2, 126.8, 126.6, 124.7, 122.3, 115.2 (Ar-C), 68.4,

33.8, 32.7, 29.0, 28.0, 25.3 (aliphatic-C), **FT-IR** (cm^{-1}): 3057 (C-H, aromatic), 2940, 2866 (C-H, aliphatic), 2253, 2144, 1972, 1599 (C=N), 1577 (C-C, aromatic) 1493, 1472, 1455 (-N=N-), 1429, 1383 (C-N), 1297 (C-O), 1261, 1181, 1138, 1064 (benzothiazole), 1003, 839, 758, 728, 692, 642 (C-S-C).

2-[4'-(6-methacryloyloxyhexyloxy)phenylazo]benzothiazole (M1)

The synthesis of *2-[4'-(6-methacryloyloxyhexyloxy)phenylazo]benzothiazole (M1)* is illustrated in Scheme 3.3. Methacrylic acid (0.7740 g, 9 mmol) was added slowly into potassium hydrogen carbonate (0.9000 g, 9 mmol) for 5 min at room temperature to form potassium methacrylate.



Scheme 3.3: Synthesis of *2-[4'-(6-methacryloyloxyhexyloxy)phenylazo]benzothiazole (M1)*

The reaction mixture was heated with stirring at 100°C for 24 h. After cooling to room temperature, the reaction mixture was poured into water (200mL) and the product was

extracted with dichloromethane (DCM). The organic layer was washed several times with water and then dried over anhydrous magnesium sulfate. The solid was filtered off and solvent was removed under reduced pressure. The colored solid was recrystallized with ethanol and finally the product was purified by column chromatography using silica gel as stationary phase and CHCl_3 as eluent. The obtained orange colored crystal 2-[4'-(6-methacryloyloxyhexyloxy)phenylazo]benzothiazole (**M1**) was dried at 40°C in vacuum oven overnight.

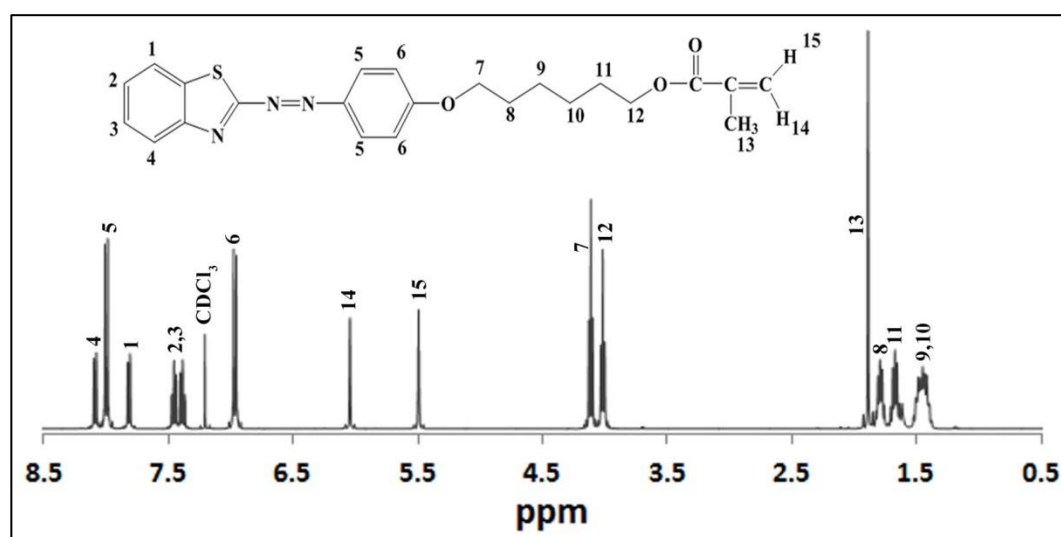


Figure 3.1: ^1H NMR spectrum of monomer **M1**

Yield: 83%, mp: $104\text{-}106^\circ\text{C}$, ^1H NMR (400 MHz, CDCl_3) δ (ppm): 8.12-8.06 (d, 1H, benzo-H), 8.04-7.97 (d, 2H, Ar-H), 7.86-7.8 (d, 1H, benzo-H), 7.48-7.43 (t, 2H, benzo-H), 7.41-7.35 (t, 2H, benzo-H), 6.99-6.93 (d, 2H, Ar-H), 6.05 (s, 1H, $=\text{CH}_2$), 5.50 (s, 1H, $=\text{CH}_2$), 4.15-4.09 (t, 2H, $-\text{OCH}_2-$), 4.05-3.97 (t, 2H, $-\text{OCH}_2-$), 1.90 (s, 3H, $-\text{CH}_3$), 1.83-1.75 (m, 2H, $-\text{CH}_2-$), 1.71-1.61 (m, 2H, $-\text{CH}_2-$), 1.53-1.37 (m, 4H, $-\text{CH}_2-$), ^{13}C NMR (100 MHz, CDCl_3) δ (ppm): 176.3 ($-\text{O}-\text{C}=\text{O}-$), 167.6 (benzo- $\text{C}-\text{N}=\text{N}-$), 164.0 (Ar- $\text{C}-\text{O}-$), 152.8 (benzo- $\text{C}-\text{N}$), 146.2 (benzo- $\text{C}-\text{S}$), 136.6 ($-\text{C}(\text{CH}_3)=\text{CH}_2$), 134.4 (Ar- $\text{C}-\text{N}=\text{N}-$), 126.8, 126.6 (Ar- C), 125.3 ($-\text{C}(\text{CH}_3)=\text{CH}_2$), 124.7, 122.3, 115.3 (Ar- C), 68.5, 64.7 ($-\text{OCH}_2$), 29.1, 28.6, 25.8, 25.7, 18.4 (aliphatic- C), FT-IR (cm^{-1}): 3064 (C-H,

aromatic), 2936 2870 (C-H, aliphatic), 2130, 1974, 1711 (C=O), 1636 (C=C), 1601 (C=N), 1574 (C-C, aromatic), 1491, 1471, 1453 (-N=N-), 1390 (C-N), 1312, 1296 (C-O), 1265, 1244, 1163, 1141, 1110, 1060 (benzothiazole), 1002, 936, 836, 805, 764, 730, 689, 629 (C-S-C).

3.3.2. Synthesis of monomer M2

2-(4'-hydroxyphenylazo)-6-methylbenzothiazole (1b)

The synthesis of compound **1b** was similar to that described for compound **1a**. Orange-red solid, yield: 72%, mp: 297-299°C, ¹H NMR (400 MHz, DMSO-D₆) δ (ppm): 10.97 (s, 1H, -OH), 7.96-7.91 (d, 1H, benzo-H), 7.90-7.85 (d, 2H, Ar-H), 7.81 (s, 1H, benzo-H), 7.36-7.31 (d, 1H, benzo-H), 7.02-6.95 (d, 2H, Ar-H), 2.41 (s, 3H, -CH₃), ¹³C NMR (100 MHz, DMSO-D₆) δ (ppm): 175.3 (benzo-C-N=N-), 164.3 (Ar-C-OH), 150.9 (benzo-C-N), 145.1 (benzo-C-S), 138.1 (Ar-C-CH₃), 134.1 (Ar-C-N=N-), 128.9, 127.3, 124.3, 122.9, 117.3 (Ar-C), 21.8 (-CH₃), FT-IR (cm⁻¹): 3042 (C-H, aromatic), 2938, 2696, 2696, 2618, 1899, 1605 (C=N), 1581 (C-C, aromatic), 1498, 1464 (-N=N-), 1382 (C-N), 1299 (C-O), 1243, 1178, 1137 (benzothiazole), 910, 840, 806, 704, 636 (C-S-C).

2-[4'-(6-bromohexyloxy)phenylazo]-6-methylbenzothiazole (2b)

The synthesis of compound **2b** was similar to that described for compound **2a**. Orange-yellow crystal, yield: 70%, mp: 126-128°C, ¹H NMR (400 MHz, CDCl₃) δ (ppm): 8.08-7.95 (m, 3H, benzo + Ar-H), 7.64 (s, 1H, benzo-H), 7.32-7.28 (m, 1H, benzo-H), 7.30 (d, 2H, Ar-H), 4.13-4.01 (t, 2H, -OCH₂-), 3.46-3.36 (t, 2H, -CH₂-Br), 2.48 (s, 3H, -CH₃), 1.95 (m, 4H, -CH₂-), 1.49-1.42 (m, 4H, -CH₂-), ¹³C NMR (100 MHz, CDCl₃) δ (ppm): 175.4 3 (benzo-C-N=N-), 163.8 (Ar-C-O-), 151.0 (benzo-C-N), 146.2 (benzo-C-S), 137.7 (Ar-C-CH₃), 134.5 (Ar-C-N=N-), 128.3, 126.7, 124.3, 122.0,

115.2 (Ar-C), 68.4, 33.8, 32.7, 29.0, 28.0, 25.3 (aliphatic-C), **FT-IR** (cm⁻¹): 3055 (C-H, aromatic), 2942, 2871 (C-H, aliphatic), 2212, 2151, 1987, 1597 (C=N), 1572 (C-C, aromatic), 1493, 1471 (-N=N-), 1430, 1387 (C-N), 1298 (C-O), 1261, 1170, 1142, 1032 (benzothiazole), 1003, 945, 853, 817, 740, 694, 628 (C-S-C).

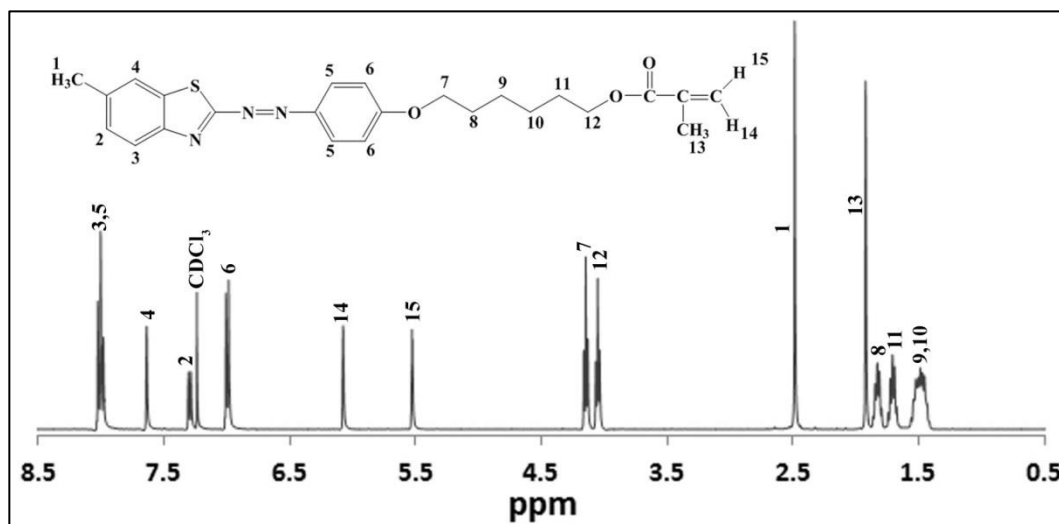


Figure 3.2: ¹H NMR spectrum of monomer **M2**

2-[4'-(6-methacryloyloxyhexyloxy)phenylazo]-6-methylbenzothiazole, (M2)

The synthesis of monomer **M2** was similar to that described for monomer **M1**. Orange-yellow crystal, yield: 80%, mp: 114-116°C, ¹H NMR (400 MHz, CDCl₃) δ (ppm): 8.0-7.9 (m, 3H, benzo + Ar-H), 7.6 (s, 1H, benzo-H), 7.27-7.24 (d, 1H, benzo-H), 6.98-6.92 (d, 2H, Ar-H), 6.05 (s, 1H, =CH₂), 5.48 (s, 1H, =CH₂), 4.12-4.06 (t, 2H, -OCH₂-), 4.01-3.96 (t, 2H, -OCH₂-), 2.42 (s, 3H, -CH₃), 1.9 (s, 3H, -CH₃) 1.78-1.72 (m, 2H, -CH₂-), 1.70-1.60 (m, 2H, -CH₂-), 1.50-1.32 (m, 4H, -CH₂-), ¹³C NMR (100 MHz, CDCl₃) δ (ppm): 175.4 (-O-CO-), 167.6 (benzo-C-N=N-), 163.8 (Ar-C-O-), 151.0 (benzo-C-N), 146.2 (benzo-C-S), 137.7 (-C(CH₃)=CH₂), 136.6 (Ar-C-CH₃), 134.5 (Ar-C-N=N-), 128.3, 126.7 (Ar-C), 125.3 (-C(CH₃)=CH₂), 124.3, 122.0, 115.2 (Ar-C), 68.5, 64.7, 29.1, 28.6, 25.8, 25.7, 21.9, 18.4 (aliphatic-C), **FT-IR** (cm⁻¹): 3055 (C-H, aromatic), 2936, 2870, 2855 (C-H, aliphatic), 2396, 2136, 1970, 1711 (C=O), 1636

(C=C), 1601 (C=N), 1577 (C-C, aromatic), 1557, 1491, 1473 (-N=N-), 1438, 1386 (C-N), 1297 (C-O), 1263, 1170, 1144, 1112, 1069 (benzothiazole), 1003, 934, 837, 808, 727, 682, 630 (C-S-C).

3.3.3. Synthesis of monomer M3

2-(4'-hydroxyphenylazo)-6-methoxybenzothiazole (1c)

The synthesis of compound **1c** was similar to that described for compound **1a**. Dark-red solid, yield: 86%, mp: 276-278°C, $^1\text{H NMR}$ (400 MHz, DMSO- D_6) δ (ppm): 10.84 (s, 1H, -OH), 7.96-7.93 (d, 1H, benzo-H), 7.88-7.84 (d, 2H, Ar-H), 7.62 (s, 1H, benzo-H), 7.13-7.07 (m, 1H, benzo-H), 6.97-6.93 (d, 2H, Ar-H), 3.84 (s, 3H, -OCH₃), $^{13}\text{C NMR}$ (100 MHz, DMSO- D_6) δ (ppm): 173.8 (benzo- $\underline{\text{C}}$ -N=N-), 163.9 (Ar- $\underline{\text{C}}$ -OH), 159.5 (Ar- $\underline{\text{C}}$ -OCH₃), 147.3 (benzo- $\underline{\text{C}}$ -N), 145.1 (benzo- $\underline{\text{C}}$ -S), 135.9 (Ar- $\underline{\text{C}}$ -N=N-), 127.1, 125.5, 117.2, 116.9, 105.7 (Ar- $\underline{\text{C}}$), 56.4 (-OCH₃), **FT-IR** (cm^{-1}): 3053 (C-H, aromatic), 2950, 2835, 2695, 1904, 1655, 1603 (C=N), 1581 (C-C, aromatic), 1469 (-N=N-), 1378 (C-N), 1298(C-O), 1136, 1057 (benzothiazole), 1027, 909, 841, 765, 697, 637 (C-S-C).

2-[4'-(6-bromohexyloxy)phenylazo]-6-methoxybenzothiazole (2c)

The synthesis of compound **2c** was similar to that described for compound **2a**. Orange crystal, yield: 65%, mp: 107-109°C, $^1\text{H NMR}$ (400 MHz, CDCl₃) δ (ppm): 8.05-7.95 (m, 3H, benzo + Ar-H), 7.3-7.28 (d, 1H, benzo-H), 7.11-7.07 (m, 1H, benzo-H), 7.03-6.98 (d, 2H, Ar-H), 4.09-4.03 (t, 2H, -O-CH₂-), 3.89 (s, 3H, -CH₃), 3.48-3.38 (t, 2H, -CH₂-Br), 1.98-1.72 (4H, m, -CH₂-), 1.48-1.40 (4H, m, -CH₂-). $^{13}\text{C NMR}$ (100 MHz, CDCl₃) δ (ppm): 174.1 (benzo- $\underline{\text{C}}$ -N=N-), 163.6 (Ar- $\underline{\text{C}}$ -O-), 159.4 (Ar- $\underline{\text{C}}$ -OCH₃), 147.5 (benzo- $\underline{\text{C}}$ -N), 146.2 (benzo- $\underline{\text{C}}$ -S), 136.2 (Ar- $\underline{\text{C}}$ -N=N-), 126.5, 125.5, 116.3, 115.2, 104.5 (Ar- $\underline{\text{C}}$), 68.9, 55.9, 33.8, 32.7, 29.0, 28.0, 25.3 (aliphatic- $\underline{\text{C}}$), **FT-IR** (cm^{-1}): 3000

(C-H, aromatic), 2938, 2868 (C-H, aliphatic), 2115, 1596 (C=N), 1577 (C-C, aromatic), 1552, 1493, 1462 (-N=N-), 1436, 1383 (C-N), 1319, 1297 (C-O), 1258, 1225, 1167, 1143, 1114, 1053 (benzothiazole), 1024, 891, 835, 811, 729, 693, 646 (C-S-C).

2-[4'-(6-methacryloyloxyhexyloxy)phenylazo]-6-methoxybenzothiazole, (**M3**)

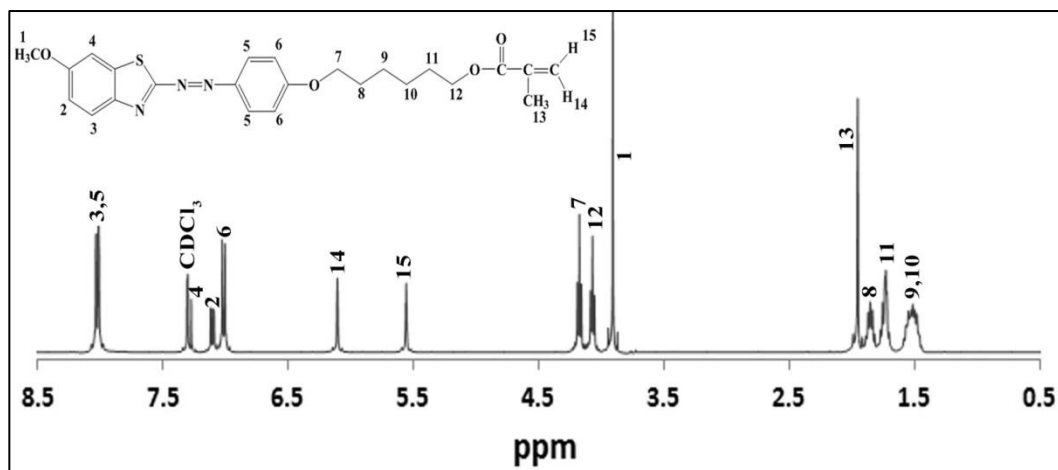


Figure 3.3: ^1H NMR spectrum of monomer **M3**

The synthesis of monomer **M3** was similar to that described for monomer **M1**. Orange crystal, yield: 75%, mp: 90-92°C, ^1H NMR (400 MHz, CDCl_3) δ (ppm): 8.08-7.9 (m, 3H, benzo + Ar-H), 7.33-7.30 (d, 1H, benzo-H), 7.13-7.08 (m, 1H, benzo-H), 7.06-7.0 (d, 2H, Ar-H), 6.11 (s, 1H, =CH₂), 5.58 (s, 1H, =CH₂), 4.20-4.12 (t, 2H, -OCH₂-), 4.10-4.02 (t, 2H, -OCH₂-), 3.89 (s, 3H, -OCH₃), 1.93 (s, 3H, -CH₃) 1.88-1.82 (m, 2H, -CH₂-), 1.80-1.70 (m, 2H, -CH₂-), 1.58-1.45 (m, 4H, -CH₂-), ^{13}C NMR (100 MHz, CDCl_3) δ (ppm): 174.1(-O-C=O), 167.6 (benzo-C-N=N-), 163.6 (Ar-C-O-), 159.4 (Ar-C-OCH₃), 147.5 (benzo-C-N), 146.2 (benzo-C-S), 136.6 (-C(CH₃)=CH₂), 136.2 (Ar-C-N=N-), 126.5, 125.5 (Ar-C), 125.3 (-C(CH₃)=CH₂), 116.2, 115.1, 104.5 (Ar-C), 68.4, 64.7, 55.9, 29.1, 28.6, 25.8, 25.7, 18.4 (aliphatic-C), **FT-IR** (cm^{-1}): 3065 (C-H, aromatic), 2941, 2868 (C-H, aliphatic), 2140, 1974, 1713 (C=O), 1637 (C=C), 1597 (C=N), 1576 (C-C, aromatic), 1489, 1467 (-N=N-), 1438, 1388 (C-N), 1338, 1318,

1296 (C-O), 1261, 1225, 1163, 1143, 1111, 1052 (benzothiazole), 1004, 942, 852, 829, 727, 692, 628 (C-S-C).

3.3.4. Synthesis of monomer M4

2-(4'-hydroxyphenylazo)-6-ethoxybenzothiazole (1d)

The synthesis of compound **1d** was similar to that described for compound **1a**. Dark-red solid, yield: 80%, mp: 256-258°C, **¹H NMR** (400 MHz, DMSO-D₆) δ (ppm): 10.94 (s, 1H, -OH), 7.98-7.94 (d, 1H, benzo-H), 7.80-7.84 (d, 2H, Ar-H), 7.59 (s, 1H, benzo-H), 7.15-7.08 (d, 1H, benzo-H), 7.04-6.94 (d, 2H, Ar-H), 4.16-4.04 (q, 2H, -OCH₂-), 1.38-1.31 (t, 3H, -CH₃), **¹³C NMR** (100 MHz, DMSO-D₆) δ (ppm): 173.8 (benzo-C-N=N-), 163.9 (Ar-C-OH), 158.8 (Ar-C-OCH₂CH₃), 147.2 (benzo-C-N), 145.1 (benzo-C-S), 135.9 (Ar-C-N=N-), 127.1, 125.5, 117.1, 115.1, 106.2 (Ar-C), 64.4 (-O-CH₂CH₃), 15.1 (-O-CH₂CH₃), **FT-IR** (cm⁻¹): 3042 (C-H, aromatic), 2981, 2935, 2695, 1605 (C=N), 1576 (C-C, aromatic), 1498, 1465 (-N=N-), 1381 (C-N), 1297 (C-O), 1217, 1135, 1061 (benzothiazole), 945, 898, 842, 824, 703, 619, 637 (C-S-C).

2-[4'-(6-bromohexyloxy)phenylazo]-6-ethoxybenzothiazole (2d)

The synthesis of compound **2d** was similar to that described for compound **2a**. Radish-brown crystal, yield: 62%, mp: 110-112°C, **¹H NMR** (400 MHz, CDCl₃) δ (ppm): 8.06-7.96 (m, 3H, benzo + Ar-H), 7.28-7.26 (d, 1H, benzo-H), 7.10-7.05 (m, 1H, benzo-H), 7.03-6.96 (d, 2H, Ar-H), 4.15-4.03 (m, 4H, -O-CH₂-), 3.45-3.38 (t, 2H, -CH₂-Br), 1.95-1.78 (4H, m, -CH₂-), 1.54-1.50 (4H, m, -CH₂-), 1.48-1.43 (t, 3H, -CH₃), **¹³C NMR** (100 MHz, CDCl₃) δ (ppm): 174.0 (benzo-C-N=N-), 163.6 (Ar-C-O-), 158.8 (Ar-C-OCH₂CH₃), 147.4 (benzo-C-N), 146.2 (benzo-C-S), 136.2 (Ar-C-N=N-), 126.5, 125.5, 116.6, 115.1 (Ar-C), 68.4, 64.2, 33.8, 32.7, 29.0, 28.0, 25.3, 15.0 (aliphatic-C), **FT-IR** (cm⁻¹): 3070 (C-H, aromatic), 2981, 2938, 2868 (C-H, aliphatic), 2137, 1595

(C=N), 1575 (C-C, aromatic), 1492, 1472, 1455 (-N=N-), 1438, 1385 (C-N), 1314, 1297 (C-O), 1258, 1225, 1144, 1112, 1053 (benzothiazole), 1032, 941, 891, 836, 730, 695, 654 (C-S-C).

2-[4'-(6-methacryloyloxyhexyloxy)phenylazo]-6-ethoxybenzothiazole, (**M4**)

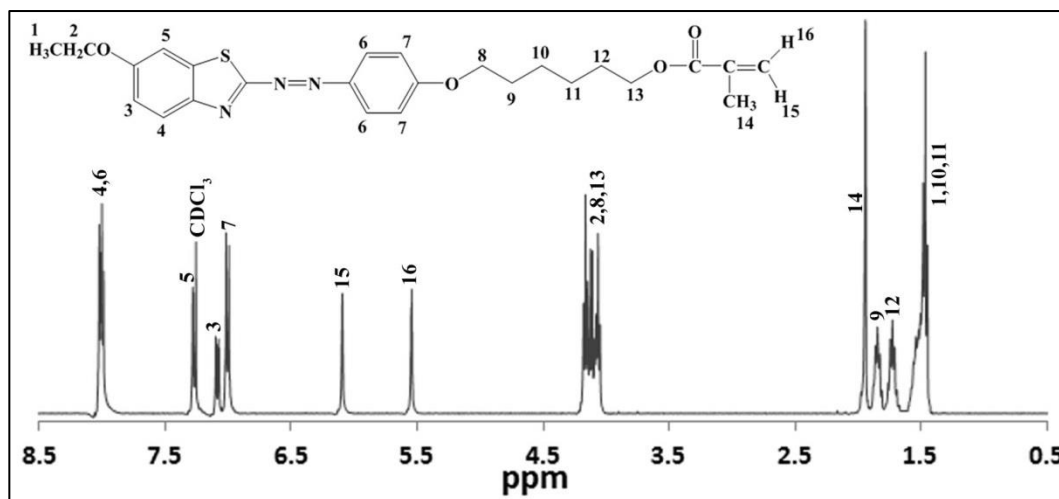


Figure 3.4: ^1H NMR spectrum of monomer **M4**

The synthesis of monomer **M4** was similar to that described for monomer **M1**. Orange crystal, yield: 78%, mp: 95-97°C, ^1H NMR (400 MHz, CDCl_3) δ (ppm): 8.04-7.97 (m, 3H, benzo + Ar-H), 7.30-7.27 (d, 1H, benzo-H), 7.11-7.06 (m, 1H, benzo-H), 7.03-6.97 (d, 2H, Ar-H), 6.09 (s, 1H, =CH₂), 5.54 (s, 1H, =CH₂), 4.19-4.04 (m, 6H, -OCH₂-), 1.94 (s, 3H, -CH₃), 1.88-1.80 (m, 2H, -CH₂-), 1.77-1.69 (m, 2H, -CH₂-), 1.57-1.50 (m, 4H, -CH₂-), 1.48-1.43 (t, 3H, -CH₃), ^{13}C NMR (100 MHz, CDCl_3) δ (ppm): 174.0 (-O-C=O), 167.6 (benzo-C-N=N-), 163.6 (Ar-C-O-), 158.8 (Ar-C-OCH₂CH₃), 147.4 (benzo-C-N), 146.2 (benzo-C-S), 136.6 (-C(CH₃)=CH₂), 136.2 (Ar-C-N=N-), 126.5, 125.5 (Ar-C), 125.3 (-C(CH₃)=CH₂), 116.6, 115.1, 105.1 (Ar-C), 68.4, 64.7, 64.2, 29.1, 28.6, 25.9, 25.8, 18.4, 14.9 (aliphatic-C), FT-IR (cm⁻¹): 3045 (C-H, aromatic), 2943, 2865 (C-H, aliphatic), 2130, 1974, 1710 (C=O), 1633 (C=C), 1600 (C=N), 1574 (C-C, aromatic), 1491, 1471, 1453 (-N=N-), 1390 (C-N), 1312, 1296 (C-

O), 1265, 1244, 1163, 1141, 1110, 1060 (benzothiazole), 1002, 936, 836, 805, 764, 730, 689, 629 (C-S-C).

3.3.5. Synthesis of monomer M5

2-(4'-hydroxyphenylazo)-6-fluorobenzothiazole (1e)

The synthesis of compound **1e** was similar to that described for compound **1a**. Dark-red solid, yield: 80%, mp: 306-308°C, ¹H NMR (400 MHz, DMSO-D₆) δ (ppm): 11.01 (s, 1H, -OH), 8.14-8.09 (m, 1H, benzo-H), 8.02–7.97 (m, 1H, benzo-H), 7.93-7.90 (d, 2H, Ar-H), 7.45-7.39 (m, 1H, benzo-H), 7.04-6.99 (d, 2H, Ar-H), ¹³C NMR (400 MHz, DMSO-D₆) δ (ppm): 176.3 (benzo-C-N=N-), 164.6 (Ar-C-OH), 149.6 (Ar-C-F), 144.9 (benzo-C-N), 135.2 (benzo-C-S), 127.5 (Ar-C-N=N-), 126.2, 117.2, 115.9, 109.7 (Ar-C), FT-IR (cm⁻¹): 2992 (C-H, aromatic), 1605 (C=N), 1577 (C-C, aromatic), 1500, 1458 (-N=N-), 1383 (C-N), 1296 (C-O), 1202, 1132, 1051 (benzothiazole), 945, 892, 852, 838, 733, 696, 634 (C-S-C).

2-[4'-(6-bromohexyloxy)phenylazo]-6-fluorobenzothiazole (2e)

The synthesis of compound **2e** was similar to that described for compound **2a**. Radish-brown crystal, yield: 62%, mp: 136-138°C, ¹H NMR (400 MHz, CDCl₃) δ (ppm): 8.03-7.95 (m, 3H, benzo + Ar-H), 7.49-7.46 (m, 1H, benzo-H), 7.20-7.15 (m, 1H, benzo-H), 6.98-6.94 (d, 2H, Ar-H), 4.11-4.08 (t, 2H, -O-CH₂-), 3.45-3.38 (t, 2H, -CH₂-Br), 1.80-1.62 (4H, m, -CH₂-), 1.49 -1.38 (4H, m, -CH₂-), ¹³C NMR (400 MHz, CDCl₃) δ (ppm): 176.2 (benzo-C-N=N-), 164.1 (Ar-C-O-), 149.2 (Ar-C-F), 146.0 (benzo-C-N), 135.7 (benzo-C-S), 126.6 (Ar-C-N=N-), 126.0, 115.8, 115.3, 108.6, 108.4 (Ar-C), 68.3, 33.8, 32.6, 29.1, 28.0, 25.2 (aliphatic-C), FT-IR (cm⁻¹): 3050 (C-H, aromatic), 2944, 2912, 2864 (C-H, aliphatic), 1597 (C=N), 1576 (C-C, aromatic), 1496,

1471 (-N=N-), 1383, 1341 (C-N), 1319, 1297 (C-O), 1247, 1202, 1136, 1109, 1048 (benzothiazole), 1021, 996, 892, 834, 724, 694, 648 (C-S-C).

2-[4'-(6-methacryloyloxyhexyloxy)phenylazo]-6-fluorobenzothiazole, (M5)

The synthesis of monomer **M5** was similar to that described for monomer **M1**. Orange crystal, yield: 73%, mp: 119-121°C, ¹H NMR (400 MHz, CDCl₃) δ (ppm): 8.03-7.95 (m, 3H, benzo + Ar-H), 7.49-7.46 (m, 1H, benzo-H), 7.19-7.16 (m, 1H, benzo-H), 6.97-6.93 (d, 2H, Ar-H), 6.02 (s, 1H, =CH₂), 5.48 (s, 1H, =CH₂), 4.11-3.99 (m, 4H, -OCH₂-), 1.87 (s, 3H, -CH₃), 1.80-1.74 (m, 2H, -CH₂-), 1.70-1.62 (m, 2H, -CH₂-), 1.49-1.38 (m, 4H, -CH₂-), ¹³C NMR (100 MHz, CDCl₃) δ (ppm): 175.9 (-O-C=O), 167.6 (benzo-C-N=N-), 164.1 (Ar-C-O-), 149.2 (Ar-C-F), 145.9 (benzo-C-N), 136.4 (benzo-C-S), 135.6 (-C(CH₃)=CH₂), 126.2(Ar-C-N=N-), 125.9, 115.4 (Ar-C), 115.2 (-C(CH₃)=CH₂), 108.6, 108.4, (Ar-C), 68.3, 64.6, 29.2, 28.8, 25.6, 25.8, 18.4 (aliphatic-C), FT-IR (cm⁻¹): 3036 (C-H, aromatic), 2946, 2911, 2872, 2855 (C-H, aliphatic), 2120, 1915, 1707 (C=O), 1635 (C=C), 1600 (C=N), 1577 (C-C, aromatic), 1493, 1472, 1458 (-N=N-), 1394 (C-N), 1337, 1316, 1297 (C-O), 1255, 1207, 1163, 1136, 1109 (benzothiazole), 1001, 938, 890, 863, 833, 803, 730, 695, 631 (C-S-C).

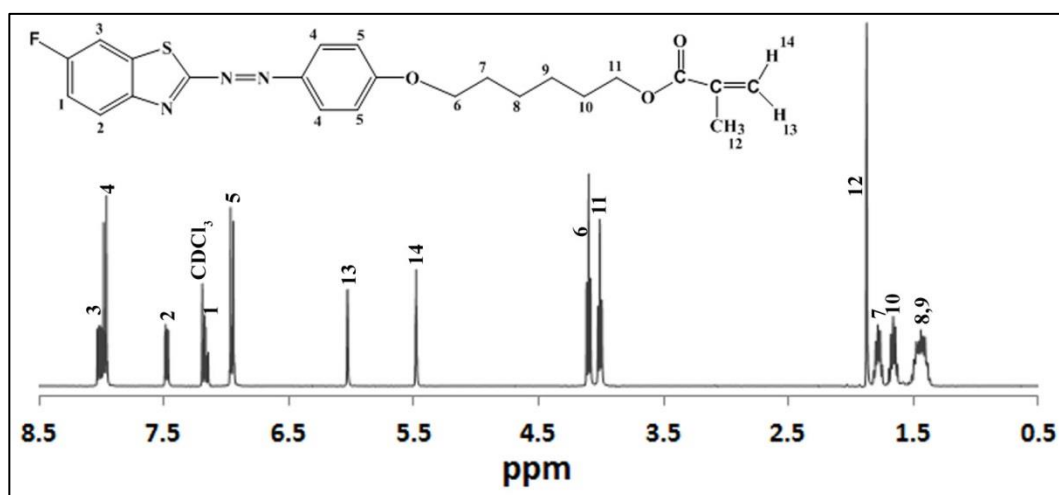


Figure 3.5: ¹H NMR spectrum of monomer **M5**

3.3.6. Synthesis of monomer M6

2-(4'-hydroxyphenylazo)-6-chlorobenzothiazole (1f)

The synthesis of compound **1f** was similar to that described for compound **1a**. Dark-red solid, yield: 80%, mp: 314-316°C, ¹H NMR (400 MHz, DMSO-D₆) δ (ppm): 11.05 (s, 1H, -OH), 8.26-8.22 (d, 1H, benzo-H), 8.10-8.05 (d, 1H, benzo-H), 7.94-7.89 (d, 2H, Ar-H), 7.60-7.56 (m, 1H, benzo-H), 7.04-6.98 (d, 2H, Ar-H), ¹³C NMR (400 MHz, DMSO-D₆) δ (ppm): 176.8 (benzo-C-N=N-), 164.7 (Ar-C-OH), 151.4 (Ar-C-Cl), 144.9 (benzo-C-N), 135.6 (benzo-C-S), 132.1 (Ar-C-N=N-), 127.9, 127.7, 125.8, 122.9, 117.2 (Ar-C), FT-IR (cm⁻¹): 3042 (C-H, aromatic), 2951, 2829, 2700, 2621, 1602 (C=N), 1574 (C-C, aromatic), 1496, 1461 (-N=N-), 1367 (C-N), 1293 (C-O), 1231, 1188, 1128, 1051 (benzothiazole), 897, 854, 839, 812, 774, 724, 694 (C-S-C).

2-[4'-(6-bromohexyloxy)phenylazo]-6-chlorobenzothiazole (2f)

The synthesis of compound **2f** was similar to that described for compound **2a**. Radish-brown crystal, yield: 62%, mp: 144-146°C, ¹H NMR (400 MHz, CDCl₃) δ (ppm): 8.06-7.81 (m, 3H, benzo + Ar-H), 7.84-7.81 (d, 1H, benzo-H), 7.46-7.43 (m, 1H, benzo-H), 7.03-6.97 (d, 2H, Ar-H), 4.10-4.02 (t, 2H, -O-CH₂-), 3.45-3.38 (t, 2H, -CH₂-Br), 1.93-1.78 (4H, m, -CH₂-), 1.55-1.45 (m, 4H, -CH₂-), ¹³C NMR (400 MHz, CDCl₃) δ (ppm): 176.5 (benzo-C-N=N-), 164.0 (Ar-C-O-), 151.3 (Ar-C-Cl), 145.8 (benzo-C-N), 135.6 (benzo-C-S), 132.8 (Ar-C-N=N-), 127.4, 126.9, 121.8, 115.1 (Ar-C), 68.4, 33.9, 32.5, 28.8, 27.9, 25.2 (aliphatic-C), FT-IR (cm⁻¹): 3065 (C-H, aromatic), 2936, 2865 (C-H, aliphatic), 2278, 1709, 1601 (C=N), 1575, 1545 (C-C, aromatic), 1489, 1471, 1463 (-N=N-), 1435, 1387 (C-N), 1339, 1305 (C-O), 1259, 1201, 1180, 1136, 1112, 1047 (benzothiazole), 1024, 918, 889, 838, 817, 765, 723, 690, 643 (C-S-C).

2-[4'-(6-methacryloyloxyhexyloxy)phenylazo]-6-chlorobenzothiazole (**M6**)

The synthesis of monomer **M6** was similar to that described for monomer **M1**. Orange crystal, yield: 72%, mp: 112-114°C, $^1\text{H NMR}$ (400 MHz, CDCl_3) δ (ppm): 8.04-7.94 (m, 3H, benzo + Ar-H), 7.83-7.79 (d, 1H, benzo-H), 7.47-7.40 (m, 1H, benzo-H), 7.04-6.96 (d, 2H, Ar-H), 6.07 (s, 1H, =CH₂), 5.52 (s, 1H, =CH₂), 4.19-4.10 (t, 2H, -OCH₂-), 4.10-4.02 (t, 2H, -OCH₂-), 1.92 (s, 3H, -CH₃), 1.89-1.77 (m, 2H, -CH₂-), 1.77-1.66 (m, 2H, -CH₂-), 1.56-1.40 (m, 4H, -CH₂-), $^{13}\text{C NMR}$ (400 MHz, CDCl_3) δ (ppm): 176.6 (-O-C=O), 167.8 (benzo-C-N=N-), 164.1 (Ar-C-O-), 150.9 (Ar-C-Cl), 146.2 (benzo-C-N), 136.7 (benzo-C-S), 135.4 (-C(CH₃)=CH₂), 132.9 (Ar-C-N=N-), 127.5, 127.1 (Ar-C), 125.3 (-C(CH₃)=CH₂), 122.2, 115.1 (Ar-C), 68.6, 64.3, 29.2, 28.6, 25.6, 18.3, (aliphatic-C), **FT-IR** (cm^{-1}): 3068 (C-H, aromatic), 2947, 2868 (C-H, aliphatic), 1903, 1709 (C=O), 1638 (C=C), 1601 (C=N), 1576 (C-C, aromatic), 1496, 1472, 1440 (-N=N-), 1390 (C-N), 1311, 1295 (C-O), 1255, 1172, 1138, 1109, 1053, 1026 (benzothiazole), 1009, 996, 965, 938, 835, 822, 768, 732, 691, 648 (C-S-C).

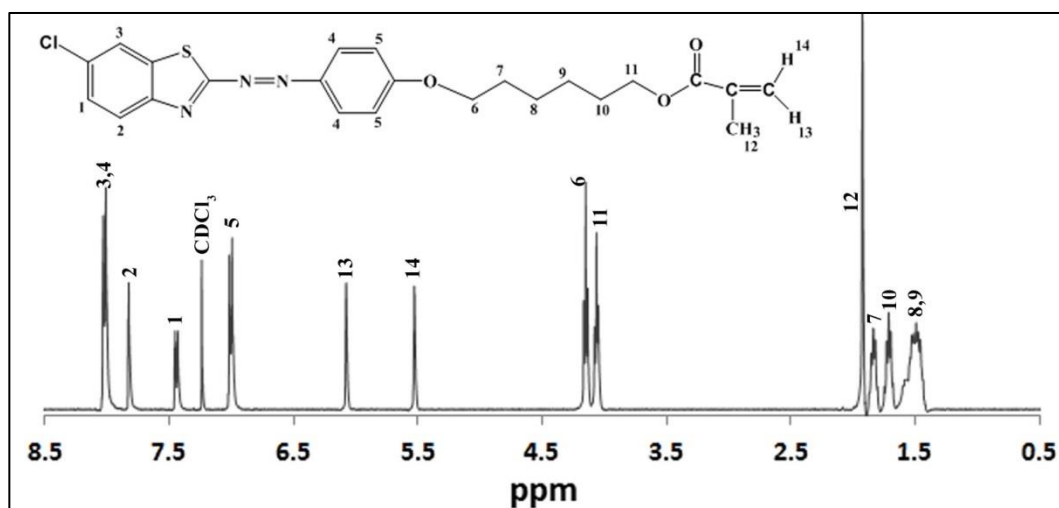


Figure 3.6: $^1\text{H NMR}$ spectrum of monomer **M6**

3.4. Synthesis and characterization of monomers M7-M10

The synthetic method and structural characterization of intermediate compounds *4-(6-hydroxyhexyloxy)benzoic acid* (**HHBA**), *4-(6-methacryloxyhexyloxy)benzoic acid* (**MHBA**) and final LC monomers **M7-M10** are described in the following sections. The structural identification of compounds was conducted by FT-IR, ¹H and ¹³C NMR spectroscopic techniques.

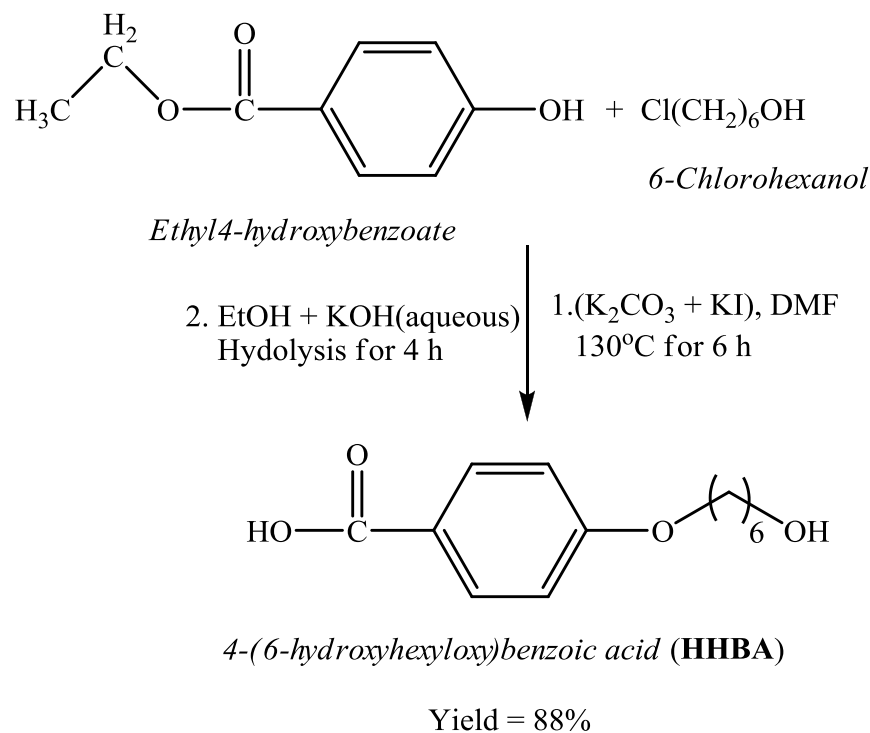
3.4.1. Synthesis of azo-benzothiazole dyes, **1w-1z**

The synthesis and characterization of *2-(4'-hydroxyphenylazo)benzothiazole* (**1w**); *2-(4'-hydroxyphenylazo)-6-methyl benzothiazole* (**1x**); *2-(4'-hydroxy phenylazo)-6-methoxybenzothiazole* (**1y**) and *2-(4'-hydroxyphenylazo)-6-ethoxy benzothiazole* (**1z**) were carried out by similar method that described for **1a-1d**.

3.4.2. Synthesis of *4-(6-hydroxyhexyloxy)benzoic acid* (**HHBA**)

4-(6-hydroxyhexyloxy)benzoic acid (**HHBA**) was synthesized according to Scheme 3.1. In a reaction flask, ethyl 4-hydroxybenzoate (7.5 g, 45 mmol), potassium carbonate (7.48 g, 54 mmol), potassium iodide (trace amount) and 6-chlorohexanol (7.34 g, 54 mmol) were dissolved in 100 mL DMF and the resulting mixture was heated at 130°C for 8 h. After completion of the reaction, the mixture was cooled to room temperature and then poured into water (200 mL). The product was then extracted with DCM and the organic phase was separated and dried over anhydrous magnesium sulphate. Next, DCM was evaporated under reduced pressure and a concentrated yellowish liquid was found. The obtained product was further dissolved in ethanol (100 mL) and then aqueous potassium hydroxide (7.6 g in 50 mL water) was added into the mixture. The resultant mixture was refluxed for 4 h and then cooled to room temperature. After that, the mixture was poured into water (200mL) and acidified with dilute hydrochloric acid

(2M). The obtained white product was then filtered off, washed with water and recrystallized from ethanol-water (10:1) mixture to get 4-(6-hydroxyhexyloxy)benzoic acid (**HHBA**).



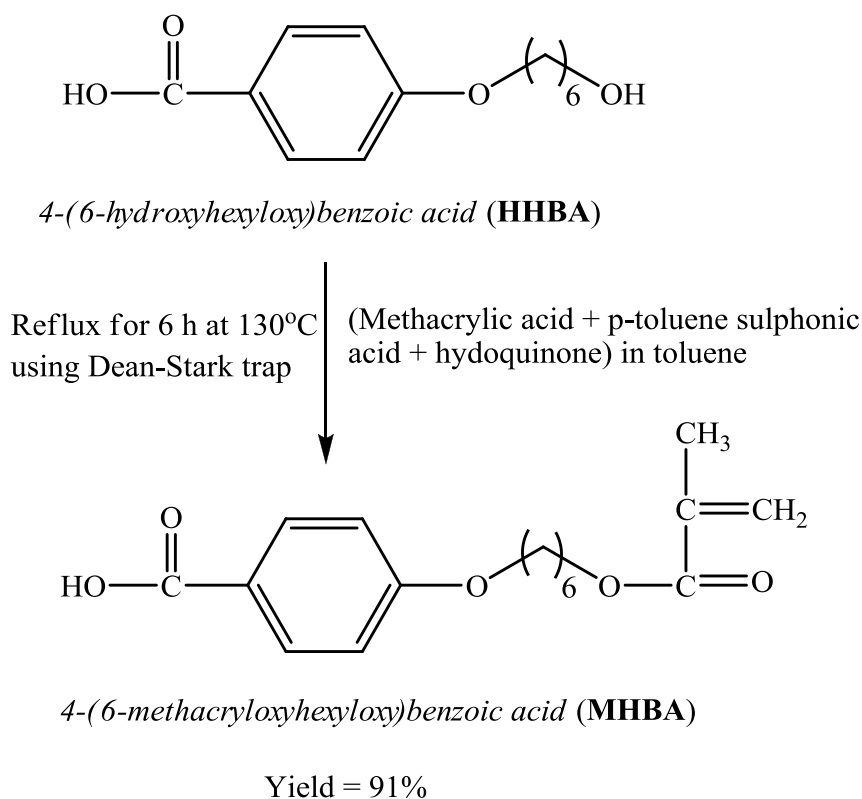
Scheme 3.4: Synthesis of 4-(6-hydroxyhexyloxy)benzoic acid (**HHBA**)

Yield: 88%, $^1\text{H NMR}$ (400 MHz, $\text{DMSO}-\text{D}_6$) δ (ppm): 12.56 (s, 1H, $-\text{COOH}$), 7.91-7.81 (d, 2H, Ar-H), 7.04-6.94 (d, 2H, Ar-H), 4.32 (1H, $-\text{OH}$), 4.07-3.96 (t, 2H, $-\text{OCH}_2-$), 3.43-3.36 (t, 2H, $-\text{CH}_2\text{OH}$), 1.78-1.64 (m, 2H, $-\text{CH}_2-$), 1.48-1.29 (m, 6H, $-\text{CH}_2-$). $^{13}\text{C NMR}$ (400 MHz, $\text{DMSO}-\text{D}_6$) δ (ppm): 166.9 ($-\text{C}=\text{O}$), 162.2, 131.2, 122.7, 114.1 (Ar-C), 67.6 ($-\text{OCH}_2-$), 60.6 ($-\text{CH}_2\text{OH}$), 32.4, 28.5, 25.3, 25.2 (aliphatic-C), **FT-IR** (cm^{-1}): 3337 ($-\text{OH}$), 2947, 2859 ($-\text{C}-\text{H}$, aliphatic), 1662 ($-\text{C}=\text{O}$), 1603, 1474 ($\text{C}=\text{C}$, aromatic), 1577 ($\text{C}-\text{C}$, aromatic), 1278, 1250 ($\text{C}-\text{O}$).

3.4.3. Synthesis of 4-(6-methacryloxyhexyloxy)benzoic acid (**MHBA**)

4-(6-Methacryloxyhexyloxy)benzoic acid (**MHBA**) was synthesized as shown in Scheme 3.5. Compound **HHBA** (5.0 g, 21 mmol), methacrylic acid (6.8840 g, 80

mmol), p-toluene sulphonic acid (1.3315 g, 7 mmol) and hydroquinone (0.4625g, 4.2 mmol) were added into a 500 mL two neck round bottom flask containing 100 mL toluene. The resultant mixture was refluxed at 130°C for 6 h using Dean-Stark trap to remove produced water from the reaction vessel. The obtained clear solution was diluted with diethyl ether and the resultant mixture was washed several times with warm water. The organic layer was separated, dried over anhydrous magnesium sulphate and then solvent was removed under reduced pressure. The obtained dull-white solid was recrystallized twice from isopropanol-water mixture (1:10) to get *4-(6-methacryloxyhexyloxy)benzoic acid (MHBA)*.



Scheme 3.5: Synthesis of *4-(6-methacryloxyhexyloxy)benzoic acid (MHBA)*

Yield: 91%, ¹H NMR (400 MHz, DMSO-D₆) δ (ppm): 12.56 (1H, -COOH), 7.91-7.81 (d, 2H, Ar-H), 7.03-6.92 (d, 2H, Ar-H), 6.00 (s, 1H, =CH₂), 5.64 (s, 1H, =CH₂), 4.14-3.96 (m, 4H, -OCH₂-), 1.85 (t, 3H, (-CH₃)), 1.78-1.68 (m, 2H, -CH₂-), 1.68-1.57 (m, 2H, -CH₂-), 1.49-1.33 (m, 4H, -(CH₂-)), ¹³C NMR (400 MHz, DMSO-

After stirring 24 h at room temperature, the precipitated solid was filtered out and DCM was removed under reduced pressure and then the resulting concentrated mixture was poured into distilled water (100 mL). The obtained colored product was again extracted with DCM and then the organic phase was washed with water several times, separated and dried over anhydrous magnesium sulphate. DCM was removed under reduced pressure and obtained orange colored solid was recrystallized twice from 2-propanol to get crystalline product monomer **M7**. Finally, monomer **M7** was purified by column chromatography using silica gel as stationary phase and chloroform as eluent.

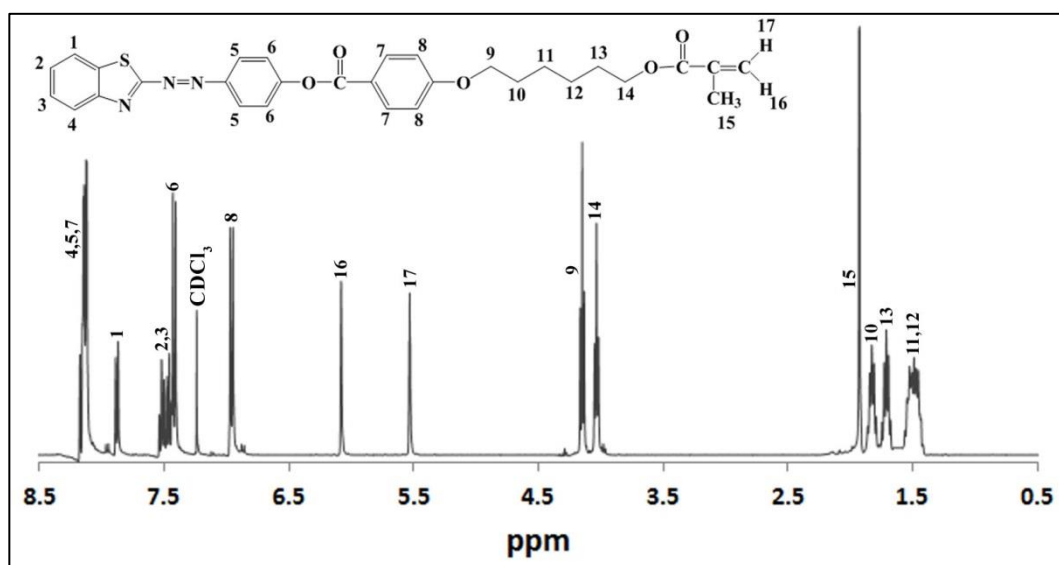


Figure 3.7: ^1H NMR spectrum of monomer **M7**

Yield: 40%, mp: 103-105°C, ^1H NMR (400 MHz, CDCl_3) δ (ppm): 8.18-8.05 (m, 5H, benzo + Ar-H), 7.90-7.83 (d, 1H, benzo-H), 7.56-7.39 (m, 4H, benzo + Ar-H), 6.99-6.91 (d, 2H, Ar-H), 6.08 (s, 1H, =CH₂), 5.54 (s, 1H, =CH₂), 4.18-4.12 (t, 2H, -OCH₂-), 4.06-3.99 (t, 2H, -OCH₂-), 1.92 (s, 3H, -CH₃), 1.89-1.77 (m, 2H, -CH₂-), 1.77-1.66 (m, 2H, -CH₂-), 1.68-1.40 (m, 4H, -CH₂-), ^{13}C NMR (400 MHz, CDCl_3) δ (ppm): 175.6 (-O-CO-), 167.5 (benzo-C-N=N-), 164.3 (Ar-O-CO-Ar), 163.8 (Ar-C-O-), 155.3 (Ar-C-O-CO-), 152.7 (benzo-C-N), 149.2 (benzo-C-S), 136.5 (-C(CH₃)=CH₂), 134.4 (Ar-C-N=N-), 132.5, 131.5, 127.6, 126.7, 126.7, 125.7, 125.0, 122.9, 122.3, 121.0,

114.4, 114.0 (Ar-C), 125.2 (-C(CH₃)=CH₂), 68.2 (-OCH₂-), 64.7 (-CH₂-O-), 30.9, 29.0, 28.7, 28.6, 25.8, 25.7, 18.4 (aliphatic-C), **FT-IR** (cm⁻¹): 3063 (C-H, aromatic), 2938, 2909, 2866 (C-H, aliphatic), 1717, 1706 (C=O), 1639 (C=C), 1604 (C=N), 1578 (C-C, aromatic), 1491, 1472, 1456 (-N=N-), 1396 (C-N), 1315, 1301, 1259 (C-O), 1220, 1195, 1167, 1122, 1106, 1060 (benzothiazole), 1005, 939, 844, 804, 756, 728, 691, 665 (C-S-C).

3.4.5. Synthesis of monomer **M8**

2-[4-(4'-(6-methacryloxyhexyloxybenzoyloxy))phenylazo]-6-methylbenzothiazole (**M8**)

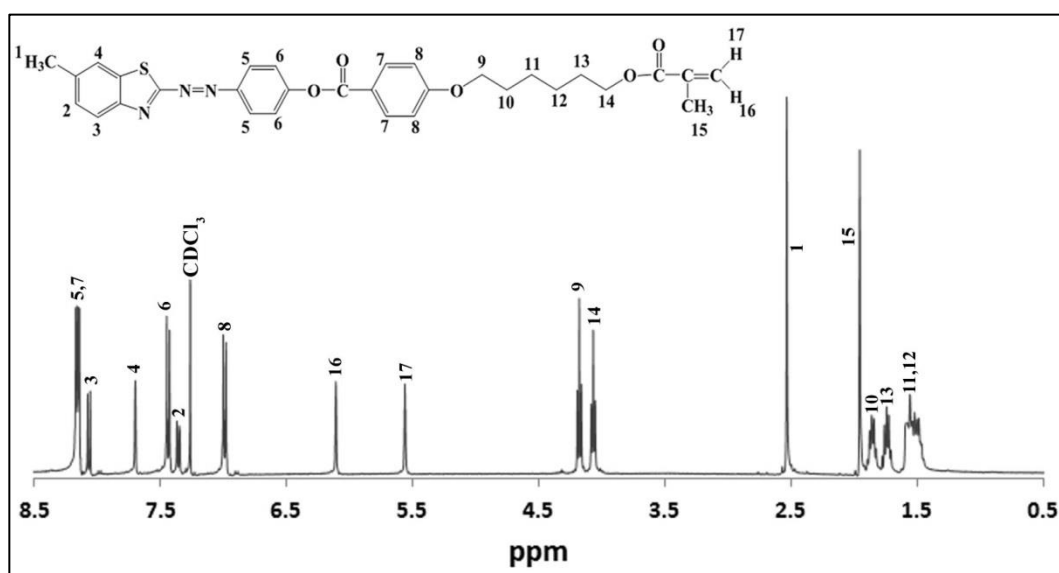


Figure 3.8: ¹H NMR spectrum of monomer **M8**

The synthesis of monomer **M8** was similar to that described for monomer **M7**. Yield: 30% , orange crystal; mp: 110-112°C, **¹H NMR** (400 MHz, CDCl₃) δ (ppm): 8.22-8.13 (m, 4H, Ar-H), 8.09-8.04 (d, 1H, benzo-H), 7.70 (s, 1H, benzo-H), 7.49-7.42 (d, 2H, Ar-H), 7.39-7.34 (d, 1H, benzo-H), 7.03-6.98 (d, 2H, Ar-H), 6.11(s, 1H, =CH₂), 5.56 (s, 1H, =CH₂), 4.21-4.14 (t, 2H, -OCH₂-), 4.11-4.01 (t, 2H, -OCH₂-), 2.53 (s, 3H, -CH₃), 1.95 (s, 3H, -CH₃), 1.91-1.79 (m, 2H, -CH₂-), 1.78-1.68 (m, 2H, -CH₂-), 1.67-1.43 (m, 4H, -CH₂-), **¹³C NMR** (100 MHz, CDCl₃) δ (ppm): 174.7 (-O-CO-), 167.5 (benzo-

$\underline{\text{C}}\text{-N}=\text{N}\text{-}$), 164.3 (Ar-O-CO-Ar), 163.8 (Ar-C-O-), 155.3(Ar-C-O-CO-), 150.9 (benzo-C-N), 149.3 (benzo-C-S), 136.5 ($\text{-C(CH}_3\text{)=CH}_2\text{}$), 138.2 ($\text{CH}_3\text{-Ar-C}$), 134.4 ($\text{Ar-C-N}=\text{N-}$), 132.4, 128.4, 125.7,124.6, 122.8, 122.0, 121.0, 114.4 (Ar-C), 125.2 ($\text{-C(CH}_3\text{)=CH}_2\text{}$), 68.2 ($\text{-OCH}_2\text{-}$), 64.6 ($\text{-CH}_2\text{-O-}$), 29.0, 28.6, 25.8, 25.7, 21.9, 18.3 (aliphatic-C), **FT-IR** (cm^{-1}): 3060 (C-H, aromatic), 2940, 2910, 2867 (C-H, aliphatic), 1720, 1705 (C=O), 1640 (C=C), 1608 (C=N), 1579 (C-C, aromatic), 1492, 1475, 1429 ($\text{-N}=\text{N-}$), 1396 (C-N), 1315, 1301, 1261 (C-O), 1222, 1182, 1168, 1125, 1107, 1060 (benzothiazole), 1006, 942, 844, 805, 756, 730, 691, 655 (C-S-C).

3.4.6. Synthesis of monomer M9

2-[4-(4'-(6-methacryloxyhexyloxybenzoyloxy))phenylazo]-6-methoxybenzothiazole (M9)

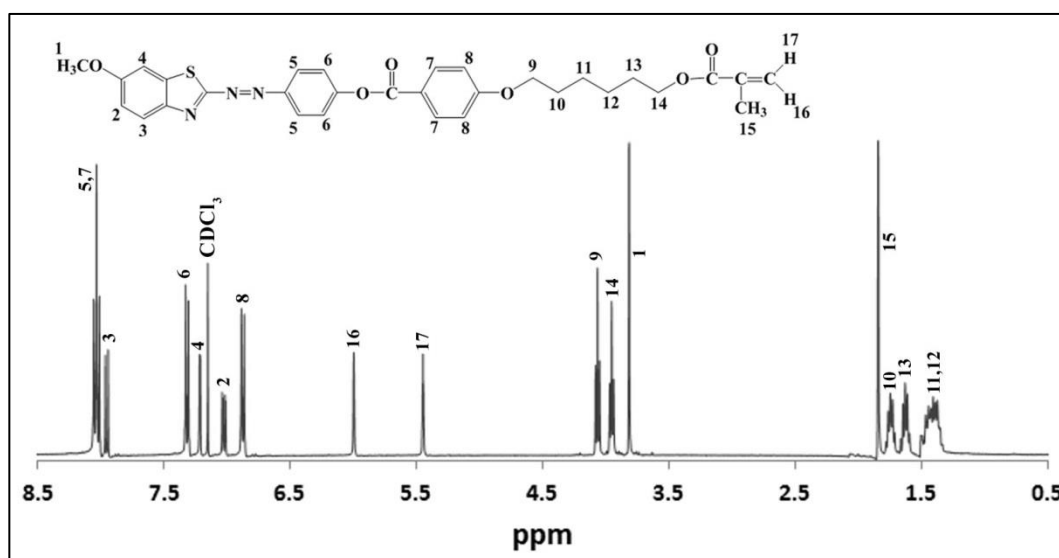


Figure 3.9: ^1H NMR spectrum of monomer **M9**

The synthesis of monomer **M9** was similar to that described for monomer **M7**. Yield: 35% , orange crystal; mp: 120-122°C, ^1H NMR (400 MHz, CDCl_3) δ (ppm): 8.08-8.01 (m, 4H, Ar-H), 7.98-7.93 (d, 1H, benzo-H), 7.34-7.30 (d, 2H, Ar-H), 7.22 (s, 1H, benzo-H), 7.05-7.01 (d, 1H, benzo-H), 6.91-6.85 (d, 2H, Ar-H), 6.00 (s, 1H, =CH₂), 5.55 (s, 1H, =CH₂), 4.09-4.03 (t, 2H, -OCH₂-), 3.98-3.92 (t, 2H, -OCH₂-), 3.81 (-OCH₃) 1.84 (s, 3H, -CH₃), 1.79-1.69 (m, 2H, -CH₂-), 1.67-1.57 (m, 2H, -CH₂-), 1.50-1.33 (m,

4H, -CH₂-), ¹³C NMR (100 MHz, CDCl₃) δ (ppm): 173.3 (-O-CO-), 167.5 (benzo-C-N=N-), 164.3 (Ar-O-CO-Ar), 163.7 (Ar-C-O-), 159.7 (CH₃O-Ar-C), 154.9 (Ar-C-O-CO-), 149.3 (benzo-C-N), 147.5 (benzo-C-S), 136.5 (-C(CH₃)=CH₂), 136.4 (Ar-C-N=N-), 132.4, 125.8, 125.4, 122.8, 121.1, 116.6, 104.3 (Ar-C), 125.2 (-C(CH₃)=CH₂), 68.2 (-OCH₂-), 64.6 (-CH₂-O-), 55.9 (-OCH₃) 30.9, 29.0, 28.9, 28.6, 25.8, 25.7, 18.3 (aliphatic-C), FT-IR (cm⁻¹): 3062 (C-H, aromatic), 2938, 2867, 2833 (C-H, aliphatic), 1729, (C=O), 1636 (C=C), 1595 (C=N), 1579 (C-C, aromatic), 1496, 1476, 1436 (-N=N-), 1393 (C-N), 1325, 1310, 1264 (C-O), 1217, 1194, 1164, 1129, 1103, 1062 (benzothiazole), 1008, 988, 937, 876, 843, 760, 725, 691, 652 (C-S-C).

3.4.7. Synthesis of monomer M10

2-[4-(4'-(6-methacryloxyhexyloxybenzoyloxy))phenylazo]-6-ethoxybenzothiazole (M10)

The synthesis of monomer **M10** was similar to that described for monomer **M7**. Yield: 50%, orange crystal; mp: 126-128°C, ¹H NMR (400 MHz, CDCl₃) δ (ppm): 8.15-8.05 (m, 4H, Ar-H), 8.2-7.97 (d, 1H, benzo-H), 7.41-7.34 (d, 2H, Ar-H), 7.27-7.23 (d, 1H, benzo-H), 7.09-7.04 (m, 1H, benzo-H), 6.96-6.90 (d, 2H, Ar-H), 6.04 (s, 1H, =CH₂), 5.49 (s, 1H, =CH₂), 4.15-3.98 (m, 6H, -OCH₂-), 1.88 (s, 3H, -CH₃), 1.83-1.74 (m, 2H, -CH₂-), 1.72-1.64 (m, 2H, -CH₂-), 1.57-1.38 (m, 7H, -CH₃ and -CH₂-), ¹³C NMR (100 MHz, CDCl₃) δ (ppm): 173.2 (-O-CO-), 167.5 (benzo-C-N=N-), 164.3 (Ar-O-CO-Ar), 163.7 (Ar-C-O-), 159.1 (CH₃O-Ar-C), 154.8 (Ar-C-O-CO-), 149.3 (benzo-C-N), 147.5 (benzo-C-S), 136.5 (-C(CH₃)=CH₂), 136.4 (Ar-C-N=N-), 132.4, 131.5, 125.9, 125.4, 123.0, 122.8, 121.1, 117.0, 114.4, 114.0, 104.9 (Ar-C), 125.2 (-C(CH₃)=CH₂), 68.2 (-OCH₂-), 64.6 (-CH₂-O-), 64.2 (-OCH₂-), 29.0, 28.9, 28.7, 28.6, 25.8, 25.7, 18.3, 14.8 (aliphatic-C), FT-IR (cm⁻¹): 3087 (C-H, aromatic), 2949, 2896 (C-H, aliphatic), 1726, 1707 (C=O), 1644 (C=C), 1603 (C=N), 1572 (C-C, aromatic),

1495, 1477, 1460 (-N=N-), 1404 (C-N), 1329, 1310, 1261 (C-O), 1222, 1197, 1165, 1143, 1116, 1060 (benzothiazole), 1000, 940, 897, 839, 760, 732, 688, 655 (C-S-C).

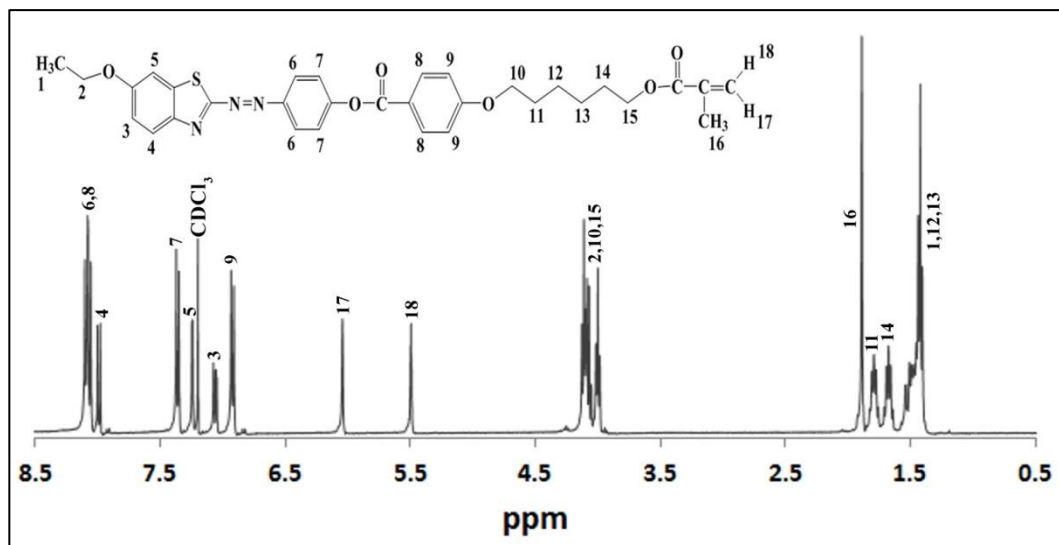


Figure 3.10: ^1H NMR spectrum of monomer **M10**

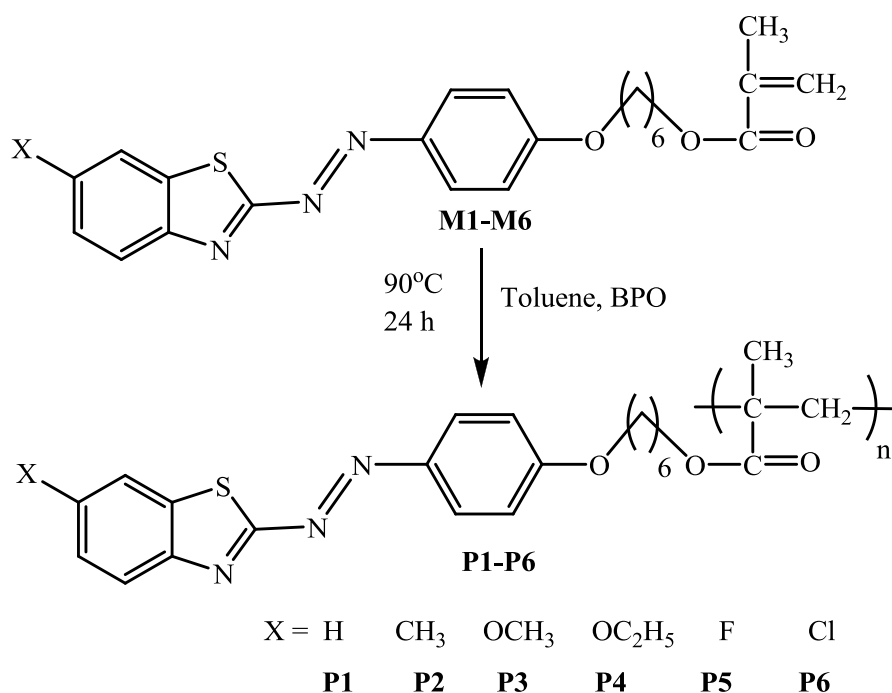
3.5. Synthesis and characterization of SCLCPs

The synthetic method and structural characterization of SCLCPs **P1-P10** are described in the following sections. The purities and structural identification of polymers were conducted by FT-IR and ^1H NMR spectroscopic techniques.

3.5.1. Synthesis of polymers P1-P6

Side chain liquid crystalline polymers, **P1- P6** were synthesized as shown in Scheme 3.7. The monomers **M1- M6** were polymerized via conventional free radical polymerization in anhydrous toluene using BPO as initiator. A typical polymerization procedure for **M1** is presented as follows: **M1** (0.8381 g, 1.8 mmol), BPO (5 mol% with respect to the monomer) and anhydrous toluene (4 mL) were added into Schlenk tube (50 mL) and the reaction mixture was degassed under high vacuum and then purged with nitrogen for one hour. The reaction flask was then sealed under nitrogen atmosphere and immersed into a thermostated oil bath at 90°C. After 24 h, the

polymerization mixture was cooled to room temperature and then poured into large excess of ethanol under vigorous stirring. The precipitated solid was filtered off and the obtained polymer (**P1**) was purified by dissolving several times in chloroform and re-precipitated with excess hot ethanol. The synthesis of polymers **P2- P6** was similar to that described for **P1**.



Scheme 3.7: Synthesis of polymers **P1-P6**

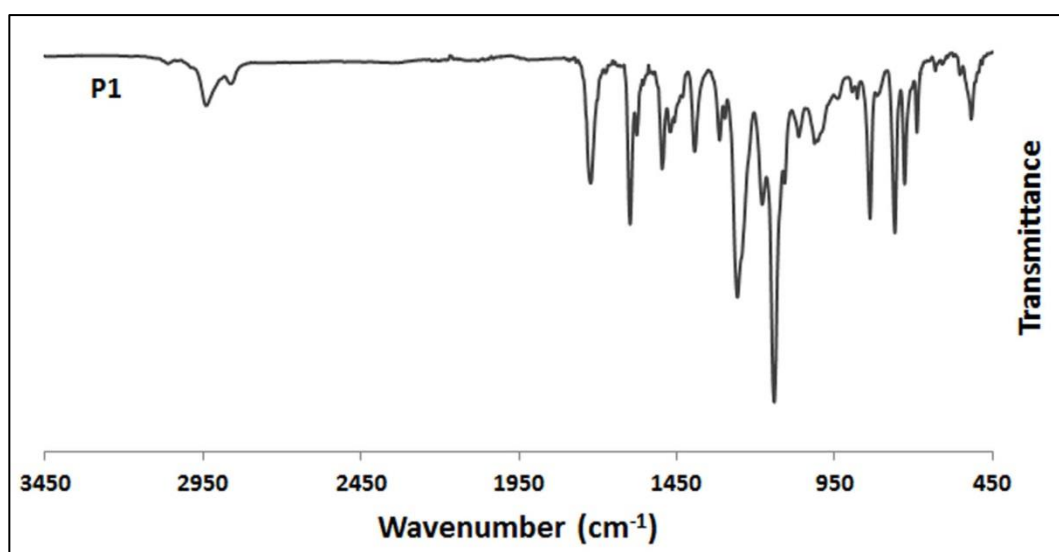


Figure 3.11: FT-IR spectrum of polymer **P1**

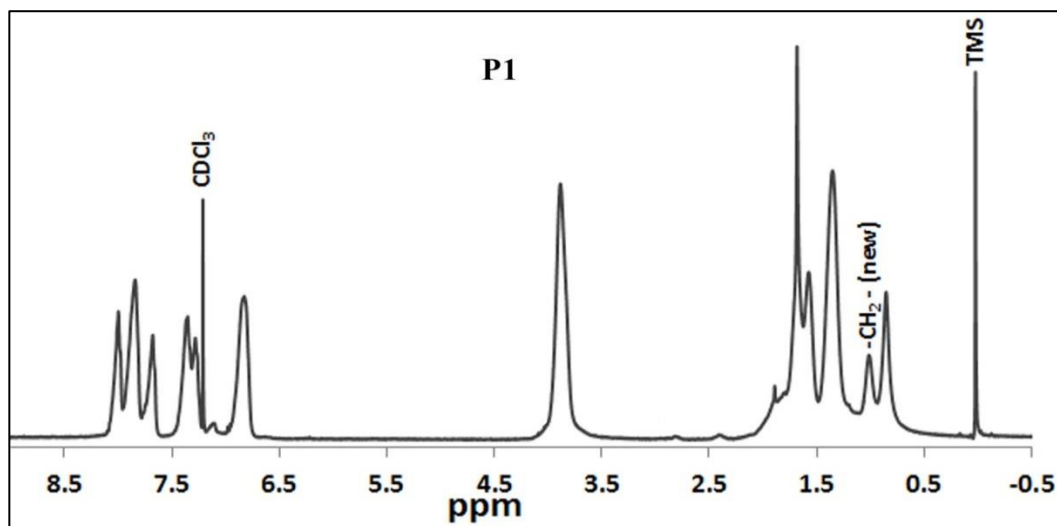
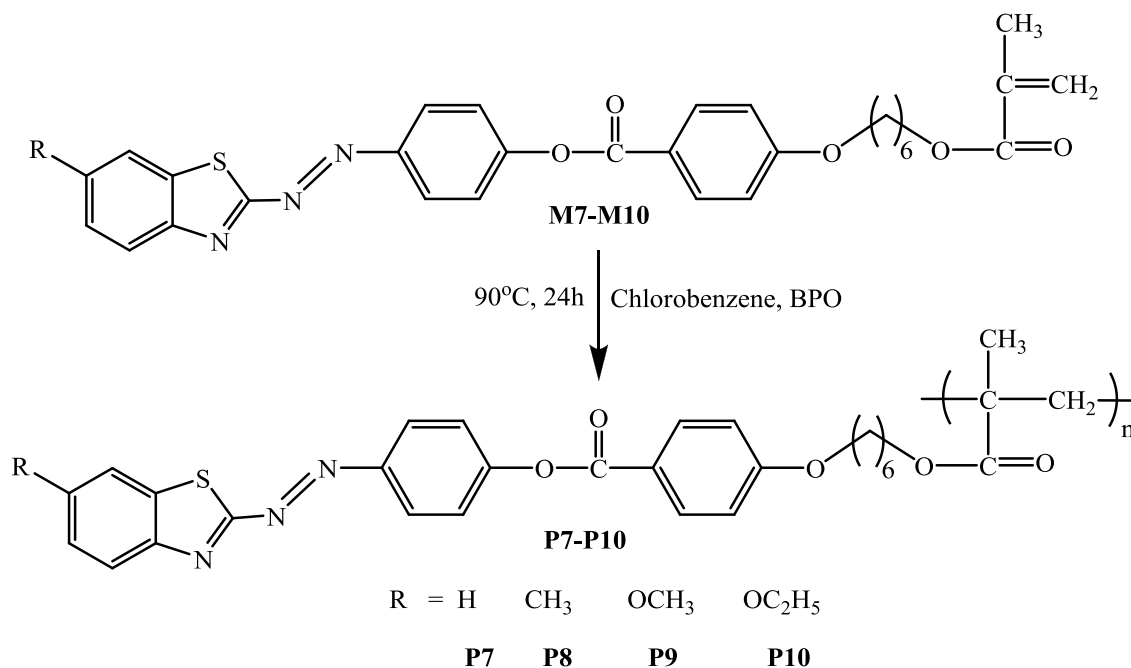


Figure 3.12: ^1H NMR spectrum of polymer **P1**

3.5.1. Synthesis of polymers **P7-P10**

SCLCPs, **P7- P10** were synthesized according to Scheme 3.8. Monomers, **M7-M10** were polymerized via conventional free radical polymerization in chlorobenzene using BPO as initiator. The rest of the steps were identical to that described for the synthesis of polymer **P1**.



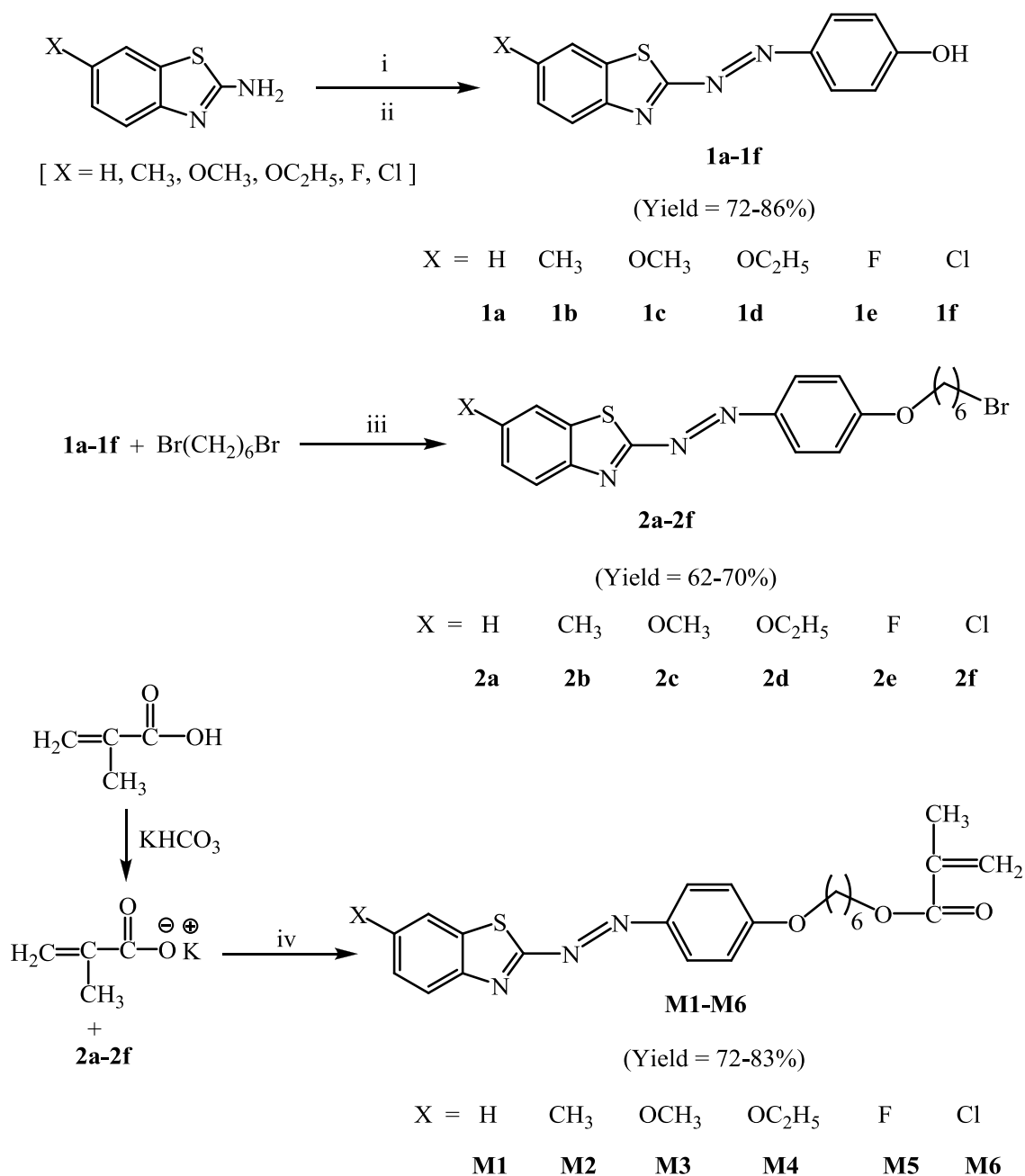
Scheme 3.8: Synthesis of polymers **P7-P10**

CHAPTER 4 : RESULTS AND DISCUSSION

4.1. Synthesis and characterization of LC monomers

4.1.1. Synthesis of LC monomers M1-M6

The synthetic routes of LC monomers **M1-M6** are depicted in Scheme 4.1. LC monomers **M1-M6** were synthesized via three step reactions: (i) azo-coupling, (ii) etherification and (iii) esterification reactions. The syntheses of azo-benzothiazole dyes **1a-1f** were carried out by simple azo coupling reaction between diazonium salts of 2-amino-6-substituted benzothiazoles and alkaline phenol at low temperature. Due to the poor solubility of 2-amino-6-substituted benzothiazoles and low stability of the diazonium salt, glacial acetic acid was used as reaction medium. To maintain temperature around 0-5°C, ice flakes were frequently added to the reaction mixture. Consequently, a satisfactory yield of 72-86% was obtained. In the second steps, a long alkyl spacer containing six carbon atoms was attached to azo-benzothiazole moiety by etherification reaction. Azo-benzothiazole dyes **1a-1f** were refluxed with 1,6-dibromohexane in presence of potassium carbonate and catalytic amount of potassium iodide in acetone for 24 h and then pure compounds **2a-2f** were isolated in good yields (62-70%). Finally, the synthesis of monomers **M1-M6** was performed via esterification reaction between compounds **2a-2f** and potassium methacrylate in DMF at 100°C. As the esterification reaction was carried at 100°C, a trace amount of hydroquinone was added to the reaction mixtures to inhibit polymerization of produced monomers. As a result, monomers **M1-M6** were obtained in higher yields (72-83%). All the azo-benzothiazole containing LC monomers were obtained as orange to orange-red crystal, which showed good solubility in common organic solvents including THF, DMF, DMSO, CHCl₃, CH₂Cl₂, toluene, chlorobenzene and acetonitrile.



Reaction conditions:

(i) NaNO₂ + (CH₃COOH + H₂SO₄); (ii) phenol + NaOH, 0-5°C

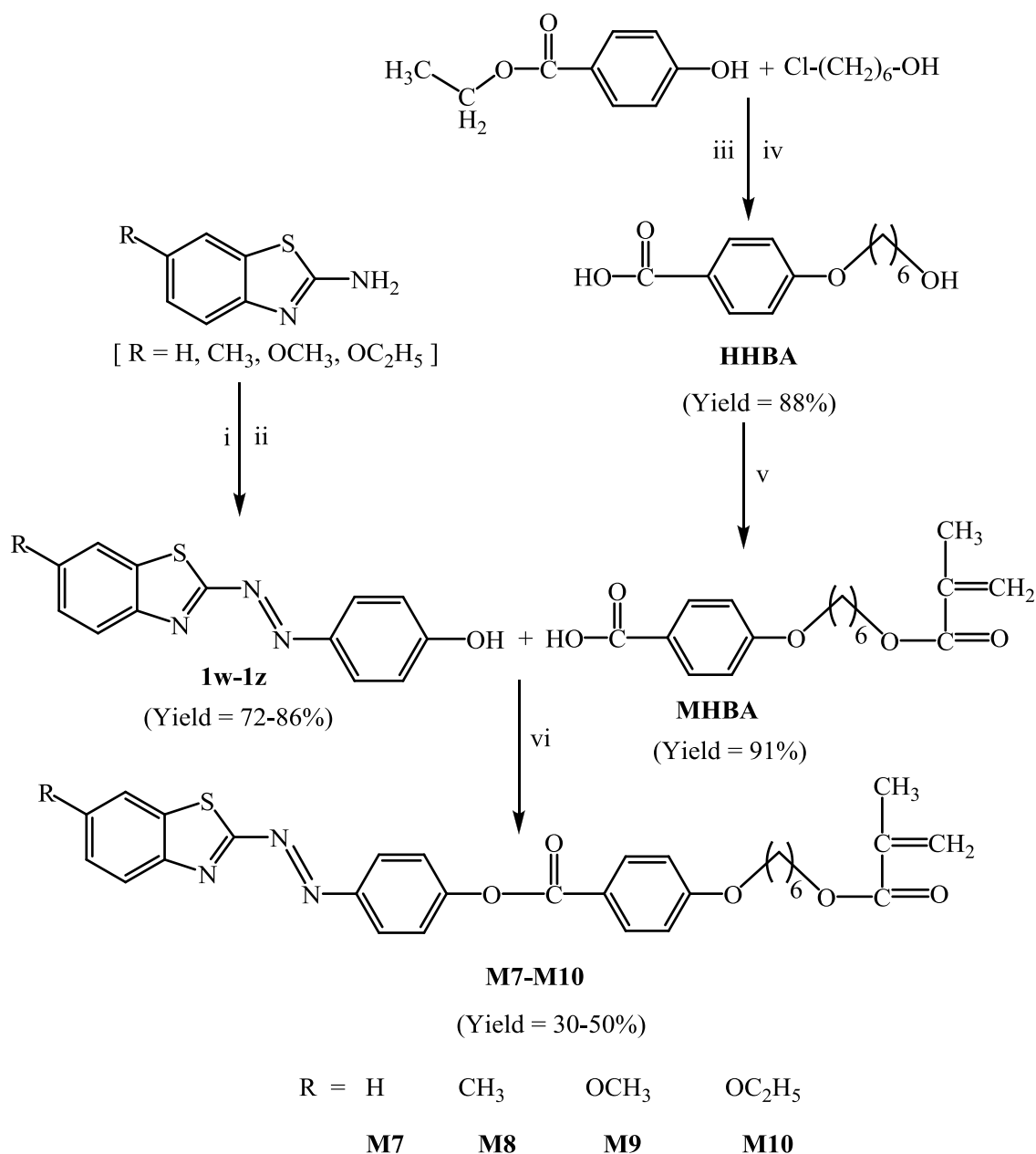
(iii) K₂CO₃, KI, acetone, reflux for 24 h

(iv) (Hydroquinone + DMF), heat at 100°C for 24 h

Scheme 4.1: Synthetic routes of monomers **M1-M6**

4.1.2. Synthesis of LC monomers M7-M10

The synthetic routes of monomers **M7-M10** are illustrated in Scheme 4.2. Azo-ester bridged LC monomers **M7-M10** were synthesized through a multistep reaction routes. First, the synthesis of azo-benzothiazole dyes **1w-1z** was carried out by similar method that described for compounds **1a-1d**. Compound *4-(6-hydroxyhexyloxy)benzoic acid* (**HHBA**) was synthesized via etherification between ethyl 4-hydroxybenzoate and 6-chlorohexanol in DMF at 130°C for 6 h. The interaction of ethyl 4-hydroxybenzoate and 6-chlorohexanol gave yellowish oily product which was then hydrolysed by aqueous KOH solution in ethanol at refluxing temperature for 4 h. The obtained mixture was acidified with dilute HCl solution to afford white powder **HHBA** in excellent yield (88%). Intermediate compound *4-(6-methacryloxyhexyloxy)benzoic acid* (**MHBA**) was prepared through condensation reaction by refluxing **HHBA** and methacrylic acid in anhydrous toluene at 130°C for 6 h using Dean-Stark trap. After recrystallization from isopropanol-water mixture (1:15), a dull-white solid was obtained in excellent yield (91%). Finally, the synthesis of LC monomers **M7-M10** was carried out between azo-benzothiazole dyes **1w-1z** and intermediate compound **MHBA** in a mixture of DMF and DCM via Steglich esterification reaction by using *N, N'*-dicyclohexylcarbodiimide (DCC) as a coupling reagent and 4-dimethylaminopyridine (DMAP) as a catalyst. The reaction mixture was stirred at 0°C for 1 h and then at room temperature for 24 h. The orange coloured crystalline product was obtained in fairly good yield (30-50%). The obtained LC monomers **M7-M10** were soluble in common organic solvents including chlorobenzene, THF, DMSO, CHCl₃ and CH₂Cl₂. From the structural viewpoint, monomers **M7-M10** bear one additional benzene ring and ester group than those of monomers **M1-M6**.



Reaction conditions:

i. $\text{NaNO}_2 + (\text{CH}_3\text{COOH} + \text{H}_2\text{SO}_4)$; ii. (Phenol + NaOH), 0-5°C

iii. (KI + K_2CO_3) in DMF; heat at 130°C for 6 h

vi. $\text{C}_2\text{H}_5\text{OH} + \text{KOH}$ (aqueous); reflux for 4 h

v. (Methacrylic acid + p-toluene sulphonic acid + hydroquinone) in toluene;

Reflux for 6 h at 130°C

vi. (DCC + DMAP) in (DMF + DCM); stir at 0°C for 1 h and room temperature for 24 h

Scheme 4.2: Synthetic routes of monomers **M7-M10**

4.1.3. Characterization of LC monomers

The chemical structure of the synthesized monomers **M1-M10** was confirmed by FT-IR, ^1H and ^{13}C NMR spectroscopic techniques. The chemical shifts and peak integrations of all the protons in the monomers are in excellent agreement with their expected molecular structure. The characteristic FT-IR vibrational frequencies, ^1H and ^{13}C NMR chemical shifts of monomers **M1-M10** have elaborately been described in the experimental section. However, the range of major FT-IR vibrational frequencies for different functional groups, ^1H NMR chemical shifts of different protons and ^{13}C NMR chemical shifts of various carbon atoms in monomers **M1-M10** are summarized in Table 4.1, Table 4.2 and Table 4.3 respectively. As an example, the spectral properties of monomer **M1** are discussed below.

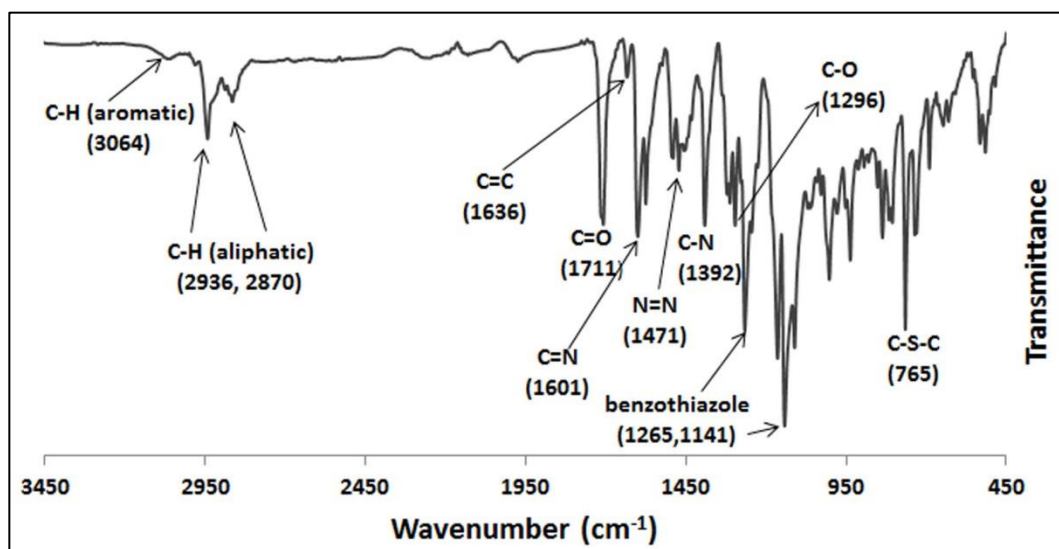


Figure 4.1: Representative FT-IR spectrum of monomer **M1**

FT-IR spectrum of monomer **M1** is shown in Figure 4.1. Monomer **M1** exhibits different vibrational modes corresponding to stretching and bending of various functional groups present in the molecule. A very weak band near 3064 cm^{-1} is attributed to aromatic $\nu(\text{C-H})$ stretching vibration. Two medium intensity bands around

2936 cm^{-1} and about 2870 cm^{-1} are due to aliphatic $\nu(\text{C-H})$ asymmetric and symmetric stretching vibration of methylene ($-\text{CH}_2$) groups of alkyl chain.

Table 4.1: FT-IR absorption frequencies of monomers **M1-M10**

Functional groups	Wavenumber (cm^{-1})
C-H (aromatic)	3068 - 3036
C-H (aliphatic)	2947-2909, 2872-2833
C=O (ester)	1720-1705
C=C (aliphatic)	1640-1633
C=N (benzothiazole)	1608-1597
C-C (aromatic)	1579-1574
N=N	1475-1467
C-N	1396-1382
C-O	1301-1296
benzothiazole	1265-1110
C-S-C	764-727

The strong absorption band at 1711 cm^{-1} corresponds to $\nu(\text{C=O})$ stretching vibration of ester group in the terminal methacrylate group. The medium intensity band around 1636 cm^{-1} is ascribed to $\nu(\text{C=C})$ stretching vibration in the terminal methacrylate functional group. The stretching vibration at 1601 cm^{-1} is attributed to $\nu(\text{C=N})$ of benzothiazole ring. The medium intensity absorption band around 1471 cm^{-1} corresponds to $\nu(\text{N=N})$ stretching vibration. The intense vibrational band around 1392 cm^{-1} is assigned to $\nu(\text{C-N})$. The band at 1296 cm^{-1} is ascribed to $\nu(\text{C-O})$ stretching vibration. The strong

absorption bands around 1265-1110 cm^{-1} are attributed to benzothiazole ring. The intense vibrational band at 764 cm^{-1} corresponds to $\nu(\text{C-S-C})$ stretching vibration.

^1H NMR spectrum of monomer **M1** is illustrated in Figure 4.2. The signals around δ 1.37-1.83 ppm in the multiplet form are observed due to methylene ($-\text{CH}_2-$) protons of straight alkyl chain.

Table 4.2: ^1H NMR chemical shifts of different type of protons present in monomers **M1-M10**

Type of protons	Chemical shifts (ppm)
Benzo- H (4 th position)	8.12-8.06
Benzo- H (5 th position)	7.48-7.08
Benzo- H (6 th position)	7.41-7.35
Benzo- H (7 th position)	7.90-7.27
(Benzo + Ar)- H	8.18-7.90
Ar- H (ortho to -N=N-)	8.04-7.97
Ar- H (ortho to -O-C)	7.56-6.92
-O CH ₂ -	4.19-3.96
- CH ₂ -	1.88-1.32
-C(CH ₃)=CH ₂	1.9
-C(CH ₃)= CH ₂	6.09-6.05 and 5.50-5.48
Ar- CH ₃	2.53-2.42
-O CH ₃	3.89-3.81
- CH ₃	1.48-1.43

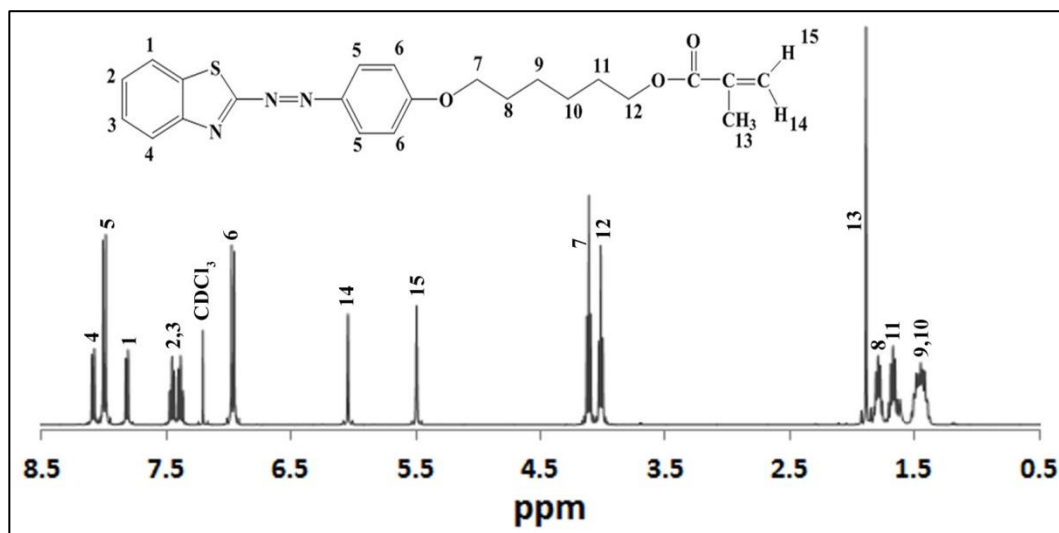


Figure 4.2: Representative ^1H NMR spectrum of monomer **M1**

The signal at δ 1.9 ppm in the singlet form is attributed to $-\text{CH}_3$ proton of methacrylate group. Two triplets signals around 4.15 ppm and at δ 3.97 ppm are ascribed for $-\text{OCH}_2-$ and $-\text{CH}_2\text{O}-$ alkoxy protons respectively. Characteristic vinylidene proton peaks of methacrylate group are observed as form of singlet at δ 6.05 ppm and around δ 5.50 ppm. The signals between δ 6.93-8.12 ppm as doublet and multiplet form are assigned to benzothiazole and aromatic ring protons.

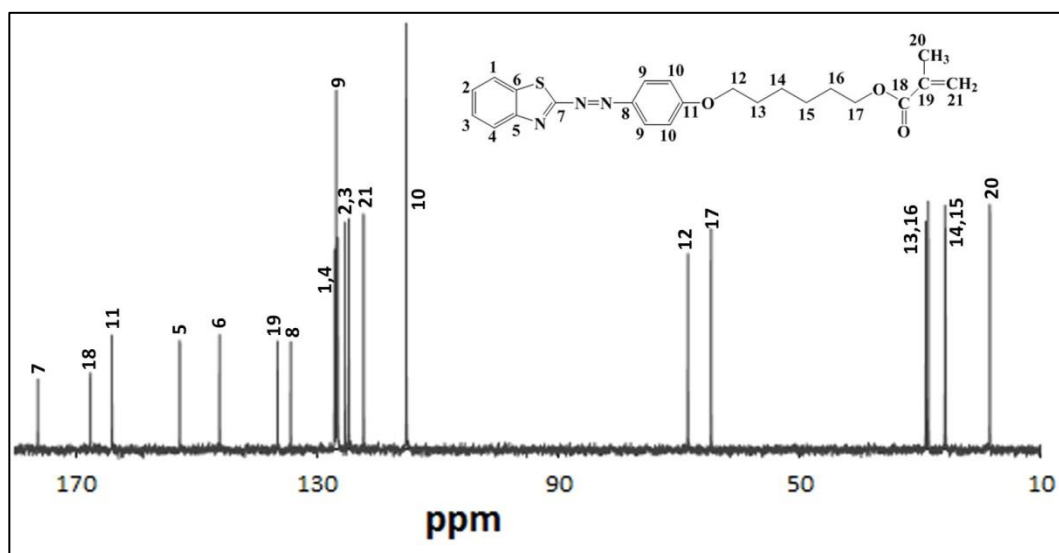


Figure 4.3: Representative ^{13}C spectrum of monomer **M1**

Table 4.3: ^{13}C NMR chemical shifts of different type of carbons present in monomers

M1-M10

Type of carbons	Chemical shift δ (ppm)
-O- <u>C</u> O-	176.3-174.0
Benzo- <u>C</u> -N=N-	167.6
Ar- <u>C</u> -O-	164.1-163.6
Benzo- <u>C</u> -N	145.9-146.2
Benzo- <u>C</u> -S	146.4-146.2
(- <u>C</u> (CH ₃)=CH ₂)	137.7-136.6
Ar- <u>C</u> -N=N-	136.2-134.4
(-C(CH ₃)= <u>C</u> H ₂)	125.3
Ar- <u>C</u>	138.2.-104.5
-O <u>C</u> H ₂ -	68.5-64.7
Aliphatic- <u>C</u>	30.9-14.8

^{13}C NMR spectrum of monomer **M1** is depicted in Figure 4.3. The signals at δ 18.4-29.4 ppm are observed due to methylene (CH₂-) carbons of straight alkyl chain and methyl (CH₃-) carbon. Two signals around δ 68.5 ppm and 64.7 ppm are assigned to -OCH₂- and -CH₂O- group carbons respectively. The signal at δ 176.3 ppm is attributed to ester group carbon (-O-CO-). The signals at δ 167.6 ppm, δ 152.8 ppm and δ 146.2 ppm are due to benzothiazole ring carbons. The signals at δ 136.6 ppm and δ 125.3 ppm are assigned for double bond carbon in methacrylate group. The signals at δ 164.0 ppm and δ 134.4 ppm are attributed to aromatic ring carbons (4,4'-position) where substitution has occurred. The signals at around δ 126.8-115.3 ppm are due to aromatic carbons.

4.2. Synthesis and characterization of SCLCPs

4.2.1. Synthesis of SCLCPs

Atom transfer radical polymerization (ATRP) is a well-established method to prepare nearly monodispersed polymers because all polymer chains grow at the same speed [188]. However, heterocyclic moiety containing molecules are very difficult to polymerize by ATRP because heteroatoms such as S and N can easily coordinate [189] with the metal catalyst used in the ATRP process leading unexpected side reactions. As all the synthesized monomers **M1-M10** possess S and N atoms in their molecular constituent, conventional free radical polymerization were adopted for this study.

Table 4.4: Yields and GPC results of polymers **P1-P10**

	M_n	M_w	PDI	Yield (%)
P1	8370	13820	1.65	50
P2	8647	13989	1.62	38
P3	9262	15162	1.64	43
P4	8221	13108	1.59	52
P5	8818	14550	1.65	65
^a P6	-	-	-	55
^a P7	-	-	-	40
^a P8	-	-	-	35
^a P9	-	-	-	36
P10	7863	12818	1.63	42

M_n , M_w and PDI were determined by GPC using polystyrene standards in THF. ^aDue to solubility problem in THF, molecular weight could not measure with existing GPC.

Azo-benzothiazole moiety containing LC methacrylate monomers **M1-M10** were polymerized via conventional free radical polymerization at 90°C for 24 h using BPO as initiator and anhydrous toluene (for **M1-M6**) and chlorobenzene (for **M7-M10**) as solvents (Scheme 3.7). Temperature, time and monomer to initiator ratio were chosen by error and trial method to achieve optimum polymerization conditions. The synthesized polymers **P1-P10** and their GPC results are listed in Table 4.4. The weight average molecular weights (M_w) obtained from GPC measurements were in the range of 13108-15162 with polydispersity range of 1.59-1.65 and the yields were found in the range of 40-65%. Although adopting a high initiator concentration (5 mol.% with respect to the monomer) and elevated temperature (90°C), the conversion rate and obtained average molecular weights of prepared polymers are not satisfactory. However, these values are typical for azobenzene containing polymers [190-192]. The lower molecular weights of polymers may be linked to a relatively high concentration of growing chain radicals in the reaction mixture, as a result of the high BPO/monomer ratio adopted, which could favour the termination of reactions [46].

4.2.2. Characterization of polymers P1-P6

The chemical structure and purity of polymers were confirmed by FT-IR and ^1H NMR spectroscopies. Figure 4.4 exhibits the FT-IR spectra of monomer **M1** and its corresponding polymer **P1**. After polymerization, the absorption band at about 1636 cm^{-1} in **M1**, which was assigned to the stretching vibration of carbon-carbon double bond, disappeared completely and the vibrational frequency of carbonyl group simultaneously shifted from 1711 cm^{-1} to 1732 cm^{-1} . This shifting of vibrational frequency may be due to the reduced electron delocalization of the carbonyl double bond in methacrylic group. Similar observation has been reported by Cristina and Paul [46] for their polymethacrylate with benzothiazole azo chromophore in the side chain.

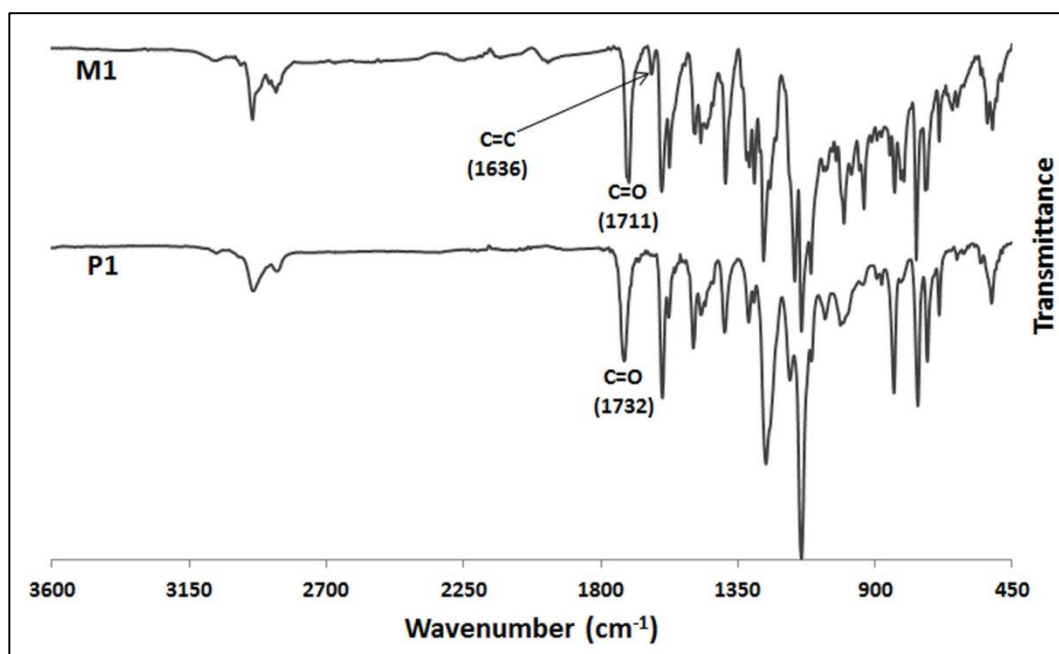


Figure 4.4: FT-IR spectra of monomer **M1** and polymer **P1**

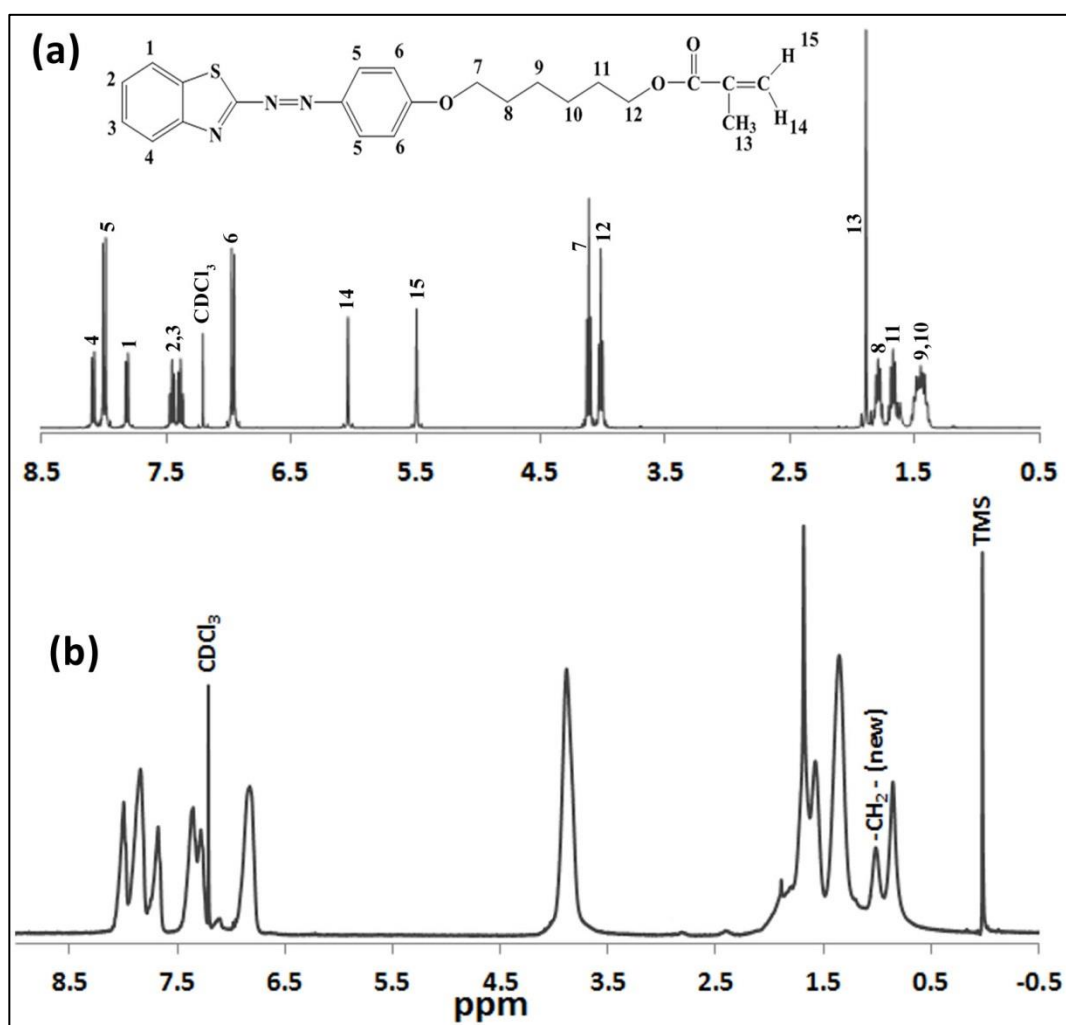


Figure 4.5: ¹H NMR spectra of (a) monomer **M1** and (b) polymer **P1**

Figure 4.5 shows ^1H NMR spectra of monomer **M1** and its corresponding polymer **P1**. After polymerization, the characteristic vinylidene protons peaks of the monomer located at δ 5.5 ppm and δ 6.1 ppm completely disappeared. Moreover, all the chemical shifts of polymer became quite broad which is consistent with the expected polymer structure. At the same time, an additional chemical shift for methylene ($-\text{CH}_2-$) protons is observed at δ 1.03 ppm in ^1H NMR spectrum of polymer. All of these observations confirmed that unsaturated methacrylic functional group was involved in the polymerization process. As polymers **P1-P6** bear similar structure except terminal tail in the mesogen, polymers **P2-P6** showed analogous spectral properties (^1H NMR and FT-IR) as described for **P1**. The FT-IR and ^1H NMR spectra of polymers **P2-P6** are shown in APPENDIX A and APPENDIX B.

4.2.3. Characterization of polymers **P7-P10**

From the structural viewpoint, polymers **P7-P10** bear one additional benzene ring and ester linking group in the mesogenic side chain than those of polymers **P1-P6**. As a result, the spectral properties of polymers **P7-P10** are almost similar like polymers **P1-P6**. The terminal methacrylate functional group was involved in the polymerization process of polymers **P7-P10** as in polymers **P1-P6**. The disappearance of vinylidene proton peaks in ^1H NMR spectrum and carbon-carbon double bond peak in FT-IR spectrum confirmed the polymerization of monomers. The FT-IR and ^1H NMR spectra of polymers **P7-P10** are presented in APPENDIX A and APPENDIX B.

4.3. Thermal properties of LC monomers and their SCLCPs

The thermal studies of LC monomers and their corresponding SCLCPs were carried out to give more insight into structures of the synthesized monomers and polymers. The thermogravimetric measurements were performed in a temperature range of 50-900°C at a heating rate of 20°C min⁻¹ in nitrogen atmosphere. The obtained

thermogravimetric results of the synthesized monomers and polymers are discussed below.

4.3.1. Thermal properties of LC monomers M1-M10

The TG and DTG curves of LC monomers **M1- M6** are depicted in Figure 4.6 and Figure 4.7 respectively and their relevant thermal results are presented in Table 4.5. The thermal decomposition temperatures corresponding to 5% weight loss ($T_{d, 5\%}$) for monomers **M1-M6** are above 280°C and these results indicate that the synthesized LC monomers **M1-M6** have good thermal stability [17].

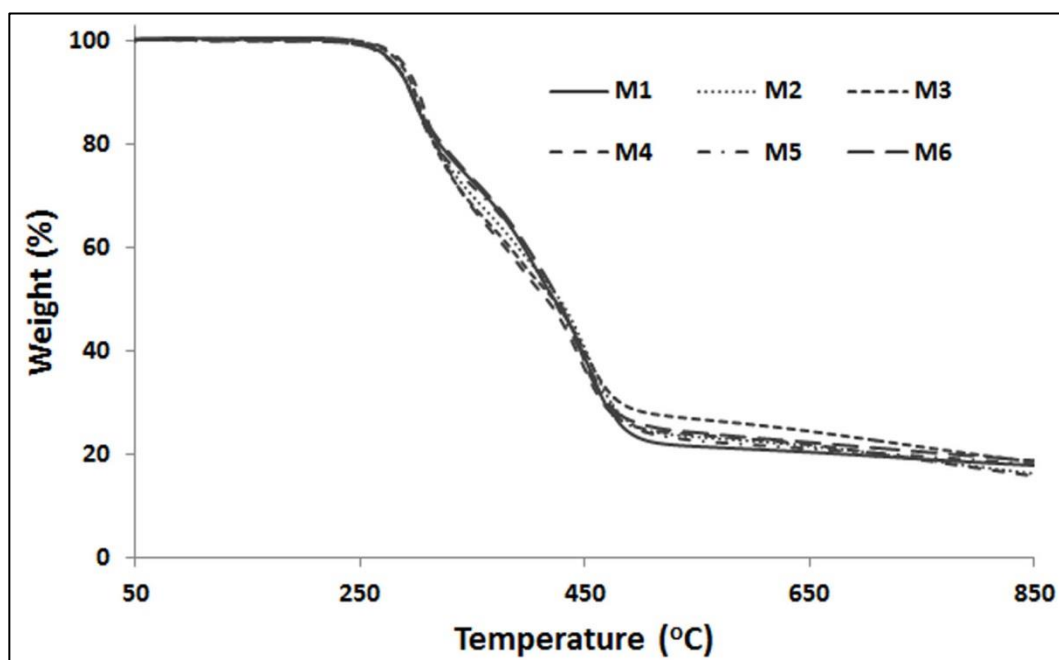


Figure 4.6: TG curves of LC monomers **M1-M6**

Although monomers **M1-M6** bear structural similarities except terminal tails, monomers **M1-M4** exhibited three-staged decomposition while monomers **M5-M6** showed two-staged decomposition pattern. It is clearly seen from Table 4.5 that the first staged-decomposition took place at different temperatures depending on the various terminal substituents on the benzothiazole moiety. The first-staged decomposition of monomers **M1-M6** started around 206-236°C and completed around 348-370°C with

estimated mass loss of 26-38%. The first-staged decomposition of **M1-M6** may be attributed to the thermal cleavage of the azo-heterocyclic segments [193-195].

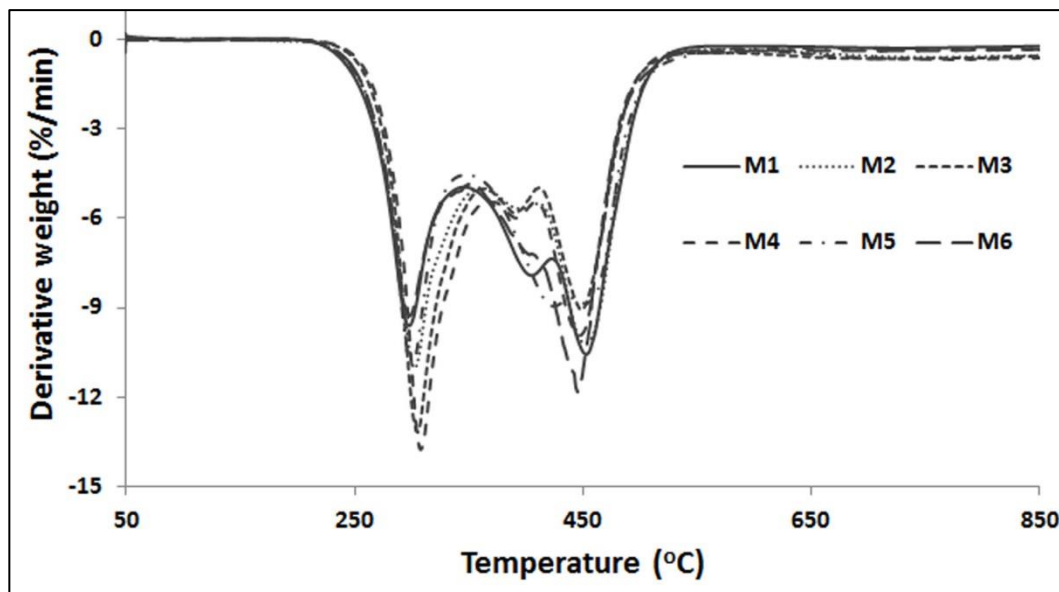


Figure 4.7: DTG curves of LC monomers **M1-M6**

The second-staged decomposition of **M1-M4** happened around 350-424°C while that of **M5-M6** occurred about 351-556°C with corresponding weight loss of 11-23% and 48-50% respectively. The third staged cleavage of compounds **M1-M4** took place around 410-529°C and corresponding weight loss of 25-29%. The second and third-staged decomposition of **M1-M4** and the second-staged decomposition of **M5-M6** may be ascribed to the thermal breakage of aliphatic spacer and heat resistant aromatic moiety [196-198].

The TG and DTG traces of **M7-M10** are depicted in Figure 4.8 and Figure 4.9 respectively and their thermal analysis results are presented in Table 4.5. The thermal decomposition temperatures corresponding to 5% weight loss ($T_{d, 5\%}$) for monomers **M7-M10** are above 315°C and this result indicates that the thermal stability of synthesized LC monomers **M7-M10** is excellent [56, 146, 199, 200]. Monomers **M7-M10** also exhibited two- staged thermal decomposition like **M5-M6**.

Table 4.5: Thermal analysis data of LC monomers **M1-M10**

	T _d (5%)	1 st decomposition		2 nd decomposition		3 rd decomposition		Char yield (%) at 850°C
	(°C)	Temp.	Wt. loss	Temp.	Wt. loss	Temp.	Wt. loss	
	(°C)	(°C)	(%)	(°C)	(%)	(°C)	(%)	
M1	281	206-348	27	350-424	23	425-525	27	17
M2	282	212-359	33	360-414	14	414-529	29	16
M3	284	218-363	35	363-410	12	410-526	25	18
M4	285	223-370	38	370-410	11	410-525	27	16
M5	282	224-350	27	351-556	50	-	-	18
M6	282	236-351	26	352-533	48	-	-	19
M7	316	256-340	9	340-521	62	-	-	21
M8	318	263-342	11	345-541	59	-	-	17
M9	318	268-339	8	342-530	61	-	-	14
M10	321	270-341	9	342-524	62	-	-	14

The first-staged decomposition occurred at 256-342°C and the corresponding weight loss obtained was 8-11%. The second-staged cleavage happened around 340-541°C and the corresponding weight loss was found to be 59-61%. The first-staged cleavage may be attributed to the decomposition of azo-heterocyclic segments [193-195] and the second-staged decomposition may be ascribed to the degradation of aliphatic spacer and heat resistant aromatic moiety [196-198]. Monomers **M7-M10** exhibited an improved

thermal stability of ca. 40°C compared to monomers **M1-M6**. The improved thermal stability of monomers **M7-M10** may due to the greater molecular length provided by the additional aromatic ring and ester linkage [118].

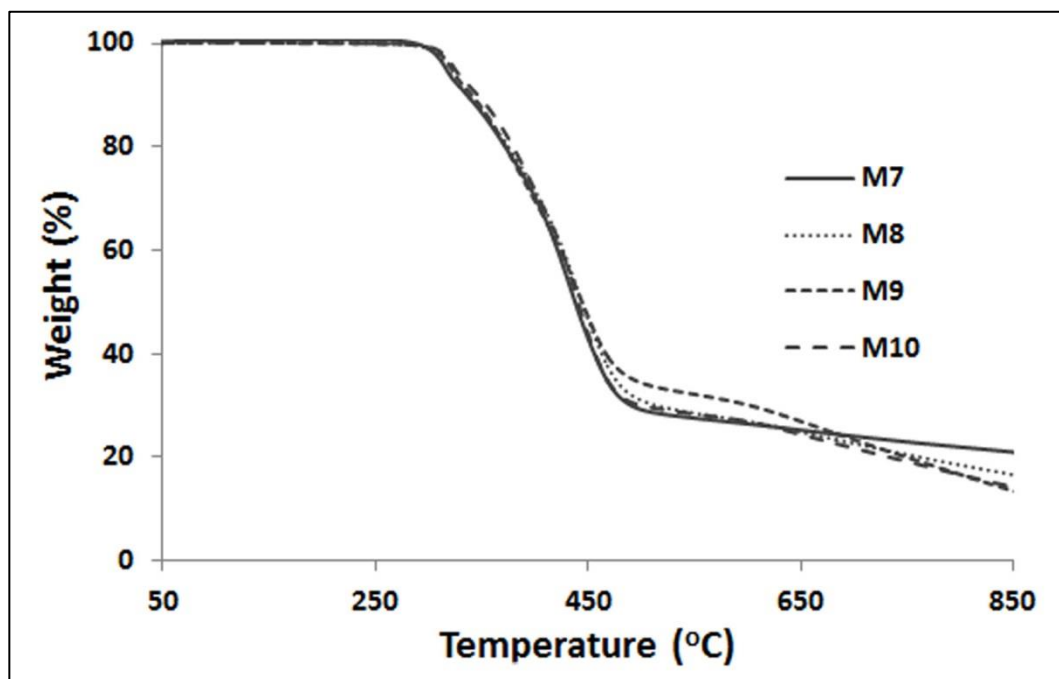


Figure 4.8: TG curves of LC monomers **M7-M10**

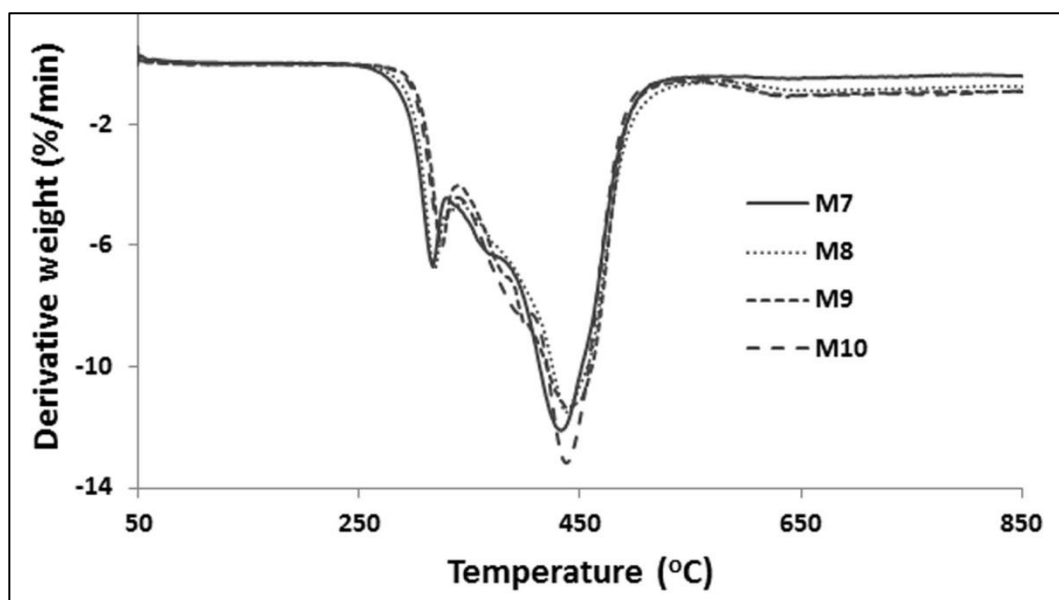


Figure 4.9: DTG traces of LC monomers **M7-M10**

4.3.2. Thermal properties of SCLCPs P1-P10

The TG and DTG traces of polymers **P1-P6** are shown in Figure 4.10 and Figure 4.11 respectively and their characteristic thermal analysis results are summarized in Table 4.6. The thermal decomposition temperatures corresponding to 5% weight loss ($T_{d, 5\%}$) for polymers **P1-P6** are above 300°C. This result indicates that the thermal stability of the synthesized polymers is excellent [56, 146, 199, 200]. Two-staged thermal degradation was observed for polymers **P1-P6** (Figure 4.11). The first-staged decomposition of polymers **P1-P6** started around 260°C and completed about 369°C and their corresponding weight loss was estimated to be 22-31%. This decomposition may be ascribed to degradation the of azo-heterocyclic segments [193-195] which are situated in side chain of the polymers. The second-staged cleavage around 365-538°C with corresponding weight loss of 43-55% may be attributed to the degradation of main chain of polymers, aliphatic flexible spacer and heat resistant aromatic moiety [196-198].

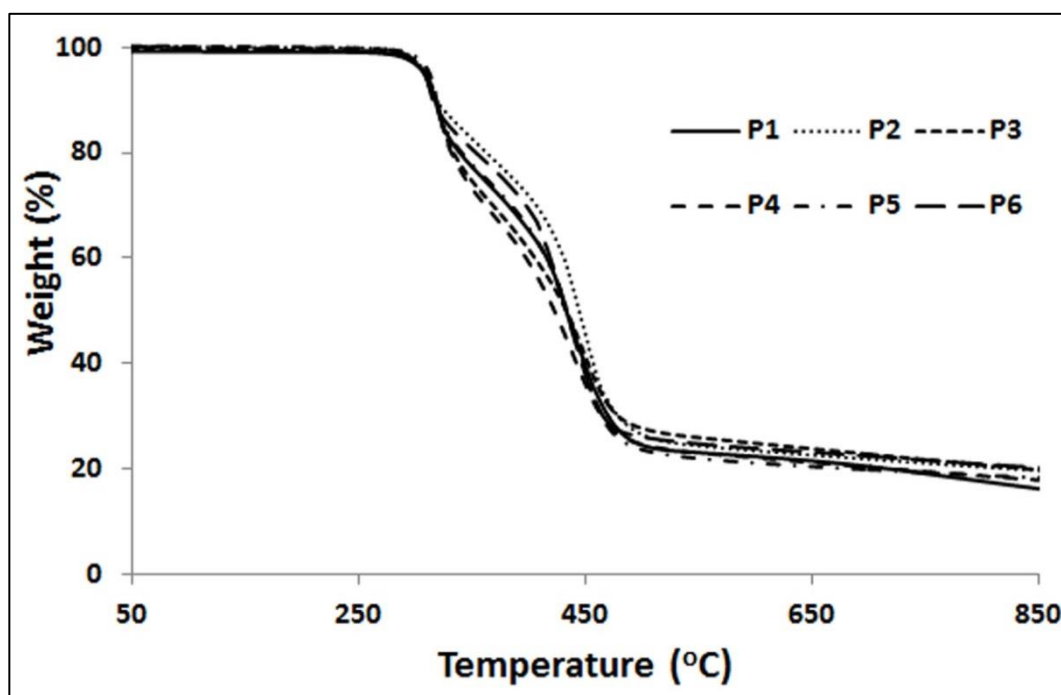


Figure 4.10: TG traces of polymers **P1-P6**

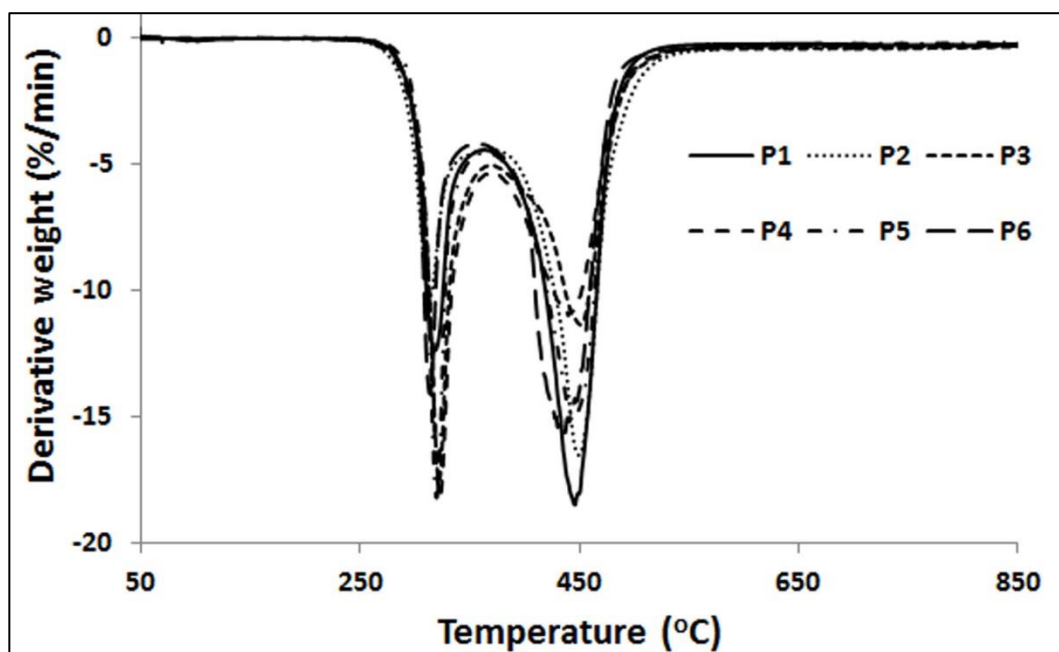


Figure 4.11: DTG curves of polymers **P1-P6**

It can clearly be seen from Table 4.5 and Table 4.6 that the decomposition temperatures corresponding to 5% weight loss ($T_{d, 5\%}$) of polymers **P1-P6** are higher than those of the corresponding monomers **M1-M6**. This result may be ascribed to the fact that the introduction of the mesogenic groups as side chains into the polymethacrylate structures has enhanced the thermal stability of the polymers [201]. In addition, the improved thermal stability of polymers **P1-P6** may be attributed to the “jacket effect” of the bulky azo-benzothiazole pendant attached to the poly-methacrylate backbone [202].

Polymers **P7-P10** exhibited similar thermal degradation behaviour as observed for polymers **P1-P6**. Two-staged decomposition was also detected in polymers **P7-P10**. The TG and DTG traces of polymers **P7-P10** are shown in Figure 4.12 and Figure 4.13 and their thermal analysis data are tabulated in Table 4.6. The first-staged cleavage occurred around 300-358°C with a mass loss of 8-11% and this may be ascribed to the decomposition of azo-heterocyclic segments [193-195] which are situated in side chain of the polymers. On the other hand, the second-staged cleavage happened around 359-537°C with a mass loss of 60-64% which may be attributed to the degradation of main

chain of polymers, aliphatic flexible spacer and heat resistant aromatic moiety [196-198].

Table 4.6: Thermal analysis results of polymers **P1-P10**

	T _d (5%)	1 st decomposition		2 nd decomposition		Char yield (%) at 600°C	Char yield (%) at 850°C
		Temp. (°C)	Wt. loss (%)	Temp. (°C)	Wt. loss (%)		
P1	308	260-364	23	365-536	56	22	16
P2	308	265-363	22	369-538	55	23	20
P3	309	261-366	29	368-521	43	25	20
P4	310	265-369	31	372-520	44	23	18
P5	312	278-364	23	368-540	53	22	18
P6	308	274-355	18	360-552	55	24	20
P7	343	302-355	8	358-534	64	25	21
P8	340	287-349	8	352-537	61	29	17
P9	340	293-358	11	359-534	63	32	14
P10	344	300-359	10	359-525	60	28	14

The thermal decomposition temperatures corresponding to 5% weight loss (T_d, 5%) are above 340°C which indicates that the thermal stability of polymers **P7-P10** is excellent [56, 146, 199, 200]. The thermal stability of polymers **P7-P10** is higher than those of polymers **P1-P6**. The improved thermal stability of polymers **P7-P10** may be due to the

greater molecular length which is provided by the additional aromatic ring and ester linking group in the mesogen. However, no significant effect of terminal substituent was observed on the thermal degradation of polymers.

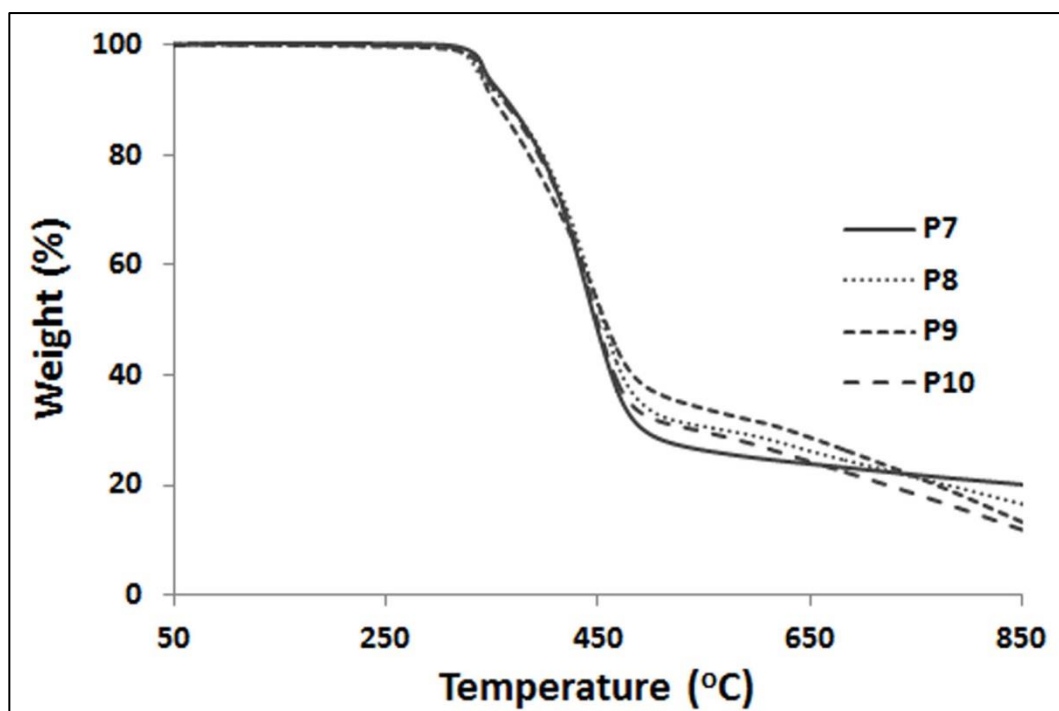


Figure 4.12: TG curves of polymers **P7-P10**

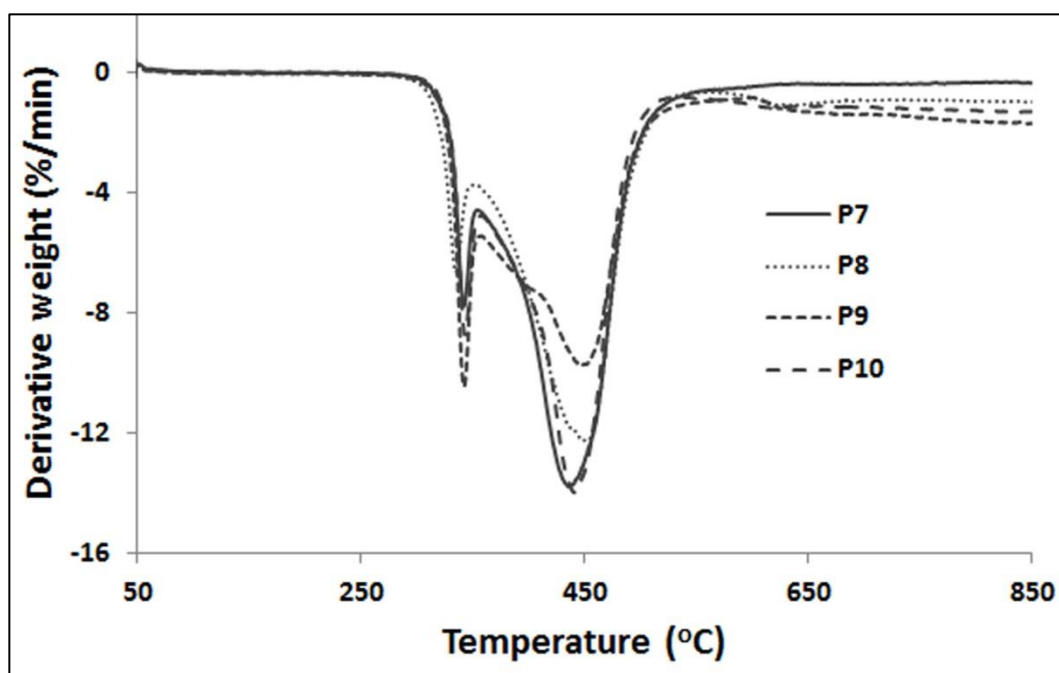


Figure 4.13: DTG traces of polymers **P7-P10**

The char yields of the polymers **P1-P10** were estimated around 14-21% and 22-32% at 850°C and 600°C respectively. The obtained char yields were good for these polymers. A good char is a useful indication of polymer being a fire retardant and thick char becomes a better thermal insulating layer and undergoes slow oxidative degradation, protecting the remaining polymer from heat radiation [203]. Moreover, increasing char formation can limit the production of combustible gases and decrease the exothermicity of the pyrolysis reaction [204].

4.4. Mesomorphic behaviour of monomers

The mesophase behaviour of monomers **M1-M10** was studied by differential scanning calorimetry (DSC) and polarizing optical microscope (POM). Phase transition temperatures and associated enthalpy changes of the synthesized monomers are summarized in Table 4.8. The mesophase assignments according to POM observation are in good agreement with the corresponding DSC thermograms. All the monomers exhibited clear-cut transition temperatures in their DSC thermograms. The identification of nematic and smectic phases was made by the comparing of observed textures with those reported in the literatures [205, 206].

4.4.1. Mesomorphic behaviour of monomers M1-M6

Figure 4.14 shows the DSC thermograms of monomer **M1**. In the second heating process, monomer **M1** exhibited an endothermic peak at 107.3°C, representing a thermal transition from a well ordered crystalline phase into an order less isotropic state. On the other hand, during the cooling scan **M1** exhibited three thermal transitions: (i) isotropic to smectic transition at 90.1°C, which is 17.2°C lower (due to supercooling) than the crystal to isotropic transition determined during heating, (ii) and (iii) transitions for crystallization at 65.5°C and 63.2°C. Therefore, monomer **M1** is a monotropic LC

compound whereby the melting points are always equal to or higher than the clearing points, hence enabling it to exhibit supercooling properties [3].

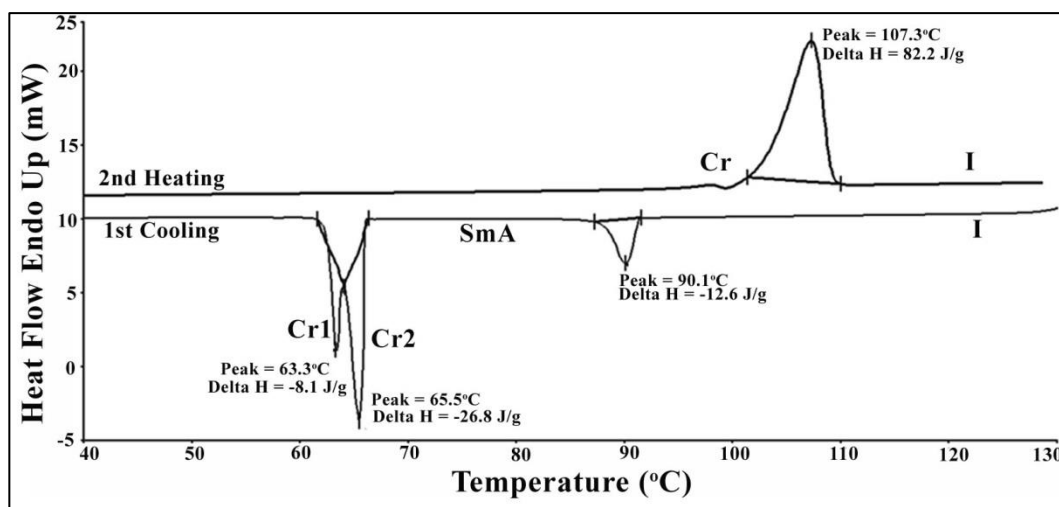


Figure 4.14: DSC thermograms of **M1** on heating and cooling at 5°C/min

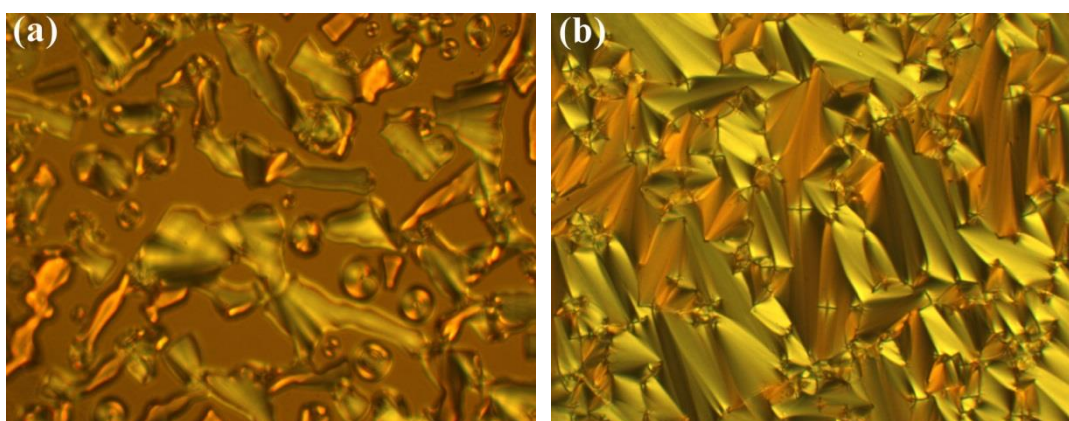


Figure 4.15: POM images of **M1** (a) smectic phase emerged as bâtonnet at 90.3°C upon cooling from isotropic liquid; (b) fan-shaped smectic A phase at 89.5°C (magnification: 50×)

POM observation also supports supercooling property of monomer **M1**. The POM images of monomer **M1** are depicted in Figure 4.15. On cooling from the isotropic liquid, monomer **M1** started forming smectic phase which emerged as bâtonnet at 90.3°C and then coalesced to form fan-shaped smectic phase at 89.5°C. The POM observations are in good agreement with the DSC thermal transition temperatures. Monomer **M2** also exhibited monotropic LC behaviour (Figure 4.16) like **M1**. During

the second heating scan, **M2** showed an endothermic peak at 116.5°C, representing a crystal to isotropic thermal transition. On the other hand, upon cooling process **M2** experienced three thermal transitions: (i) isotropic to nematic transition at 112.3°C, (ii) nematic to smectic transition at 102.6°C and (iii) crystallization at 89.2°C. Figure 4.17 exhibits polarized optical micrographs of monomer **M2**. On cooling from the isotropic melt, monomer **M2** revealed nematic droplet texture at 111.2°C and fan-shaped smectic phase at 101.5°C.

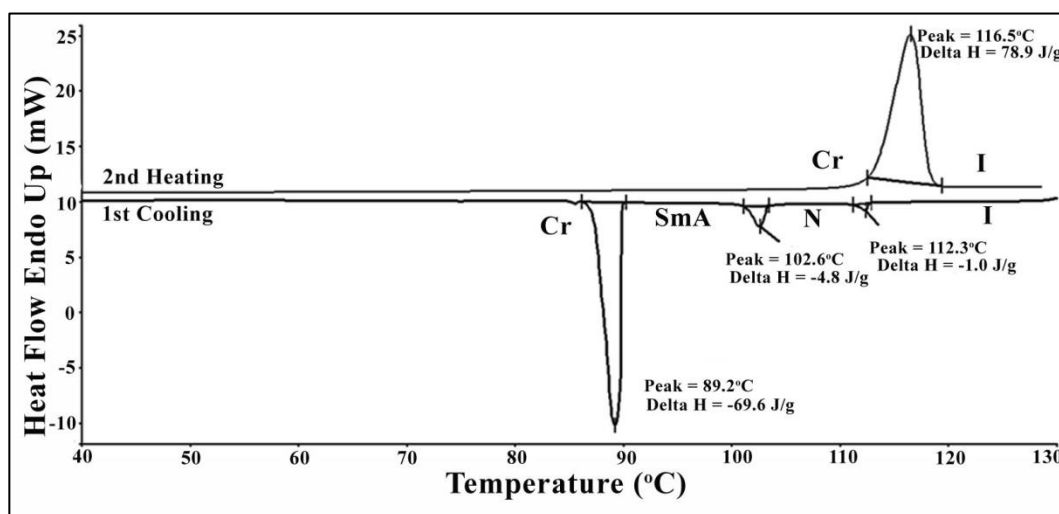


Figure 4.16: DSC thermograms of **M2** on heating and cooling at 5°C/min

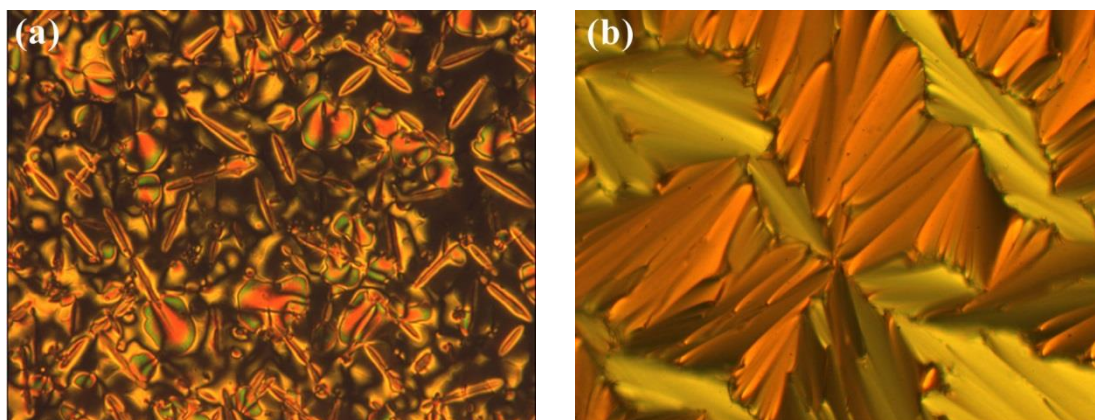


Figure 4.17: POM images of **M2**: (a) nematic phase at 112.0°C; (b) smectic A phase at 101.5°C (magnification: 50×)

The thermal transition traces of monomer **M3** are shown in Figure 4.18. The second heating process of **M3** exhibited four thermal transitions: (i) a crystal to crystal

at 91.8°C, (ii) crystal to smectic at 94.3°C, (iii) smectic to nematic at 105.2°C and (iv) nematic to isotropic at 106.9°C. The cooling scan also displayed four thermal transitions: (i) isotropic to nematic at 106.1°C, (ii) nematic to smectic at 77.0°C, (iii) and (iv) transitions for crystallization at 56.2°C and 51.0°C.

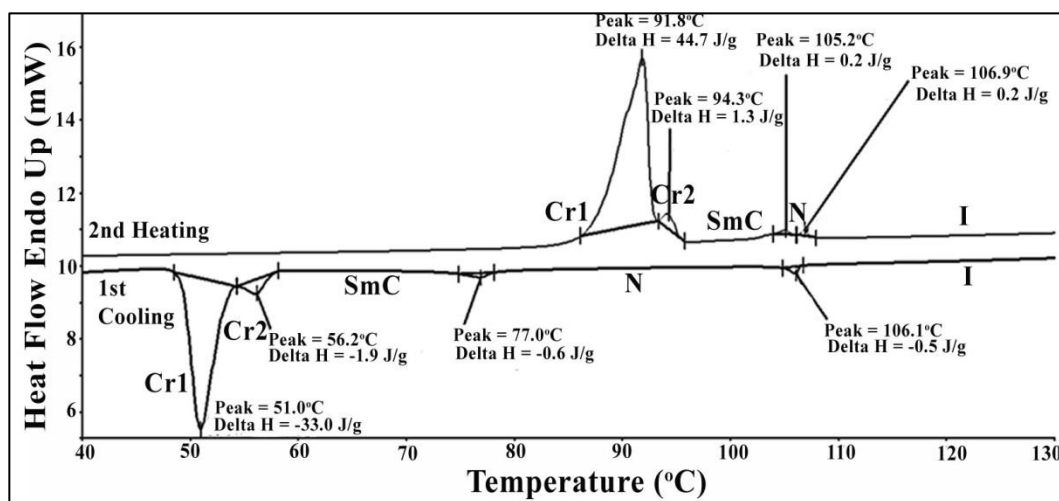


Figure 4.18: DSC thermograms of **M3** on heating and cooling at 5°C/min

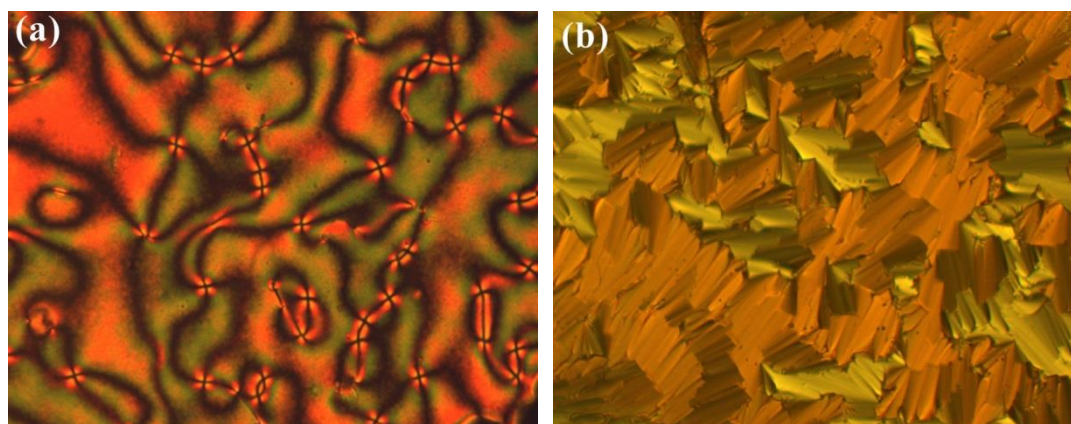


Figure 4.19: POM images of **M3**: (a) nematic phase at 105.8°C; (b) smectic C phase at 76.5°C (magnification: 50×)

The nematic and smectic transitions occur during both of heating and cooling scans, indicating an enantiotropic phase transitions of monomer **M3**. The optical photomicrographs of monomer **M3** are illustrated in Figure 4.19. On cooling from isotropic melt, monomer **M3** revealed schlieren texture of nematic phase with fourfold brush at 105.8°C and fan-shaped smectic phase at 76.5°C and both the transitions were enantiotropic. The thermal behaviour of monomer **M4** is quite different (Figure 4.20)

than that of **M3**. Monomer **M4** showed two thermal transitions during the second heating process: (i) crystal to nematic at 97.3°C and (ii) nematic to isotropic at 111.2°C. On the contrary, upon cooling scan monomer **M4** exhibited three thermal transitions: (i) isotropic to nematic at 110.5°C, (ii) nematic to smectic at 76.2°C and (iii) crystallization at 54.8°C.

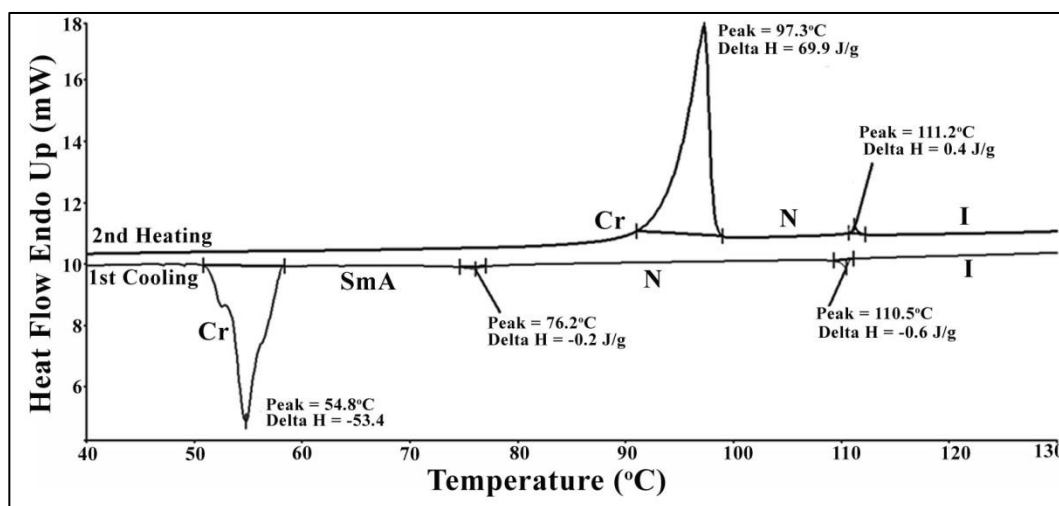


Figure 4.20: DSC thermograms of **M4** on heating and cooling at 5°C/min

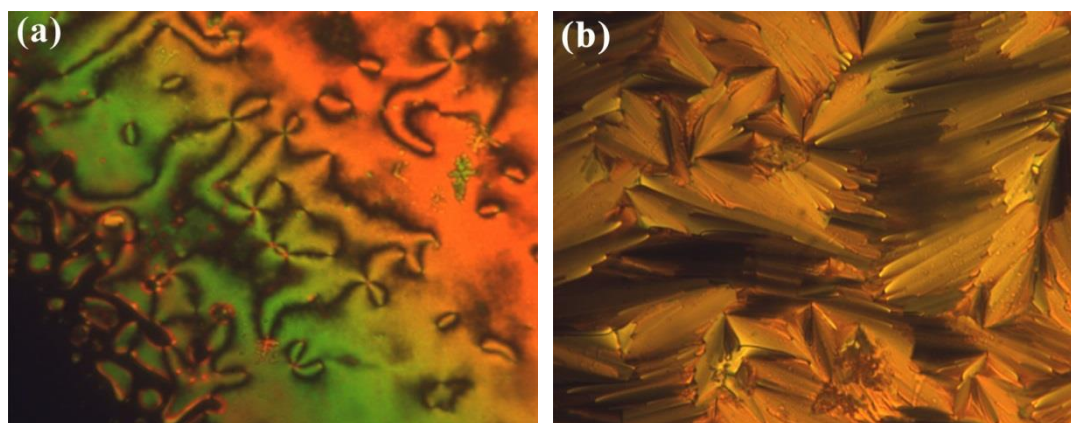


Figure 4.21: POM images of **M4**: (a) nematic phase at 109.8°C; (b) smectic A phase at 75.5°C (magnification: 50×)

It is evident from the DSC thermograms (Figure 4.20) that the nematic phase transition is enantiotropic whereas smectic phase transition is monotropic in nature for monomer **M4**. The optical photomicrographs of monomer **M4** are given in Figure 4.21. Upon cooling from isotropic liquid, **M4** exhibited schlieren texture of nematic phase with fourfold brush at 109.8°C and this transition was enantiotropic. On further cooling, **M4**

displayed fan-shaped texture of smectic phase with narrow and elongated ellipses at 75.5°C.

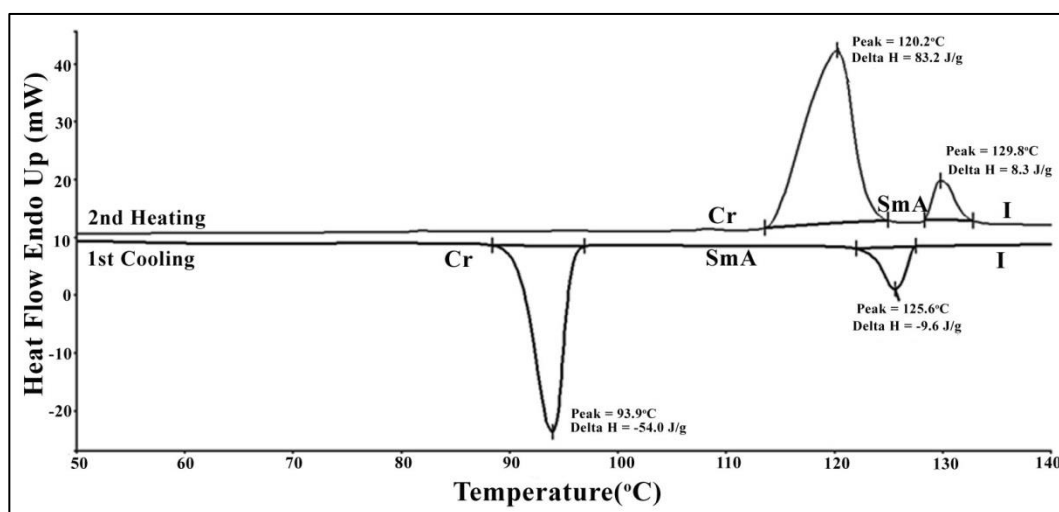


Figure 4.22: DSC thermograms of **M5** on heating and cooling at 10°C/min

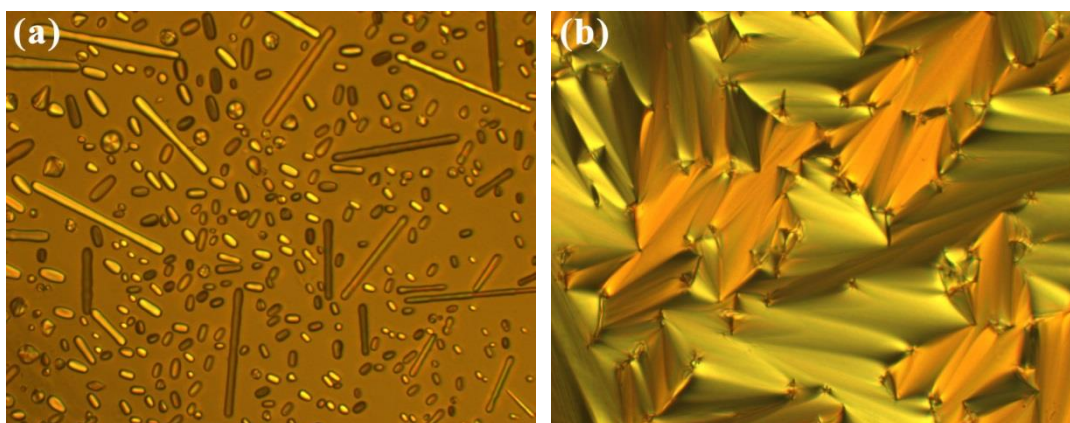


Figure 4.23: POM images of **M5**: (a) smectic phase emerged as bâtonnet at 125.8°C upon cooling from isotropic liquid; (b) fan-shaped smectic A phase at 124.5°C (magnification: 50×)

Figure 4.22 gives the thermal transition traces of **M5** and the obtained results are different than those of monomer **M1-M4**. Monomer **M5** exhibited two thermal transitions during both of heating and cooling processes. The second heating scan displayed a crystal to smectic transition at 120.2°C and smectic to isotropic transition at 129.8°C. During cooling process an isotropic to smectic transition is identified at 125.6°C and crystallization was detected at 93.8°C. Figure 4.23 gives the optical

photomicrographs of monomer **M5**. The POM observations revealed that monomer **M5** started forming smectic phase which emerged as bâtonnet at 125.8°C upon cooling from isotropic melt and further cooling a well-defined fan-shaped smectic A phase appeared at 124.5°C. Like **M5**, monomer **M6** exhibited similar thermal transitions and LC behaviours (Figure 4.24).

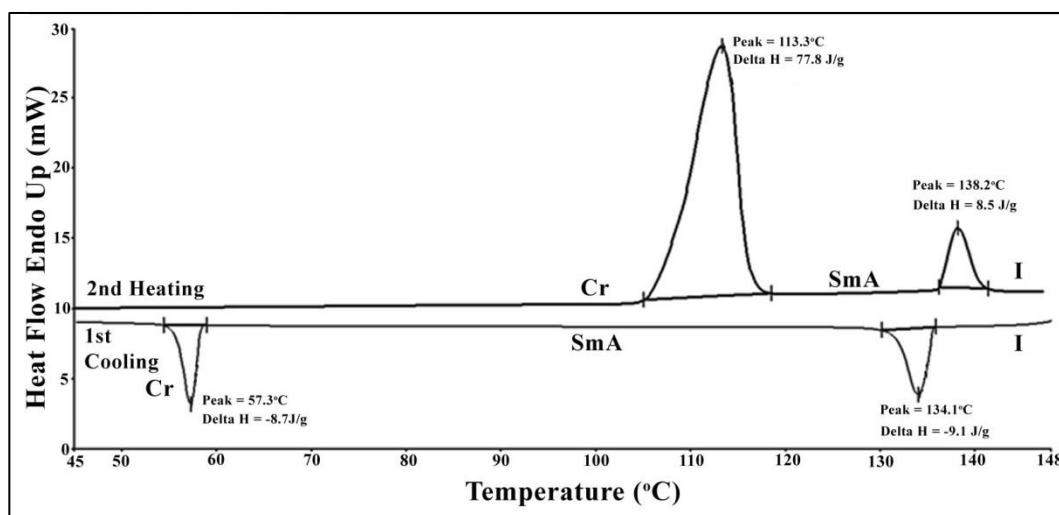


Figure 4.24: DSC thermogram of **M6** on heating and cooling at 10°C/min

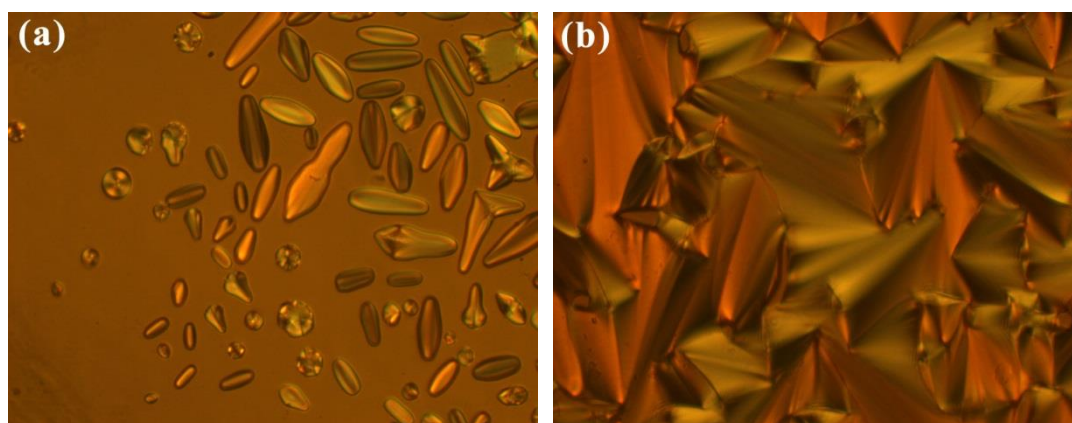


Figure 4.25: POM images of **M6** (a) smectic phase emerged as bâtonnet at 134.5°C upon cooling from isotropic liquid; (b) fan-shaped smectic A phase at 133.5°C (magnification: 50×)

Two thermal transitions were also observed for **M6** during both of heating and cooling scans. The second heating scan exhibited a crystal to smectic transition at 113.3°C and smectic to isotropic transition at 138.2°C. On cooling scan, an isotropic to smectic transition was detected at 134.1°C and crystallization was observed at 57.3°C. Figure

4.25 shows the optical photomicrographs of monomer **M6**. The POM study of monomer **M6** revealed that a smectic phase emerged as bâtonnet at 134.5°C on cooling from isotropic melt and further cooling a clear fan-shaped smectic A phase appeared at 133.5°C.

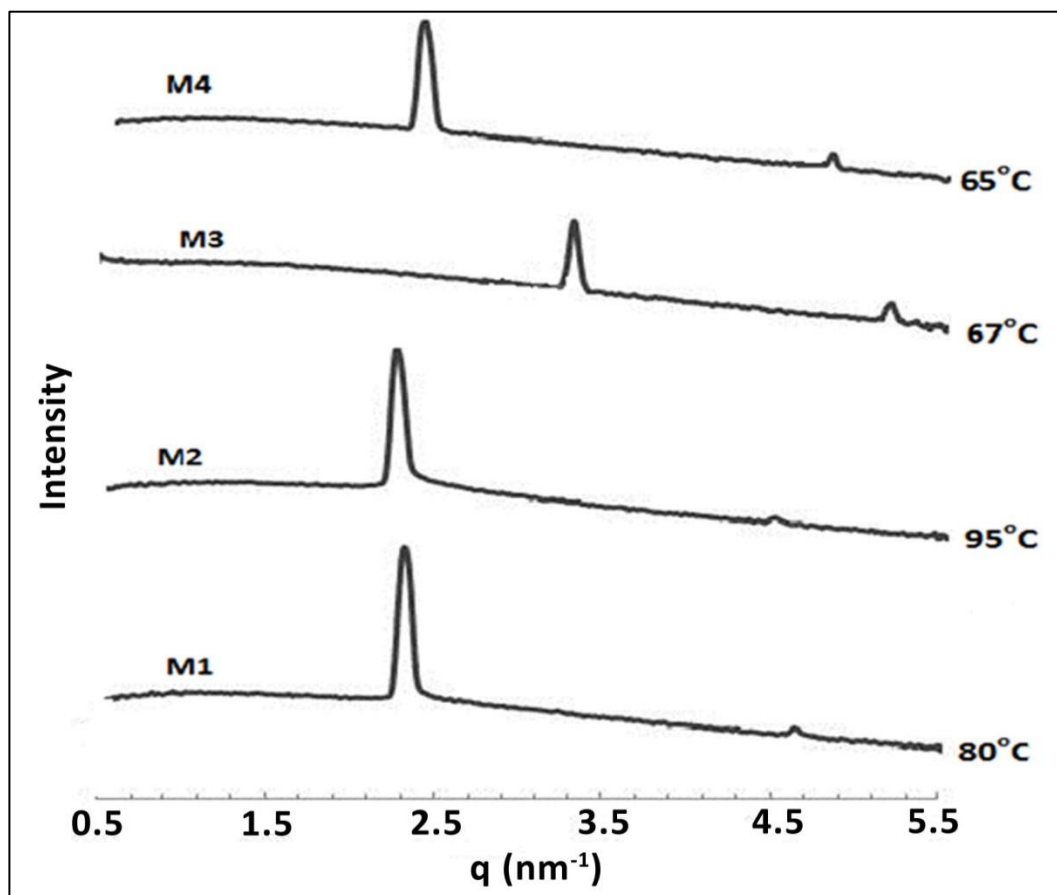


Figure 4.26: SAXS patterns of **M1- M4** at 80°C, 95°C, 67°C and 65°C respectively

The LC phases of monomers **M1-M4** were further studied by SAXS to confirm their mesophase assignment. Figure 4.26 exhibits the SAXS patterns of studied monomers which were obtained for the LC temperatures upon cooling from their isotropic states. The scattering vector ($q = 4\pi\sin\theta/\lambda$) and layer spacing ($d = 2\pi/q$) were estimated for the temperatures where monomers **M1- M4** showed smectic phase. The calculated molecular lengths (l), estimated layer spacing values (d), and data collecting temperatures of monomers **M1-M4** are listed in Table 4.7. The q values for the first peak of **M1**, **M2**, and **M4** are 2.29 nm⁻¹, 2.22 nm⁻¹, 2.35 nm⁻¹ and their corresponding d

values are 2.74 nm, 2.83 nm and 2.67 nm respectively. The ratio of q_1 to q_2 for **M1**, **M2** and **M4** is 1: 2, indicating the presence of a long range ordered lamellar structure [207].

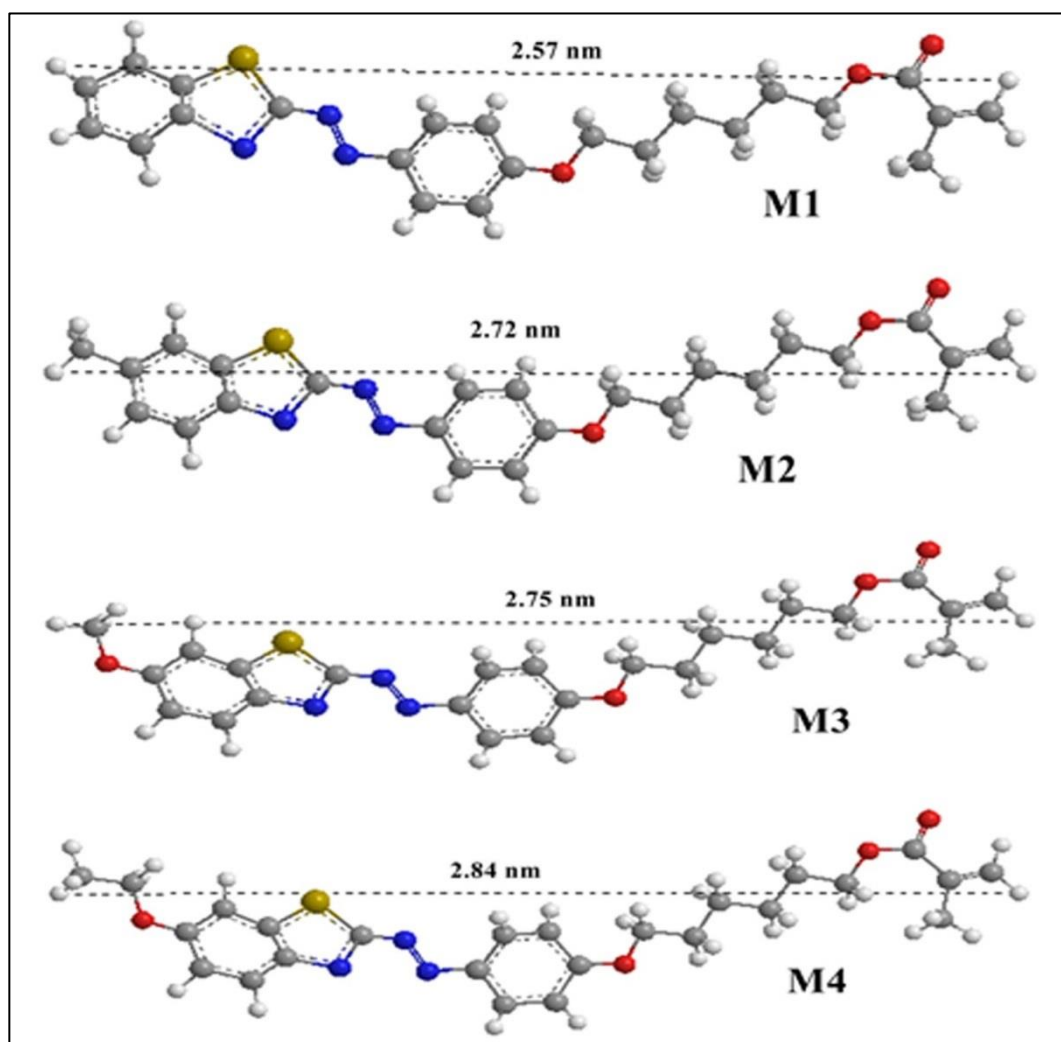


Figure 4.27: Molecular structures and molecular lengths of **M1-M4**. The molecular lengths of the studied compounds were calculated from the most extended conformation with optimized energy level by simple molecular modelling (ChemBio3D Ultra 11.0).

Furthermore, the observed d values of **M1**, **M2** and **M4** are in good agreement with the calculated molecular length (l) (Figure 4.27 & Table 4.7) for the fully extended conformation, suggesting an ordered smectic A phase. On the other hand, q value for the first scattering peak of **M3** is 3.33 nm^{-1} and corresponding d value is 1.89 nm. The estimated d value (1.89 nm) of **M3** is smaller than the calculated molecular length ($l = 2.75 \text{ nm}$) for the fully extended conformation, revealing the presence of smectic C structure [173].

Table 4.7: Scattering vector q (nm^{-1}), layer spacing, d (nm), calculated molecular length, l (nm) and data collecting temperature ($^{\circ}\text{C}$) of monomers **M1-M4**

	Data collecting temperature ($^{\circ}\text{C}$)	First Peak q_1 (nm^{-1})	Layer spacing d (nm)	Second peak q_2 (nm^{-1})	$q_1 : q_2$	Calculated molecular length l (nm)
M1	80	2.29	2.74	4.56	1 : 2	2.57
M2	95	2.22	2.83	4.42	1 : 2	2.72
M3	67	3.33	1.89	5.22	1 : 1.6	2.75
M4	65	2.35	2.67	4.77	1 : 2	2.84

4.4.2. The effect of terminal substituents on mesophase behaviours of M1-M6

The mesophase ranges, phase transition temperatures and corresponding enthalpy changes of monomers **M1-M6** are presented in Table 4.8. Although monomers **M1-M6** have similar molecular structure except terminal sixth position substituent on the benzothiazole ring, different LC phases were exhibited during heating and cooling. In order to investigate the terminal substituent effect on mesophase formation, X = H, CH₃, OCH₃, OC₂H₅, F and Cl groups situated at the sixth position on the benzothiazole ring were chosen for this study. It can be clearly seen from figures (Figure 4.14 to Figure 4.25) and Table 4.8 that the terminal methacrylate group and the sixth position substituents on benzothiazole ring have significant role on the mesophase formation. Comparison among the six monomers reveals that **M1**, **M5** and **M6** showed only smectic mesophase whereas monomers **M2**, **M3** and **M4** exhibited both nematic and smectic phases. Monomers with an electron donating substituent (CH₃, OCH₃ and

OC₂H₅) exhibited both nematic and smectic mesophases; however, monomer without terminal substituent (**M1**) revealed only SmA phase.

Table 4.8: Mesophase lengths, phase transition temperatures and enthalpy changes for monomers **M1- M6** upon heating and cooling scans.

	Phase transitions, (°C) (enthalpy changes, J g ⁻¹)		Mesophase range (°C)	
	Second Heating	First Cooling	Nematic	Smectic
M1	Cr 107.3 (82.2) I	Cr ₁ 63.3 (-8.1) Cr ₂ 65.5 (-26.8) SmA 90.1 (-12.6) I	-	24.6
M2	Cr 116.5 (78.9) I	Cr 89.2 (-69.6) SmA 102.6 (-4.8) N 112.3 (-1.0) I	9.7	13.4
M3	Cr ₁ 91.8 (44.7) Cr ₂ 94.3(1.3) SmC 105.2 (0.2) N 106.9 (0.2) I	Cr ₁ 51.0 (-33.0) Cr ₂ 56.2 (-1.9) SmC 77.0 (-0.6) N 106.1 (-0.5) I	29.1	20.8
M4	Cr 97.3 (69.9) N 111.2 (0.4) I	Cr 54.8 (-53.4) SmA 76.2 (-0.2) N 110.5 (-0.6) I	34.3	21.4
M5	Cr 120.2 (83.2) SmA 129.8 (8.3) I	Cr 93.9 (-54.0) SmA 125.6 (-9.6) I	-	31.7
M6	Cr 113.3 (77.8) SmA 138.2 (8.5) I	Cr 57.3 (-8.7) SmA 134.1 (-9.1) I	-	76.8

Transition temperatures (°C) and enthalpies (in parentheses, J g⁻¹) were measured by DSC. Cr = Crystalline phase; SmA = Smectic A phase; SmC = Smectic C phase; N = Nematic phase; I = Isotropic liquid.

The terminal methacrylate group attached with alkyl spacer could play an important role to the formation of smectic phase in monomer **M1**. This statement can be explained by comparing the mesophase behaviour of **M1**- **M4** with recently reported structurally similar compounds [118, 122] whereby only nematic LC phase of same mesogenic unit containing molecules was reported. This result may be attributed to the fact that the terminal polar methacrylate group enhanced the polarisability anisotropy and could favour the lateral attraction between molecules to generate a strong smectic phase. On the other hand, monomers **M2**, **M3** and **M4** exhibited nematic phase along with smectic phase. Replacement of hydrogen atom by the methyl, methoxy and ethoxy groups at the sixth position on the benzothiazole ring may play vital role to the formation of the nematic phase because the relatively short terminal chains in conjugation with a core of high longitudinal polarisability facilitates the generation of nematic phase [3]. Polarization or electron distribution in electron-deficient benzothiazole moiety may also be affected by the electron-donating substituents which could facilitate the formation of nematic phase. The mesophase temperature ranges were significantly influenced (Table 4.8) by the size of the sixth position substituent on benzothiazole ring. Monomer with ethoxy substituent exhibited greater mesophase stability than those of compounds with methoxy and methyl substituents. Like **M1**, monomers **M5** and **M6** having terminal electron withdrawing F and Cl atom respectively exhibited only SmA phase. However, monomer **M6** containing a larger or more polarized group (X = Cl) which enhanced the SmA phase stability than monomers with a smaller polarized substituent (X = F) and without polarized group (X = H). The clearing temperature of monomer **M6** (138.3°C) was higher than those of compounds **M5** (129.2°C) and **M1** (107.3°C), i.e., 138.3°C > 129.2°C > 107.3°C. On the other hand, monomer **M6** (76.8°C) exhibited greater mesophase stability than those of monomers **M5** (31.7°C) and **M1** (24.6°C), i.e., 76.8°C > 31.7°C > 24.6°C on cooling. The higher clearing temperature and greater mesophase

stability of monomer **M6** may be due to the strong polarizing power of Cl atom. Therefore, it can obviously be concluded that the terminal sixth position substituent on the benzothiazole moiety has profound influence on the formation of mesophase as well as mesophase stability of the synthesized LC monomers.

4.4.3. Mesomorphic behaviours of LC monomers M7-M10

Figure 4.28 shows DSC thermograms of synthesized monomers **M7-M10**. The isotropization temperatures of monomers **M7-M10** determined from DSC were almost identical with the onset thermal decomposition temperatures of azo-benzothiazole segment as observed from TGA analysis. As a result, no distinct DSC peaks were identified for monomers **M7-M10** during cooling scan due to the partial decomposition of the studied monomers. Wei et al. [208] also reported similar observation for their studied compounds. Thus, only first heating data of monomers **M7-M10** are considered for further discussion.

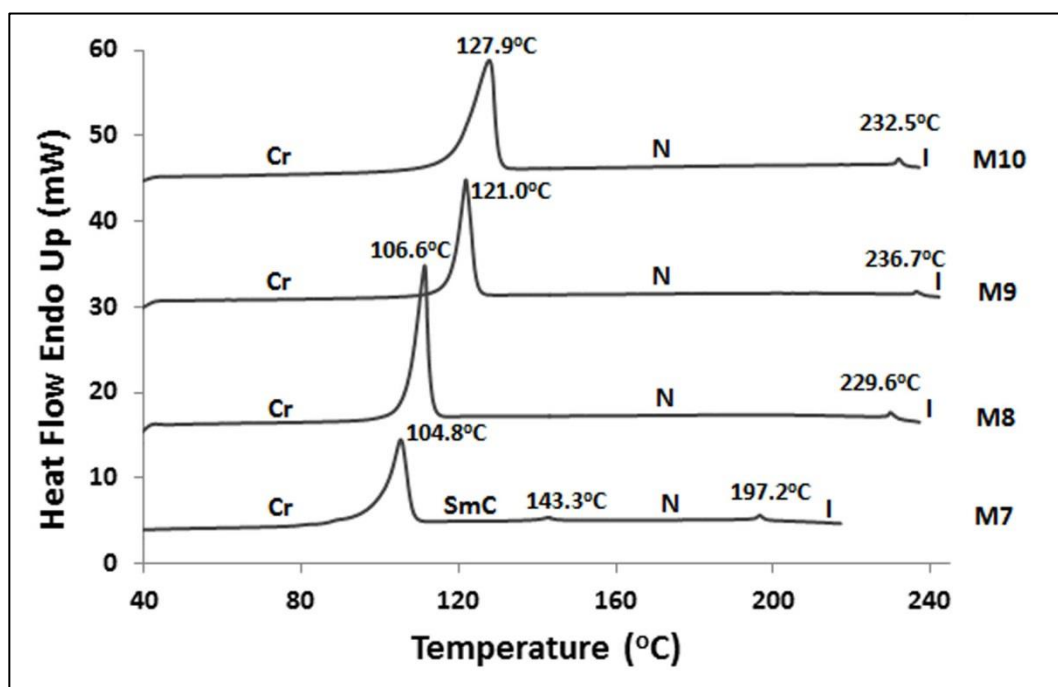


Figure 4.28: DSC traces of monomers **M7-M10** on first heating scan at 10°C/min

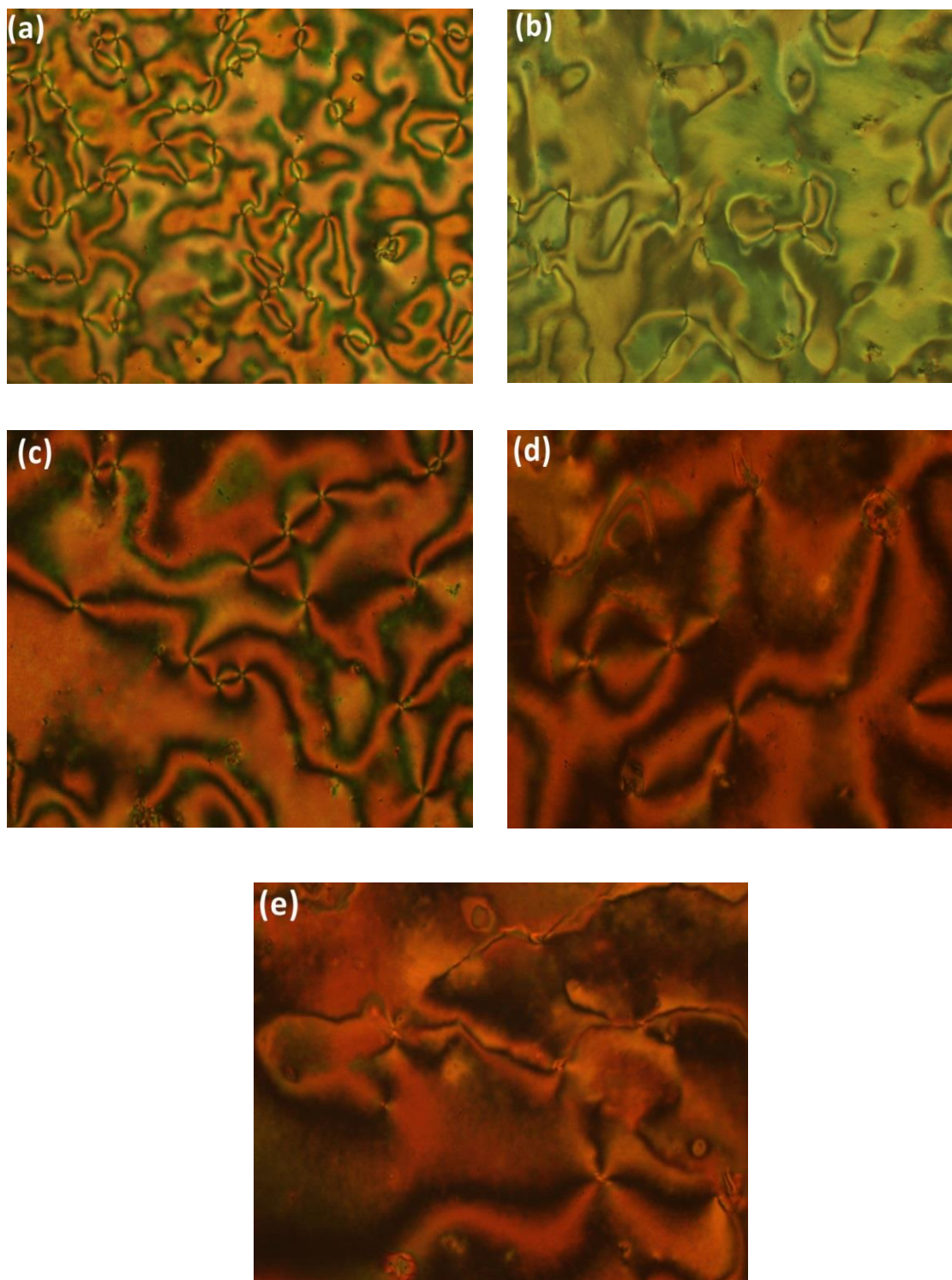


Figure 4.29: POM images of compounds **M7- M10**: (a) & (b) **M7** displays schlieren texture of nematic phase at 196.8°C and smectic C phase at 140.5°C; (c) **M8** shows nematic phase at 225.5°C; (d) **M9** exhibits nematic phase at 229.4°C (e) **M10** reveals nematic (threaded) phase at 226.5°C (magnification: 50×)

It can be seen from Figure 4.28 that monomer **M7** exhibits three thermal transitions: (i) a crystal to smectic at 104.8°C, (ii) smectic to nematic at 143.3°C and

(iii) nematic to isotropic at 197.2°C. On the other hand, monomer **M8** shows two thermal transitions: (i) a crystal to nematic at 106.6°C and (ii) nematic to isotropic at 229.6°C. Similarly, monomer **M9** exhibits a crystal to nematic transition at 121.0°C and (ii) nematic to isotropic transition at 236.7°C. Likewise **M8** and **M9**, monomer **M10** shows two thermal transitions: (i) crystal to nematic at 127.9°C and (ii) nematic to isotropic at 232.5°C.

The observed optical photomicrographs of **M7-M10** are shown in Figure 4.29. The optical photomicrographs of monomer **M7** were taken during cooling scan whereas POM images of **M8-M10** were recorded during heating scan. Monomer **M7** exhibited schlieren texture of nematic phase at 196.8°C upon cooling from isotropic liquid and further cooling schlieren texture of smectic C phase appeared at 140.5°C. The identification of SmC phase was made on the basis of the characteristic grey schlieren texture (Figure 4.29b) which appeared during nematic to smectic C transition [209]. During heating, monomer **M8** melted around 107.0°C and upon further heating schlieren texture of nematic phase with four-fold brushes (Figure 4.29c) started appearing and the image was taken at 225.5°C. Monomers **M9** and **M10** also exhibited schlieren texture of nematic phases upon heating scan and the POM images of **M9** and **M10** were recorded at 229.4°C and 226.5°C respectively.

4.4.4. The effect of terminal substituent and mesogen length on mesomorphic behaviour of M7-M10

Monomers **M7-M10** possess an additional benzene ring and ester linkage in their molecular structure than those of monomers **M1-M4**. It can be compared from Table 4.8 and Table 4.9 that the clearing temperatures of monomers **M7-M10** are much higher than those of monomers **M1-M4**. This result may be attributed to the fact that additional aromatic ring and ester linkage enhance the molecular length of monomers

M7-M10 which leads to increase clearing temperatures tremendously. In addition, mesomorphic behaviours of **M7-M10** are completely different than those of **M1-M4**. Monomer **M1** exhibited only smectic phase whereas **M7** showed both nematic and smectic phases.

Table 4.9: Mesophase lengths, phase transition temperatures and enthalpy changes for **M7-M10** upon first heating scan.

	Phase transition temperatures (°C) (enthalpy changes, J g ⁻¹)	Mesophase length(°C)	
		N	SmC
^a M7	Cr 104.8 (46.1) SmC 143.3(0.5) N 197.2 (0.6) I	53.4	38.5
^a M8	Cr 106.6(36.5) N 229.6 (0.7) I	123.0	-
^a M9	Cr 121.0 (58.7) N 236.7 (0.5) I	115.7	-
^a M10	Cr 127.9 (56.4) N 232.5(0.6) I	104.6	-

^a Only first heating data are provided. No distinct peak was detected during the cooling scan due to their partial decomposition. Transition temperatures (°C) and enthalpies (in parentheses, J g⁻¹) were measured by DSC. Cr = Crystalline phase; SmC = Smectic C phase; N = Nematic phase; I = Isotropic liquid.

M2-M4 displayed both nematic and smectic phases but **M8-M10** revealed only nematic phase. These results may be ascribed to fact that the additional ester linkage which conferred stepped core structure leading to the broadening effect, thus disrupting the lamellar packing, and therefore stabilizing the nematic phase [3]. Moreover, polarization or electron distribution in electron-deficient benzothiazole moiety may also be affected by the electron-donating substituent (CH₃, OCH₃ and OC₂H₅) which could facilitate the formation of nematic phase. Replacement of hydrogen atom by methyl, methoxy and ethoxy groups at the sixth position on benzothiazole moiety has

substantial influence on mesophase stability. Methyl substituted compound (**M8**) exhibited greater mesophase stability (123.0°C) than those of methoxy (115.7°C) and ethoxy (104.6°C) substituted compounds (**M9** and **M10**). The reduced nematic phase stability of monomer **M9** and **M10** may be attributed to the fact that the oxygen being in conjugation with the heteroaromatic core, extends the length of the rigid core as well as enhances the polarizability anisotropy [3].

4.5. Mesomorphic behaviour of SCLCPs

4.5.1. Mesomorphic behaviour of polymers P1-P6

The thermal transition temperatures and mesomorphic behaviours of polymers were studied by differential scanning calorimetry (DSC) and polarizing optical microscope (POM). The DSC thermograms of polymers **P1-P4** during heating and cooling scans are shown in Figure 4.30. It can be observed from Figure 4.30 that polymer **P1** exhibits two thermal transitions: (i) glass transition temperature to smectic at 122°C and (ii) smectic to isotropic at 180.0°C during second heating scan. Upon cooling scan, **P1** shows an isotropic to smectic transition at 165.5°C, which is 14.5°C lower than heating process, due to supercooling. Polymer **P2** also displays two thermal transitions: (i) glass transition to nematic at 134°C and (ii) nematic to isotropic at 184.2°C upon heating scan. On the other hand, an isotropic to nematic transition is observed at 180.5°C and nematic to smectic transition is detected at 164.5°C during cooling scan. Polymer **P3** reveals three thermal transitions during heating process: (i) glass transition to smectic at 93°C, (ii) smectic to nematic at 145.3°C and (iii) nematic to isotropic at 185.8°C. An isotropic to nematic transition is observed at 179.5°C and nematic to smectic transition is detected at 130.8°C during cooling scan. Similarly, **P4** exhibits two thermal transitions: (i) glass transition to nematic at 89°C and nematic to

isotropic at 175.1°C during heating cycle and an isotropic to nematic transition is identified at 169.5°C on cooling process.

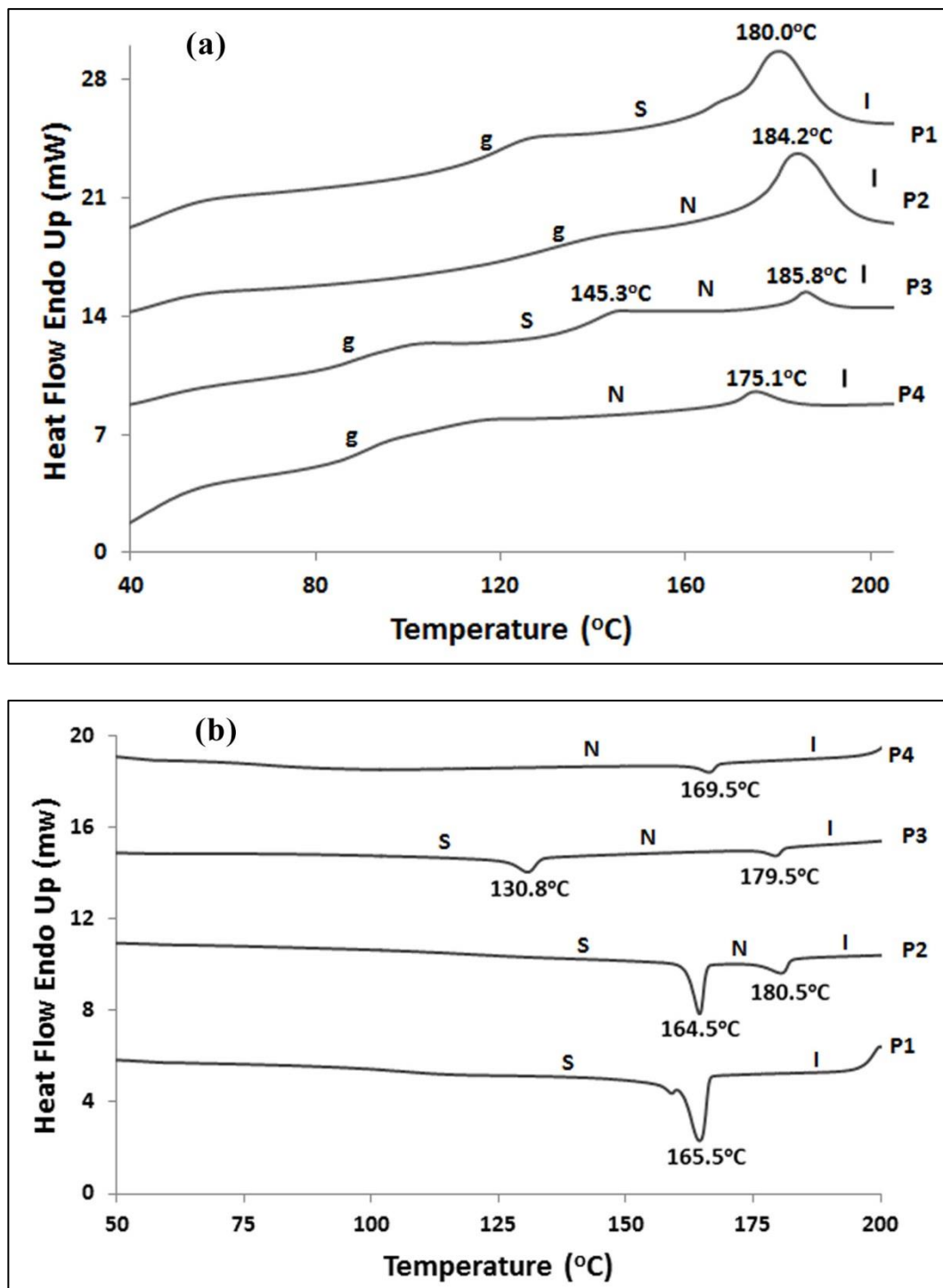


Figure 4.30: DSC curves of **P1-P4** on (a) second heating scan rate at 20°C and (b) first cooling scan at 10°C/min

The DSC traces of polymers **P5** and **P6** are depicted in Figure 4.31. During heating cycle polymer **P5** showed glass transition to smectic phase transition at 99°C

and smectic to isotropic transition was detected at 215.2°C while an isotropic to smectic transition was identified at 210.8°C during cooling scan. However, polymer **P6** exhibited two well-defined thermal transitions during the first heating cycle: (i) glass transition to smectic phase at 107°C and (ii) smectic to isotropic transition at 239.8°C. Due to the high clearing temperature, partial decomposition of polymer **P6** may have happened during heating scan. As a result, no distinct thermal transition peak was identified upon cooling process.

Table 4.10: Phase transition temperatures and corresponding enthalpy changes of **P1-P6** upon second heating and first cooling scans

	Phase transition temperatures (°C) (enthalpy changes, J g ⁻¹)		T _g (°C)
	Heating	Cooling	
P1	g 122 S 180.0 (8.2) I	S 165.5 (-10.2) I	122
P2	g 134 N 184.2 (9.3) I	S 164.5(-4.6) N 180.5(-1.7) I	134
P3	g 93 S 145.3 (0.2) N 185.8(0.9) I	S 130.8(-2.9) N 179.5 (-1.0) I	93
P4	g 89 N 175.1 (0.9) I	N 169.5 (-1.0) I	89
P5	g 99 S 215.2 (5.4) I	S 210.8 (-5.4) I	99
^a P6	g 107 S 239.8 (0.6) I	-	107

^aNo distinct peak was detected during the cooling scan due to its partial decomposition. Transition temperatures (°C) and enthalpies (in parentheses, J g⁻¹) were measured by DSC. g = glassy state; S = Smectic phase; N = Nematic phase; I = Isotropic liquid; T_g = Glass transition temperature

The glass transition temperatures (T_g) of polymers **P1-P6** are in the range of 89°C to 134°C (Table 4.10). Polymer **P1** exhibited T_g of 122°C whereas polymer **P2**

displayed exceptionally high T_g of 135°C among all the studied polymers. The T_g values of other polymers **P3-P6** were shifted toward lower temperature region with the incorporation of short terminal tails i.e., OCH_3 , OC_2H_5 , F and Cl in the mesogen. This observation may be ascribed to the fact that terminal tails attached to the mesogenic unit could induce flexibility which may lower the T_g values [210]. Moreover, the decreasing tendency of T_g values could be ascribed to the combined effects of the steric hindrance and plasticization function of the terminal tails of the polymers [211].

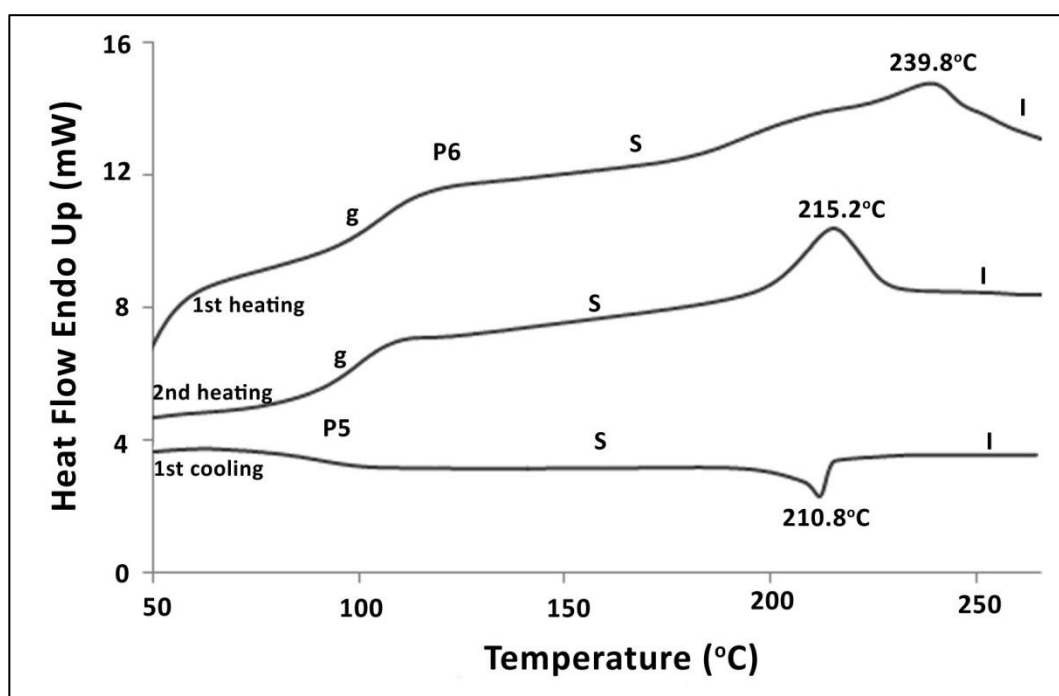


Figure 4.31: DSC traces of **P5** and **P6** on heating at $20^\circ\text{C}/\text{min}$ and cooling at $10^\circ\text{C}/\text{min}$

Figure 4.32 shows the optical photomicrographs of polymers **P1-P6**. The mesophase assignments according to POM observation are in good agreement with the corresponding DSC thermograms. Upon cooling from the isotropic liquid, polymer **P1** exhibited fan-shaped smectic phase at 164.8°C . POM study revealed that polymers **P2** and **P3** showed both nematic and smectic phases upon cooling from isotropic state. On cooling from isotropic liquid, **P2** exhibited schlieren texture of nematic phase at 179.8°C and further cooling smectic phase appeared at 162.6°C . Similarly, **P3** revealed

schlieren texture of nematic phase at 180.2°C upon cooling from isotropic melt and again cooling smectic phase emerged at 132.3°C .

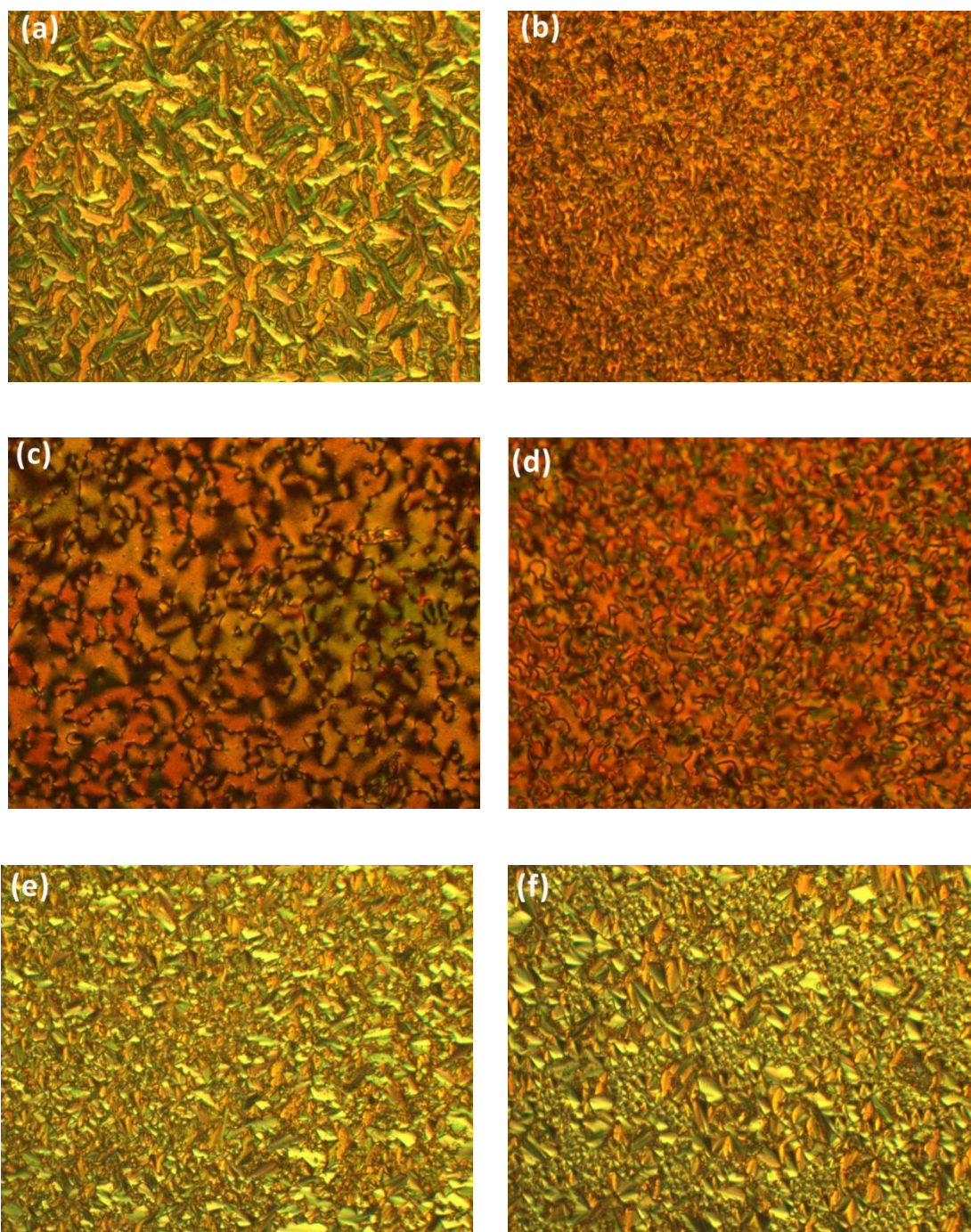


Figure 4.32: POM images of **P1**- **P6**: (a) **P1** exhibits smectic phase at 164.8°C ; (b) **P2** shows nematic phase at 179.8°C ; (c) **P3** displays nematic phase at 180.2°C ; (d) **P4** reveals nematic phase at 169.9°C ; (e) **P5** exhibits smectic phase at 209.5°C and (f) **P6** shows smectic phase at 233.8°C (magnification: $50\times$)

However, polymers **P2** and **P3** could not exhibit well-defined smectic phases. Polymer **P4** displayed only schlieren texture of nematic phase at 170.5°C on cooling from

isotropic liquid. Polymer **P5** revealed smectic phase at 209.5°C on cooling from isotropic liquid whereas polymer **P6** displayed smectic phase 233.8°C upon cooling from isotropic melt.

4.5.2. Mesomorphic behaviour of polymers **P7-P10**

Figure 4.33 shows DSC traces of polymers **P7-P10**. As isotropization temperatures of polymers **P7-P10** are higher or equal to the decomposition temperatures, only glass transition temperatures are identified from DSC traces. The DSC curves of **P7-P10** start declining before/after isotropic points. Polymer **P7** shows slightly higher T_g than polymers **P8-P10**.

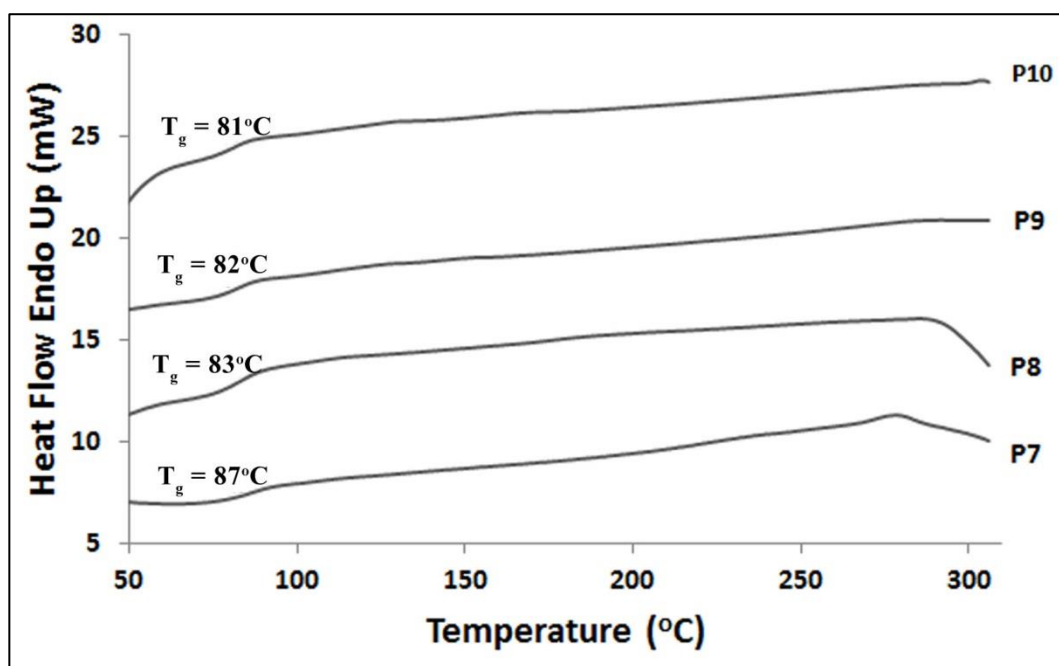


Figure 4.33: DSC traces of polymers **P7-P10** under heating scan at 20°C/min

The decreasing tendency of T_g values of polymer **P8-P10** may be due to the terminal tail which could induce flexibility and thus lowers the T_g values. Figure 4.34 displays the optical photomicrographs of polymers **P7-P10**. All the POM images were recorded during heating process. Each polymer exhibited nematic liquid crystalline phases. The POM images were taken at 200.5°C, 210.8°C, 220.4°C and 215.6°C for **P7-P10**

respectively. Although polymers **P1-P10** were annealed for rather long time at their LC temperatures, the POM images were not observed clearly. This observation may be due to the high polymer viscosity which could hinder the formation of well-defined LC phases [173].

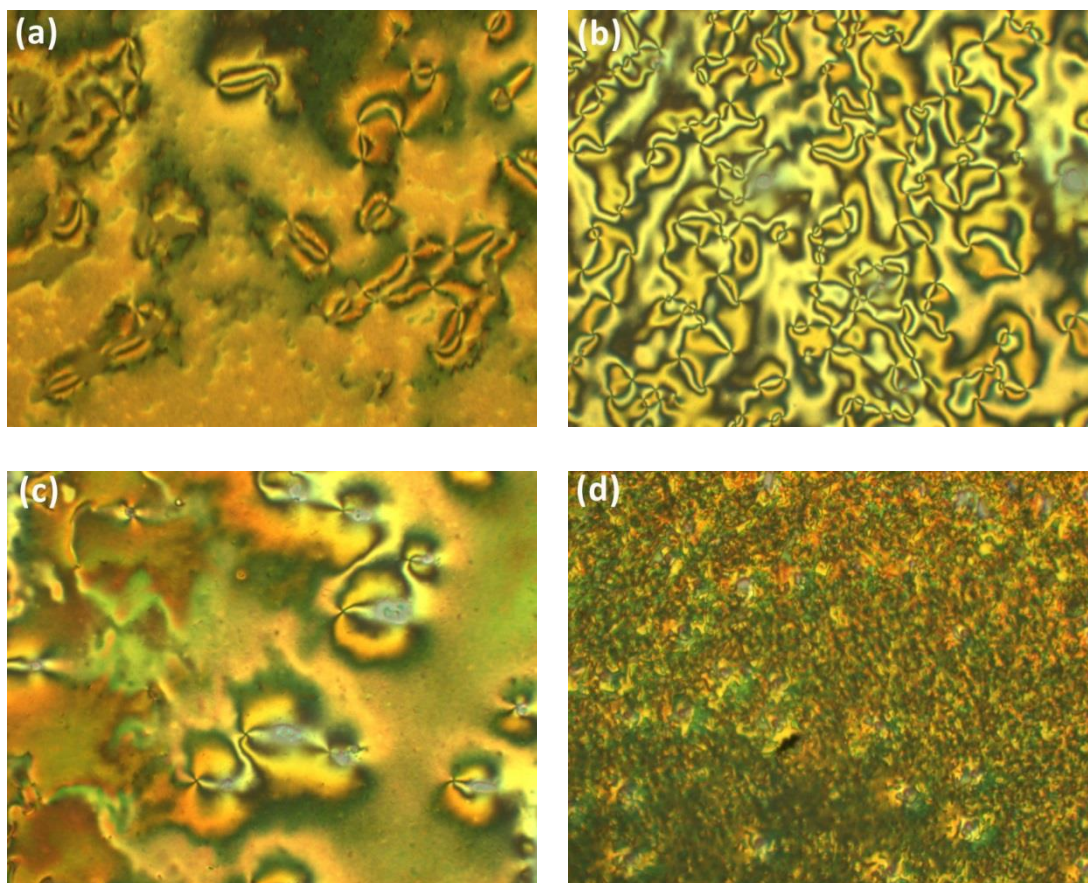


Figure 4.34: POM images of polymers **P7- P10**: (a) **P7** shows nematic phase at 200.5°C; (b) **P8** exhibits nematic phase at 210.8°C; (c) **P9** displays nematic phase at 220.4°C; (d) **P10** reveals nematic phase at 215.6°C (magnification: 50×)

4.6. Optical properties of SCLCPs

4.6.1. Optical properties of polymers P1-P6

Figure 4.35 shows the UV-vis absorption spectra of SCLCPs **P1-P6** in dilute chloroform solutions (1×10^{-6} M) and the obtained results are summarized in Table 4.11.

The absorption spectra of polymers **P1-P6** are very similar in shape because the spectral

properties of polymers **P1-P6** are governed by the structurally similar azo-benzothiazole mesogen in the side chain of the polymers.

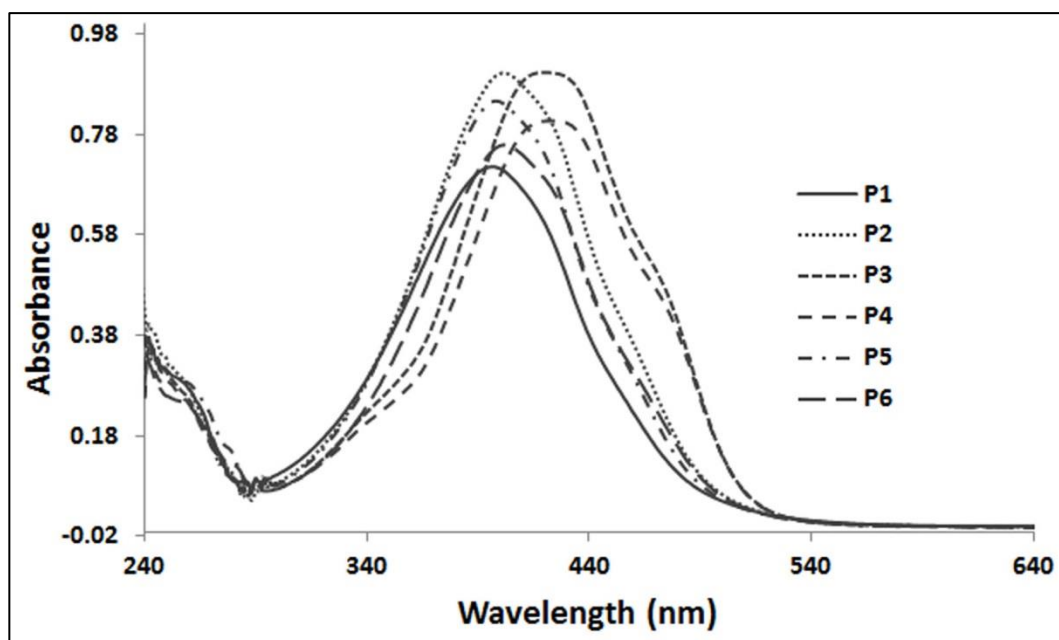


Figure 4.35: UV-vis spectra of **P1-P6** in dilute CHCl_3 solutions (1×10^{-6} M)

All the polymers exhibited similar absorption bands in their UV-vis spectra with strong and broad absorption bands found in the range of 300–530 nm and the absorption maxima (λ_{max}) appearing at 397 nm, 401 nm, 420 nm, 423 nm, 398 nm and 402 nm for **P1-P6** respectively. These absorption bands may be regarded as a π - π^* transition involving the π -electronic system throughout the whole mesogenic unit with a considerable charge transfer (CT) character [212-214]. The absorption maxima (λ_{max}) of polymers were bathochromically shifted by the influence of electron pushing/donating (CH_3 , OCH_3 , OC_2H_5) terminal substituent situated at the sixth position on the benzothiazole moiety. These shifts of absorption maxima (λ_{max}) may be ascribed to the electronic effect that lowers the LUMO energy level and reduces the energy gap [215]. However, electron withdrawing group (F and Cl) could not play significant role to the shifting of absorption maxima.

Table 4.11: UV-vis and photoluminescence results of polymers **P1-P10**

	Absorption λ_{\max} (nm)	Absorption edge λ_{onset} (nm)	PL λ_{\max} (nm)
P1	397	490	461
P2	401	498	474
P3	420	510	482
P4	423	513	482
P5	398	495	453
P6	402	500	458
P7	262 & 376	454	522
P8	262 & 388	471	523
P9	261 & 411	502	522
P10	261 & 413	507	524

Figure 4.36 illustrates photoluminescence (PL) spectra of SCLCPs **P1-P6** in dilute chloroform solutions (1×10^{-6} M) and the experimental results are summarized in Table 4.11. Emission spectra of the polymers were recorded using excitation wavelengths where polymers show maximum UV-vis absorption. All the polymers exhibited emission spectra of identical pattern because of the structural similarities in the mesogenic side chain. The fluorescence emission maxima of polymers are in the range 461-482 nm which may be categorized as blue emission.

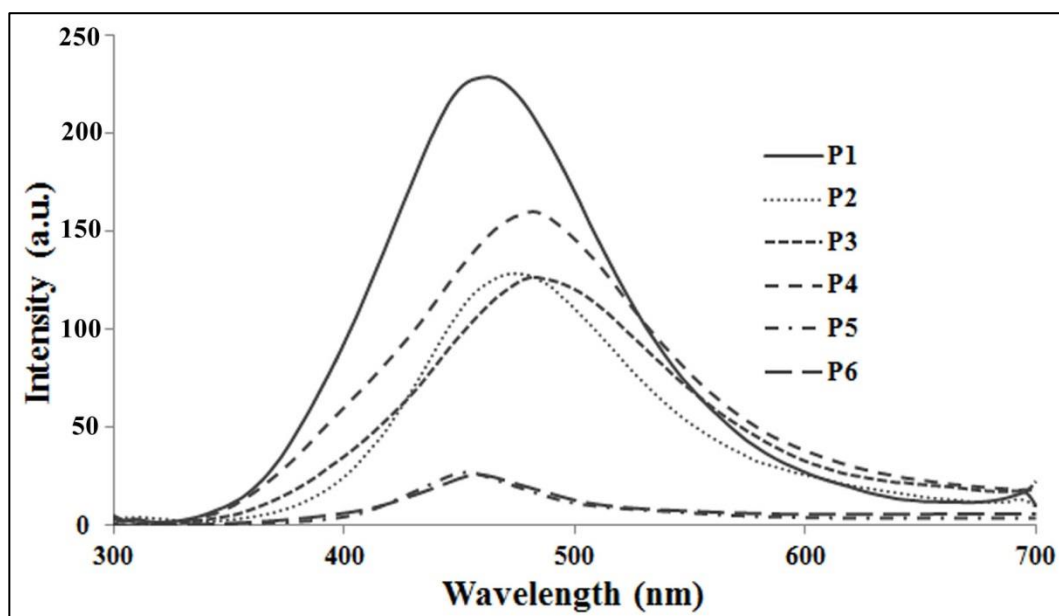


Figure 4.36: PL spectra of **P1-P6** in dilute CHCl_3 solutions (1×10^{-6} M)

Like UV-vis absorption spectra, PL emission maxima were also bathochromically shifted due to the electronic effect which could lower the HOMO-LUMO energy gap. Polymer **P1** exhibited highest emission intensity compared to the other polymers which could be originated from the efficient intermolecular charge transfer in the excited state [216]. However, polymers **P5** and **P6**, having terminal F and Cl substitution respectively showed very poor emission compared to polymers **P1-P4**. It is well known that the concentration and kind of solvent have profound influence on PL property of materials. The poor fluorescence intensities of polymers **P5** and **P6** can be linked to the concentration of the polymers solutions. At lower concentration (1×10^{-6} M), intermolecular distances between polymer molecules may be so large that the molecules could not interact properly [217]. As a result, polymers **P5** and **P6** exhibited very poor fluorescence emission. Iwan et al. [44] reported similar observation for their studied materials.

4.6.2. Optical properties of polymers P7-P10

The UV-vis absorption spectra of SCLCPs **P7-P10** in dilute chloroform solutions (1×10^{-6} M) are depicted in Figure 4.37 and their spectral results are summarized in Table 4.11. All the polymers show two absorption bands in their UV-vis spectra: (i) a high-energy absorption bands at 245-295 nm and (ii) a low-energy absorption bands at 320-520 nm. The absorption maxima (λ_{\max}) of short wavelength region are in the range 260-262 nm and this high-energy absorption band may be attributed to a $\pi-\pi^*$ transition of the heterocyclic moiety and phenyl rings [218, 219].

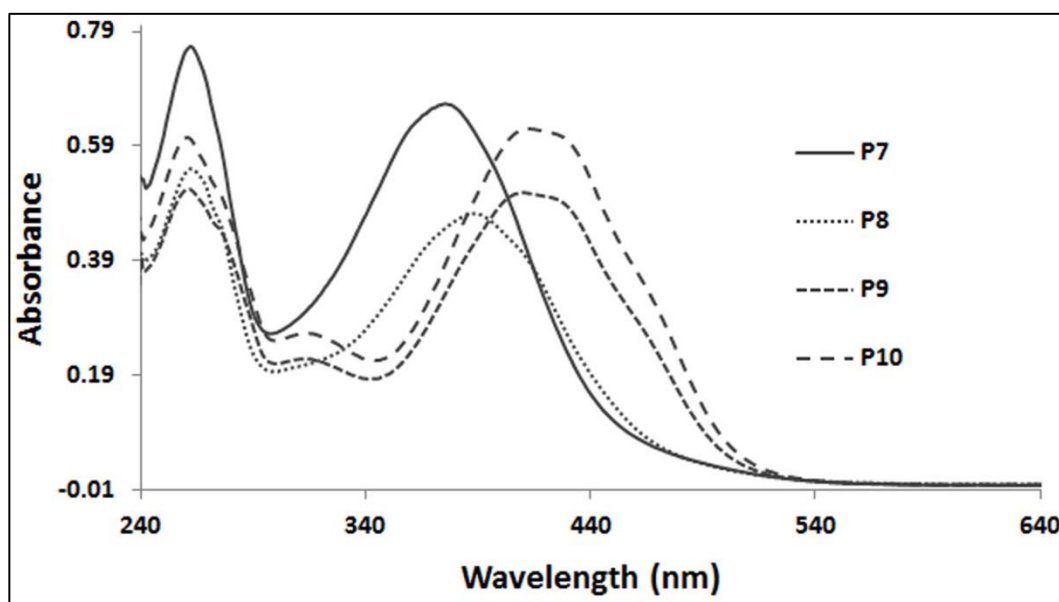


Figure 4.37: UV-vis absorption spectra of **P7-P10** in dilute CHCl_3 solutions (1×10^{-6} M)

On the other hand, the absorption maxima (λ_{\max}) of longer wavelength region are in the range 376-413 nm and this low-energy absorption band may be regarded as a $\pi-\pi^*$ transition involving the π -electronic system throughout the whole molecule with a considerable charge transfer (CT) character [212-214]. Like polymers **P1-P6**, the absorption maxima (λ_{\max}) of polymers **P7-P10** were also red shifted by the incorporation of electron donating/pushing terminal substituent at the sixth position on benzothiazole ring. The electron donating/pushing group tends to provide extra electron

density toward benzothiazole moiety through resonance effect which could reduce HOMO-LUMO energy gaps of the molecules.

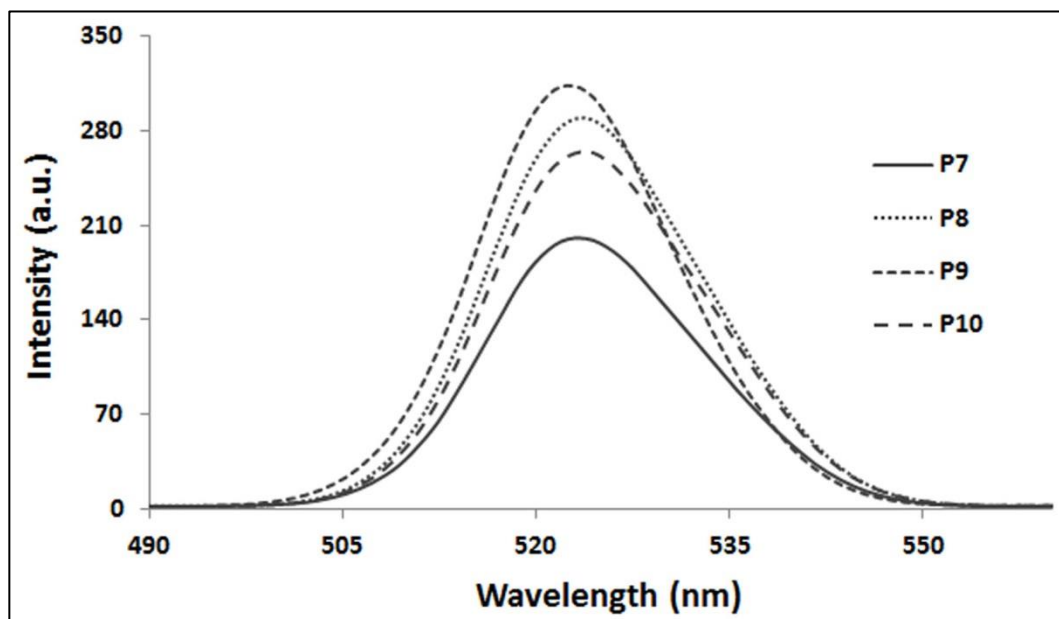


Figure 4.38: PL spectra of **P7-P10** in dilute CHCl_3 solutions ($1 \times 10^{-6} \text{ M}$)

Figure 4.38 exhibits photoluminescence (PL) spectra of SCLCPs **P7-P10** in dilute chloroform solutions ($1 \times 10^{-6} \text{ M}$) and the obtained results are summarized in Table 4.11. The emission spectra of polymers **P7-P10** have identical pattern because of the structural similarities in the mesogenic side chain. The fluorescence emission maxima of polymers are in the range of 522-524 nm which may be categorized as green emission. The PL emission maxima of polymers **P7-P10** were red shifted ca. 40-50 nm compared to polymers **P1-P6**. This is because of the additional benzene ring in the mesogenic side chain of polymers **P7-P10**, which could elongate the effective conjugation length of mesogen and lowers the HOMO-LUMO energy gap. Like UV-vis absorption spectra, PL emission maxima of polymers **P7-P10** also bathochromically shifted due to the electronic effect. The fluorescence emission intensity of standard compound pyrene is shown in Figure 4.39. It is clearly seen from figures (Figure 4.36, Figure 4.38 and Figure 4.39) that the fluorescence intensities of the synthesized

polymers are comparable with pyrene. Thus, these polymers may be potential candidate as fluorescent materials in polymer light emitting diode (PLED) applications.

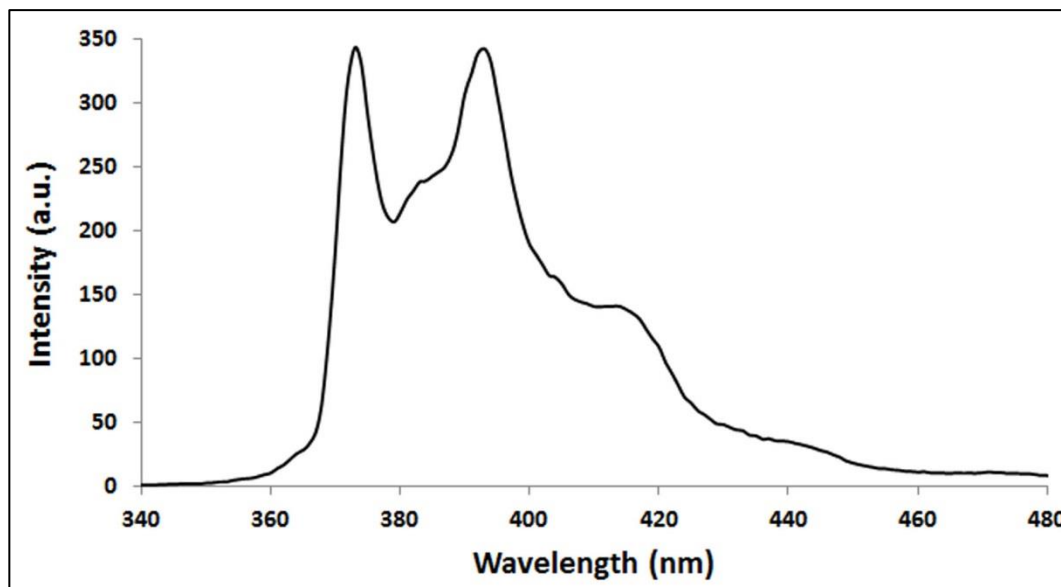


Figure 4.39: PL spectrum of standard compound pyrene in dilute CHCl_3 solutions ($1 \times 10^{-6} \text{ M}$)

4.7. Electrochemical properties of SCLCPs, P1-P10

Cyclic voltammetric (CV) measurements were performed to evaluate the electrochemical properties of new SCLCPs as well as to estimate HOMO and LUMO energy levels, which are important for determining the band gaps. As mentioned in experimental section, three conventional electrode systems were employed to carry out the measurements: (i) Ag/AgCl as reference electrode, (ii) Pt wire as counter electrode and (iii) glassy carbon as working electrode. All the measurements were performed at room temperature in the potential range from - 1.0 V to + 2.0 V with a scan rate of 50 mV s^{-1} and 0.1 M tetrabutylammonium perchlorate (Bu_4NClO_4) was used as supporting electrolyte in anhydrous chloroform. It is assumed that the redox potential of Fc/Fc^+ has an absolute energy level of -4.80 eV to vacuum [220]. The HOMO and LUMO energy levels of polymers were calculated by using the following equations.

$$\text{HOMO} = - [E_{\text{ox}} (\text{onset}) - E_{\text{Fc}/\text{Fc}^+} + 4.8] \text{ eV} \text{ and } \text{LUMO} = [\text{HOMO} + E_{\text{g}} (\text{opt.})] \text{ eV}$$

where E_{ox} is the onset oxidation potential and $E_{Fc/Fc+}$ is the external standard potential of the ferrocene/ferricenium ion couple and E_g (opt.) is the optical band gap. The external standard potential of the ferrocene/ferricenium ion couple ($E_{Fc/Fc+}$), was estimated under the same experimental condition and the value was located at 0.30 V to the Ag/AgCl electrode.

Table 4.12: Cyclic voltammetric results of polymers **P1- P10**

	$E_g(\text{opt.})^a(\text{eV})$	$E_{ox}(\text{onset}) (\text{V})$	HOMO ^b (eV)	LUMO ^c (eV)
P1	2.53	1.40	-5.90	-3.37
P2	2.49	1.41	-5.91	-3.42
P3	2.43	1.36	-5.86	-3.43
P4	2.42	1.35	-5.85	-3.43
P5	2.50	1.66	-6.16	-3.66
P6	2.48	1.50	-6.00	-3.52
P7	2.73	0.37	-4.87	-2.14
P8	2.63	0.35	-4.85	-2.22
P9	2.47	0.32	-4.82	-2.35
P10	2.44	0.30	-4.80	-2.36

^aOptical band gaps were calculated from onset absorption wavelengths using equation, $E_g = 1240/\lambda_{\text{onset}}$

^bThe HOMO energy levels were estimated from cyclic voltammetric onset oxidation potential and ferrocene/ferricenium ion was used as standard.

^cLUMO = HOMO + E_g (opt.)

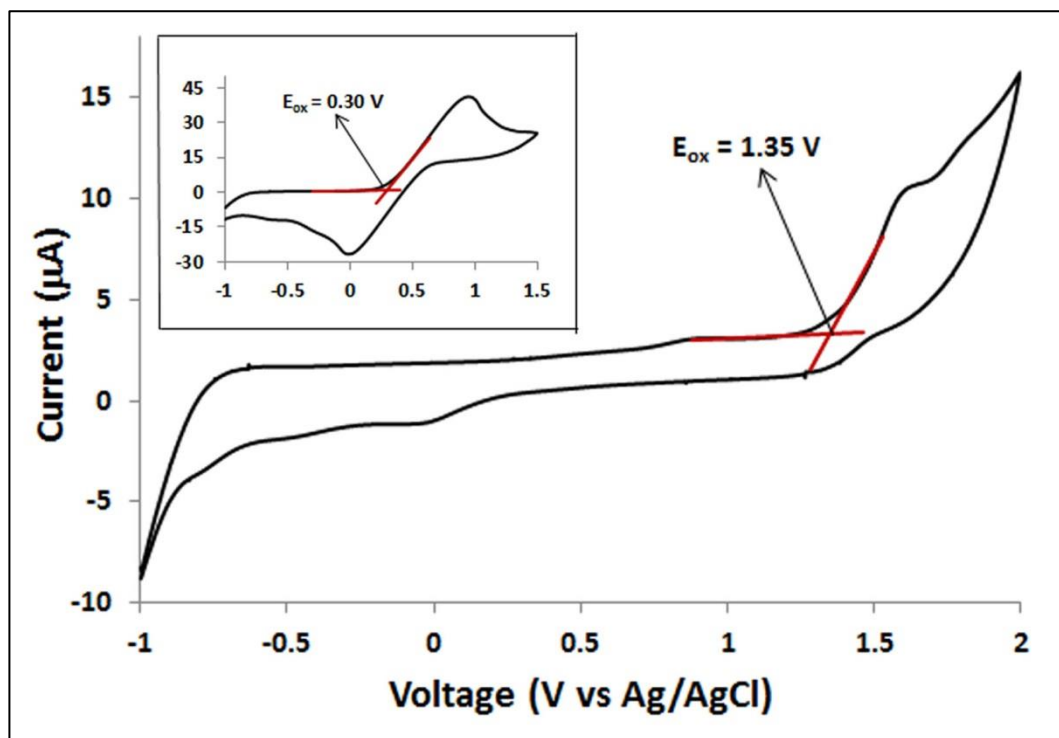


Figure 4.40: Cyclic voltammograms of **P4** in CHCl_3 with 0.1M tetrabutylammonium perchlorate (Bu_4NClO_4) as supporting electrolyte. Inset figure shows CV of ferrocene, run under identical condition as **P4**

The onset oxidation potentials of **P1-P10** were calculated from the intersection of two tangents drawn at the rising and background currents of the cyclic voltammogram. The voltammogram of **P4** is shown in Figure 4.40 which is typical for the polymers. The HOMO-LUMO energies of **P1-P10** and their corresponding band gap values are summarized in Table 4.12. All the polymers showed analogous redox behavior due to their structural similarities and also irreversible redox behaviour under investigated potential ranges. The oxidation potentials of polymers **P1-P6** is characterized by an irreversible wave with onset potentials at 1.40, 1.41, 1.36, 1.35, 1.66 and 1.50 V respectively. The HOMO energy levels of the polymers were estimated to be -5.90, -5.91, -5.86, -5.85, -6.16 and -6.00 eV; the LUMO energy levels were found to be -3.37, -3.42, -3.43, -3.43, -3.53 and -3.47 eV for **P1-P6** respectively. It can be noticed from Table 4.12 that polymer **P5** shows the lowest HOMO energy value among six polymers **P1-P6**. The introduction of electron-withdrawing fluorine atom at the sixth position on the benzothiazole mesogenic unit in the side chain of polymer may play

crucial role to lower the HOMO energy level. This observation on electrochemical behaviour of polymers **P1-P6** can be well explained on the basis of their structure-property relationship. It is well recognized matter that an electron-withdrawing substituent attached with a conjugated molecular system, can decrease π -electron density of the conjugated molecular system. As a result, the molecule will be stabilized and it is necessary to apply higher potential to oxidize the molecule. This results in a shift of the HOMO energy level to lower energy [221].

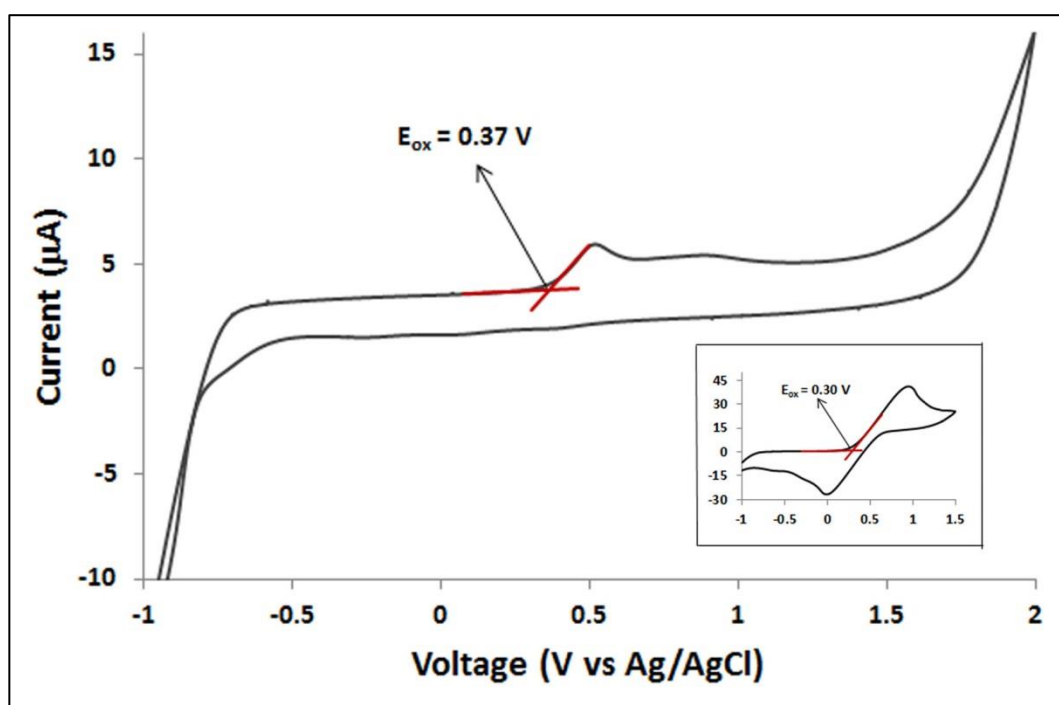


Figure 4.41: Cyclic voltammogram of **P7** in CHCl_3 with 0.1M tetrabutylammonium perchlorate (Bu_4NClO_4) as supporting electrolyte. Inset figure shows CV of ferrocene run under identical condition as **P7**

Similar observation has been reported by Liang et al. [222] for their highly efficient solar cell polymers. The HOMO energy level of polymers **P1-P6** is comparable with the most widely used hole-transporting material 4,4'-bis(1-naphthylphenylamino)biphenyl (NBP)[38]. Recently, many research groups [42, 143, 214] have reported electrochemical behaviour of benzothiazole derivatives and their obtained results are comparable with SCLCPs **P1-P6**. The obtained electrochemical results indicate that the newly synthesized SCLCPs **P1-P6** are conjugated p-type polymers and they may exhibit

hole-transporting properties [223]. Therefore, SCLCPs **P1-P6** could be potential candidate for hole-transporting materials in OLED applications [224].

Figure 4.41 exhibits a typical cyclic voltammogram of the polymer (**P7**) and the estimated HOMO-LUMO energy levels are shown in Table 4.12. The HOMO and LUMO energy values of polymers **P7-P10** are in the range -4.80 eV to -4.87 eV and -2.14 eV to -2.36 eV respectively. These HOMO energy values are significantly different from those of polymers **P1-P6** (Table 4.12). These variations in electrochemical behaviour of polymers **P7-P10** may be originated from the different molecular structure of mesogenic side chain of polymers. Generally, the electrochemical properties of any conjugated polymer may be influenced by the effective conjugation length, solid-state intermolecular ordering and the presence of electron withdrawing or donating moieties [225]. Thus, electrochemical behaviours of conjugated polymers can be tuned by varying above mentioned properties. Polymers, **P7-P10** possess an additional benzene ring and ester linkage than those of polymers **P1-P6**, which could extend the conjugation length in the mesogenic side chain of polymers **P7-P10**. As a result, the effective conjugation lengths in the mesogenic unit of polymers **P7-P10** may be longer than those of polymers **P1-P6**. Therefore, the oxidation potential of **P7-P10** will be decreased and the HOMO energy levels will be shifted to a higher energy level.

4.8. Rheology of SCLCPs P1, P3 and P4

Rheological properties of LC polymers are relatively complex due to the long range orientational order and inherent anisotropy of the materials. Among the ten synthesized SCLCPs, three polymers (**P1, P5** and **P6**) exhibited smectic phase, two polymers (**P2** and **P3**) showed both nematic and smectic phases and five polymers (**P4, P7, P8, P9** and **P10**) revealed only nematic phase. The precise temperature control of existing rheometer was around 200°C, however, only four polymers **P1-P4** showed

isotropization temperature of less than 200°C. As a result, polymer having only smectic phase (**P1**), both nematic and smectic phases containing polymer (**P3**) and polymer (**P4**) exhibiting nematic phase have been chosen for rheological study. In this study, amplitude sweep and frequency sweep experiments have been carried out to study the linear viscoelasticity range and dynamic viscoelastic properties of the selected polymers **P1**, **P3** and **P4**.

4.8.1. The strain sweep behaviour of polymer **P1**

The dynamic strain sweep experiments were carried out in order to determine the existence and extent of linear viscoelasticity range. In Figure 4.42, the storage (G') and loss (G'') moduli are shown as a function of the strain amplitude for polymer **P1** at 182°C, at a constant frequency of 10 rad/s.

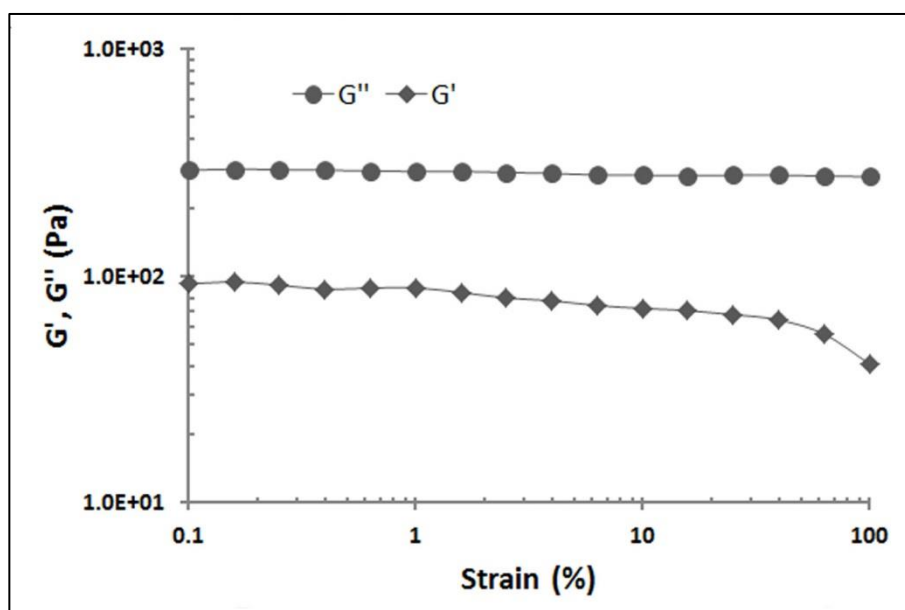


Figure 4.42: Storage (G') modulus and loss modulus (G'') vs strain amplitude sweep at a constant frequency 10 rad/s for polymer **P1** at 182°C

It can be seen from Figure 4.42 that polymer **P1** shows linear viscoelastic behaviour at small and medium strain amplitude and finally the onset of non-linearity is observed when the strain amplitude overcomes the limit of linear viscoelasticity. The loss

modulus (G'') is always greater than storage modulus (G') and the values of G'' are largely insensitive to strain amplitude.

Figure 4.43 demonstrates the plots of $\log \eta$ vs $\log \dot{\gamma}$ for polymer **P1** over the phase transition temperatures. The shear viscosity behaviour can be divided into two categories, (i) temperatures below 162°C , where polymer exhibits smectic A phase, which is evident from POM and DSC observations and (ii) temperatures above 162°C , where **P1** shows isotropic phase. Within the smectic state, polymer **P1** shows a strong shear thinning behaviour over the shear rate range investigated and there is no sign of Newtonian plateau down to the lowest shear rate of $1 \times 10^{-2} \text{ s}^{-1}$. In the isotropic region, **P1** exhibits shear thinning behaviour at low shear rate and this shear thinning behaviour was also observed at high shear rate without exhibiting Newtonian plateau.

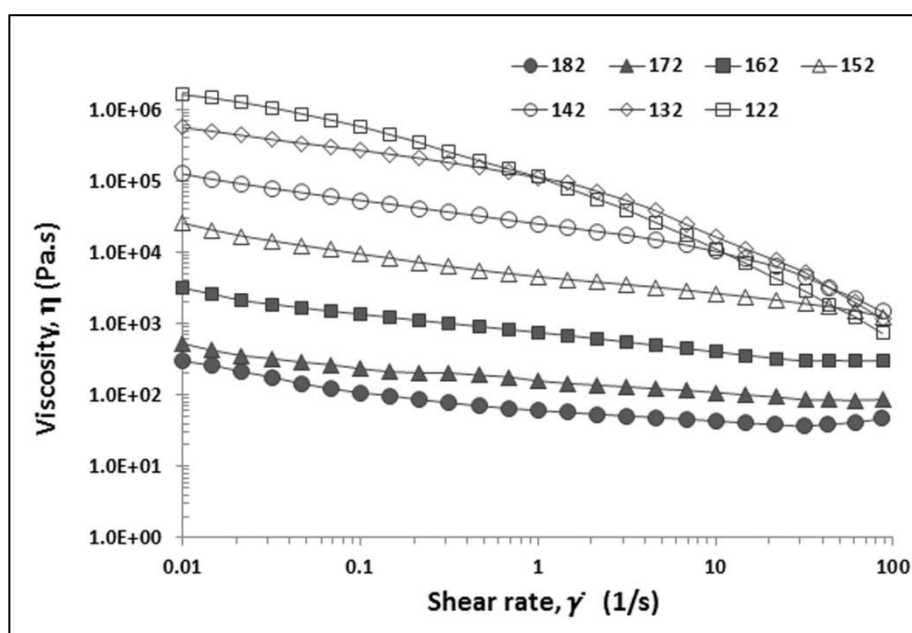


Figure 4.43: Steady shear viscosity (η) as a function of shear rate ($\dot{\gamma}$) for polymer **P1** at indicated temperatures ($^\circ\text{C}$)

In the temperature region where smectic to isotropic transition occurs, the shear viscosity rapidly decreases and this effect is regarded as a pre-transitional phenomenon [226]. This result indicates the destruction of ordered smectic layer structure into the order less isotropic phase. Polymer **P1** exhibits shear thinning slopes around -0.4 in the

smectic region at low shear rate and this result is consistent with the low molar mass smectic SCLCPs with polymethacrylate backbone as reported by Zentel and Wu [227]. The strong shear thinning behaviour of low molar mass SCLCPs in the smectic phase may be resorted to the alignment of the smectic layers normal to the direction of the vorticity [226]. In addition to the alignment, the diminishing of the disclinations may also play a crucial role in the shear thinning for polymer **P1**.

4.8.2. The linear viscoelastic response of smectic polymer P1

There are very few reports published on rheology of smectic SCLCPs and such as the information available are limited. In addition, rheological properties of SCLCPs containing azo-heterocyclic mesogen have so far not been addressed in the literature yet. However, an effort has been made to explain obtained rheological results by only comparing published results [13, 179, 185, 226, 228, 229].

The frequency dependence of storage modulus (G') and loss modulus (G'') is depicted in Figure 4.44 for polymer **P1** in the smectic phase (122°C to 162°C) and in the isotropic state (162°C to 182°C). The values of both G' and G'' in the smectic region are much higher than those in the isotropic state. This observation may be due to the breakdown of two dimensional layered smectic structures to dimensionless isotropic state. The slope of $\log G'$ vs $\log \omega$ plots for polymer **P1** over the entire range of ω tested remains much less than two at various temperatures ranging from 122°C to 182°C. Instead, an elastic plateau is observed at temperature greater than 162°C as the frequency approaches lower values. The level-off tendency of storage modulus in the low frequency region has been reported for thermotropic co-polyester [230], cholesteric liquid crystal [231], and polymeric smectic phases [13, 179]. The very weak frequency dependence of G' of the smectic polymer **P1** is the characteristic of gel-like behaviour of side chain liquid crystalline polymers [232, 233].

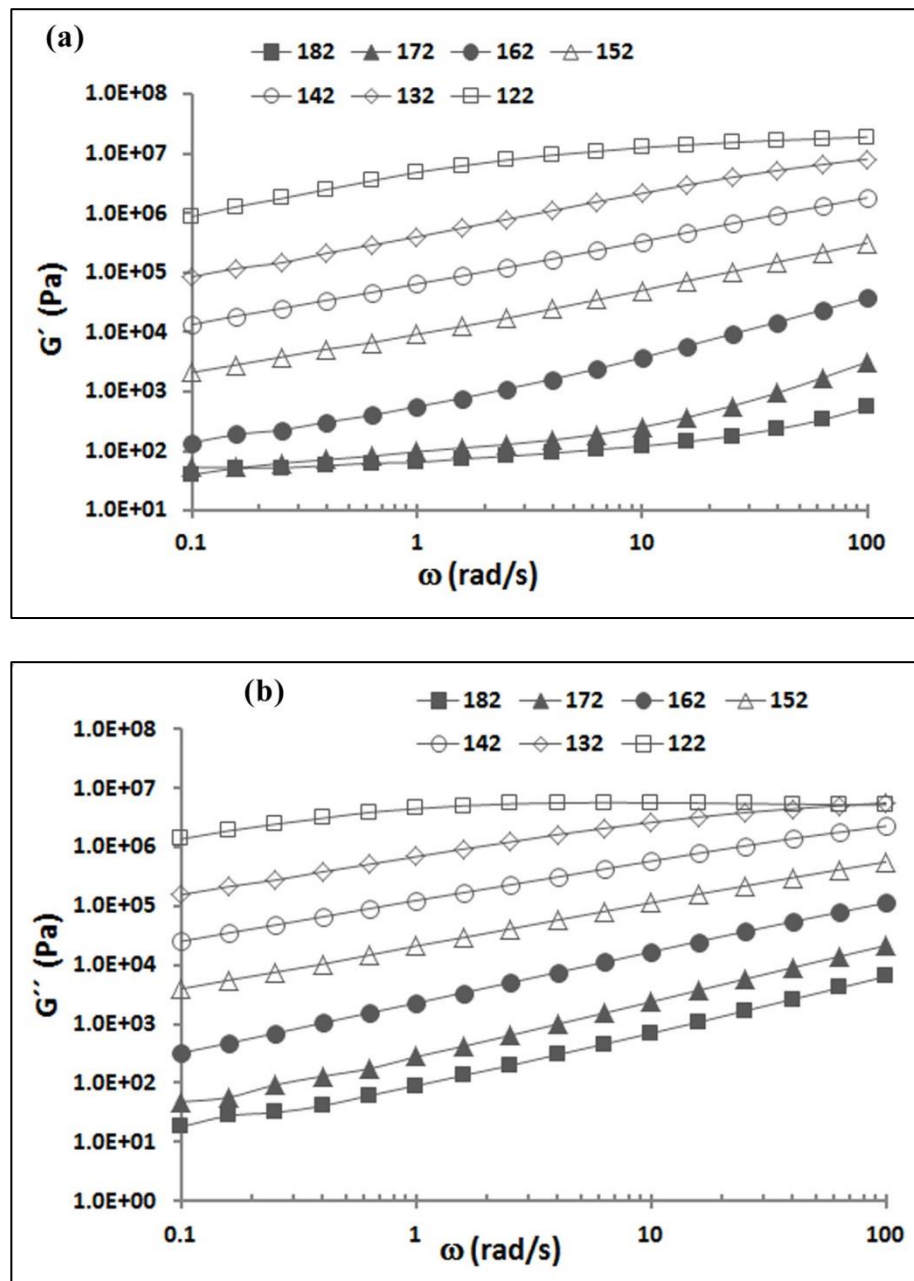


Figure 4.44 : (a) Storage modulus (G') and (b) loss modulus (G'') as a function of frequency for polymer **P1** at indicated temperatures ($^{\circ}\text{C}$)

Polymer **P1** greatly deviated from the typical terminal behaviour which follows $G' \propto \omega^2$ and $G'' \propto \omega$ as shown by the homogenous polymeric systems. It has been reported that the deviation from such terminal behaviour is the characteristic of unaligned layered liquids [234, 235]. Moreover, the non-terminal low frequency response is an identifying signature of smectic mesophases, irrespective of whether the mesogenic units are in the main chain or in the side chains [178, 234]. On the other

hand, the slope of $\log G''$ vs $\log \omega$ plots for **P1** remains unchanged (~ 0.6) over the entire range of ω investigated, indicating that the dynamic loss modulus G'' of **P1** is not as sensitive as the dynamic storage modulus G' to variation in the morphological state from the smectic phase to the isotropic phase.

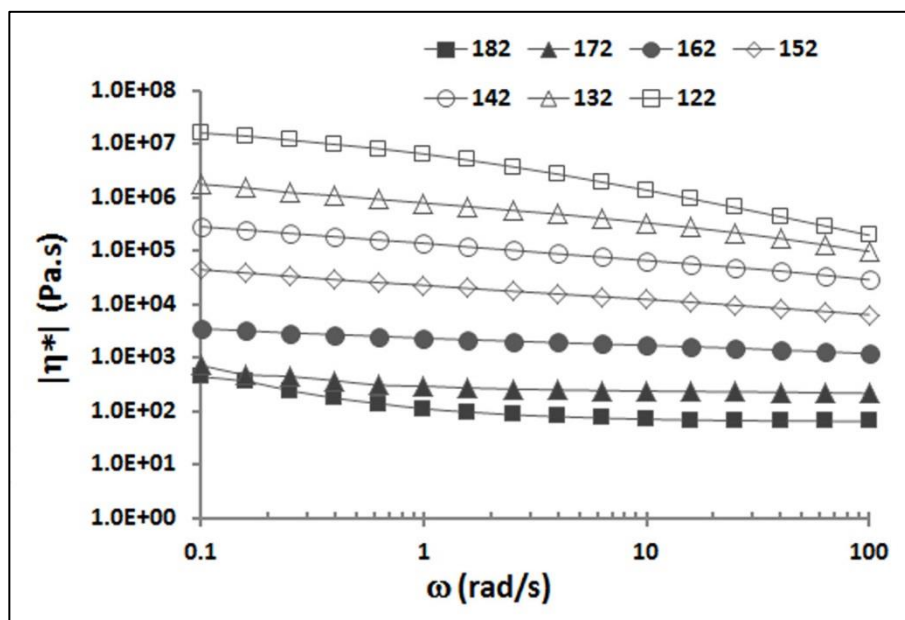


Figure 4.45: Complex viscosity ($|\eta^*|$) as a function of frequency (ω) for **P1** at indicated temperatures ($^{\circ}\text{C}$)

Figure 4.45 exhibits dependence of complex viscosity ($|\eta^*|$) on frequency (ω) for polymer **P1** at various temperatures ranging from 122°C to 182°C , where $|\eta^*| = [(G'/\omega)^2 + [(G''/\omega)^2]^{1/2}$. The $|\eta^*|$ of **P1** shows shear thinning behaviour with almost the same slope at temperatures below smectic-isotropic transition. In the isotropic phase, the $|\eta^*|$ of **P1** gives shear thinning behaviour at low angular frequencies and Newtonian behaviour at medium and higher frequencies. Lee and Han [185] observed similar results for their studied SCLCPs.

The frequency dependence of storage modulus (G'), loss modulus (G'') and complex viscosity ($|\eta^*|$) for polymer **P1** at 182°C (isotropic phase) is presented in Figure 4.46a. The complex viscosity shows an upward concavity over the frequency

range investigated. The G' and G'' profiles of **P1** indicate a viscous response ($G'' > G'$) at higher frequencies and an elastic response is dominant at lower frequency ($G' > G''$) region. In addition, a level off tendency for G' is observed, indicating a solid-like elasticity of polymer **P1** at higher temperature region (isotropic state). Somma et al. [236] reported similar results for their thermotropic liquid crystalline polymers.

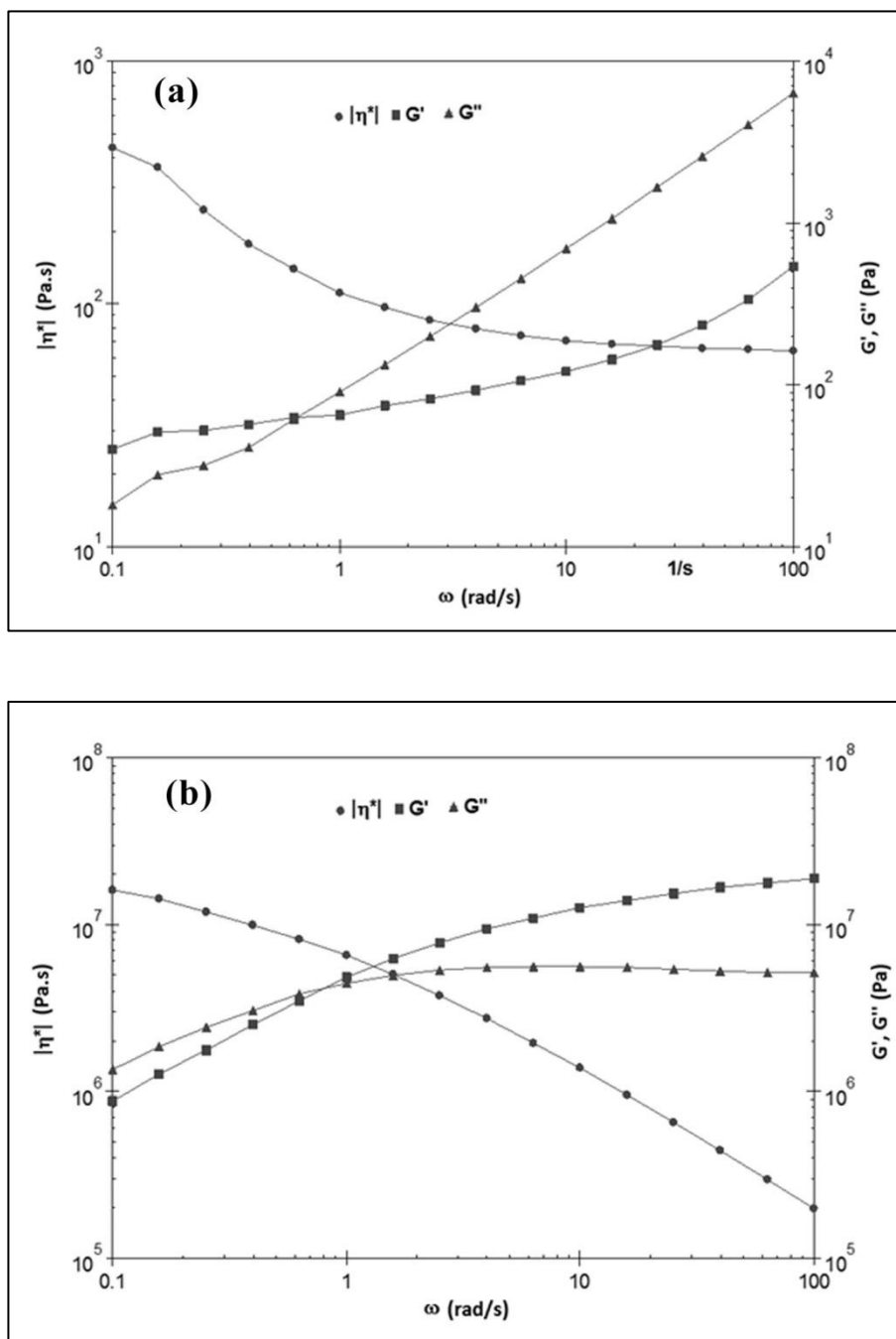


Figure 4.46: Storage modulus (G'), loss modulus (G'') and complex viscosity ($|\eta^*|$) as a function of frequency (ω) for polymer **P1** (a) at 182°C and (b) at 122°C

On the other hand, the plots of $\log G'$, $\log G''$ and $\log (\eta^*)$ vs $\log \omega$ for **P1** at 122°C (smectic phase) in Figure 4.46b shows different behaviour than those at 182°C. In the smectic region, neither complex viscosity shows an upward concavity nor is a plateau observed for G' at low frequencies. At high frequencies, polymer **P1** predominantly shows solid like behaviour ($G' > G''$) and moduli crossover is noticed at $\omega_c = 0.63$ rad/s ($G' = G'' = 3.8 \times 10^6$ Pa). At lower frequencies, P1 exhibits liquid like behaviour ($G' < G''$) which can easily be evident from the G' and G'' profiles (Figure 4.46). This behaviour of **P1** is analogous with the thixotropic materials [237] which exhibit solid like properties at higher frequencies and liquid like properties at lower frequencies.

4.8.3. The strain amplitude sweep behaviour of polymer **P3**

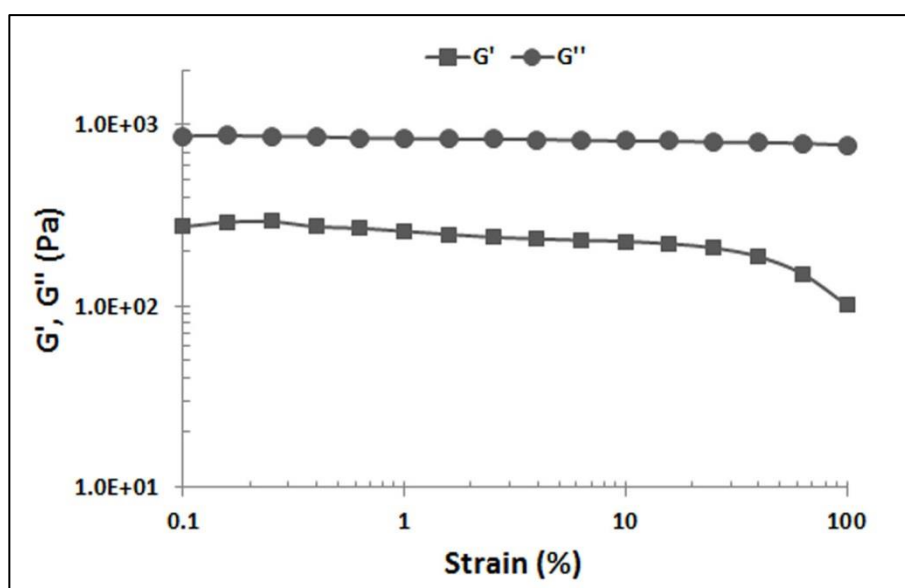


Figure 4.47: Storage (G') modulus and loss modulus (G'') vs strain amplitude sweep at a constant frequency 10 rad/s for polymer **P3** at 190°C

The appearance and limit of linear viscoelasticity range for polymer **P3** were studied by strain amplitude sweep experiments. Figure 4.47 depicts the storage (G') and loss (G'') moduli as a function of the strain amplitude for polymer **P3** at 190°C, at a constant frequency of 10 rad/s. Polymer **P3** exhibits linear viscoelastic behaviour at small and medium strain amplitude and then non-linearity is observed when the strain

amplitude overcomes the limit of linear viscoelasticity. The loss modulus (G'') is always greater than storage modulus (G') and the values of G'' are largely insensitive to strain amplitude. Similar results were also observed for smectic polymer **P1**.

4.8.4. The linear dynamic viscoelasticity of polymer **P3**

Figure 4.48 depicts $\log G'$ vs $\log \omega$ and $\log G''$ vs $\log \omega$ plots for **P3** (i) at 120°C and 130°C in the smectic phase, (ii) at 150, 160, 170 and 180 °C in the nematic phase and (iii) at 190 °C in the isotropic state. The storage and loss moduli in the smectic phase are much higher than those of either the nematic or isotropic phases. In addition, both the moduli fail to reach terminal behaviour even at the lowest accessible frequencies. The higher values of G' and G'' in the smectic region may be due to the two-dimensional orientational order and lower values in the nematic phase may be attributed to the one-dimensional orientational order. Similar to **P1**, polymer **P3** also fails to exhibit the typical terminal behaviour which follows $G' \propto \omega^2$ and $G'' \propto \omega$ as shown by the homogenous polymeric systems. The deviation from the terminal behaviour may be due to the unaligned layered structure, low molecular weight and polydispersity of SCLCPs [181, 185, 238]. The slopes in the terminal region for G' and G'' are 0.4 and 0.7 respectively for polymer **P3** and this result indicates the pseudo solid-like behaviours [239] of polymer in the terminal region. A careful observation of Figure 4.48 indicates that the loss modulus is always greater than the storage modulus ($G' < G''$) at all the frequencies tested in the nematic and isotropic phases. This result reveals a liquid-like (viscous) behaviour of polymer **P3** in the nematic and isotropic states. The trend is comparable with the results reported by Somma et al. [236] for thermotropic liquid crystalline co-polyester Rodrun 3000. On the other hand, the storage modulus is greater than the loss modulus ($G' > G''$) at all the frequencies investigated in the smectic region, indicating a solid like (elastic) behaviour of polymer in that region.

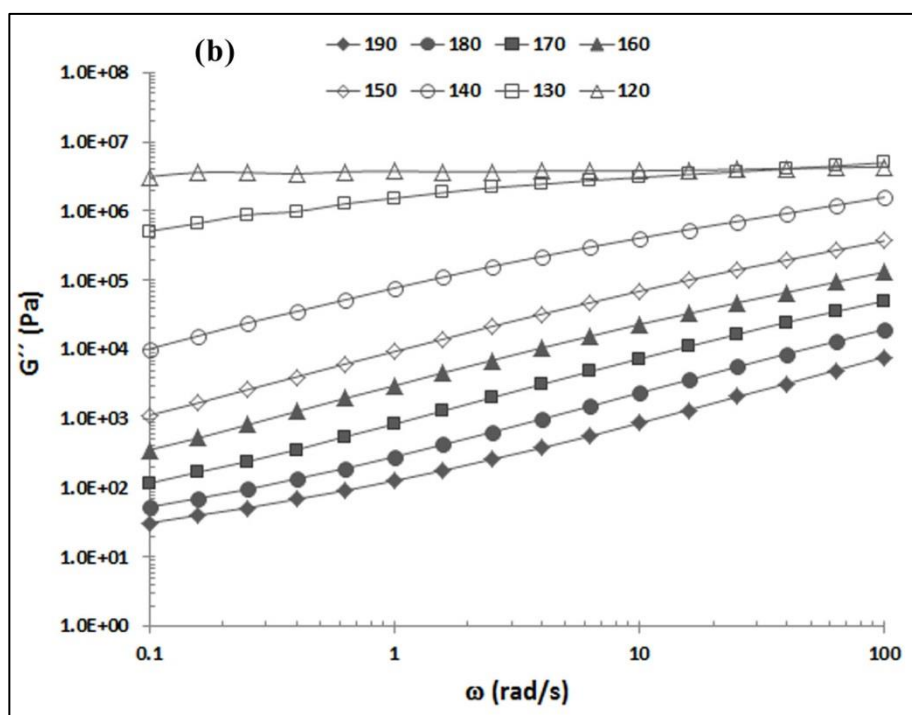
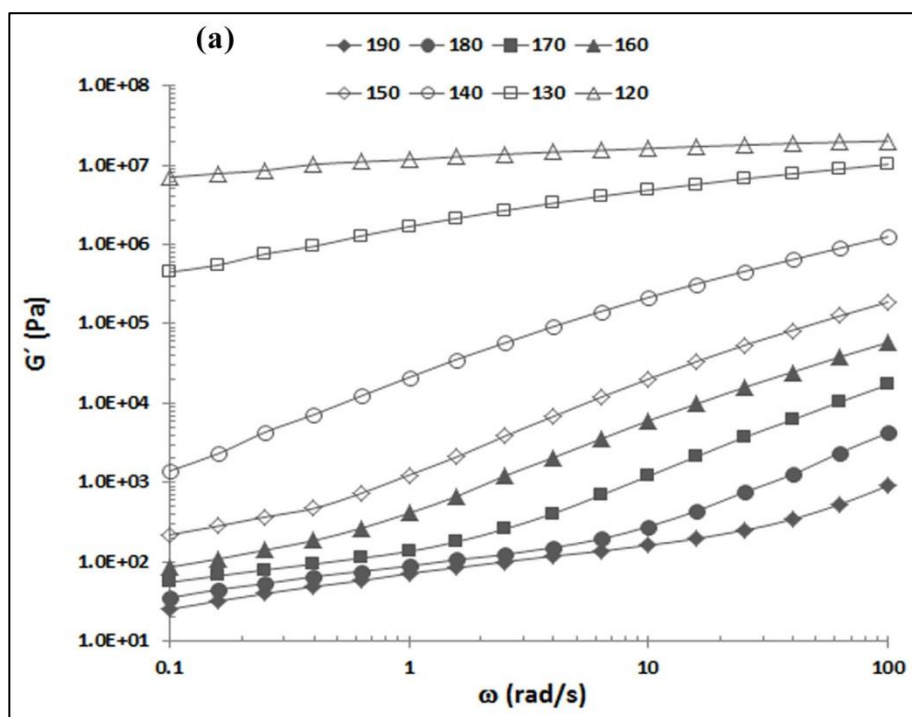


Figure 4.48: (a) Storage modulus (G') and (b) loss modulus (G'') as a function of frequency for polymer **P3** at indicated temperatures ($^{\circ}\text{C}$)

Figure 4.49 shows variation of complex viscosity ($|\eta^*|$) as a function of frequency for polymer **P3** at various temperatures ranging from 120°C to 190°C , where $|\eta^*| = [(G'/\omega)^2 + [(G''/\omega)^2]^{1/2}$. The plots of $\log |\eta^*|$ vs $\log \omega$ for polymer **P3** show strong frequency dependence at 130°C and 120°C , a very mild frequency dependence at

140°C and then weak frequency dependence at temperatures greater than 150°C. The complex viscosity for polymer **P3** exhibits strong shear thinning behaviour in the smectic region and during smectic to nematic transition (~140°C) complex viscosity decreases rapidly. This abrupt decrease of viscosity for polymer **P3** may be due to the breakdown of three-dimensional smectic order to one-dimensional nematic order [240]. At higher temperatures region (150°C - 190°C), the complex viscosity of polymer **P3** shows shear thinning behaviour at low frequencies and Newtonian behaviour at medium and higher frequencies.

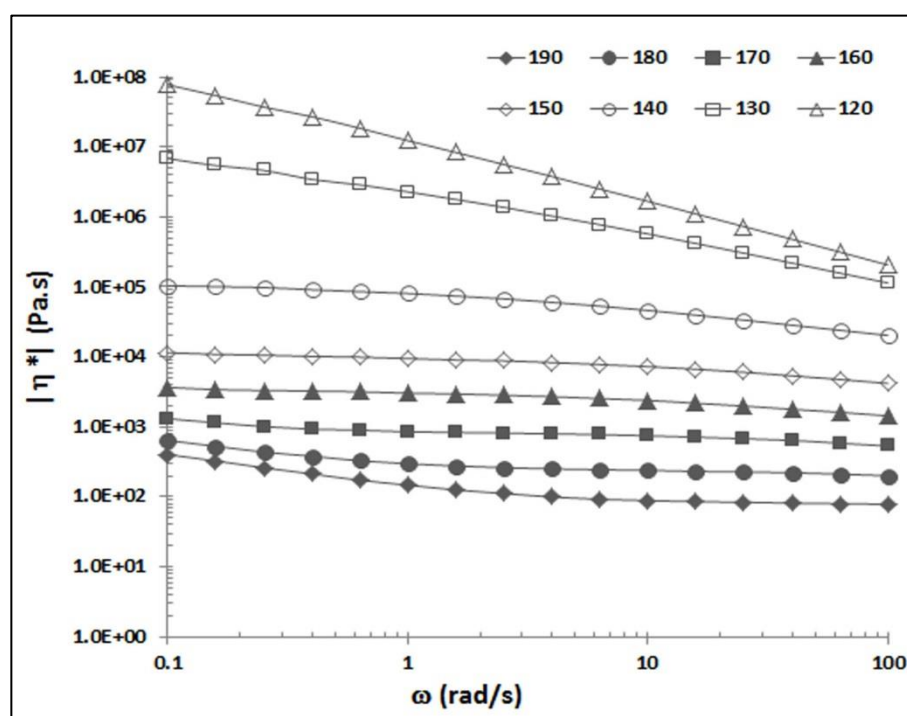


Figure 4.49: Complex viscosity ($|\eta^*|$) as a function of frequency (ω) for **P3** at indicated temperatures (°C)

4.8.5. The linear dynamic viscoelasticity of polymer **P4**

Figure 4.50 depicts $\log G'$ vs $\log \omega$ and $\log G''$ vs $\log \omega$ plots for **P4** (i) from 185°C to 175°C in the isotropic state and (ii) from 165°C to 120 °C in the nematic phase. From Figure 4.50, it is very difficult to distinguish between nematic and isotropic phases in the experimental condition covered for polymer **P4**.

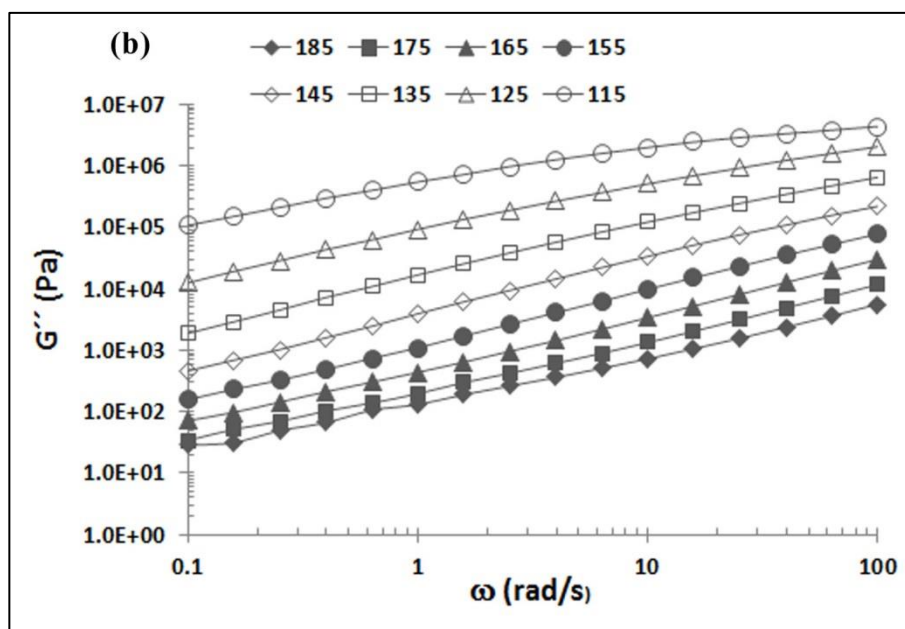
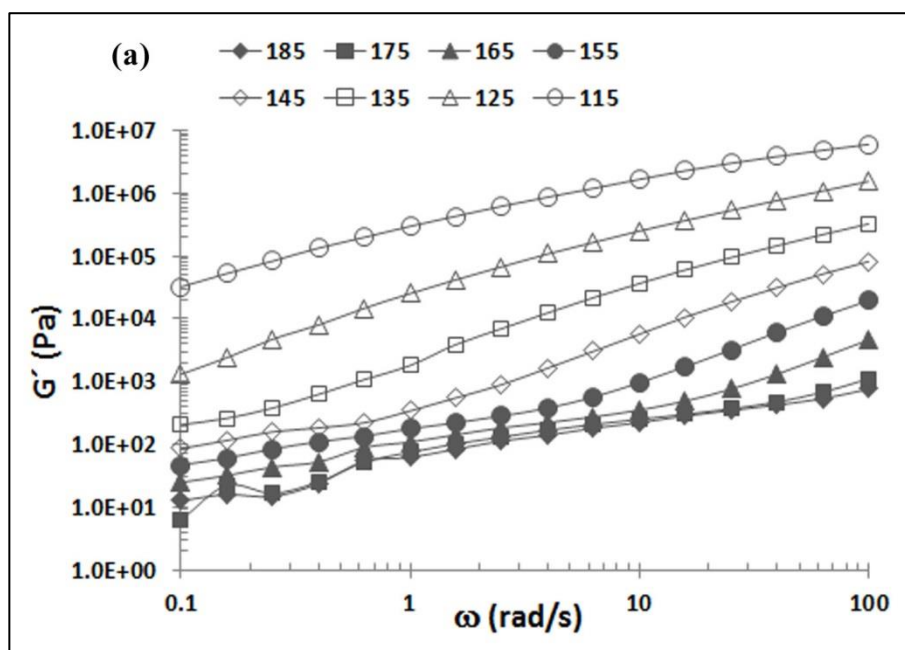


Figure 4.50: (a) Storage modulus (G') and (b) loss modulus (G'') as a function of frequency for polymer **P4** at indicated temperatures ($^{\circ}\text{C}$)

Although both the nematic-isotropic and the smectic-isotropic transitions for SCLCPs exhibit thermo-rheological complexity, the nematic-isotropic transition is far less sensitive compared to the smectic-isotropic transition. So, the above statement is applicable for polymer **P4** which shows nematic phase only. The slope of $\log G'$ vs $\log \omega$ plots for polymer **P4** is greater than one but much less than two over the frequency range investigated. On the other hand, the slope of $\log G''$ vs $\log \omega$ plots is slightly less

than one and remains unchanged over the entire range of temperatures tested. This result indicates that the dynamic loss modulus G'' of **P4** is not as sensitive as the dynamic storage modulus G' to a variation in the morphological state from the nematic phase to the isotropic phase as the temperature is increased. Likewise polymer **P1** and **P3**, polymer **P4** also fails to follow the typical terminal behaviour because of low molecular weight ($M_n = 8221$) and high polydispersity (1.59) of SCLCPs [185].

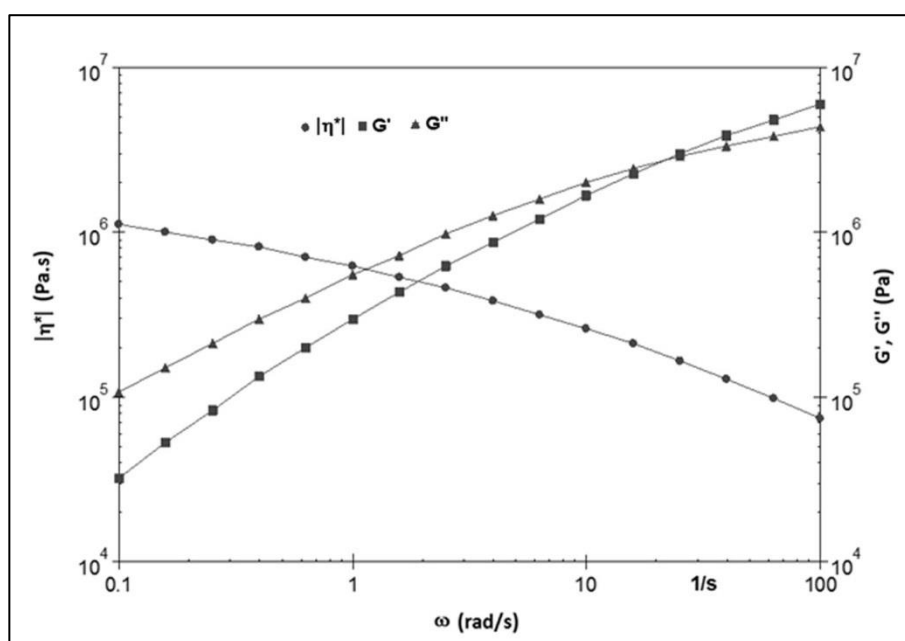


Figure 4.51: Storage modulus (G'), loss modulus (G'') and complex viscosity ($|\eta^*|$) as a function of frequency (ω) for polymer **P4** at 115°C

It can also be observed from Figure 4.50 that the loss modulus is always greater than the storage modulus ($G' < G''$) at all investigated temperatures over the entire frequency range applied, indicating a liquid-like behaviour of polymer **P4** in the nematic and isotropic phases. However, the storage modulus is greater than the loss modulus ($G' > G''$) at 115°C in the high frequency region and moduli crossover (Figure 4.51) is noticed at $\omega_c = 25.1$ rad/s ($G' = G'' = 3.0 \times 10^6$ Pa), indicating solid-like behaviour of polymer in that region.

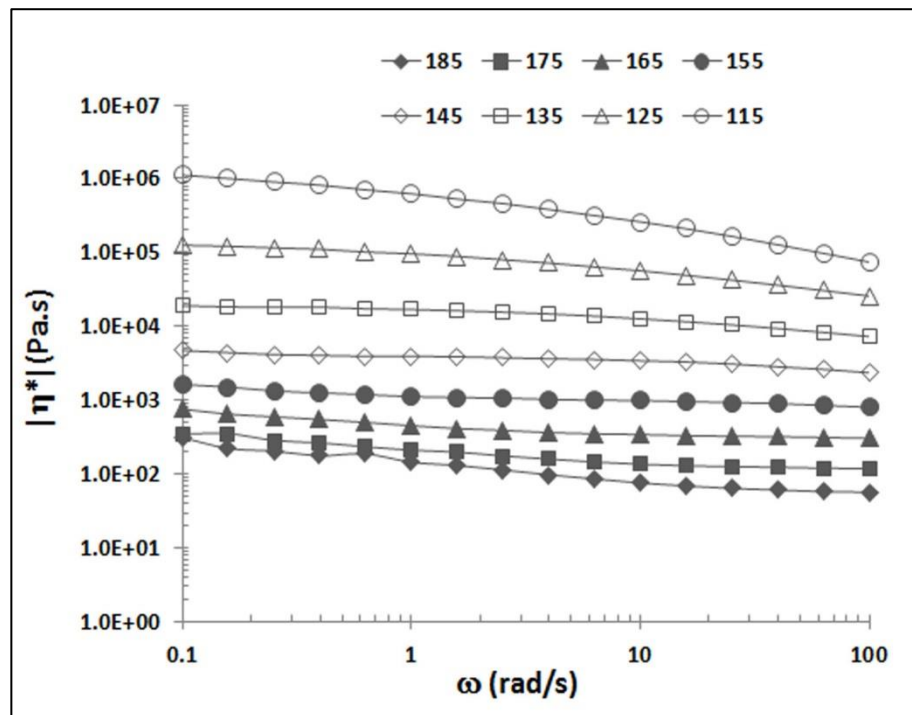


Figure 4.52: Complex viscosity ($|\eta^*|$) as a function of frequency (ω) for **P4** at indicated temperatures ($^{\circ}\text{C}$)

Figure 4.52 shows frequency dependence of complex viscosity ($|\eta^*|$) for polymer **P4** at various temperatures ranging from 115°C to 185°C , where $|\eta^*| = [(G'/\omega)^2 + [(G''/\omega)^2]^{1/2}]$. The plots of $\log |\eta^*|$ vs $\log \omega$ for polymer **P4** show mild frequency dependence over the temperatures range investigated (115°C to 185°C). The complex viscosity for polymer **P4** exhibits shear thinning behaviour at temperatures range from 120°C to 145°C over the frequency range tested. On the other hand, at temperatures range from 155°C to 185°C , the complex viscosity shows shear thinning at low and medium frequency region and exhibit Newtonian behaviour at higher frequencies.

CHAPTER 5 : CONCLUSIONS

5.1. Conclusions

New polymerizable LC methacrylate monomers, **M1-M10**, bearing azo-benzothiazole mesogen were successfully synthesized via azo coupling followed by etherification and esterification reactions. The chemical structures of the prepared monomers were confirmed by FT-IR, ^1H and ^{13}C NMR spectroscopic techniques. The newly synthesized LC monomers showed good to excellent thermal stability with decomposition temperatures corresponding to 5% weight loss ($T_{d,5\%}$) in the range of 280-320°C. Monomers **M7-M10** exhibited an improved thermal stability of ca. 40°C compared to monomers **M1-M6** due to the greater molecular length of **M7-M10**. DSC and POM observations confirmed that all the synthesized monomers exhibited LC properties. The electron donating/pushing terminal substituents facilitate the formation of nematic phase while electron withdrawing terminal substituents help to generate strong smectic phase. The mesophase formation as well as the mesophase stability of monomers **M1-M10** was greatly influenced by the terminal substituents located at the sixth position on the benzothiazole moiety and the length of the mesogen.

Azo-benzothiazole mesogen containing new SCLCPs, **P1-P10**, were successfully synthesized via conventional free radical polymerization using the synthesized LC methacrylate monomers, **M1-M10**. The purity and chemical structures of the prepared polymers were confirmed by FT-IR and ^1H NMR spectroscopic techniques. SCLCPs **P1-P10** showed excellent thermal stability with decomposition temperatures corresponding to 5% weight loss ($T_{d,5\%}$) in the range of 310-340°C. However, the synthesized SCLCPs **P1-P10** exhibited enhanced thermal stability of ca. 30°C compared to their corresponding LC monomers **M1-M10**. All the polymers gave good char yields at 600°C (22-32%) and 850°C (14-21%) supporting the oxidative

stability of the polymers. Polymers **P1**, **P5** and **P6** showed only smectic phase while polymers **P2** and **P3** displayed both nematic and smectic phases. On the other hand, polymers **P4**, **P7**, **P8**, **P9** and **P10** revealed only nematic phase. Like monomers **M1-M10**, the mesophase formation as well as the mesophase stability of polymers **P1-P10** was greatly influenced by the terminal substituents located in the mesogenic side chain and the length of the mesogen. The glass transition temperatures (T_g) of SCLCPs **P1-P10** were in the range of 134-81°C and decreased with the incorporation of short terminal tails in mesogenic side chain. The thermal stability and the T_g values indicate that the synthesized polymers may be a suitable candidate for optoelectronic applications.

Polymers **P1-P6** showed a broad absorption band with λ_{max} values in the range of 397-423 nm while **P7-P10** exhibited two strong absorption bands with λ_{max} values in the range of 261-262 nm and 376-413 nm due to the structural differences in the mesogenic side chain of the polymers. The UV-vis absorption maxima (λ_{max}) of polymers were red shifted with the incorporation of electron donating/pushing terminal substituent located in the mesogen of polymers. Polymers **P1-P6** exhibited fluorescence maxima in the range of 461-482 nm while polymers **P7-P10** showed fluorescence emission maxima in the range of 522-524 nm. Like UV-vis absorption, the emission maxima were also bathochromically shifted by the influence of electron donating/pushing terminal substituents. From cyclic voltammetric studies the HOMO and LUMO energy levels of polymers were found in the range of -4.80 to -6.16 eV and -2.14 to -3.53 eV respectively and the obtained HOMO-LUMO values were influenced by the terminal substituents located in the mesogenic side chain. Polymer having terminal fluorine atom (**P5**) exhibited the lowest HOMO value of -6.16 eV while polymer **P10** showed highest HOMO value of -4.80 eV. The HOMO-LUMO energy levels of polymers support that the newly synthesized SCLCPs are conjugated p-type

polymers and they could be potential candidate as hole-transporting materials in organic light emitting diodes (OLEDs).

Rheological behaviour of all the studied polymers (**P1**, **P3** and **P4**) showed linear viscoelastic region at small and medium strain amplitudes, while, non-linearity was observed at high strain amplitude. Within the smectic state, polymer **P1** exhibited a strong shear thinning behaviour over the shear rate range investigated. The shear viscosity of polymer **P1** rapidly decreased within the temperature region where smectic to isotropic transition occurred due to the pre-transitional phenomenon. Polymer **P1** exhibited gel-like behaviour in the terminal region which is characteristics of smectic polymers. In addition, **P1** exhibited solid-like properties at higher frequency and liquid-like at lower frequency and these behaviours are analogous with the thixotropic materials. The storage and loss moduli of polymer **P3** in the smectic region were much higher than those of either the nematic or isotropic phases. On the other hand, the storage and loss moduli of polymer **P4** were not so sensitive during nematic-isotropic transition. Like polymer **P1**, the complex viscosity of polymer **P3** exhibited strong shear thinning in the smectic region. Polymers **P3** and **P4** failed to follow the typical terminal behaviour as exhibited by the homogeneous polymeric system due to the low molecular weight and high polydispersity of the polymers.

5.2. Suggestions for further research

In the present study, SCLCPs have been synthesized by conventional free radical polymerization technique. For many applications, a monodispersed polymer is desirable. Atom transfer radical polymerization (ATRP) may be adopted for further investigation to produce high molecular weight with narrow polydispersity SCLCPs. In addition, co-polymerization may be carried out to obtain SCLCPs with improved

thermal, optical and electrochemical properties. Moreover, the synthesized SCLCPs may be further studied as photo switching, NLO and hole-transporting materials.

REFERENCES

1. Chandrasekhar, S., *Liquid Crystals*. 2nd ed. 1992, New York: Cambridge University Press.
2. Wang, X.J. and Zhou, Q.F., *Liquid Crystalline Polymers*. 2004: World Scientific Publishing Company.
3. Collings, P.J. and Hird, M., *Introduction to Liquid Crystals: Chemistry and Physics*. 1997: Taylor & Francis.
4. Gray, G.W., Harrison, K.J., and Nash, J.A., New family of nematic liquid crystals for displays. *Electronics Letters*, 1973. 9(6): 130-131.
5. Crawford, G.P., Woltman, S.J., and Jay, G.D., *Liquid Crystals: Frontiers in Biomedical Applications*. 2007: World Scientific.
6. Carlton, R.J., Hunter, J.T., Miller, D.S., Abbasi, R., Mushenheim, P.C., Tan, L.N., and Abbott, N.L., Chemical and biological sensing using liquid crystals. *Liquid Crystals Reviews*, 2013. 1(1): 29-51.
7. Nalwa, H.S., *Handbook of Advanced Electronic and Photonic Materials and Devices: Liquid crystals, display and laser materials*. 2001: Academic Press.
8. Ritter, O.M.S., Silveira, N.P.d., and Merlo, A.A., Synthesis and mesomorphic properties of side chain liquid-crystalline biphenyl-phenyl polyacrylates. *Journal of the Brazilian Chemical Society*, 2006. 17: 348-356.
9. Finkelmann, H., Ringsdorf, H., and Wendorff, J.H., Model considerations and examples of enantiotropic liquid crystalline polymers. Polyreactions in ordered systems, 14. *Makromol. Chem.*, 1978. 179(1): 273-276.
10. Finkelmann, H., Ringsdorf, H., Siol, W., and Wendorff, J.H., Synthesis of cholesteric liquid crystalline polymers. Polyreactions in ordered systems, 15. *Makromol. Chem.*, 1978. 179(3): 829-832.
11. Mishra, G. and Srivastava, A.K., Side-Chain Liquid Crystalline Polymers with [α -terpineol-co-MMA] Main Chain: Synthesis and Characterization of Polymers with Phenyl Benzoate Mesogenic Group. *Polymer Bulletin*, 2007. 58(2): 351-358.
12. Craig, A.A., Winchester, I., Madden, P.C., Larcey, P., Hamley, I.W., and Imrie, C.T., Synthesis, thermal characterization and rheological properties of a homologous series of polymethacrylate-based side-chain liquid crystal polymers. *Polymer*, 1998. 39(5): 1197-1205.
13. Wewerka, A., Viertler, K., Vlassopoulos, D., and Stelzer, F., Structure and rheology of model side-chain liquid crystalline polymers with varying mesogen length. *Rheologica Acta*, 2001. 40(5): 416-425.
14. Hsu, C.-S., The application of side-chain liquid-crystalline polymers. *Progress in Polymer Science*, 1997. 22(4): 829-871.

15. Blinov, L.M., Kozlovsky, M.V., and Cipparrone, G., Photochromism and holographic grating recording on a chiral side-chain liquid crystalline copolymer containing azobenzene chromophores. *Chemical Physics*, 1999. 245(1): 473-485.
16. Åstrand, P.-O., Ramanujam, P.S., Hvilsted, S., Bak, K.L., and Sauer, S.P.A., Ab Initio Calculation of the Electronic Spectrum of Azobenzene Dyes and Its Impact on the Design of Optical Data Storage Materials. *Journal of the American Chemical Society*, 2000. 122(14): 3482-3487.
17. Nejati, K., Rezvani, Z., and Seyedahmadian, M., The synthesis, characterization, thermal and optical properties of copper, nickel, and vanadyl complexes derived from azo dyes. *Dyes and Pigments*, 2009. 83(3): 304-311.
18. Zhang, X., Wang, C., Lu, X., and Zeng, Y., Nonlinear optical properties of a series of azobenzene liquid-crystalline materials. *Optik - International Journal for Light and Electron Optics*, 2012. 123(1): 26-29.
19. Raposo, M.M.M., Fonseca, A.M.C., Castro, M.C.R., Belsley, M., Cardoso, M.F.S., Carvalho, L.M., and Coelho, P.J., Synthesis and characterization of novel diazenes bearing pyrrole, thiophene and thiazole heterocycles as efficient photochromic and nonlinear optical (NLO) materials. *Dyes and Pigments*, 2011. 91(1): 62-73.
20. Hrozhyk, U., Serak, S., Tabiryan, N., Hoke, L., Steeves, D.M., Kedziora, G., and Kimball, B. *High optical nonlinearity of azobenzene liquid crystals for short laser pulses*. in *Proc. SPIE 7050, Liquid Crystals XII*. 2008.
21. Xie, H.-Q., Liu, Z.-H., Liu, H., and Guo, J.-S., Nonlinear optical crosslinked polymers and interpenetrating polymer networks containing azo-benzothiazole chromophore groups. *Polymer*, 1998. 39(12): 2393-2398.
22. Tabiryan, N., Hrozhyk, U., and Serak, S., Nonlinear Refraction in Photoinduced Isotropic State of Liquid Crystalline Azobenzenes. *Physical Review Letters*, 2004. 93(11): 113901.
23. Hrozhyk, U.A., Serak, S.V., Tabiryan, N.V., Hoke, L., Steeves, D.M., and Kimball, B.R., Azobenzene liquid crystalline materials for efficient optical switching with pulsed and/or continuous wave laser beams. *Optics Express*, 2010. 18(8): 8697-8704.
24. Yager, K.G. and Barrett, C.J., Novel photo-switching using azobenzene functional materials. *Journal of Photochemistry and Photobiology A: Chemistry*, 2006. 182(3): 250-261.
25. Gibbons, W.M., Shannon, P.J., Sun, S.-T., and Swetlin, B.J., Surface-mediated alignment of nematic liquid crystals with polarized laser light. *Nature*, 1991. 351(6321): 49-50.
26. Shishido, A., Tsutsumi, O., Kanazawa, A., Shiono, T., Ikeda, T., and Tamai, N., Rapid Optical Switching by Means of Photoinduced Change in Refractive Index of Azobenzene Liquid Crystals Detected by Reflection-Mode Analysis. *Journal of the American Chemical Society*, 1997. 119(33): 7791-7796.

27. Luk, Y.-Y. and Abbott, N.L., Surface-Driven Switching of Liquid Crystals Using Redox-Active Groups on Electrodes. *Science*, 2003. 301(5633): 623-626.
28. Aoki, K.i., Nakagawa, M., and Ichimura, K., Self-Assembly of Amphoteric Azopyridine Carboxylic Acids: Organized Structures and Macroscopic Organized Morphology Influenced by Heat, pH Change, and Light. *Journal of the American Chemical Society*, 2000. 122(44): 10997-11004.
29. Kadota, S., Aoki, K., Nagano, S., and Seki, T., Photocontrolled Microphase Separation of Block Copolymers in Two Dimensions. *Journal of the American Chemical Society*, 2005. 127(23): 8266-8267.
30. De Sio, L., Ricciardi, L., Serak, S., La Deda, M., Tabiryman, N., and Umeton, C., Photo-sensitive liquid crystals for optically controlled diffraction gratings. *Journal of Materials Chemistry*, 2012. 22(14): 6669-6673.
31. Thieghi, L.T., Bonvent, J.J., Oliveira, E.A., Giacometti, J.A., and Balogh, D.T., Competition between anchoring and reversible photo-induced alignment of a nematic liquid crystal. *Applied Physics A*, 2003. 77(7): 911-914.
32. He, X., Yan, D., and Mai, Y., Synthesis of novel multi-arm star azobenzene side-chain liquid crystalline copolymers with a hyperbranched core. *European Polymer Journal*, 2004. 40(8): 1759-1765.
33. Matsui, M., Nakagawa, H., Joglekar, B., Shibata, K., Muramatsu, H., Abe, Y., and Kaneko, M., Synthesis of perfluoroalkylated azo dyes and their application to guest-host liquid crystal display. *Liquid Crystals*, 1996. 21(5): 669-682.
34. Li, X., Fang, L., Hou, L., Zhu, L., Zhang, Y., Zhang, B., and Zhang, H., Photoresponsive side-chain liquid crystalline polymers with amide group-substituted azobenzene mesogens: effects of hydrogen bonding, flexible spacers, and terminal tails. *Soft Matter*, 2012. 8(20): 5532-5542.
35. Xu, X., Liao, Y., Yu, G., You, H., Di, C.a., Su, Z., Ma, D., Wang, Q., Li, S., Wang, S., Ye, J., and Liu, Y., Charge Carrier Transporting, Photoluminescent, and Electroluminescent Properties of Zinc(II)-2-(2-hydroxyphenyl)benzothiazolate Complex. *Chemistry of Materials*, 2007. 19(7): 1740-1748.
36. Hamada, Y.T., S. Fujii, H. Nishio, Y. Takahashi, H. Shibata, K., White-Light-Emitting Material for Organic Electroluminescent Devices. *Japanese Journal of Applied Physics*, 1996. 35(10B): 1339-1344.
37. Jose, B. and Manoharan, S.S., Photo-physical and semi-empirical studies of a dominant blue light emitting 1,4-dibenzthiazolyl benzene. *Journal of Physics and Chemistry of Solids*, 2007. 68(4): 617-621.
38. Yu, G., Yin, S., Liu, Y., Shuai, Z., and Zhu, D., Structures, Electronic States, and Electroluminescent Properties of a Zinc(II) 2-(2-Hydroxyphenyl)benzothiazolate Complex. *Journal of the American Chemical Society*, 2003. 125(48): 14816-14824.

39. Wang, X., Yang, K., Kumar, J., Tripathy, S.K., Chittibabu, K.G., Li, L., and Lindsay, G., Heteroaromatic Chromophore Functionalized Epoxy-Based Nonlinear Optical Polymers. *Macromolecules*, 1998. 31(13): 4126-4134.
40. Xiao-Juan, L., Ji-Kang, F., Ai-Min, R., Xin, Z., and Wei-Nan, L., Second-order Nonlinear Optical Properties of a Series of Benzothiazole Derivatives. *Chinese Journal of Chemistry*, 2003. 21(1): 9-15.
41. Fu, H.-y., Ye, X.-t., Zhong, G.-y., Zhong, Z.-y., and Xiao, F., White organic light-emitting diodes based on benzothiazole derivative. *Current Applied Physics*, 2010. 10(5): 1326-1330.
42. Wang, H., Chen, G., Xu, X., Chen, H., and Ji, S., The synthesis and optical properties of benzothiazole-based derivatives with various π -electron donors as novel bipolar fluorescent compounds. *Dyes and Pigments*, 2010. 86(3): 238-248.
43. Fu, H.-y., Gao, X.-d., Zhong, G.-y., Zhong, Z.-y., Xiao, F., and Shao, B.-x., Synthesis and electroluminescence properties of benzothiazole derivatives. *Journal of Luminescence*, 2009. 129(10): 1207-1214.
44. Iwan, A., Palewicz, M., Krompiec, M., Grucela-Zajac, M., Schab-Balcerzak, E., and Sikora, A., Synthesis, materials characterization and opto(electrical) properties of unsymmetrical azomethines with benzothiazole core. *Spectrochimica Acta Part A: Molecular and Biomolecular Spectroscopy*, 2012. 97(0): 546-555.
45. Li, H., Li, N., Gu, H., Xu, Q., Yan, F., Lu, J., Xia, X., Ge, J., and Wang, L., Two Different Memory Characteristics Controlled by the Film Thickness of Polymethacrylate Containing Pendant Azobenzothiazole. *The Journal of Physical Chemistry C*, 2010. 114(13): 6117-6122.
46. Cojocariu, C. and Rochon, P., Synthesis and optical storage properties of a novel polymethacrylate with benzothiazole azo chromophore in the side chain. *Journal of Materials Chemistry*, 2004. 14(19): 2909-2916.
47. Wang, D., Li, H., Li, N., Zhao, Y., Zhou, Q., Xu, Q., Lu, J., and Wang, L., A new DRAM-type memory devices based on polymethacrylate containing pendant 2-methylbenzothiazole. *Materials Chemistry and Physics*, 2012. 134(1): 273-278.
48. Faustino, H., El-Shishtawy, R.M., Reis, L.V., Santos, P.F., and Almeida, P., 2-Nitrosobenzothiazoles: useful synthons for new azobenzothiazole dyes. *Tetrahedron Letters*, 2008. 49(48): 6907-6909.
49. Zheng, M.-Q., Yin, D.-Z., Qiao, J.-P., Zhang, L., and Wang, Y.-X., Syntheses and evaluation of fluorinated benzothiazole anilines as potential tracers for β -amyloid plaques in Alzheimer's disease. *Journal of Fluorine Chemistry*, 2008. 129(3): 210-216.
50. Ono, M., Hayashi, S., Kimura, H., Kawashima, H., Nakayama, M., and Saji, H., Push-pull benzothiazole derivatives as probes for detecting β -amyloid plaques in Alzheimer's brains. *Bioorganic & Medicinal Chemistry*, 2009. 17(19): 7002-7007.

51. Cui, M.-C., Li, Z.-J., Tang, R.-K., and Liu, B.-L., Synthesis and evaluation of novel benzothiazole derivatives based on the bithiophene structure as potential radiotracers for β -amyloid plaques in Alzheimer's disease. *Bioorganic & Medicinal Chemistry*, 2010. 18(7): 2777-2784.
52. Bingol, H., Kocabas, E., Zor, E., and Coskun, A., A novel benzothiazole based azocalix[4]arene as a highly selective chromogenic chemosensor for Hg^{2+} ion: A rapid test application in aqueous environment. *Talanta*, 2010. 82(4): 1538-1542.
53. Misra, A. and Shahid, M., Chromo and Fluorogenic Properties of Some Azo-Phenol Derivatives and Recognition of Hg^{2+} Ion in Aqueous Medium by Enhanced Fluorescence. *The Journal of Physical Chemistry C*, 2010. 114(39): 16726-16739.
54. Misra, A., Shahid, M., and Srivastava, P., An efficient fluoroionophore for selective recognition of Hg^{2+} and Cu^{2+} ions. *Thin Solid Films*, 2010. 519(3): 1235-1239.
55. Ha, S.-T., Koh, T.-M., Yeap, G.-Y., Lin, H.-C., Lee, S.-L., Win, Y.-F., and Ong, S.-T., Mesogenic Schiff base esters with benzothiazole core: synthesis and phase transition studies. *Phase Transitions*, 2010. 83(3): 195-204.
56. Dutta, G.K., Guha, S., and Patil, S., Synthesis of liquid crystalline benzothiazole based derivatives: A study of their optical and electrical properties. *Organic Electronics*, 2010. 11(1): 1-9.
57. Schmidt-Mende, L., Fechtenkötter, A., Müllen, K., Moons, E., Friend, R.H., and MacKenzie, J.D., Self-Organized Discotic Liquid Crystals for High-Efficiency Organic Photovoltaics. *Science*, 2001. 293(5532): 1119-1122.
58. De Feyter, S. and De Schryver, F.C., Two-dimensional supramolecular self-assembly probed by scanning tunneling microscopy. *Chemical Society Reviews*, 2003. 32(3): 139-150.
59. Liu, J.-H. and Yang, P.-C., Synthesis and characterization of novel monomers and polymers containing chiral (-)-menthyl groups. *Polymer*, 2006. 47(14): 4925-4935.
60. Singh, S. and Dunmur, D.A., *Liquid Crystals: Fundamentals*. 2002: World Scientific.
61. Kardas, D., Mieczkowski, J., Pocięcha, D., Szydłowska, J., and Gorecka, E., Synthesis and properties of a new series of mesogenic compounds with pyridine, oxidopyridinium, thienyl and furyl moieties. *Journal of Materials Chemistry*, 2001. 11(3): 741-748.
62. Wu, L.-H., Wang, Y.-C., and Hsu, C.-S., Synthesis and characterization of thiophene-containing liquid crystals. *Liquid Crystals*, 2000. 27(11): 1503-1513.
63. Wang, C.-S., Wang, I.W., Cheng, K.-L., and Lai, C.K., The effect of polar substituents on the heterocyclic benzoxazoles. *Tetrahedron*, 2006. 62(40): 9383-9392.

64. Thaker, B.T., Patel, B.S., Dhimmar, Y.T., Chothani, N.J., Solanki, D.B., Patel, N., Patel, K.B., and Makawana, U., Mesomorphic studies of novel azomesogens having a benzothiazole core: Synthesis and characterisation. *Liquid Crystals*, 2012. 40(2): 237-248.
65. Khoo, I.C., *Liquid Crystals*. 2nd ed. 2007, New Jersey: John Wiley & Sons.
66. Kelker, H. and Hatz, R., *Handbook of liquid crystals*. 1980: Verlag Chemie.
67. Rego, J.A. *Introduction to Liquid Crystals* [cited 2013 26 August]; Available from: http://www.csupomona.edu/~jarego/pages/LC_intro.html.
68. Goodby, J.W., A Pictorial Approach to Helical Macrostructures in Smectic Liquid Crystals. *Molecular Crystals and Liquid Crystals Science and Technology. Section A. Molecular Crystals and Liquid Crystals*, 1997. 292(1): 245-263.
69. Kumar, S., *Chemistry of Discotic Liquid Crystals: From Monomers to Polymers*. 2011, New York: Taylor and Francis.
70. Madhusudana, N.V., Recent advances in thermotropic liquid crystals. *Current Science*, 2001. 80(8): 1018-1025.
71. Barrett, C.J., Mamiya, J.-i., Yager, K.G., and Ikeda, T., Photo-mechanical effects in azobenzene-containing soft materials. *Soft Matter*, 2007. 3(10): 1249-1261.
72. H. Kelker, B.S., R. Hatz and W. Bartsch Liquid-crystalline phases with a very low freezing point. *Angew. Chem.*, 1970. 82: 984.
73. Murase, K. and Watanabe, H., Liquid Crystalline Properties of Substituted Azo- and Azoxy-benzenes. I. *Bulletin of the Chemical Society of Japan*, 1973. 46(10): 3142-3143.
74. Hrozhyk, U., Serak, S., Tabiryan, N., and Bunning, T.J., Wide Temperature Range Azobenzene Nematic and Smectic LC Materials. *Molecular Crystals and Liquid Crystals*, 2006. 454(1): 235/[637]-245/[647].
75. Yang, P.-C., Li, C.-Y., Wu, H., and Chiang, J.-C., Synthesis and mesomorphic properties of photoresponsive azobenzene-containing chromophores with various terminal groups. *Journal of the Taiwan Institute of Chemical Engineers*, 2012. 43(3): 480-490.
76. Rahman, M.L., Asik, J., Kumar, S., Silong, S., and Rahman, M.Z.A., Synthesis and mesomorphic properties of nonsymmetric liquid crystalline dimers containing azobenzene groups. *Phase Transitions: A Multinational Journal*, 2009. 82(3): 228-239.
77. Al-Hamdani, U.J., Mesomorphic Properties of an Homologous Series of Thioalkyl-Terminated Azomesogens. *International Journal of Molecular Sciences*, 2011. 12(5): 3182-3190.
78. Cook, A.G., Inkster, R.T., Martinez-Felipe, A., Ribes-Greus, A., Hamley, I.W., and Imrie, C.T., Synthesis and phase behaviour of a homologous series of

- polymethacrylate-based side-chain liquid crystal polymers. *European Polymer Journal*, 2012. 48(4): 821-829.
79. Prasad, S.K., Nair, G.G., and Rao, D.S.S., Photoinduced phase transitions. *Liquid Crystals*, 2009. 36(6-7): 705-716.
 80. Tamba, M.-G., Bobrovsky, A., Shibaev, V., Pelzl, G., Baumeister, U., and Weissflog, W., Photochromic azobenzene functionalised banana–calamitic dimers and trimers: mesophase behaviour and photo-orientational phenomena. *Liquid Crystals*, 2011. 38(11-12): 1531-1550.
 81. Ichimura, K., Oh, S.-K., and Nakagawa, M., Light-Driven Motion of Liquids on a Photoresponsive Surface. *Science*, 2000. 288(5471): 1624-1626.
 82. Shibaev, V., Bobrovsky, A., and Boiko, N., Photoactive liquid crystalline polymer systems with light-controllable structure and optical properties. *Progress in Polymer Science*, 2003. 28(5): 729-836.
 83. Deng, W., Albouy, P.-A., Lacaze, E., Keller, P., Wang, X., and Li, M.-H., Azobenzene-Containing Liquid Crystal Triblock Copolymers: Synthesis, Characterization, and Self-Assembly Behavior. *Macromolecules*, 2008. 41(7): 2459-2466.
 84. Fujii, T., Shiotsuki, M., Inai, Y., Sanda, F., and Masuda, T., Synthesis of Helical Poly(N-propargylamides) Carrying Azobenzene Moieties in Side Chains. Reversible Arrangement-Disarrangement of Helical Side Chain Arrays upon Photoirradiation Keeping Helical Main Chain Intact. *Macromolecules*, 2007. 40(20): 7079-7088.
 85. Tomatsu, I., Hashidzume, A., and Harada, A., Contrast Viscosity Changes upon Photoirradiation for Mixtures of Poly(acrylic acid)-Based α -Cyclodextrin and Azobenzene Polymers. *Journal of the American Chemical Society*, 2006. 128(7): 2226-2227.
 86. Chen, X., Hong, L., You, X., Wang, Y., Zou, G., Su, W., and Zhang, Q., Photo-controlled molecular recognition of [small alpha]-cyclodextrin with azobenzene containing polydiacetylene vesicles. *Chemical Communications*, 2009(11): 1356-1358.
 87. Ruchmann, J., Fouilloux, S., and Tribet, C., Light-responsive hydrophobic association of surfactants with azobenzene-modified polymers. *Soft Matter*, 2008. 4(10): 2098-2108.
 88. Pouliquen, G., Amiel, C., and Tribet, C., Photoresponsive Viscosity and Host–Guest Association in Aqueous Mixtures of Poly-Cyclodextrin with Azobenzene-Modified Poly(acrylic)acid. *The Journal of Physical Chemistry B*, 2007. 111(20): 5587-5595.
 89. Zhao, Y.-L. and Stoddart, J.F., Azobenzene-Based Light-Responsive Hydrogel System†. *Langmuir*, 2009. 25(15): 8442-8446.
 90. Gao, J., He, Y., Xu, H., Song, B., Zhang, X., Wang, Z., and Wang, X., Azobenzene-Containing Supramolecular Polymer Films for Laser-Induced Surface Relief Gratings. *Chemistry of Materials*, 2006. 19(1): 14-17.

91. Isayama, J., Nagano, S., and Seki, T., Phototriggered Mass Migrating Motions in Liquid Crystalline Azobenzene Polymer Films with Systematically Varied Thermal Properties. *Macromolecules*, 2010. 43(9): 4105-4112.
92. Yamamoto, T., Hasegawa, M., Kanazawa, A., Shiono, T., and Ikeda, T., Holographic gratings and holographic image storage photochemical phase transitions of polymer azobenzene liquid-crystal films. *Journal of Materials Chemistry*, 2000. 10(2): 337-342.
93. Natansohn, A. and Rochon, P., Photoinduced Motions in Azo-Containing Polymers. *Chemical Reviews*, 2002. 102(11): 4139-4176.
94. Zettsu, N., Ubukata, T., Seki, T., and Ichimura, K., Soft Crosslinkable Azo Polymer for Rapid Surface Relief Formation and Persistent Fixation. *Advanced Materials*, 2001. 13(22): 1693-1697.
95. You, F., Paik, M.Y., Häckel, M., Kador, L., Kropp, D., Schmidt, H.W., and Ober, C.K., Control and Suppression of Surface Relief Gratings in Liquid-Crystalline Perfluoroalkyl-Azobenzene Polymers. *Advanced Functional Materials*, 2006. 16(12): 1577-1581.
96. Grimes, A.F., Call, S.E., Vicente, D.A., English, D.S., and Harbron, E.J., Toward Efficient Photomodulation of Conjugated Polymer Emission: Optimizing Differential Energy Transfer in Azobenzene-Substituted PPV Derivatives. *The Journal of Physical Chemistry B*, 2006. 110(39): 19183-19190.
97. Lewis, S.M. and Harbron, E.J., Photomodulated PPV Emission in a Photochromic Polymer Film. *The Journal of Physical Chemistry C*, 2007. 111(11): 4425-4430.
98. Grimes, A.F., Call, S.E., Harbron, E.J., and English, D.S., Wavelength-Resolved Studies of Förster Energy Transfer in Azobenzene-Modified Conjugated Polymers: The Competing Roles of Exciton Migration and Spectral Resonance. *The Journal of Physical Chemistry C*, 2007. 111(38): 14257-14265.
99. Harbron, E.J., Hadley, D.H., and Imm, M.R., Solvent effects on phototriggered conformational changes in an azobenzene-functionalized poly(p-phenylene vinylene). *Journal of Photochemistry and Photobiology A: Chemistry*, 2007. 186(2-3): 151-157.
100. Racané, L., Mihalić, Z., Cerić, H., Popović, J., and Tralić-Kulenović, V., Synthesis, structure and tautomerism of two benzothiazolyl azo derivatives of 2-naphthol: A crystallographic, NMR and computational study. *Dyes and Pigments*, 2013. 96(3): 672-678.
101. Keerthi Kumar, C.T.K., J. Rajesh, T. Peethambar, S.K. , Synthesis, Characterization and Biological Activity of Heterocyclic Azo Dyes Derived From 2-Aminobenzothiozole. *International Journal of Pharmacy and Pharmaceutical Sciences*, 2013. 5(Suppl 1): 296-301.
102. Yazdanbakhsh, M.R., Mohammadi, A., and Abbasnia, M., Some heterocyclic azo dyes derived from thiazolyl derivatives; synthesis; substituent effects and solvatochromic studies. *Spectrochimica Acta Part A: Molecular and Biomolecular Spectroscopy*, 2010. 77(5): 1084-1087.

103. Faustino, H., Brannigan, C.R., Reis, L.V., Santos, P.F., and Almeida, P., Novel azobenzothiazole dyes from 2-nitrosobenzothiazoles. *Dyes and Pigments*, 2009. 83(1): 88-94.
104. Marchevsky, E., Olsina, R., and Marone, C., 2-[2-(5-Chloropyridyl)azo]-5-dimethylaminophenol as indicator for the complexometric determination of zinc. *Talanta*, 1985. 32(1): 54-56.
105. Manickasundaram, S., Kannan, P., Hassan, Q.M.A., and Palanisamy, P.K., Azo dye based poly(alkyloxymethacrylate)s and their spacer effect on optical data storage. *Journal of Materials Science: Materials in Electronics*, 2008. 19(11): 1045-1053.
106. Matharu, A.S. and Chambers-Asman, D., Structure–property investigation of 2- and 3-thienylacrylates bearing laterally fluorinated azobenzene moieties. *Liquid Crystals*, 2007. 34(11): 1317-1336.
107. Gallardo, H., Magnago, R., and Bortoluzzi, A.J., Synthesis, characterization and mesomorphic properties of Ag(I) and Pd(II) complexes containing the pyridyl and tetrazoyl rings: crystal structure of [C₃₀H₄₆N₁₀Ag ClO₄]. *Liquid Crystals*, 2001. 28(9): 1343-1352.
108. Seed, A., Synthesis of self-organizing mesogenic materials containing a sulfur-based five-membered heterocyclic core. *Chemical Society Reviews*, 2007. 36(12): 2046-2069.
109. Henderson, P., Cook, A., and Imrie, C., Oligomeric liquid crystals: From monomers to trimers. *Liquid Crystals*, 2004. 31(11): 1427-1434.
110. Lee, C.-H. and Yamamoto, T., Synthesis of Liquid Crystals with Bent-Rod Structure: 4-Methylthiazole Derivatives with Nematic Phase. *Molecular Crystals and Liquid Crystals Science and Technology. Section A. Molecular Crystals and Liquid Crystals*, 2001. 369(1): 95-102.
111. Parra, M., Hernandez, S., Alderete, J., and Zuniga, C., New Schiff's bases containing 1,3,4-thiadiazole and 1,3,4-oxadiazole units: a study of the effect of the heterocyclic ring and the position of the lateral alkoxy group on liquid crystalline properties. *Liquid Crystals*, 2000. 27(8): 995-1000.
112. Dave, J. and Menon, M., Azomesogens with a heterocyclic moiety. *Bulletin of Materials Science*, 2000. 23(3): 237-238.
113. Haramoto, Y., Yamada, T., Nanasawa, M., Funahashi, M., Hanna, J., and Ujiie, S., Conductive liquid crystalline compounds having a piperazine structure. *Liquid Crystals*, 2002. 29(8): 1109-1111.
114. Barbera, J., Clays, K., Gimenez, R., Houbrechts, S., Persoons, A., and Luis Serrano, J., Versatile optical materials: fluorescence, non-linear optical and mesogenic properties of selected 2-pyrazoline derivatives. *Journal of Materials Chemistry*, 1998. 8(8): 1725-1730.
115. Campbell, N.L., Duffy, W.L., Thomas, G.I., Wild, J.H., Kelly, S.M., Bartle, K., O'Neill, M., Minter, V., and Tuffin, R.P., Nematic 2,5-disubstituted thiophenes. *Journal of Materials Chemistry*, 2002. 12(9): 2706-2721.

116. Thaker, B.T., Patel, P., Vansadia, A.D., and Patel, H.G., Synthesis, Characterization, and Mesomorphic Properties of New Liquid-Crystalline Compounds involving Ester–Azomethine Central Linkages, Lateral Substitution, and a Thiazole Ring. *Molecular Crystals and Liquid Crystals*, 2007. 466(1): 13-22.
117. Belmar, J., New liquid crystals containing the benzothiazol unit: amides and azo compounds. *Liquid Crystals*, 1999. 26(3): 389-396.
118. Prajapati, A. and Bonde, N., Mesogenic benzothiazole derivatives with methoxy substituents. *Journal of Chemical Sciences*, 2006. 118(2): 203-210.
119. Ha, S.T., Foo, K.L., Lin, H.C., Ito, M.M., Abe, K., Kunbo, K., and Sastry, S.S., Mesomorphic behavior of new benzothiazole liquid crystals having Schiff base linker and terminal methyl group. *Chinese Chemical Letters*, 2012. 23(7): 761-764.
120. Ha, S.-T., Koh, T.-M., Yeap, G.-Y., Lin, H.-C., Lee, S.-L., Win, Y.-F., and Ong, S.-T., Synthesis and Mesomorphic Properties of 6-Methoxy- and 6-Ethoxy-2-(2-Hydroxy-4-Alkanoyloxybenzylidenamino)Benzothiazoles. *Molecular Crystals and Liquid Crystals*, 2010. 528(1): 10-22.
121. Ha, S.-T., Koh, T.-M., Lin, H.-C., Yeap, G.-Y., Win, Y.-F., Ong, S.-T., Sivasothy, Y., and Ong, L.-K., Heterocyclic benzothiazole-based liquid crystals: synthesis and mesomorphic properties. *Liquid Crystals*, 2009. 36(9): 917-925.
122. Yeap, G.-Y., Alshargabi, A., Ito, M.M., Mahmood, W.A.K., and Takeuchi, D., Synthesis and Anisotropic Properties of Azo-Bridged Benzothiazole-Phenyl Esters. *Molecular Crystals and Liquid Crystals*, 2012. 557(1): 126-133.
123. Iwan, A., Gorecki, L., and Pocięcha, D., Liquid crystalline properties of new unsymmetrical compounds with benzothiazole core detected by TG/DSC-POM-XRD. *Journal of Thermal Analysis and Calorimetry*, 2012. 110(1): 43-49.
124. Alshargabi, A., Yeap, G.-Y., Mahmood, W.A.K., and Samikannu, R., Molecular, spectroscopic and thermal studies on catechol, 4,5-dibromocatechol, resorcinol, hydroquinone and 4-4'-dihydroxybiphenyl derivatives armed with benzothiazole moieties. *Journal of Molecular Structure*, 2013. 1039(0): 189-196.
125. Ha, S.-T., Koh, T.-M., Win, Y.-F., and Sastry, S.S., Phase transition behaviours of calamitic liquid crystals comprising phenylbenzothiazole core. *Liquid Crystals*, 2013. 40(8): 1016-1023.
126. Pudzych, R., Fuhrmann-Lieker, T., and Salbeck, J., *Spiro Compounds for Organic Electroluminescence and Related Applications*, in *Emissive Materials Nanomaterials*. 2006, Springer Berlin Heidelberg. p. 83-142.
127. Hung, L.S. and Chen, C.H., Recent progress of molecular organic electroluminescent materials and devices. *Materials Science and Engineering: R: Reports*, 2002. 39(5–6): 143-222.
128. Tang, C.W. and VanSlyke, S.A., Organic electroluminescent diodes. *Applied Physics Letters*, 1987. 51(12): 913-915.

129. Burroughes, J., Bradley, D., Brown, A., Marks, R., Mackay, K., Friend, R., Burns, P., and Holmes, A., Light-emitting diodes based on conjugated polymers. *Nature*, 1990. 347(6293): 539-541.
130. Chen, C.-T., Evolution of Red Organic Light-Emitting Diodes: Materials and Devices. *Chemistry of Materials*, 2004. 16(23): 4389-4400.
131. Huang, T.H., Lin, J.T., Chen, L.Y., Lin, Y.T., and Wu, C.C., Dipolar Dibenzothiophene S,S-Dioxide Derivatives Containing Diarylamine: Materials for Single-Layer Organic Light-Emitting Devices. *Advanced Materials*, 2006. 18(5): 602-606.
132. Kido, J. and Iizumi, Y., Fabrication of highly efficient organic electroluminescent devices. *Applied Physics Letters*, 1998. 73(19): 2721-2723.
133. Li, Z.H., Wong, M.S., Fukutani, H., and Tao, Y., Synthesis and Light-Emitting Properties of Bipolar Oligofluorenes Containing Triarylamine and 1,2,4-Triazole Moieties. *Organic Letters*, 2006. 8(19): 4271-4274.
134. Lee, J.H., Yuan, Y.Y., Kang, Y.J., Jia, W.L., Lu, Z.H., and Wang, S.N., 2,5-Functionalized Spiro-Bisiloles as Highly Efficient Yellow-Light Emitters in Electroluminescent Devices. *Advanced Functional Materials*, 2006. 16(5): 681-686.
135. Kannan, R., He, G.S., Yuan, L., Xu, F., Prasad, P.N., Dombroskie, A.G., Reinhardt, B.A., Baur, J.W., Vaia, R.A., and Tan, L.-S., Diphenylaminofluorene-Based Two-Photon-Absorbing Chromophores with Various π -Electron Acceptors. *Chemistry of Materials*, 2001. 13(5): 1896-1904.
136. Baur, J.W., Alexander, M.D., Banach, M., Denny, L.R., Reinhardt, B.A., Vaia, R.A., Fleitz, P.A., and Kirkpatrick, S.M., Molecular Environment Effects on Two-Photon-Absorbing Heterocyclic Chromophores. *Chemistry of Materials*, 1999. 11(10): 2899-2906.
137. Belfield, K.D., Morales, A.R., Kang, B.-S., Hales, J.M., Hagan, D.J., Van Stryland, E.W., Chapela, V.M., and Percino, J., Synthesis, Characterization, and Optical Properties of New Two-Photon-Absorbing Fluorene Derivatives. *Chemistry of Materials*, 2004. 16(23): 4634-4641.
138. Shao, P., Huang, B., Chen, L., Liu, Z., Qin, J., Gong, H., Ding, S., and Wang, Q., Synthesis and two-photon absorption properties of novel heterocycle-based organic molecules. *Journal of Materials Chemistry*, 2005. 15(42): 4502-4506.
139. He, G.S., Swiatkiewicz, J., Jiang, Y., Prasad, P.N., Reinhardt, B.A., Tan, L.-S., and Kannan, R., Two-Photon Excitation and Optical Spatial-Profile Reshaping via a Nonlinear Absorbing Medium†. *The Journal of Physical Chemistry A*, 2000. 104(20): 4805-4810.
140. Zhang, X.H., Wong, O.Y., Gao, Z.Q., Lee, C.S., Kwong, H.L., Lee, S.T., and Wu, S.K., A new blue-emitting benzothiazole derivative for organic electroluminescent devices. *Materials Science and Engineering: B*, 2001. 85(2-3): 182-185.

141. Chang, S.M., Tzeng, Y.J., Wu, S.Y., Li, K.Y., and Hsueh, K.L., Emission of white light from 2-(2'-hydroxyphenyl) benzothiazole in polymer electroluminescent devices. *Thin Solid Films*, 2005. 477(1-2): 38-41.
142. Ji, S.-J. and Shi, H.-B., Synthesis and fluorescent property of some novel benzothiazoyl pyrazoline derivatives containing aromatic heterocycle. *Dyes and Pigments*, 2006. 70(3): 246-250.
143. Fu, H.-Y., Sun, X.-Y., Gao, X.-d., Xiao, F., and Shao, B.-X., Synthesis and characterization of benzothiazole derivatives for blue electroluminescent devices. *Synthetic Metals*, 2009. 159(3-4): 254-259.
144. Hancock, J.M., Gifford, A.P., Tonzola, C.J., and Jenekhe, S.A., High-Efficiency Electroluminescence from New Blue-Emitting Oligoquinolines Bearing Pyrenyl or Triphenyl Endgroups. *The Journal of Physical Chemistry C*, 2007. 111(18): 6875-6882.
145. Li, H.C., Lin, Y.P., Chou, P.T., Cheng, Y.M., and Liu, R.S., Color Tuning and Highly Efficient Blue Emitters of Finite Diphenylamino-Containing Oligo(arylenevinylene) Derivatives Using Fluoro Substituents. *Advanced Functional Materials*, 2007. 17(4): 520-530.
146. Raposo, M.M.M., Castro, M.C.R., Fonseca, A.M.C., Schellenberg, P., and Belsley, M., Design, synthesis, and characterization of the electrochemical, nonlinear optical properties, and theoretical studies of novel thienylpyrrole azo dyes bearing benzothiazole acceptor groups. *Tetrahedron*, 2011. 67(29): 5189-5198.
147. Rajakumar, P., Kalpana, V., Ganesan, S., and Maruthamuthu, P., Synthesis and DSSC application of novel dendrimers with benzothiazole and triazole units. *Tetrahedron Letters*, 2011. 52(44): 5812-5816.
148. Echevarria, L., Moreno, I., Camacho, J., Salazar, M.C., and Hernández, A., A fluorescent benzothiazole probe with efficient two-photon absorption. *Spectrochimica Acta Part A: Molecular and Biomolecular Spectroscopy*, 2012. 97(0): 274-276.
149. Anzini, M., Chelini, A., Mancini, A., Cappelli, A., Frosini, M., Ricci, L., Valoti, M., Magistretti, J., Castelli, L., Giordani, A., Makovec, F., and Vomero, S., Synthesis and Biological Evaluation of Amidine, Guanidine, and Thiourea Derivatives of 2-Amino(6-trifluoromethoxy)benzothiazole as Neuroprotective Agents Potentially Useful in Brain Diseases. *Journal of Medicinal Chemistry*, 2009. 53(2): 734-744.
150. Saeed, S., Rashid, N., Jones, P.G., Ali, M., and Hussain, R., Synthesis, characterization and biological evaluation of some thiourea derivatives bearing benzothiazole moiety as potential antimicrobial and anticancer agents. *European Journal of Medicinal Chemistry*, 2010. 45(4): 1323-1331.
151. Karmakar, T., Kuang, Y., Neamati, N., and Baruah, J.B., Cadmium complexes and cocrystals of indium complexes of benzothiazole derivatives and anticancer activities of the cadmium complexes. *Polyhedron*, 2013. 54(0): 285-293.

152. Zajac, M., Hrobárik, P., Magdolen, P., Foltínová, P., and Zahradník, P., Donor- π -acceptor benzothiazole-derived dyes with an extended heteroaryl-containing conjugated system: synthesis, DFT study and antimicrobial activity. *Tetrahedron*, 2008. 64(46): 10605-10618.
153. Hu, W.-P., Chen, Y.-K., Liao, C.-C., Yu, H.-S., Tsai, Y.-M., Huang, S.-M., Tsai, F.-Y., Shen, H.-C., Chang, L.-S., and Wang, J.-J., Synthesis, and biological evaluation of 2-(4-aminophenyl)benzothiazole derivatives as photosensitizing agents. *Bioorganic & Medicinal Chemistry*, 2010. 18(16): 6197-6207.
154. Yuxia, Z., Zhao, L., Ling, Q., Jianfen, Z., Jiayun, Z., Yuquan, S., Gang, X., and Peixian, Y., Synthesis and characterization of a novel nonlinear optical polyurethane polymer. *European Polymer Journal*, 2001. 37(3): 445-449.
155. Ledoux, I., Zyss, J., Barni, E., Barolo, C., Diulgheroff, N., Quagliotto, P., and Viscardi, G., Properties of novel azodyes containing powerful acceptor groups and thiophene moiety. *Synthetic Metals*, 2000. 115(1-3): 213-217.
156. Facchetti, A., Abboto, A., Beverina, L., van der Boom, M.E., Dutta, P., Evmenenko, G., Marks, T.J., and Pagani, G.A., Azinium-(π -Bridge)-Pyrrole NLO-Phores: Influence of Heterocycle Acceptors on Chromophoric and Self-Assembled Thin-Film Properties#. *Chemistry of Materials*, 2002. 14(12): 4996-5005.
157. Albert, I.D.L., Morley, J.O., and Pugh, D., Optical Nonlinearities in Azoarenes. *The Journal of Physical Chemistry*, 1995. 99(20): 8024-8032.
158. Tasaganva, R.G., Tambe, S.M., and Kariduraganavar, M.Y., Synthesis and characterization of thermally stable second-order nonlinear optical side-chain polyurethanes containing nitro-substituted oxadiazole and thiazole chromophores. *Journal of Molecular Structure*, 2011. 1000(1-3): 10-23.
159. Leng, W.N., Zhou, Y.M., Xu, Q.H., and Liu, J.Z., Synthesis of nonlinear optical polyimides containing benzothiazole moiety and their electro-optical and thermal properties. *Polymer*, 2001. 42(22): 9253-9259.
160. Hao, J., Han, M.-J., Guo, K., Zhao, Y., Qiu, L., Shen, Y., and Meng, X., A novel NLO azothiophene-based chromophore: Synthesis, characterization, thermal stability and optical nonlinearity. *Materials Letters*, 2008. 62(6-7): 973-976.
161. Leng, W., Zhou, Y., Xu, Q., and Liu, J., Synthesis and Characterization of Nonlinear Optical Side-Chain Polyimides Containing the Benzothiazole Chromophores. *Macromolecules*, 2001. 34(14): 4774-4779.
162. Chen, L., Cui, Y., Qian, G., and Wang, M., Synthesis and spectroscopic characterization of an alkoxy silane dye containing azo-benzothiazole chromophore for nonlinear optical applications. *Dyes and Pigments*, 2007. 73(3): 338-343.
163. Tambe, S.M., Kittur, A.A., Inamdar, S.R., Mitchell, G.R., and Kariduraganavar, M.Y., Synthesis and characterization of thermally stable second-order nonlinear optical side-chain polyimides containing thiazole and benzothiazole push-pull chromophores. *Optical Materials*, 2009. 31(6): 817-825.

164. He, M., Zhou, Y., Dai, J., Liu, R., Cui, Y., and Zhang, T., Synthesis and nonlinear optical properties of soluble fluorinated polyimides containing hetarylazo chromophores with large hyperpolarizability. *Polymer*, 2009. 50(16): 3924-3931.
165. Kariduraganavar, M.Y., Tambe, S.M., Tasaganva, R.G., Kittur, A.A., Kulkarni, S.S., and Inamdar, S.R., Studies on nonlinear optical polyurethanes containing heterocyclic chromophores. *Journal of Molecular Structure*, 2011. 987(1-3): 158-165.
166. Zhang, L., Xu, Q.-F., Lu, J.-M., Li, N.-J., Yan, F., and Wang, L.-H., Synthesis, characterization and fluorescence adjustment of well-defined polymethacrylates with pendant π -conjugated benzothiazole via atom transfer radical polymerization (ATRP). *Polymer*, 2009. 50(20): 4807-4812.
167. Park, S.K., Do, J.Y., Ju, J.J., Park, S., Kim, M.-s., and Lee, M.-H., Nonlinear optical polymer applicable for all-optical wavelength converters in communications bands near 1.5 μm . *Materials Letters*, 2005. 59(23): 2872-2875.
168. Cao, Z., Qiu, F., Wang, Q., Cao, G., Zhuang, L., Shen, Q., Xu, X., Wang, J., Chen, Q., and Yang, D., Synthesis of azo benzothiazole polymer and its application of 1 \times 2 Y-branched and 2 \times 2 Mach-Zehnder interferometer switch. *Optik - International Journal for Light and Electron Optics*, 2013. 124(19): 4036-4040.
169. Yıldırım, M. and Kaya, İ., A comparative study of aminothiazole-based polymers synthesized by chemical oxidative polymerization. *Synthetic Metals*, 2012. 162(5-6): 436-443.
170. Tang, X., Gao, L., Fan, X., and Zhou, Q., Effect of the terminal substituent of azobenzene on the properties of ABA triblock copolymers via atom transfer radical polymerization. *Journal of Polymer Science Part A: Polymer Chemistry*, 2007. 45(22): 5190-5198.
171. Labarthe, F.L., Freiberg, S., Pellerin, C., Pézolet, M., Natansohn, A., and Rochon, P., Spectroscopic and Optical Characterization of a Series of Azobenzene-Containing Side-Chain Liquid Crystalline Polymers. *Macromolecules*, 2000. 33(18): 6815-6823.
172. Freiberg, S., Lagugné-Labarthe, F., Rochon, P., and Natansohn, A., Synthesis and Characterization of a Series of Azobenzene-Containing Side-Chain Liquid Crystalline Polymers. *Macromolecules*, 2003. 36(8): 2680-2688.
173. Li, Z., Zhang, Y., Zhu, L., Shen, T., and Zhang, H., Efficient synthesis of photoresponsive azobenzene-containing side-chain liquid crystalline polymers with high molecular weights by click chemistry. *Polymer Chemistry*, 2010. 1(9): 1501-1511.
174. Angiolini, L., Benelli, T., Giorgini, L., Paris, F., Salatelli, E., Fontana, M.P., and Camorani, P., Synthesis by ATRP and effects of molecular weight on photomechanical properties of liquid crystalline polymers containing side-chain azobenzene chromophores. *European Polymer Journal*, 2008. 44(10): 3231-3238.

175. Han, M. and Ichimura, K., In-Plane and Tilt Reorientation of p-Methoxyazobenzene Side Chains Tethered to Liquid Crystalline Polymethacrylates by Irradiation with 365 nm Light. *Macromolecules*, 2000. 34(1): 90-98.
176. Liu, J., Sun, K., Li, Z., Gao, J., Su, W., Yang, J., Zhang, J., Wang, P., and Zhang, Q., Banded texture of photo-aligned azobenzene-containing side-chain liquid crystalline polymers. *Polymer*, 2004. 45(12): 4331-4336.
177. Alicante, R., Cases, R., Forcén, P., Oriol, L., and Villacampa, B., Synthesis and nonlinear optical properties of side chain liquid crystalline polymers containing azobenzene push-pull chromophores. *Journal of Polymer Science Part A: Polymer Chemistry*, 2010. 48(1): 232-242.
178. Colby, R.H., Gillmor, J.R., Galli, G., Laus, M., Ober, C.K., and Hall, E., Linear viscoelasticity of side chain liquid crystal polymer. *Liquid Crystals*, 1993. 13(2): 233-245.
179. Colby, R., Ober, C., Gillmor, J., Connelly, R., Duong, T., Galli, G., and Laus, M., Smectic rheology. *Rheologica Acta*, 1997. 36(5): 498-504.
180. Kannan, R.M., Kornfield, J.A., Schwenk, N., and Boeffel, C., Rheology of side-group liquid-crystalline polymers: effect of isotropic-nematic transition and evidence of flow alignment. *Macromolecules*, 1993. 26(8): 2050-2056.
181. Rubin, S.F., Kannan, R.M., Kornfield, J.A., and Boeffel, C., Effect of Mesophase Order and Molecular Weight on the Dynamics of Nematic and Smectic Side-Group Liquid-Crystalline Polymers. *Macromolecules*, 1995. 28(10): 3521-3530.
182. Berghausen, J., Fuchs, J., and Richtering, W., Rheology and Shear Orientation of a Nematic Liquid Crystalline Side-Group Polymer with Laterally Attached Mesogenic Units. *Macromolecules*, 1997. 30(24): 7574-7581.
183. Wewerka, A., Floudas, G., Pakula, T., and Stelzer, F., Side-Chain Liquid-Crystalline Homopolymers and Copolymers. Structure and Rheology. *Macromolecules*, 2001. 34(23): 8129-8137.
184. Lee, K.M. and Han, C.D., Rheology of Nematic Side-Chain Liquid-Crystalline Polymer: Comparison with Main-Chain Liquid-Crystalline Polymer. *Macromolecules*, 2002. 35(16): 6263-6273.
185. Lee, K.M. and Han, C.D., Effect of Flexible Spacer Length on the Rheology of Side-Chain Liquid-Crystalline Polymers. *Macromolecules*, 2003. 36(23): 8796-8810.
186. Rendon, S., Burghardt, W.R., Auad, M.L., and Kornfield, J.A., Shear-Induced Alignment of Smectic Side Group Liquid Crystalline Polymers. *Macromolecules*, 2007. 40(18): 6624-6630.
187. Andreatti, L., Galli, G., Giordano, M., and Zulli, F., A Rheological Investigation of Entanglement in Side-Chain Liquid-Crystalline Azobenzene Polymethacrylates. *Macromolecules*, 2013. 46(12): 5003-5017.

188. Coessens, V. and Matyjaszewski, K., Fundamentals of Atom Transfer Radical Polymerization. *Journal of Chemical Education*, 2010. 87(9): 916–919.
189. Krzysztof Matyjaszewski, T.P.D., *Handbook of Radical Polymerization* 2003, New York: John Wiley & Sons.
190. Tourasanidis, E.V. and Karayannidis, G.P., Synthesis and characterization of new polymethacrylates bearing an azo-dye in the side chain . *Journal of Macromolecular Science, Part A*, 1999. 36(9): 1241-1258.
191. Tsutsumi, O., Kitsunai, T., Kanazawa, A., Shiono, T., and Ikeda, T., Photochemical Phase Transition Behavior of Polymer Azobenzene Liquid Crystals with Electron-Donating and -Accepting Substituents at the 4,4'-Positions. *Macromolecules*, 1998. 31(2): 355-359.
192. Ho, M.-S., Natansohn, A., Barrett, C., and Rochon, P., Azo polymers for reversible optical storage. 8. The effect of polarity of the azobenzene groups. *Canadian Journal of Chemistry*, 1995. 73(11): 1773-1778.
193. Karipcin, F., Kabalcilar, E., Ilican, S., Caglar, Y., and Caglar, M., Synthesized some 4-(2-thiazolylazo)resorcinol complexes: Characterization, thermal and optical properties. *Spectrochimica Acta Part A: Molecular and Biomolecular Spectroscopy*, 2009. 73(1): 174-180.
194. Rameshbabu, K. and Kannan, P., Synthesis and characterization of thermotropic liquid crystalline polyphosphates containing photoreactive moieties. *Liquid Crystals*, 2004. 31(6): 843-851.
195. Khanmohammadi, H. and Darvishpour, M., New azo ligands containing azomethine groups in the pyridazine-based chain: Synthesis and characterization. *Dyes and Pigments*, 2009. 81(3): 167-173.
196. Chen, B.-K., Tsay, S.-Y., and Chen, J.-Y., Synthesis and properties of liquid crystalline polymers with low T_m and broad mesophase temperature ranges. *Polymer*, 2005. 46(20): 8624-8633.
197. Cui, Y., Qian, G., Chen, L., Wang, Z., and Wang, M., Synthesis and nonlinear optical properties of a series of azo chromophore functionalized alkoxy silanes. *Dyes and Pigments*, 2008. 77(1): 217-222.
198. Karim, M.R., Sheikh, M.R.K., Salleh, N.M., Yahya, R., Hassan, A., and Hoque, M.A., Synthesis and characterization of azo benzothiazole chromophore based liquid crystal macromers: Effects of substituents on benzothiazole ring and terminal group on mesomorphic, thermal and optical properties. *Materials Chemistry and Physics*, 2013. 140(2–3): 543-552.
199. Wang, H.-Y., Chen, G., Xu, X.-P., and Ji, S.-J., Synthesis and characterization of triphenylamine–benzothiazole-based donor and acceptor materials. *Synthetic Metals*, 2010. 160(9–10): 1065-1072.
200. Giménez, R., Millaruelo, M., Piñol, M., Serrano, J.L., Viñuales, A., Rosenhauer, R., Fischer, T., and Stumpe, J., Synthesis, thermal and optical properties of liquid crystalline terpolymers containing azobenzene and dye moieties. *Polymer*, 2005. 46(22): 9230-9242.

201. Lam, J.W.Y., Kong, X., Dong, Y., Cheuk, K.K.L., Xu, K., and Tang, B.Z., Synthesis and Properties of Liquid Crystalline Polyacetylenes with Different Spacer Lengths and Bridge Orientations. *Macromolecules*, 2000. 33(14): 5027-5040.
202. A.-Zhang, X., Zhao, H., Gao, Y., Tong, J., Shan, L., Chen, Y., Zhang, S., Qin, A., Sun, J.Z., and Tang, B.Z., Functional poly(phenylacetylene)s carrying azobenzene pendants: Polymer synthesis, photoisomerization behaviors, and liquid-crystalline property. *Polymer*, 2011. 52(23): 5290-5301.
203. Kumaresan, S. and Kannan, P., Substituent effect on azobenzene-based liquid-crystalline organophosphorus polymers. *Journal of Polymer Science Part A: Polymer Chemistry*, 2003. 41(20): 3188-3196.
204. Balaji, K. and Murugavel, S.C., Synthesis and characterization of photosensitive liquid crystalline poly(benzylidene-ether)s with alkanones and methylene spacers in the main chain. *Journal of Polymer Science Part A: Polymer Chemistry*, 2011. 49(22): 4809-4819.
205. D. Demus, L.R., *Textures of Liquid Crystals*. 2nd ed. 1978, New York: Verlag Chemie.
206. Dierking, I., *Textures of Liquid Crystals*. 2003: John Wiley & Sons Incorporated.
207. Li, X., Wen, R., Zhang, Y., Zhu, L., Zhang, B., and Zhang, H., Photoresponsive side-chain liquid crystalline polymers with an easily cross-linkable azobenzene mesogen. *Journal of Materials Chemistry*, 2009. 19(2): 236-245.
208. Wei, Q., Shi, L., Cao, H., Wang, L., Yang, H., and Wang, Y., Synthesis and mesomorphic properties of two series of new azine-type liquid crystals. *Liquid Crystals*, 2008. 35(5): 581-585.
209. Guillevic, M.-A., Light, M.E., Coles, S.J., Gelbrich, T., Hursthouse, M.B., and Bruce, D.W., Synthesis of dinuclear complexes of rhenium(I) as potential metallomesogens. *Journal of the Chemical Society, Dalton Transactions*, 2000(9): 1437-1445.
210. Bagheri, M. and Pourmoazzen, Z., Synthesis and properties of new liquid crystalline polyurethanes containing mesogenic side chain. *Reactive and Functional Polymers*, 2008. 68(2): 507-518.
211. Karim, M.R., Sheikh, M.R., Yahya, R., M. Salleh, N., Azzahari, A., Hassan, A., and M. Sarih, N., Thermal, optical and electrochemical study of side chain liquid crystalline polymers bearing azo-benzothiazole chromophore in the mesogen. *Journal of Polymer Research*, 2013. 20(10): 1-7.
212. Ebead, Y.H., Selim, M.A., and Ibrahim, S.A., Solvatochromic, acid-base features and time effect of some azo dyes derived from 1,3-benzothiazol-2-ylacetonitrile: Experimental and semiempirical investigations. *Spectrochimica Acta Part A: Molecular and Biomolecular Spectroscopy*, 2010. 75(2): 760-768.
213. Mabrouk, A., Azazi, A., and Alimi, K., On the properties of new benzothiazole derivatives for organic light emitting diodes (OLEDs): A comprehensive

- theoretical study. *Journal of Physics and Chemistry of Solids*, 2010. 71(9): 1225-1235.
214. Shi, H.-p., Shi, L.-w., Dai, J.-x., Xu, L., Wang, M.-h., Wu, X.-h., Fang, L., Dong, C., and Choi, M.M.F., Synthesis, photophysical and electrochemical properties and theoretical studies on three novel indolo[3,2-b]carbazole derivatives containing benzothiazole units. *Tetrahedron*, 2012. 68(47): 9788-9794.
215. Wong, M.S., Li, Z.H., Tao, Y., and D'Iorio, M., Synthesis and Functional Properties of Donor–Acceptor π -Conjugated Oligomers. *Chemistry of Materials*, 2003. 15(5): 1198-1203.
216. Hohnholz, D., Schweikart, K.H., Subramanian, L.R., Wedel, A., Wischert, W., and Hanack, M., Synthesis and studies on luminescent biphenyl compounds. *Synthetic Metals*, 2000. 110(2): 141-152.
217. Bera, R.N., Sakakibara, Y., Abe, S., Yase, K., and Tokumoto, M., Time-resolved photoluminescence study on concentration quenching of a red emitting tetraphenylchlorin dye for organic electroluminescent devices. *Synthetic Metals*, 2005. 150(1): 9-13.
218. Issa, R.M., Khedr, A.M., and Rizk, H.F., UV–vis, IR and ¹H NMR spectroscopic studies of some Schiff bases derivatives of 4-aminoantipyrine. *Spectrochimica Acta Part A: Molecular and Biomolecular Spectroscopy*, 2005. 62(1–3): 621-629.
219. Gup, R., Giziroglu, E., and Kirkan, B., Synthesis and spectroscopic properties of new azo-dyes and azo-metal complexes derived from barbituric acid and aminoquinoline. *Dyes and Pigments*, 2007. 73(1): 40-46.
220. Pommerehne, J., Vestweber, H., Guss, W., Mahrt, R.F., Bässler, H., Porsch, M., and Daub, J., Efficient two layer leds on a polymer blend basis. *Advanced Materials*, 1995. 7(6): 551-554.
221. Vishnumurthy, K.A., Sunitha, M.S., Safakath, K., Philip, R., and Adhikari, A.V., Synthesis, electrochemical and optical studies of new cyanopyridine based conjugated polymers as potential fluorescent materials. *Polymer*, 2011. 52(19): 4174-4183.
222. Liang, Y., Feng, D., Wu, Y., Tsai, S.-T., Li, G., Ray, C., and Yu, L., Highly Efficient Solar Cell Polymers Developed via Fine-Tuning of Structural and Electronic Properties. *Journal of the American Chemical Society*, 2009. 131(22): 7792-7799.
223. Manjunatha, M.G., Adhikari, A., Hegde, P., Suchand Sandeep, C.S., and Philip, R., Synthesis and characterization of a new NLO-active donor–acceptor-type conjugated polymer derived from 3,4-diphenylthiophene. *Journal of Polymer Research*, 2010. 17(4): 495-502.
224. Zhang, X.H., Lai, W.Y., Gao, Z.Q., Wong, T.C., Lee, C.S., Kwong, H.L., Lee, S.T., and Wu, S.K., Photoluminescence and electroluminescence of pyrazoline monomers and dimers. *Chemical Physics Letters*, 2000. 320(1–2): 77-80.

225. Perzon, E., Wang, X., Admassie, S., Inganäs, O., and Andersson, M.R., An alternating low band-gap polyfluorene for optoelectronic devices. *Polymer*, 2006. 47(12): 4261-4268.
226. Yang, I.K. and Chang, S., The Smectic Rheology of a Polysiloxane Side Chain Liquid Crystalline Polymer. *Journal of Polymer Research*, 2002. 9(3): 163-168.
227. Zentel, R. and Wu, J., Rheological properties of liquid-crystalline side-group polymers in the isotropic, nematic, and smectic states. *Macromolecular Chemistry*, 1986. 187(7): 1727-1736.
228. Andreozzi, L., Faetti, M., Giordano, M., Zulli, F., Galli, G., and Laus, M., Rheological Behavior of Azobenzene Nematic Homopolymer and Copolymer. *Molecular Crystals and Liquid Crystals*, 2005. 429(1): 301-312.
229. Auad, M.L., Kempe, M.D., Kornfield, J.A., Rendon, S., Burghardt, W.R., and Yoon, K., Effect of Mesophase Order on the Dynamics of Side Group Liquid Crystalline Polymers. *Macromolecules*, 2005. 38(16): 6946-6953.
230. Kalika, D.S., Giles, D.W., and Denn, M.M., Shear and time-dependent rheology of a fully nematic thermotropic liquid crystalline copolymer. *Journal of Rheology*, 1990. 34(2): 139-154.
231. Ramos, L., Zapotocky, M., Lubensky, T.C., and Weitz, D.A., Rheology of defect networks in cholesteric liquid crystals. *Physical Review E*, 2002. 66(3): 031711.
232. Martinoty, P., Hilliou, L., Mauzac, M., Benguigui, L., and Collin, D., Side-Chain Liquid-Crystal Polymers: Gel-like Behavior below Their Gelation Points. *Macromolecules*, 1999. 32(6): 1746-1752.
233. Gallani, J.L., Hilliou, L., Martinoty, P., and Keller, P., Abnormal viscoelastic behavior of side-chain liquid-crystal polymers. *Physical Review Letters*, 1994. 72(13): 2109-2112.
234. Larson, R.G., Winey, K.I., Patel, S.S., Watanabe, H., and Bruinsma, R., The rheology of layered liquids: lamellar block copolymers and smectic liquid crystals. *Rheologica Acta*, 1993. 32(3): 245-253.
235. Hudson, S.D., Lovinger, A.J., Larson, R.G., Davis, D.D., Garay, R.O., and Fujishiro, K., Detection of nematic-smectic phase transition in a semiflexible main-chain liquid crystalline polymer. *Macromolecules*, 1993. 26(21): 5643-5650.
236. Somma, E., Iervolino, R., and Nobile, M., The viscoelasticity of thermotropic liquid crystalline polymers: effects of the chemical composition. *Rheologica Acta*, 2006. 45(4): 486-496.
237. Barnes, H.A., Thixotropy—a review. *Journal of Non-Newtonian Fluid Mechanics*, 1997. 70(1-2): 1-33.
238. Zhou, W.-J., Kornfield, J.A., Ugaz, V.M., Burghardt, W.R., Link, D.R., and Clark, N.A., Dynamics and Shear Orientation Behavior of a Main-Chain

Thermotropic Liquid Crystalline Polymer. *Macromolecules*, 1999. 32(17): 5581-5593.

239. Tang, Y., Gao, P., Ye, L., Zhao, C., and Lin, W., Organoclay/thermotropic liquid crystalline polymer nanocomposites. Part V: morphological and rheological studies. *Journal of Materials Science*, 2010. 45(11): 2874-2883.
240. Dan, K., Kim, B., and Han, Y.-K., The physical properties of thermotropic side-chain triblock copolymers of n-butyl acrylate and a comonomer with azobenzene group. *Macromolecular Research*, 2009. 17(5): 313-318.

APPENDICES

APPENDIX A : FT-IR spectra of monomers and polymers

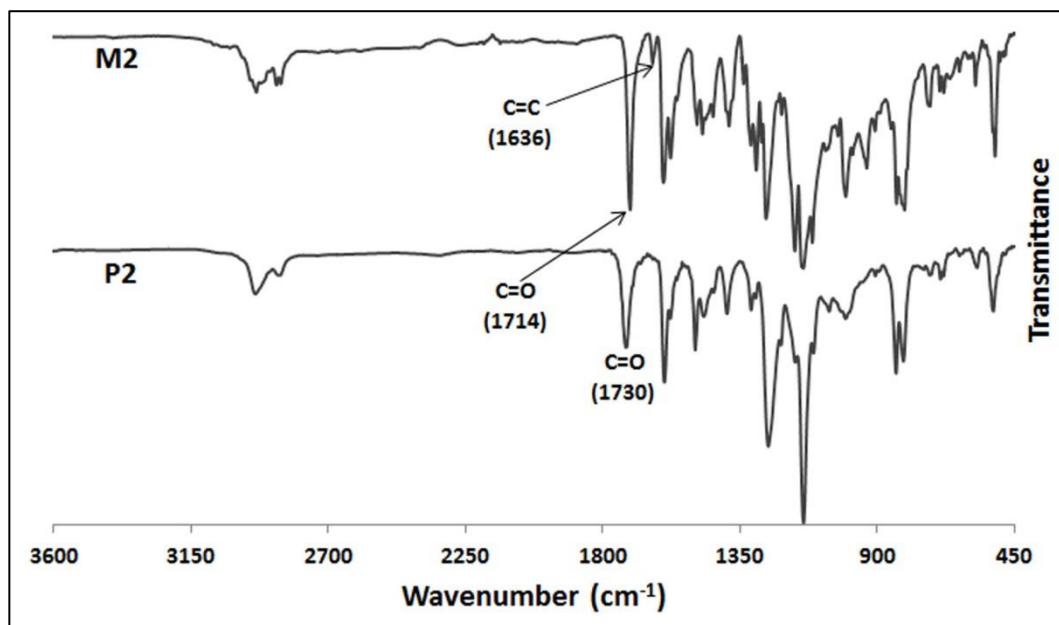


Figure 1: FT-IR spectra of monomer M2 and polymer P2

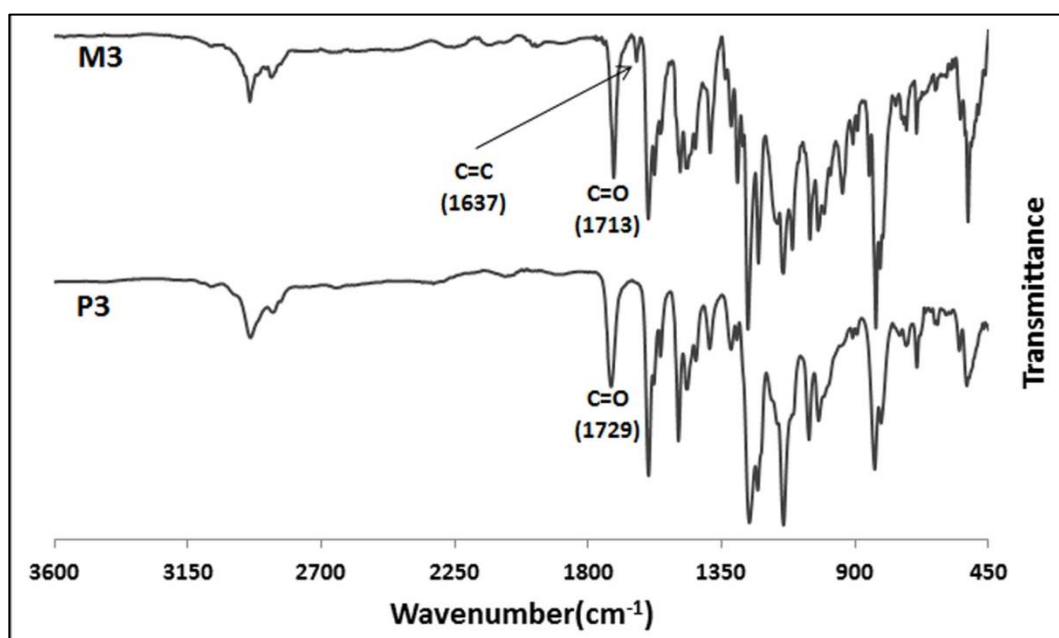


Figure 2: FT-IR spectra of monomer M3 and polymer P3

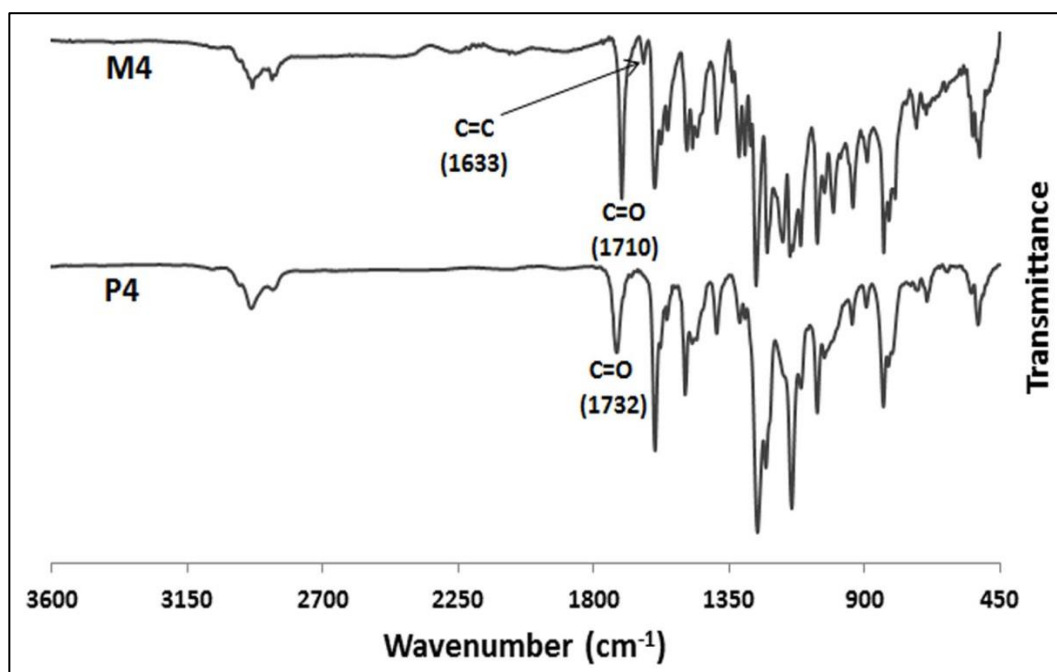


Figure 3: FT-IR spectra of monomer **M4** and polymer **P4**

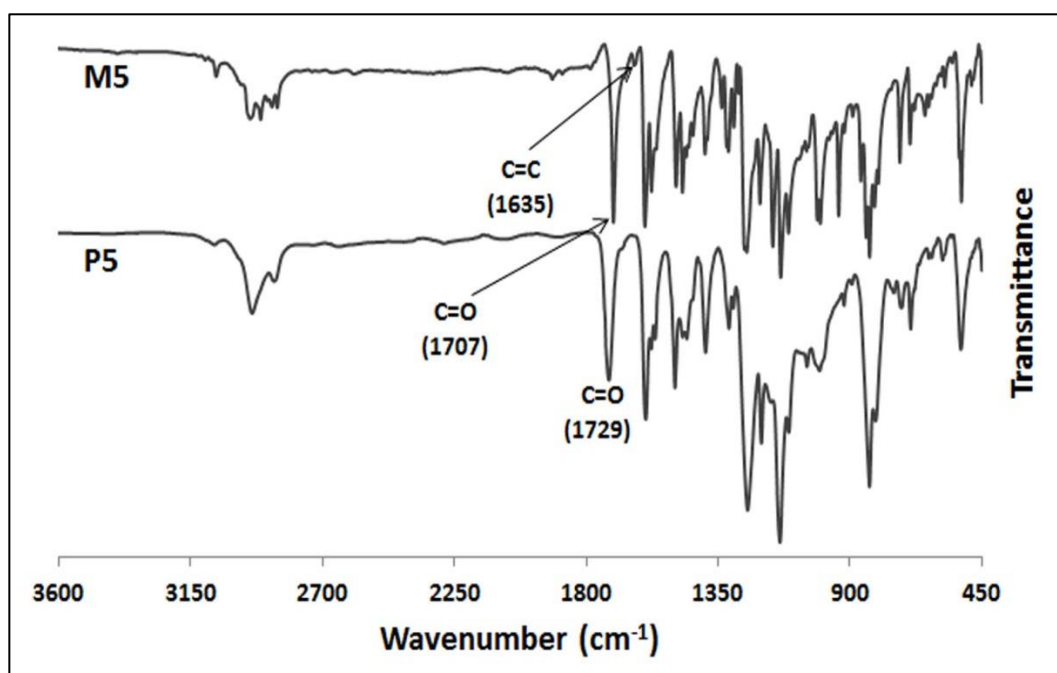


Figure 4: FT-IR spectra of monomer **M5** and polymer **P5**

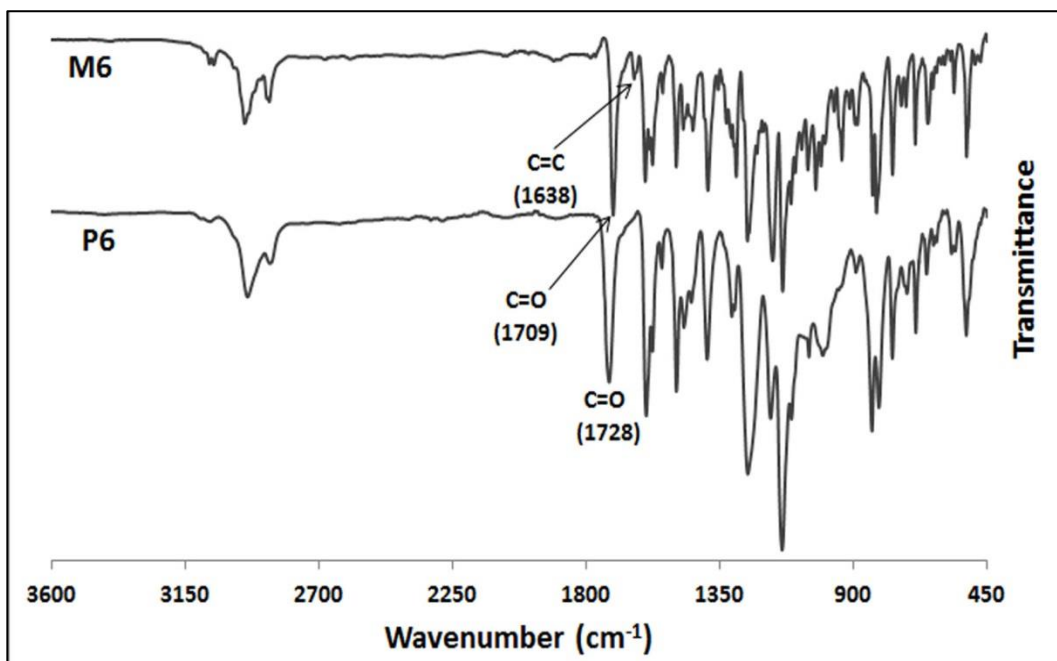


Figure 5: FT-IR spectra of monomer **M6** and polymer **P6**

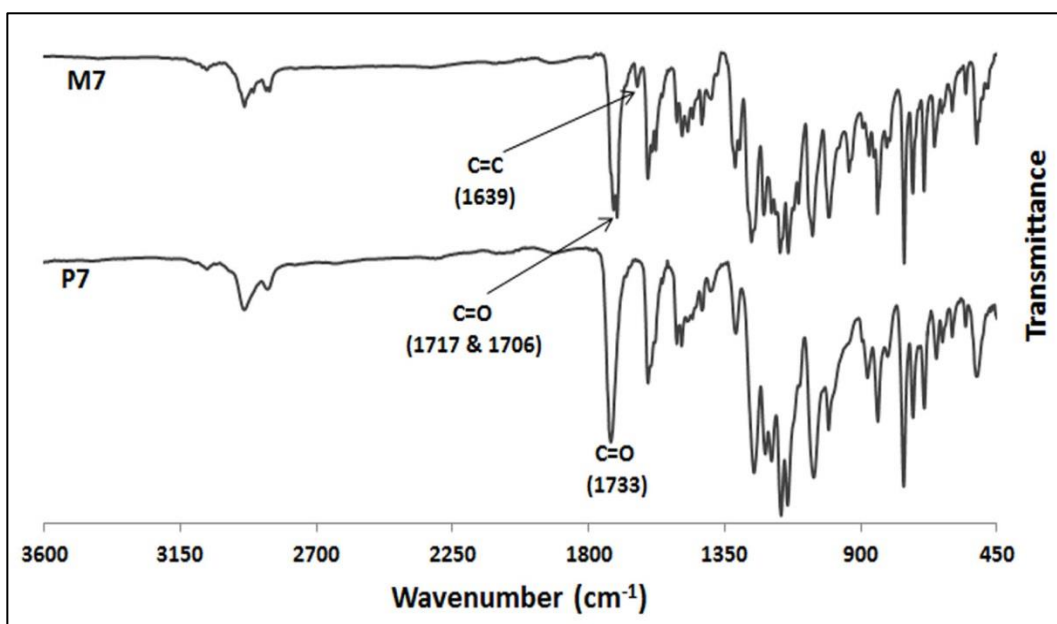


Figure 6: FT-IR spectra of monomer **M7** and polymer **P7**

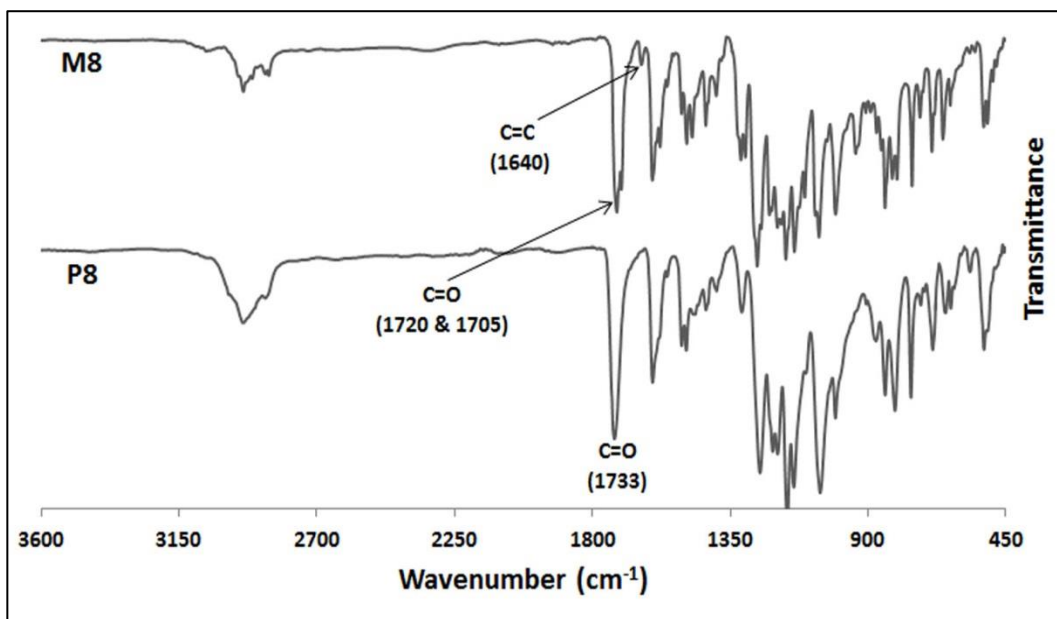


Figure 7: FT-IR spectra of monomer **M8** and polymer **P8**

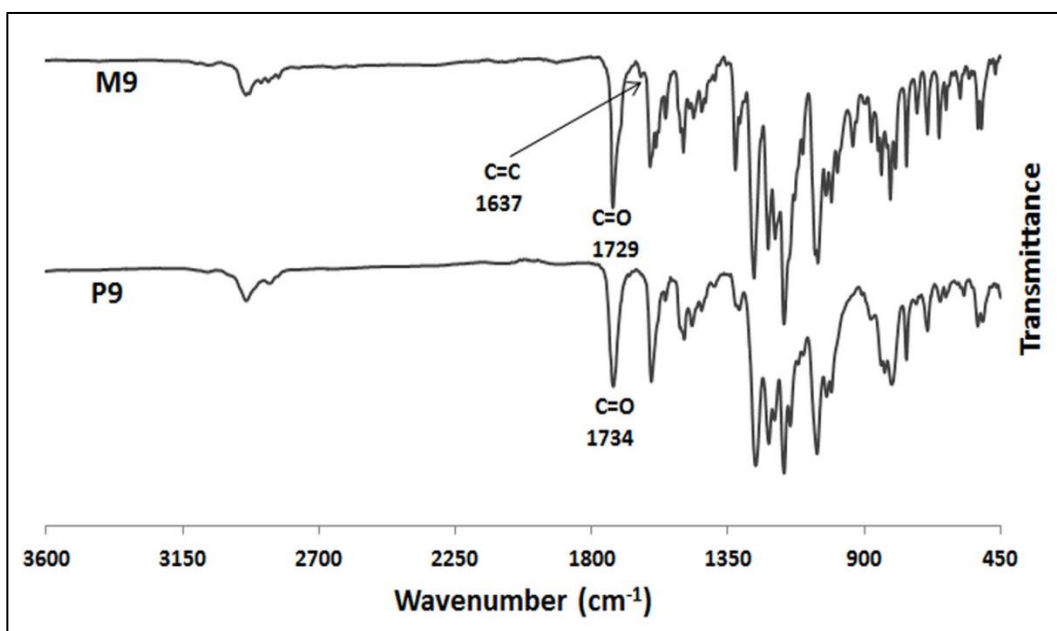


Figure 8: FT-IR spectra of monomer **M9** and polymer **P9**

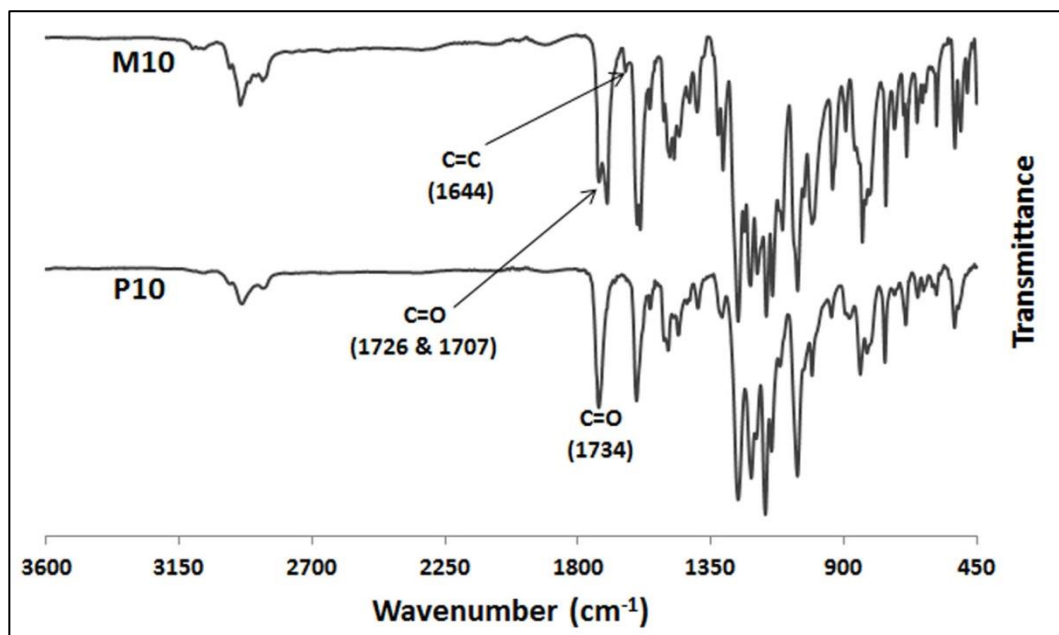


Figure 9: FT-IR spectra of monomer **M10** and polymer **P10**

APPENDIX B : ¹H NMR spectra of monomers and polymers

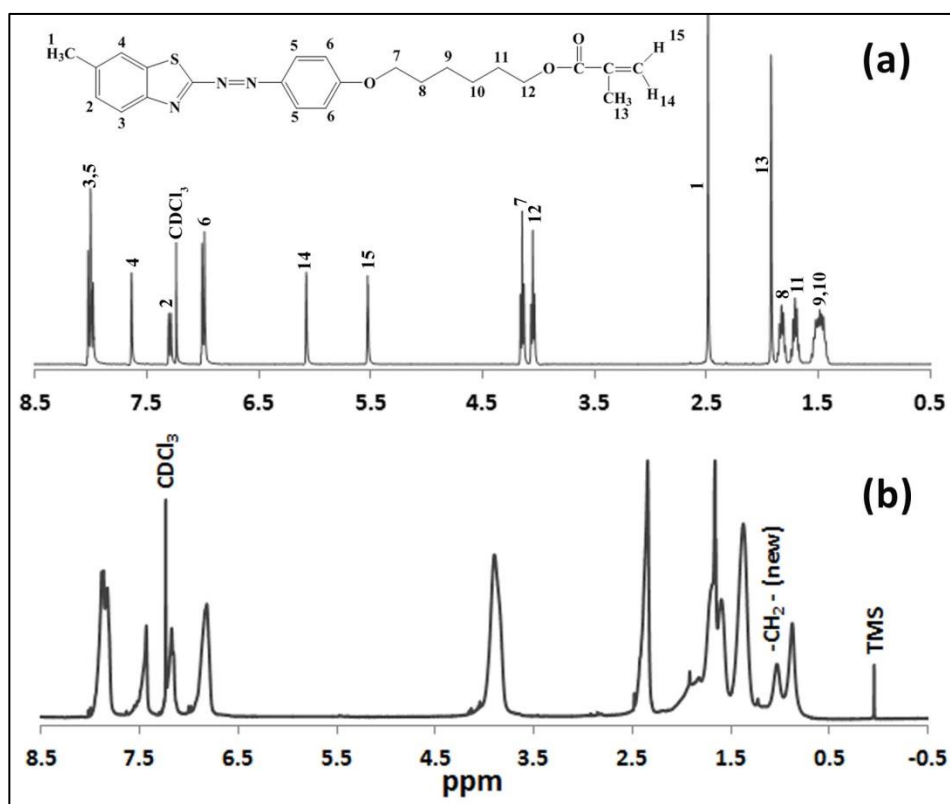


Figure 1: ¹H NMR spectra of (a) monomer **M2** and (b) polymer **P2**

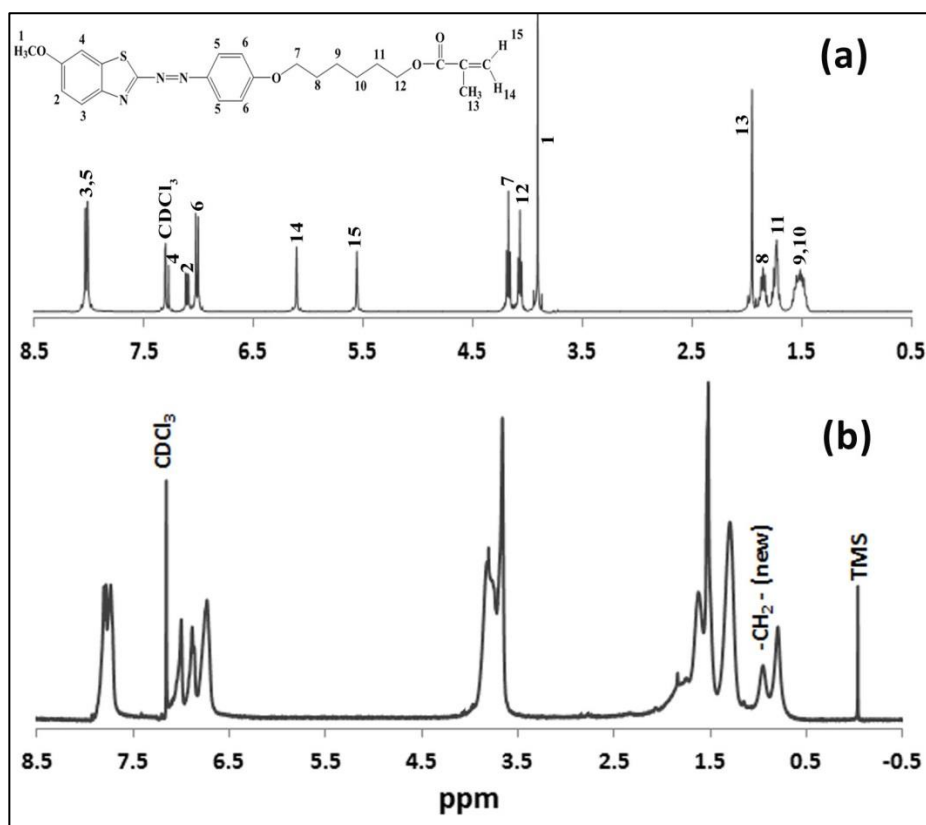


Figure 2: ^1H NMR spectra of (a) monomer **M3** and (b) polymer **P3**

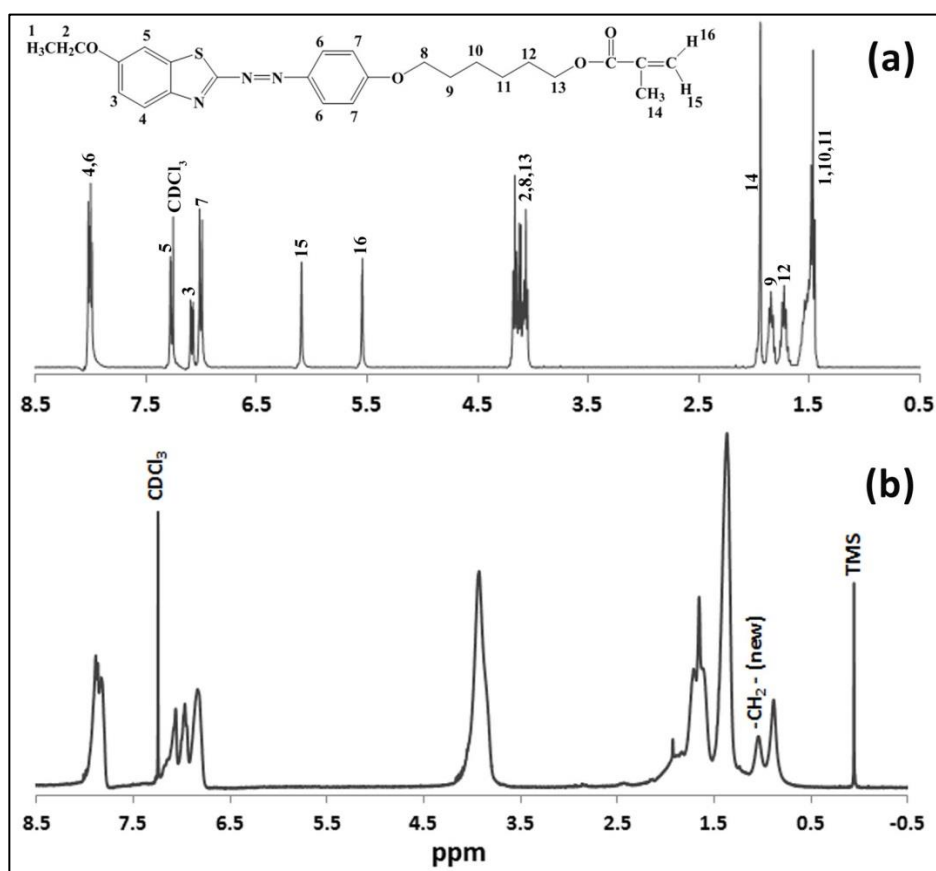


Figure 3: ^1H NMR spectra of (a) monomer **M4** and (b) polymer **P4**

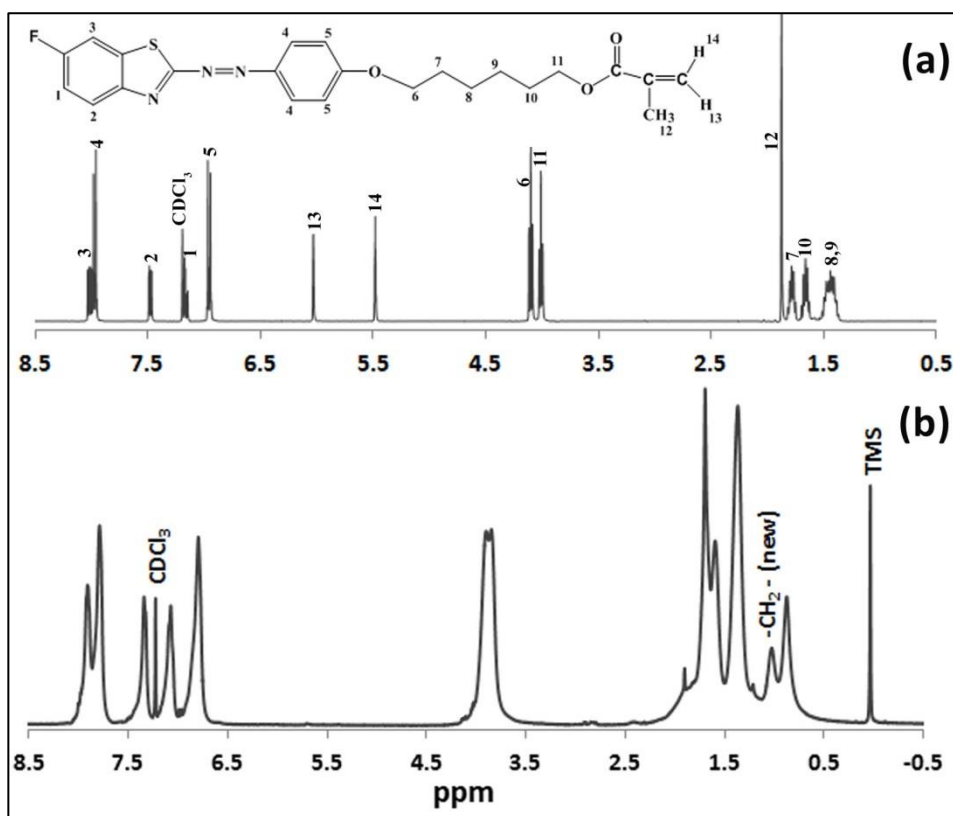


Figure 4: ^1H NMR spectra of (a) monomer **M5** and (b) polymer **P5**

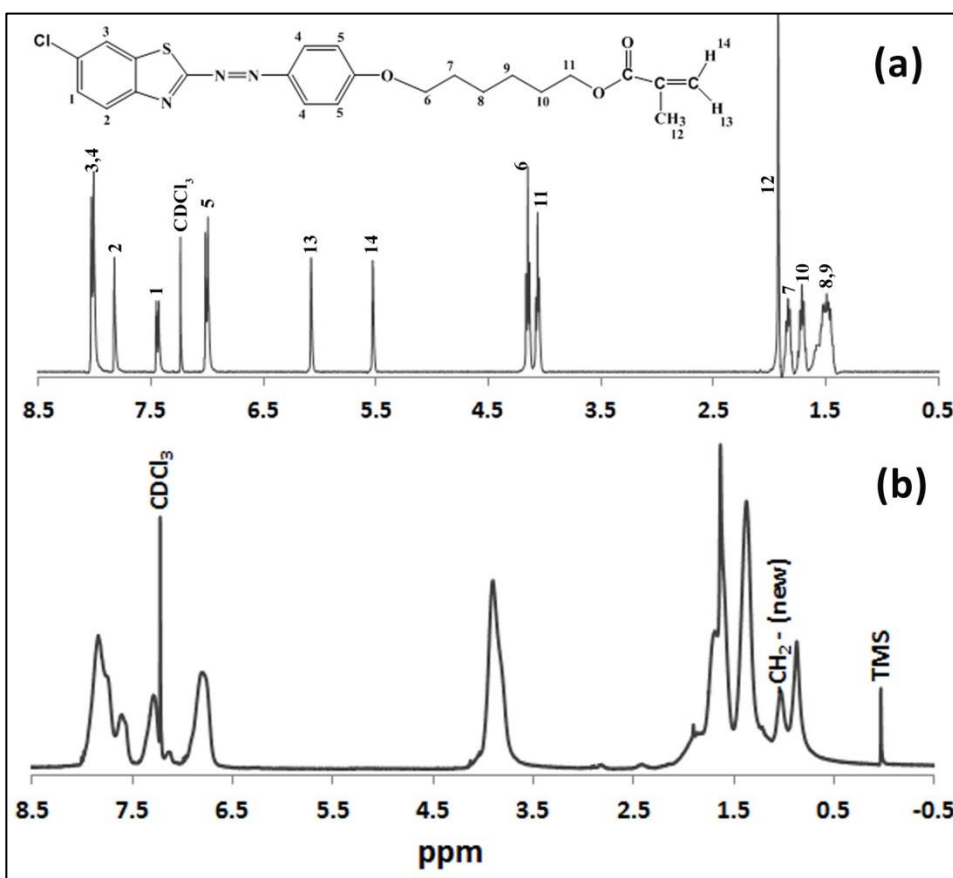


Figure 5: ^1H NMR spectra of (a) monomer **M6** and (b) polymer **P6**

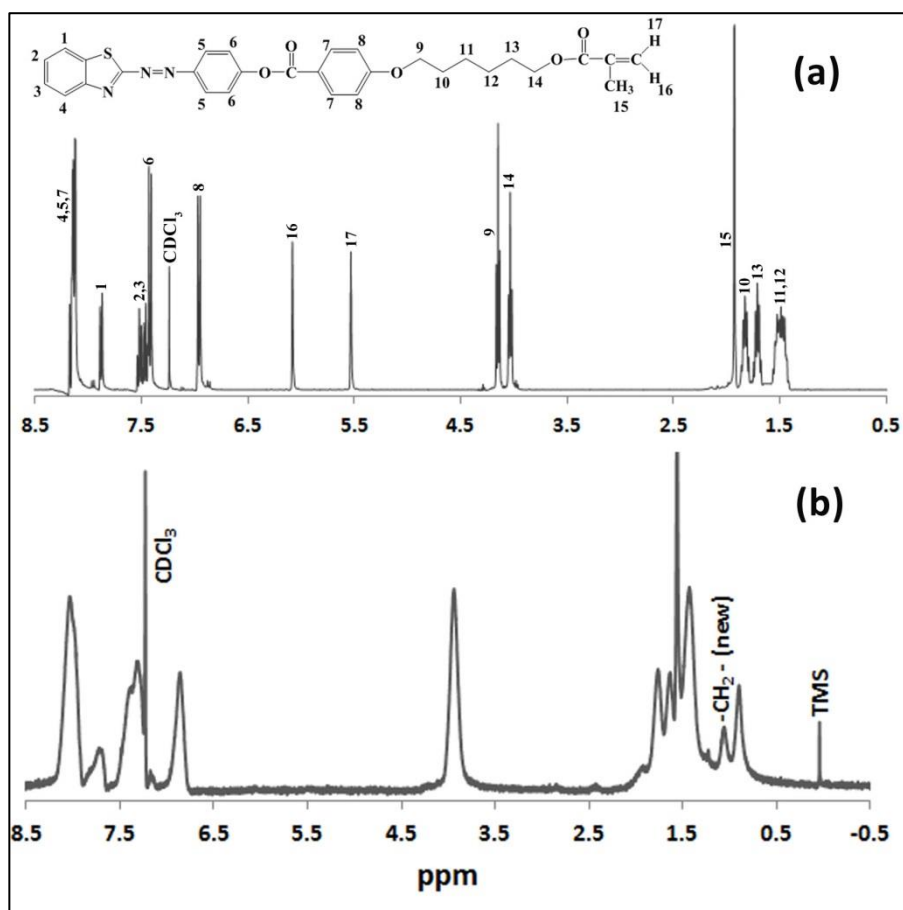


Figure 6: ^1H NMR spectra of (a) monomer **M7** and (b) polymer **P7**

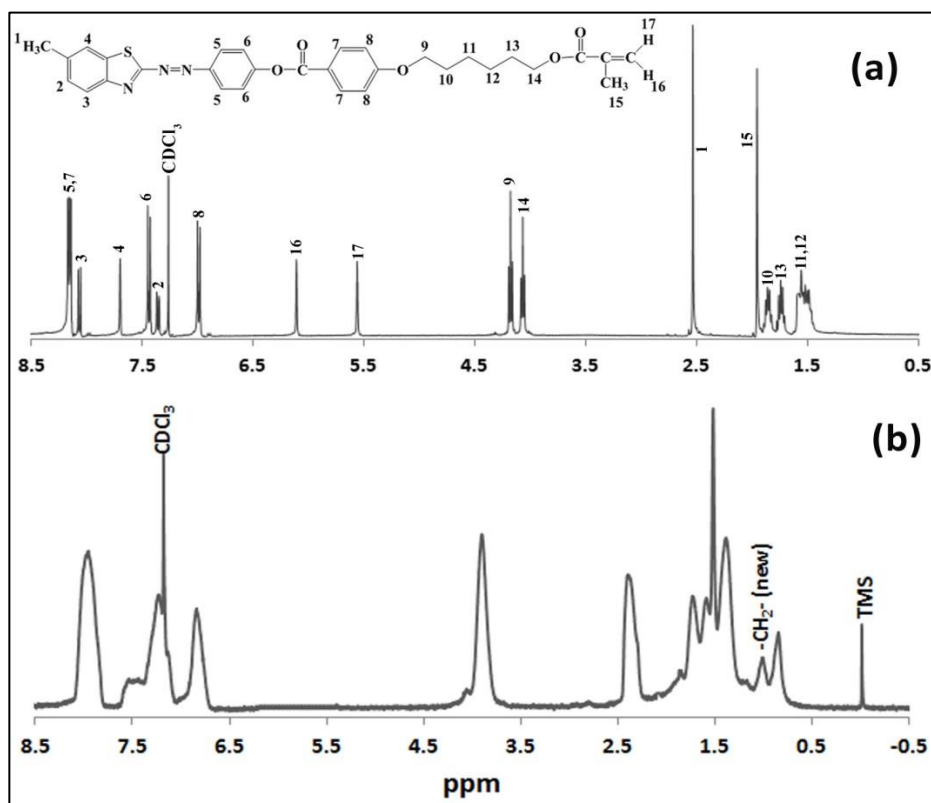


Figure 7: ^1H NMR spectra of (a) monomer **M8** and (b) polymer **P8**

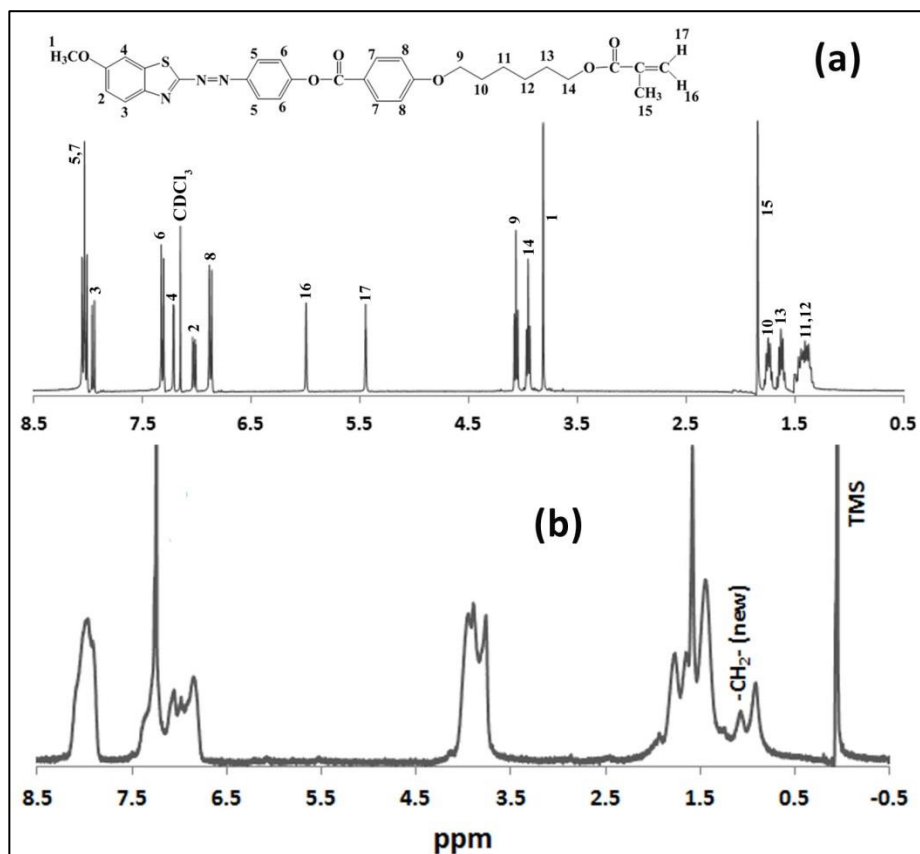


Figure 8: ^1H NMR spectra of (a) monomer **M9** and (b) polymer **P9**

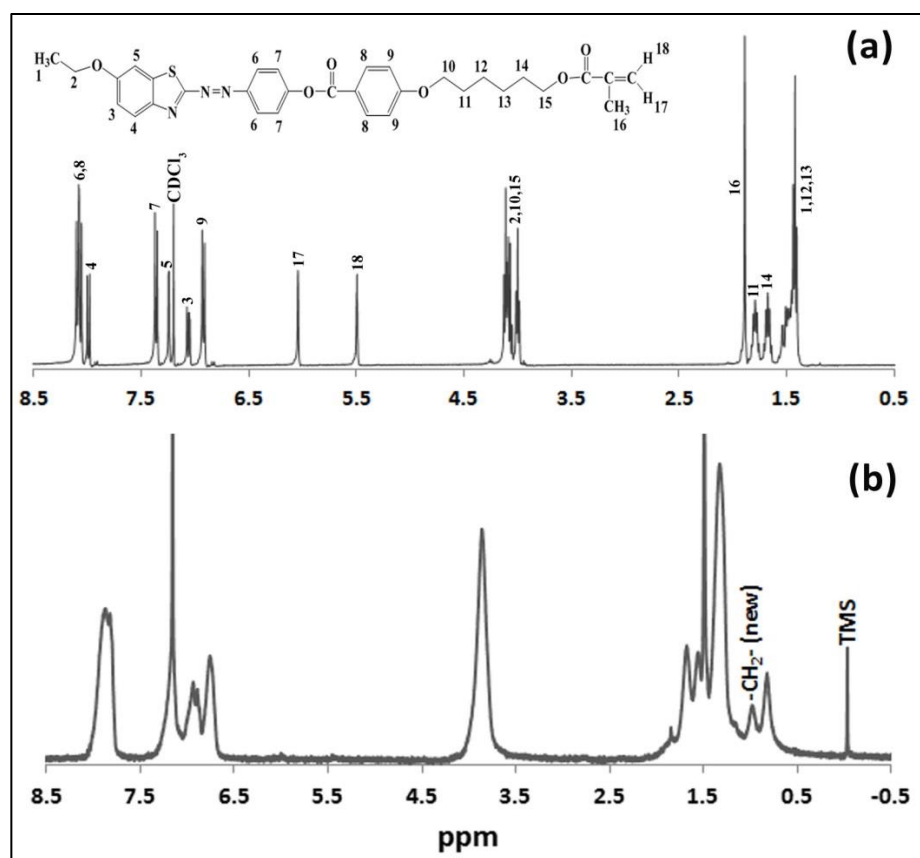


Figure 9: ^1H NMR spectra of (a) monomer **M10** and (b) polymer **P10**

APPENDIX C : Cyclic voltammograms of polymers

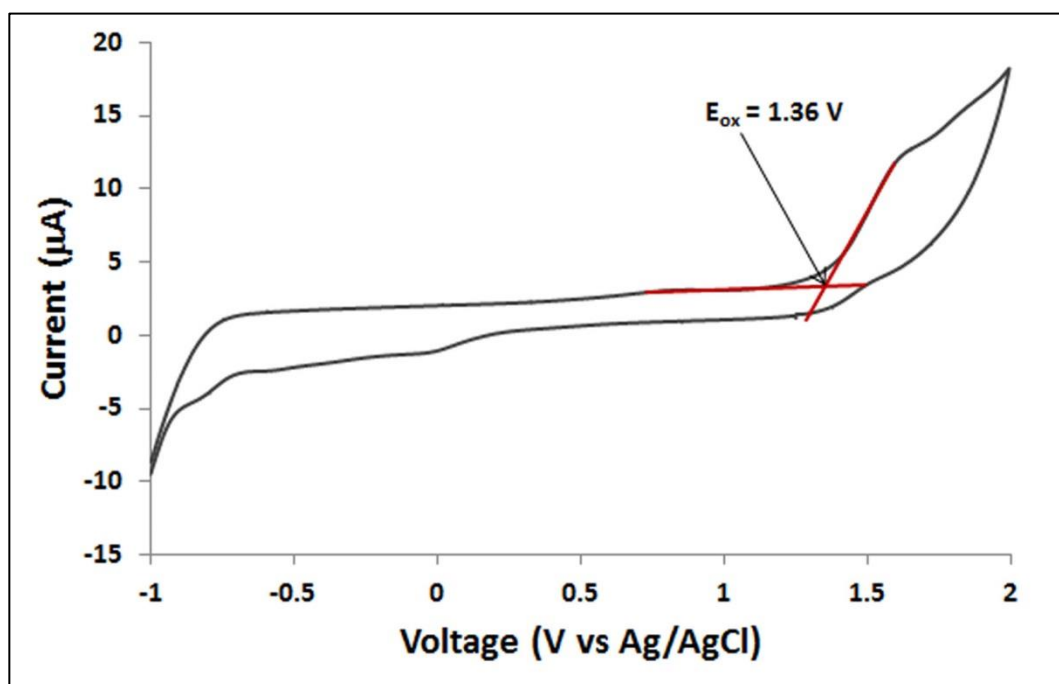


Figure 1: Cyclic voltammogram of polymer P3

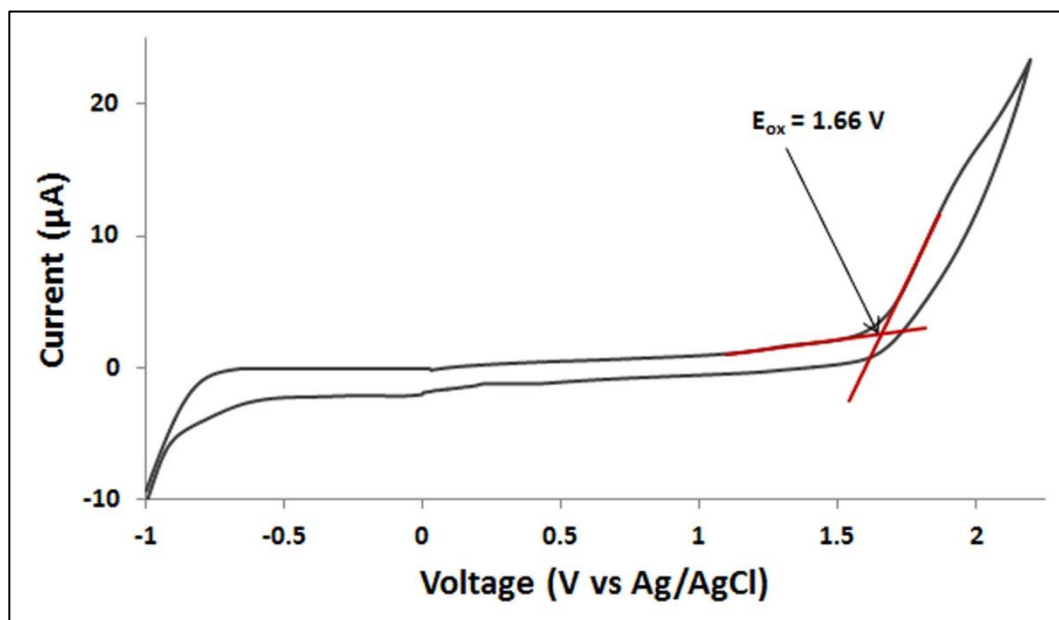


Figure 2: Cyclic voltammogram of polymer P5

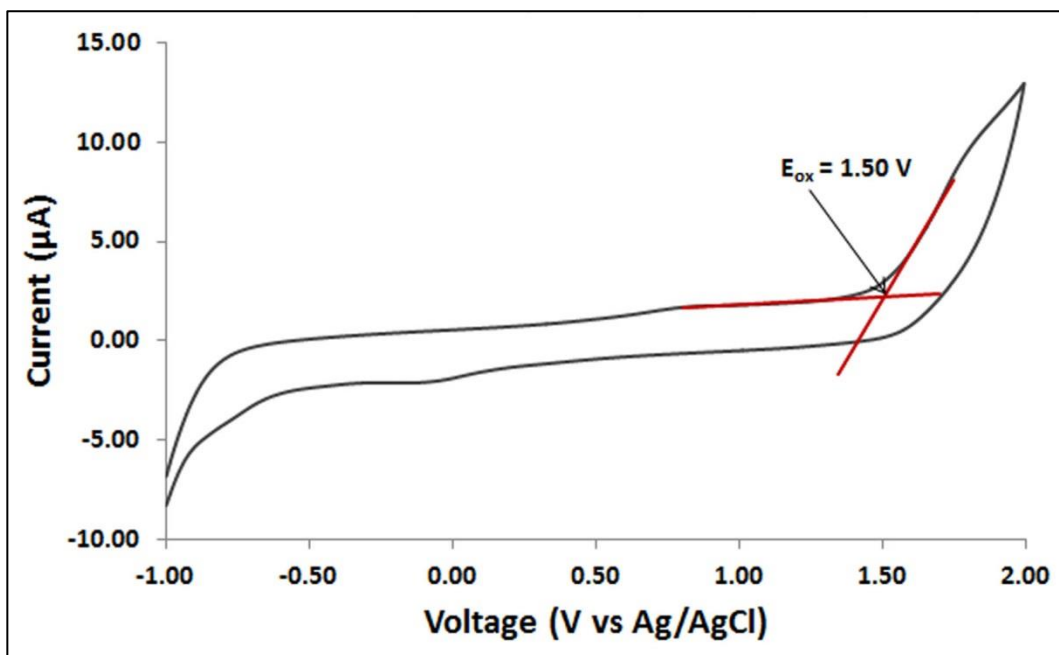


Figure 3: Cyclic voltammogram of polymer P6

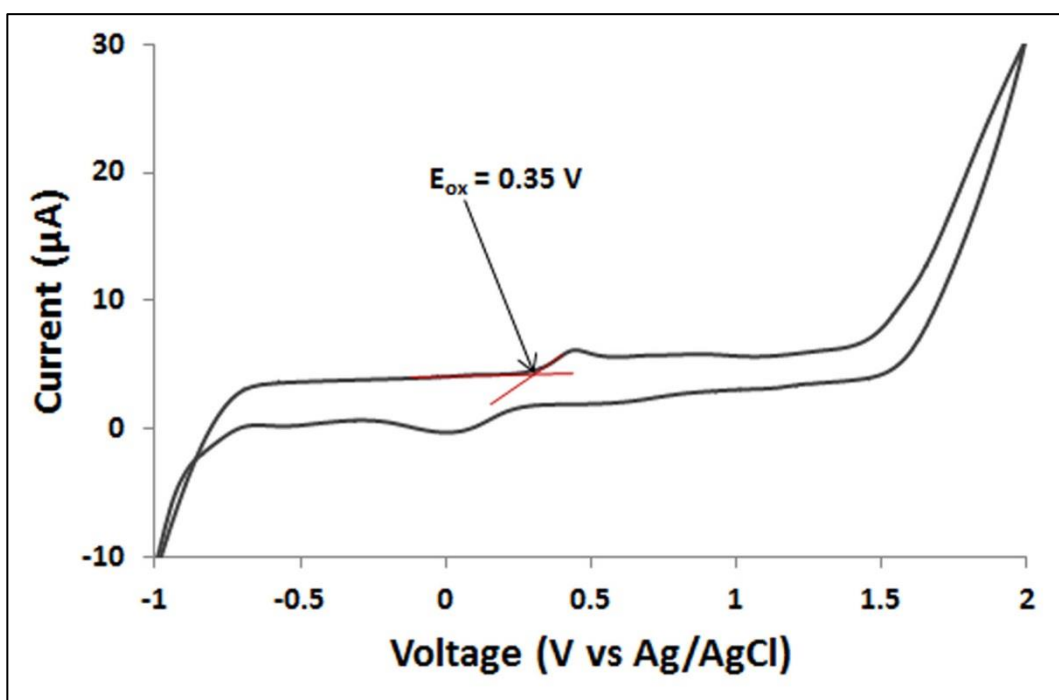


Figure 4: Cyclic voltammogram of polymer P9

APPENDIX D : Publications

1. **Md. Rabiul Karim**, Md. Rezaul Karim Sheikh , Noordini M. Salleh , Rosiyah Yahya , Aziz Hassan and Md. Asadul Hoque, Synthesis and characterization of azo benzothiazole chromophore based liquid crystal macromers: Effects of substituents on benzothiazole ring and terminal group on mesomorphic, thermal and optical properties, *Materials Chemistry and Physics* 140 (2013): 543-552
2. **Md. Rabiul Karim**, Md. Rezaul Karim Sheikh, Rosiyah Yahya, Noordini M. Salleh, Ahmad Danial Azzahari, Aziz Hassan and Norazilawati M. Sarih, Thermal, optical and electrochemical study of side chain liquid crystalline polymers bearing azo-benzothiazole chromophore in the mesogen, *Journal of Polymer Research* 20 (2013): 259-265
3. **Md. Rabiul Karim**, Rosiyah Yahya, Md. Rezaul Karim Sheikh and Noordini M. Salleh, Aziz Hassan and H. N. M. Ekramul Mahmud, Synthesis, thermal stability, optical and electrochemical properties of halogen terminated azo-benzothiazole mesogen containing smectic side chain liquid crystalline polymers, *Journal of Polymer Research* (Manuscript under review).
4. **Md. Rabiul Karim**, Rosiyah Yahya, Md. Rezaul Karim Sheikh and Noordini M. Salleh, H. N. M. Ekramul Mahmud, Ahmad Danial Azzahari, and Aziz Hassan, Synthesis of polymerizable liquid crystalline macromers and their side chain liquid crystalline polymers bearing azo linked benzothiazole moiety in the mesogen (Manuscript submitted).
5. **Md. Rabiul Karim**, Rosiyah Yahya, Md. Rezaul Karim Sheikh and Noordini M. Salleh, Rheology of side chain liquid crystalline polymers bearing azo-benzothiazole mesogen (Manuscript under preparation)